High performing sustainable thermoplastic elastomers

A DISSERTATION
SUBMITTED TO THE FACULTY OF THE
UNIVERSITY OF MINNESOTA
BY

Annabelle Watts

IN PARTIAL FULFILLMENT OF THE REQUIREMENTS
FOR THE DEGREE OF
DOCTOR OF PHILOSOPHY

Marc A. Hillmyer, Advisor

January 2019

Acknowledgements

Pursuing a PhD entails much more than the technical content of this dissertation. There are many people that I want to acknowledge for making a positive impact in my journey through graduate school. I would like to thank Prof. Marc Hillmyer for his guidance during my graduate career as his influence has shaped me to be the scientist that I am today. Aligned with his research interests, I have been able to pursue a research topic that I am passionate about in the area of sustainability. Marc's continuous enthusiasm for understanding fundamental research questions was contagious and made research exciting. We have had many honest conversations where he has always listened and provided sound advice; I strive to emulate the high level of professionalism he demonstrates on a daily basis. I have been able to grow tremendously technically and personally with the help of Marc, for which I am deeply grateful.

I would not be in graduate school were it not for having excellent undergraduate mentors Kristin Clark, Nathaniel Lynd, Louis Pitet, Craig Hawker, and Hawker group members. I am particularly grateful for the influence of Kristin Clark and Nathaniel Lynd, both of whom took a chance with me and took every moment to promote and encourage me in research.

I want to acknowledge the many members of the Hillmyer group that I have had the fortune to overlap with. I learned a lot from those who shared Southeast lab with me: James Gallagher, Lindsay Johnson, and Madalyn Radlauer. I want to thank those who shared in the responsibility of safety: Paula Delgado, Arthur Bertrand, Sam Dalsin, Alex

Todd, Guilhem De Hoe, Colin Peterson, and Gereon Yee. I am thankful for the friendships I have fostered with Helena Quilter, Michael Larsen, Stacey Saba, Derek Batiste, Leon Lillie, Ingrid Haugan Smidt, and Marie Vanderlaan. I have been fortunate to have had the opportunity to work with many collaborators during my graduate career: Dr. Kyle O'Conner, Prof. Geoffrey Coates, Jacob Trotta, Prof. Brett Fors, Dr. Adrian Amador, Dr. Angelika Neitzel, Naruki Kurokawa, Kali Johnson, Emma Rettner, Emily Abdo, and many more.

Shout out to Caleb, Ben, Laura, Timothy, Julianna, Joe, Jake, Josie, Theresa, Maggie, Sarah, Anna, Kate, Jeramiah, Deano, and Katie. You all kept my spirits high, kept me caffeinated, and helped me more than you can imagine. I want to say special thanks to Cecilia Hall who has traveled through this journey with me and helped me every step of the way. We studied together, practiced talks with each other, kept each other on track with goals, started a student group together, and helped one another in every aspect of life. I am incredibly grateful for our friendship and for her support.

I am extremely thankful to Justin Watts. He has been a partner through so much of life and I appreciate his support during the ups and downs of graduate school. His persistent encouragement to pursue my hobbies really helped me maintain work-life balance. We both grew tremendously over the years and graduate school is now one more experience we traversed together.

Abstract

Thermoplastic elastomers (TPEs) exhibit a wide range of properties and are easy to process as they are made of physical, rather than chemical, crosslinks. Many factors contribute to the varied physical properties seen in elastomeric TPEs, defining whether the resultant material is a soft elastomer suitable for adhesives, or a hard elastomer with competitive properties to vulcanized natural rubber. The sustainable polymers studied in this work are able to be synthesized through commercially available reagents and through controlled polymerization methods. Through the design of sustainable block polymers, we have gained insight into properties such as polymer entanglement that govern TPE mechanical behavior. High molar mass systems demonstrate high strength and high extensibility, yielding tough elastomers. Incorporating crystallinity or hydrogen-bonding groups results in improved mechanical properties and reduced stress relaxation. This work presents the synthesis of sustainable polymers and the investigation into the fundamental polymer properties essential to designing high performing TPEs.

Table of contents

List of Figures

List of Tables

List of Schemes

Chapter 1.

Introduction

1.1 Sustainability

Polymers play a large role in our daily lives. It would be hard to imagine a world without the plastics in computers, phones, cars, furniture, clothing, lenses, coatings, insulation. The list goes on. Despite the benefits that plastics provide society today, public perception is changing as their long-term impacts on the environment are revealed. Not only are we producing a large portion of plastics from non-renewable feedstocks, a finite resource, the fate of plastics after disposal is not well managed.[1,2] Due to the increasing concerns of persistent plastics, there is growing demand at a personal, local, and national level for environmentally-friendly replacements.

There are many innovative products that have drastically improved quality of life for society. However, the fate of these products after disposal need to be considered. The green chemistry initiative can be applied to the synthesis, use, and disposal of chemicals and plastics.[3] Processes can be engineered to reduce waste and increase efficiencies, reducing the carbon footprint of production plants.[4] We can better our local waste management policies to recover value from waste products. There are many factors that can contribute to the sustainability of a product. Here we will describe some considerations surrounding the idea of sustainability focused on polymer chemistry.

Feedstock. Most plastics are currently derived from chemicals obtained through resources that are not replenished at the same rate of consumption (crude oil, coal tar, etc.). Although plastic production from annually renewable resources is growing, the higher cost point compared to petroleum derivatives limits their widespread use. Products derived from annually renewable resources (agriculture, marine, forestry materials) can be labeled

biobased, a USDA certifiable product label for materials composed of at least 25% renewable feedstocks, though many other marketing phrases are used such as bioplastics, biorenewable, plant-based, etc.[5] There are a few approaches to obtain building blocks derived from renewable feedstocks.[6] Biomass, such as wood fibers, can be directly incorporated into plastics to form composite materials. Simple extraction of naturally occurring compounds can be used directly, such as in resin applications. Sugar from corn, sugarcane, or cellulose can be subjected to chemical transformations or biofermentation to yield high value chemicals. Chemicals with higher carbon content and aromaticity can be derived from lignocellulosic feedstocks. Bioderived chemicals that are identical to those derived from petroleum are used as drop-in replacements (e.g., biobased ethylene glycol in poly(ethylene terephthalate) (PET) bottles). The high production potential of some chemicals from renewable feedstocks has also increased the development and commercialization of new biobased plastics (e.g., polylactide (PLA)).

Production. Beyond considering raw material sources, there is a sustainability component in production of chemicals and plastics. Following the 12 principles of green chemistry, production processes can be engineered for higher efficiency, less byproducts, lower toxicity, etc.[8] There are also financial incentives to increase yields and produce less waste to decrease production costs. Although the improvements to the chemical production process are less visible to the consumer, efficient processes have a large impact in reducing the carbon footprint of plastic production.

Lifetime. Durability is a significant consideration in the design and production of plastic products. We expect long lifetimes for plastic products that go into cars, flooring,

piping, etc. Furthermore, less raw materials are used, and less waste is generated due to the durability of these materials. On the other extreme, there are many applications where the plastic products are more durable than their intended application. This is particularly rampant for single-use plastics such as cold-drink cups, plastic bags, food packaging, etc. These single-use plastics are ubiquitous due to the simplification of everyday tasks; however, these materials persist in the world far longer than the product's intended lifetime.

Recycling. Reprocessing plastics is an excellent way to recover value from a material after its intended lifetime. However, of the many different plastics that we use daily, only a small portion of them is recycled.[7] In contrast to the highly efficient process of aluminum recycling that recovers a high value product, plastic recycling faces many challenges. Recycling facilities typically do not collect low-value plastics as the cost to collect and sort for reprocessing comes at a far higher cost than obtaining the plastics from virgin feedstocks. The quality of the sorted plastic is impacted by the collection method. Many highly urban areas have turned towards single-stream collection, where all recyclables (glass, paper, plastic, aluminum, etc.) are comingled to be sorted at a processing facility, where the sorted plastic can have a variety of purities due to the imperfections in the sorting process. When plastic is recycled, it is likely to be downcycled (i.e. used to make materials that require lower quality materials). Downcycling is a result of contamination in the recycling stream or the degradation of the product, ultimately resulting in lower quality materials. Efficient recycling is heavily dependent on the infrastructure which varies widely across the world.

End-of-life. When plastics do not get recycled, the fate widely varies based on an individual's actions as well as local waste management infrastructure. Compostable plastics can be collected with organic waste to go to an industrial composting facility. However, industrial composting is not available everywhere. Some metro areas have garbage incineration facilities to burn waste and harvest energy. We can recover value from waste products through recycling, composting, and incineration. However, the waste infrastructure is not perfect, and the remaining products end up in a landfill or leaking into the environment.

Research efforts in degradable plastics have grown significantly to address the concerns of persistent plastics. *Degradable* is a vague descriptor to detail the decomposition of plastics, as most products can degrade under a specific set of conditions over long enough times. *Biodegradable* plastics are materials that can be completely broken down by naturally occurring microorganisms to form carbon dioxide, water, salts, and biomass with no other distinguishable or toxic residues.[8] Plastics such as polystyrene do not biodegrade after being buried in bioactive soil for 32 years.[9] Thin films of polyethylene begin to show evidence of biodegradation in bioactive soil, however, complete degradation does not occur within a realistic time frame.[10] *Compostable* plastics have a much more distinct definition, indicating plastics undergo biodegradation at a similar rate to other compostable materials (e.g., plant matter).[11] Therefore, plastics are compostable when they biodegrade under a specific set of composting conditions within a defined time frame as set by ASTM standards.[12]

The ideal sustainable future of plastics would be to address each of the areas above. Not only do we need to consider the impact of the resources used, we need to design materials for their intended lifetimes and consider the fate of the product after disposal. Plastics that are biobased, compostable, and affordable are the way forward. The work presented in this dissertation considers the many different facets of sustainability through the development of sustainable polymers for thermoplastic elastomers, tough plastics, and foams.

1.2 Polylactide

Natureworks LLC is the largest commercial producer of a sustainable polymer, PLA, priced at about $2.2 per kg. PLA is derived from biorenewable resources, is compostable and is used in food packaging, cold drink cups, and synthetic cushions.[13] Homopolymer PLA is a thermoplastic and can be processed at elevated temperatures using the variety of processing methods used industrially. Blending or copolymerizing PLA with other polymers produces materials with a broader range of applications. Specifically, incorporating PLA into block polymers with various architectures allows for a wide range of properties from hard plastics to soft rubbers.[14]

Lactide (LA, 3,6-dimethyl-1,4-dioxane-2,5-dione) is the cyclic dimer of lactic acid which is produced from the fermentation of corn, sugarcane, or tapioca.[15] Lactide is available as a racemic mixture, *rac*-lactide, and in three stereoisomers, (*S,S*)-lactide (LLA), (*R,R*)-lactide, and *meso*-lactide ((*R,S*)-lactide) (Figure 1.1). The thermal and mechanical properties of PLA are dictated by the tacticity and molar mass of the polymer, exhibiting a

glass transition temperature (T_g) between 45–60 °C.[14] Isotactic PLA, poly((*S*,*S*)-lactide) (PLLA) or poly((*R*,*R*)-lactide) (PDLA), exhibits a melting temperature up to 185 °C. Stereocomplexes of isotactic polymers PLLA+PDLA have the highest T_m between 220 and 230 °C.[15]

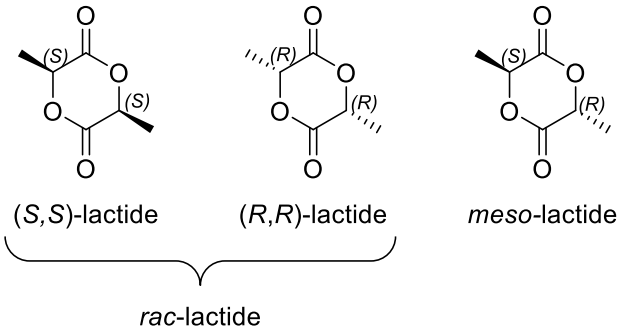

Figure 1.1.
The different stereoisomers of lactide.

PLA is susceptible to degradation through hydrolysis, depolymerization, transesterification, and random chain scission resulting in compounds ranging from monomers, cyclic oligomers, linear oligomers, and other small molecules.[16] PLA based materials can be industrially composted, chemically recycled to recover monomer, or conventionally recycled through thermal reprocessing. The thermal and mechanical properties of PLA are comparable to polystyrene, resulting in the widespread use of PLA-based materials as a sustainable alternative.

1.3 Polymerization of lactones

Polyesters like PLA can be obtained through the ring-opening transesterification polymerization (ROTEP) of lactones. Organometallic compounds, organocatalysts, or enzymes can be used to polymerize lactones with control over molar mass and architectures, with moderate dispersities ($Đ \leq 1.7$). ROTEP is superior compared to the condensation polymerization of the starting hydroxy acid, where molar masses are not well controlled, dispersities are broad, and high energy input is required.

Commercially, PLA and other polyesters are synthesized through the ROTEP of cyclic esters using tin(II) bis(2-ethylhexanoate) ($Sn(Oct)_2$) as the catalyst.[14] This catalyst is approved by the US FDA for use in food containers up to 1 wt%, leading to its widespread use and study.[17] The polymerization of lactones with $Sn(Oct)_2$ is understood to occur through a coordination-insertion mechanism.[18,19] In this mechanism, $Sn(Oct)_2$ first reacts with an alcohol species forming tin alkoxides prior reacting with a monomer. Since the catalyst can react with any alcohol in the system, polymerization results are dependent on the purity of the reagents; alcohol or water impurities act as co-initiators resulting in lower molar mass polymers. There are uncertainties about whether or not the octanoate group stays coordinated or leaves as the carboxylic acid.[19] Regardless, there is a consensus that the alkoxide bond between the alcohol and tin propagates the coordination-insertion mechanism.[18,20] This mechanism is consistent with the observation of residual tin that remains coordinated to the polymer even after extensive purification.[21,22]

Inter- and intramolecular transesterification reactions occur from the very beginning of the polymerization when using active ROTEP catalysts like $Sn(Oct)_2$. The

extent of transesterification increases with higher temperatures, longer reactions and higher concentrations of catalyst.[19,23] Intramolecular transesterification reactions result in shortened polymer chains and cyclic polymers while intermolecular transesterification reactions both lengthens and shortens chains (Scheme 1.1). These transesterification reactions have significant consequences as they broaden polymer dispersity and produce unwanted byproducts (e.g., cyclic polymers). Transesterification reactions facilitate randomization of the chain which are problematic when specific architectures are desired (e.g., block or star polymers).[24] Carbon (^{13}C) NMR spectroscopy can be used to detect the randomization of the chain.[25,26] Lowering the temperature of the polymerization to 120 °C and keeping the reaction time under 8 hours has been shown limit the degree of transesterification for $Sn(Oct)_2$ catalyzed polymerizations.[27]

Scheme 1.1.
a) Intermolecular and b) intramolecular transesterification reactions.

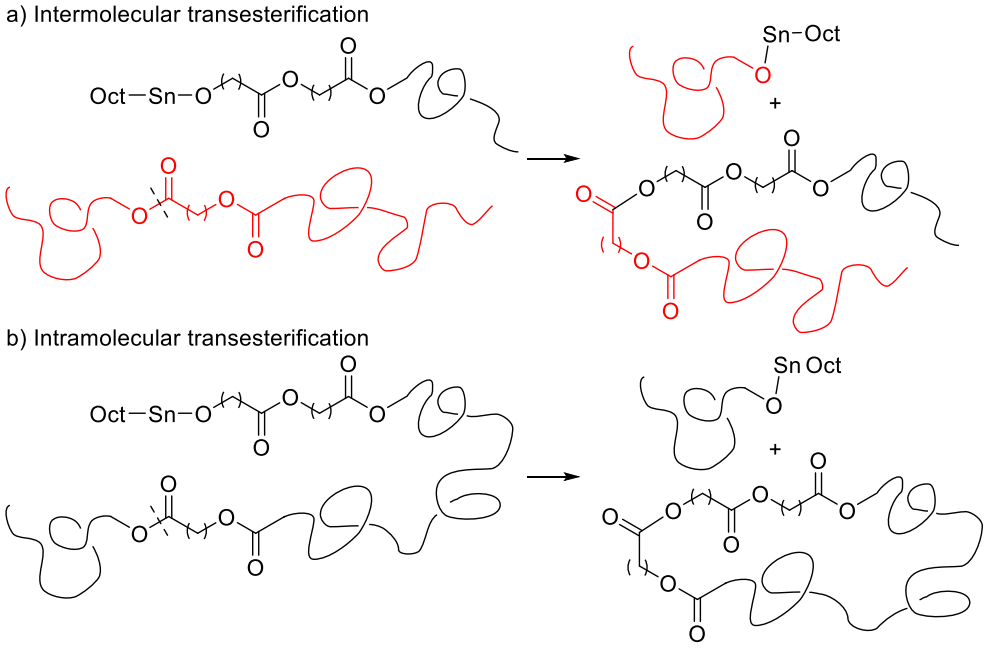

The thermodynamics of the polymerization of lactones of play an important role in forming high molar mass polymers. To preferentially form polymer, the Gibbs free energy of the system (ΔG_p) needs to be negative. This depends on the temperature (T), change in enthalpy (ΔH_p), and change in entropy (ΔS_p) of the system (1.1).

$$\Delta G_p = \Delta H_p - T\Delta S_p \tag{1.1}$$

For small and medium ring sizes (≤ 7-membered lactones), the polymerization is driven by the negative change in enthalpy due to the release of ring strain.[28] For larger lactones, the polymerization is driven by a positive change in entropy.[29] The thermodynamics of the polymerization of lactones can be monitored by the equilibrium monomer concentration ($[M]_{eq}$) using Equation 1.2, where the standard state monomer concentration ($[M]_{ss}$) is typically defined as being equal to 1.0.

$$\ln \frac{[M]_{eq}}{[M]_{ss}} = \frac{\Delta H_p^\circ}{RT} - \frac{\Delta S_p^\circ}{R} \tag{1.2}$$

This equilibrium between monomer and polymer is also dependent on temperature of the system. As the temperature increases, the rate of polymerization reaches a maximum value then declines to a rate of zero for an exothermic polymerization. The ceiling temperature (T_c) occurs where there is no polymer formation; equilibrium monomer concentration is equal to the initial monomer concentration.[30]

The equilibrium monomer concentration depends on the enthalpic contribution and the temperature of the system. Low ceiling temperatures mean that polymerizations must be carried out at low temperatures to get substantial conversion. For ease of synthesis of polymers, a high ceiling temperature is preferred. For rings with larger strain like β-

propiolactone the equilibrium lies towards forming polymer even at high temperatures (T_c > 1000 °C when $[M]_{eq}$ = 1 mol L^{-1}).[31] Substituted six-membered lactones have much lower ring strain than β-propiolactone, and polymerization only occurs closer to room temperature. LA is a substituted six-membered ring that can be polymerized at increased temperatures due to the planar configuration of the two ester groups, which increases the ring strain. The ceiling temperature is still low for LA (T_c = 290 °C when $[M]_{eq}$ = 1 mol L^{-1}) and the equilibrium monomer concentration increases with increasing temperature, 0.058 mol L^{-1} to 0.151 mol L^{-1} for 60 °C to 133 °C.[31] Although the low T_c of small rings necessitate the use of high concentration and/or low temperature during polymer synthesis, the reversibility of the reaction can be utilized to recover monomer through depolymerization.

The simple seven-membered lactone, ε-caprolactone (CL), has a much higher ceiling temperature, above 2000 °C when $[M]_{eq}$ = 1 mol L^{-1}, and the equilibrium concentration during polymerization at 130 °C is very low. A large focus in this body of work uses γ-methyl-ε-caprolactone (γMCL) (Chapter 3 and 4, Appendix A – C). The polymerization of γMCL results in a polymer that is amorphous, T_g = −60 °C.[32,33,34] The ceiling temperature of γMCL is expected to be high due to the ring strain in this seven-membered lactone, resulting in high conversion to polymer when using $Sn(Oct)_2$ at 130 °C.[35,36,37] Furthermore, efforts in our lab have demonstrated the enzyme-catalyzed hydrolysis of poly(γMCL) (PγMCL), a key step in biodegradation.[38]

Caprolactone derivatives are typically synthesized through the Baeyer-Villiger oxidation of a ketone precursor. Interestingly, when linear precursors for 7-membered

lactones undergo a ring-closing reaction, the 14-membered macrocycle and higher order oligomers are preferentially formed. Furthermore, there is a wide range of structural diversity that can be incorporated in the design of lactones in this manner. Thus, the polymerization of macrocycles through ROTEP can be utilized to yield a wide range of aliphatic polyester backbones. Macrolactone polymerizations are driven by entropic factors and the rate of polymerization is impacted by catalyst choice, concentration, and temperature. These factors are explored in the work shown in Chapter 2.

1.4 Thermoplastic elastomers

Block polymers are made up of homopolymers covalently linked together at a junction point. Based on compatibility, the blocks will either mix or microphase separate. The phase separation of incompatible blocks is constrained by the covalent linkage, forcing the polymers to adopt ordered, microphase separated structures that minimize the free energy of the system. The microphase separated structure, or morphology, is dictated by N, temperature, and the Flory-Huggins interaction parameter χ.[39] Changing these parameters, such as through heating or cooling, can change the segregation strength between the two blocks generating a disordered mix of A and B at low segregation strengths. The temperature at which this order-disorder transition occurs is designated T_{ODT}. Based on the relative volume fractions of the blocks in the polymers, the bulk material can form different morphologies (Figure 1.2). For an asymmetric system, the minority block (A) can microphase separate into spheres (S) or hexagonally packed

cylinders (C) in a matrix of the majority block. With an equivalent fraction of each block, the polymers form into a lamellar structure (L).

The architecture of the block polymers also affects properties, and this work will focus on ABA triblock copolymers where A and B represent polymers made of repeat units of A and B, respectively. A represents the glassy or semicrystalline block and B represents the soft and rubbery midblock. For an ABA triblock with a hard A minority fraction microphase separated from the soft B majority fraction, a physically crosslinked material results (Figure 1.3). Domains of A act as physical cross-links, similar to the chemical sulfur crosslinks in vulcanized rubbers, while being reversibly formed based on changes in temperature that affect the segregation strength. The hard end blocks connected by rubbery midblocks with trapped entanglements allow for the materials to have high strain at break (ε_B) and ultimate tensile strength (σ_B). These block polymers have both thermoplastic and elastomeric properties, making them thermoplastic elastomers (TPEs).

Figure 1.2.
Microphase separated morphologies of block polymers with two components.

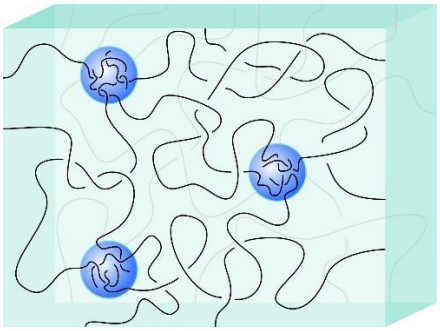

Figure 1.3.
Drawing of a physically crosslinked material, where the hard end blocks segregate from the rubbery midblocks connecting the domains. Loops that do not connect two domains do not contribute to the physical crosslinks.

TPEs can be processed with the same equipment that is used for thermoplastics and TPE waste can be reprocessed and reused like other thermoplastics.[42] TPEs are ideal for a broad range of applications such as coatings, pressure sensitive adhesives, medical devices, and automotive parts due to their tunable properties ranging from hard plastics to soft rubbers. The choice in identity and composition of the hard phase and soft phase contributes to the strength and stiffness, respectively, of the TPE.[40] Properties of TPEs are a result the system temperature lying between the T_g of the A and B blocks, giving a hard A block below its T_g and a rubbery B block above its T_g. For the desired rubber like behavior, the composition of A ranges from 15 – 40 wt% which allows A to form spheres or hexagonally packed cylinders in a matrix of B.[41]

A large fraction of commercially produced TPEs are non-degradable and use petroleum-based monomers. One example is styrenic TPEs, which are extensively used due to versatile properties and low cost.[42] For polystyrene-*block*-polybutadiene-*block*-polystyrene (S-B-S) with polystyrene (PS) in the minority component, the tensile strength

and elastic modulus at break of melt processed materials are comparable to vulcanized natural rubbers. S-B-S exhibits ultimate tensile strengths of 30 MPa, and 800% strain at break.[42]

When the molar mass between entanglements (M_e) increases, polymers with similar molar masses have a smaller number of entanglements, resulting in softer TPEs.[42] In the context of practical applications, PI has a larger M_e than PB, resulting in a softer polymer that is effective in adhesives. The lower M_e in PB-based TPEs result in tough materials used in footwear. Increasing the number of effective entanglements in the midblock of the block copolymer will improve physical properties when increasing the molar mass no longer improves properties.[42]

PLA has been utilized for the end blocks of sustainable TPE systems. Significant research efforts have been made towards finding a suitable polyester for the midblock in these sustainable ABA triblock polymers. However, previously studied systems lack a combination of improved mechanical properties and use of commercially relevant polymerization methods. These studies have revealed structure-property relationships of polyester TPEs that can be used to target new block polymer systems for optimal mechanical properties. In general, increasing overall molar mass and using semicrystalline PLA results in higher tensile strength in TPEs. The high ceiling temperatures of ε-caprolactone based monomers allow for more commercially relevant polymerization methods using $Sn(Oct)_2$ at elevated temperature, whereas the low ceiling temperature of substituted δ-valerolactones restricts the temperature used in polymerizations. Polymers of substituted ε-caprolactones also show good thermal stability.[36] Polyester-based triblock

copolymers with PLA end blocks are detailed in this section, with the tensile properties are summarized in Table 1.1.

Table 1.1.
Summary of tensile properties in various thermoplastic elastomers.

Polymer[a]	f[b]	E (MPa)	σ_B (MPa)	ε_B (%)	$\varepsilon_{residual}$ (%)
S-B-S[40] (10-52-10)	0.28	--	27.2	860	--
LA-MVL-LA[43] (16.8-70-16.8)	0.32	1.9 ± 0.6	9.0 ± 1.1	1790 ± 130	--
LLA-MVL-LLA[43] (18.6-70-18.6)	0.35	5.9 ± 0.9	28 ± 4	1720 ± 140	--
LA-M-LA[44] (7.8-29-7.8)	0.35	1.4 ± 0.3	1.7 ± 0.1	960 ± 60	30
LLA-M-LLA[45] (6.9-28-6.9)	0.34	1.5 ± 0.1	13.6 ± 1.4	900 ± 76	2.0
DLA-M-DLA[45] (6.8-28-6.8)	0.33	1.6 ± 0.3	12.6 ± 0.4	849 ± 40	2.1
LLA-M-LLA + DLA-M-DLA blend (1:1)[45]	0.34	5.6 ± 1.3	11.1 ± 0.5	754 ± 52	2.7
LA-6MCL-LA[35] (25-98-25)	0.34	31 ± 9	14.2 ± 1.9	1360 ± 120	4-6
LLA-TMC-LLA[46] (14-41-14)	0.41	62.2 ± 4.6	35.6 ± 5.0	593 ± 85	18
LLA-(DXO-co-TMC)-LLA[46]	0.40	65.6 ± 4.1	5.9 ± 0.4	1089 ± 140	16

[a] S = polystyrene; B = polybutadiene; LA = poly((±)-lactide); LLA = poly((+)-lactide); DLA = poly((−)-lactide); MVL = poly(β-methyl-δ-valerolactone); M = poly(menthide); 6MCL = poly(6-methyl caprolactone); TMC = poly(trimethylene carbonate); DXO = poly(1,5-dioxepan-2-one). [b] weight fraction of hard block: S, LA, LLA, or DLA.

Xiong et al. previously reported a completely renewable ABA triblock copolymer using the monomer β-methyl-δ-valerolactone (MVL).[43] This monomer was obtained through the dehydration and subsequent hydrogenation of the fermentation product mevalonate ((3*R*)-3,5-dihydroxy-3-methylpentanoic acid). Using both amorphous and semicrystalline PLA as the end blocks and poly(MVL) as the midblock, the triblock copolymer LLA-MVL-LLA demonstrated a high Young's modulus, ultimate tensile strength and strain at break (Table 1.1). These properties are comparable in strength while

exceeding strain at break compared to S-B-S. This polymer system, with high molar mass and PLA as the minority fraction, shows a renewable-resourced polymer that exceeds the tensile properties of a petroleum-based material. However, this monomer has a low ceiling temperature, which is not desirable. This means that at elevated temperatures, the equilibrium lies away from polymer formation and more towards the monomer, giving 91% conversion at 18 °C and only 60% conversion at 120 °C.[43]

The equilibrium concentration of monomer that persists at the end of the polymerization of MVL can affect the composition of the desired triblock copolymer. When the second monomer LA is added to PMVL, there is the potential for the residual MVL monomer to polymerize through the duration of the reaction, resulting in a gradient-like polymer. Although the conditions used in the study were ideal, analysis showed two distinct blocks with no evidence of a gradient, the low ceiling temperature adds complications to the use of PMVL precursors.

One way to avoid the issue of a low ceiling temperature is to use larger lactones, such as ε-caprolactones derivatives. Thermoplastic elastomers made with a polymenthide midblock and PLA end blocks (LA-M-LA) give a completely renewable and degradable aliphatic polyester. Menthide can be generated from (−)-menthol, a renewable, but expensive resource at $20 per kilogram.[44] Using amorphous PLA as the end blocks, a Young's modulus of 1.4 MPa, ultimate tensile strength of 1.7 MPa and strain at break of 960% was observed (Table 1.1).[44] Strain-stress behavior showed yielding that indicated a semicontinuous PLA phase in PM matrix. Subjecting samples to cycles of loading and unloading showed residual strains of 30%.[44] High residual strains indicate the TPE

undergoes permanent deformation under extension, undesirable for many TPE applications.

Although the triblock copolymers with PM are renewable and show high conversion using $Sn(Oct)_2$, the observed strengths are significantly lower than the styrenic based analogues and show high residual strain. This can be attributed to the M_e of the midblock being relatively high, between 11 and 14 kg mol^{-1}.[37] Large M_e indicates there is less contribution to the tensile strength from entanglements. This does not bode well for applications as strong TPEs, but when mixed with a renewable rosin tackifier, they showed attractive adhesion properties in pressure sensitive adhesives. [37]

Both LA-M-LA and LA-MVL-LA were compared to their semicrystalline analogues and showed significant improvements in ultimate tensile strength and no significant changes in strain at break (Table 1.1). By changing the end block from amorphous PLA to semicrystalline PLLA or PDLA, the properties of TPEs were enhanced as the physical interactions in the hard domains were strengthened. Blending PDLA and PLLA causes an increase tensile strength as the formation of stereocomplexes in the PLA domain results in a different microphase separated structure.[47] By blending LLA-M-LLA and DLA-M-DLA, the stereocomplexed PLA in the hard domains demonstrated higher Young's modulus and higher residual strain compared to the pure PLLA- or PDLA-based polymers.

Poly(6MCL) has also been explored as the elastomeric midblock in LA-6MCL-LA triblock copolymers.[35] 6MCL is synthesized from the Baeyer-Villiger (BV) oxidation of 2-methylcyclohexanone. Unlike the other monomers reviewed in this section, this monomer

is not renewably sourced. However, efforts were made in using a green oxidant, Oxone®, to synthesize the monomer (Scheme 1.2). The resulting triblock copolymers show excellent tensile properties that exceed the PM-based TPEs. A significant difference between LA-6MCL-LA and LA-M-LA is that the LA-6MCL-LA was synthesized with a 3-fold increase in molar mass. This higher molecular weight of the polymers resulted in mechanical properties that were significantly enhanced, even when using amorphous PLA.

Scheme 1.2.
BV oxidation of 2-methylcyclohexanone to yield 6MCL.[35]

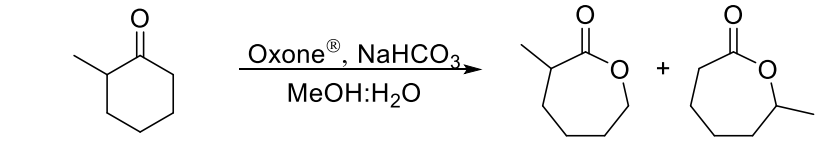

2-methylcyclohexanone

6-methyl-ε-caprolactone (6MCL)

As mentioned in Section 1.4 on TPEs, the ultimate tensile strength is improved by increasing the molecular weight of the hard block up to a critical point. The M_e of PLA has been reported as 8700 g/mol at 180 °C.[48] In the LA-M-LA (7.8-29-7.8) polymer, the molecular weight of the PLA segment is smaller than the entanglement molecular weight, leading to unentangled hard domains and weaker TPEs. In contrast, the LA-6MCL-LA polymers reported have PLA segments that are three times larger than the M_e resulting in an increase in tensile strength and strain at break. The increase in the entanglements in the P6MCL elastomer phase also contributes to the increase in tensile strength (M_e = 3.0 kg mol^{-1}).[49] Even though the properties were better for LA-P6MCL-LA than LA-M-LA, the ultimate tensile strength was still a factor of 2 smaller than the commercial S-B-S and has

more residual strain than other TPEs. Overall, the increase in molecular weight of the polymers, larger than M_e, improves tensile properties as it leads to more entanglements.

Andronova and Albertsson studied some other soft midblocks in triblock copolymers with PLLA end blocks.[46] The triblock copolymer with trimethylene carbonate (TMC), LLA-TMC-LLA, showed the highest tensile strength, exceeding the strength of S-B-S and LLA-MVL-LLA (Table 1.1). However, they show the lowest strain at break of all the polymers reported in Table 1.1. Polymerization of the mixture of TMC and 1,5-dioxepan-2-one (DXO) as the midblock resulted in triblock copolymers that had improved strain at break, but lower tensile strength. These polymers studied have small PLA end blocks, lower than the M_e, which likely contributed to their weaker tensile strengths.

The lactones discussed in this section demonstrate promising results for finding alternative plastics with similar properties to styrenic block polymers. Due to the aliphatic polyester backbone of these TPEs, they are likely to undergo biodegradation at faster rates than styrene-based derivatives. Some of these polymers that were generated from renewable resources would also address the feedstock concerns outlined in Section 1.1. However, there are still improvements that can be made in aliphatic polyester systems in their mechanical performance.

The lactone ring size as well as the position and size of the substituent impacts the thermodynamics and rate of polymerization, respectively. Both the tacticity and molecular weight of the polymers contribute to the mechanical properties. Using semicrystalline blocks resulted in increased tensile strengths, without compromising the other tensile properties. The increase in molar mass of the polymers controls the amount of

entanglements present, as well as the segregation strength between blocks. The increase in entanglements in both the hard phase and soft phase contributed to improved tensile properties.

1.5 Thesis Overview

Ultimately, the goal of this thesis is to make sustainable TPEs that have tensile properties that exceed those of commercial S-B-S polymers. Chapter 2 details the synthesis and polymerization of 14-membered cyclic esters to yield aliphatic polyesters. Chapter 3 covers the use of high molar mass polymers to yield strong and resilient aliphatic polyester TPEs. The impact of decreasing molar mass and the use of using hydrogen bonding end groups on stress relaxation and ultimate tensile properties is explored in Chapter 4. Chapter 5 details a polyolefin TPE system comparing triblock polymers and multiblock polymers derived from renewable feedstocks. Appendices A–C detail other work done on the PγMCL system beyond elastomeric materials: Appendix A expands on the impact of crystallinity on PLLA block polymers for tough plastics, Appendix B outlines preliminary results in utilizing PγMCL to make soft polyurethane foams, and Appendix C expands on the feedstock and environmental impacts of the synthesis of γMCL monomer.

1.6 References

(1) Garcia, J. M.; Robertson, M. L. The Future of Plastics Recycling. *Science* **2017**, *358*, 870–872.

(2) Albertsson, A.-C.; Hakkarainen, M. Designed to Degrade. *Science* **2017**, *358*, 872–873.

(3) Anastas, P.; Eghbali, N. Green Chemistry: Principles and Practice. *Chem. Soc. Rev.* **2010**, *39*, 301–312.

(4) Dubé, M. A.; Salehpour, S. Applying the Principles of Green Chemistry to Polymer Production Technology. *Macromol. React. Eng.* **2014**, *8*, 7–28.

(5) United States Department of Agriculture. USDA Biopreferred® program guidelines, June 2016; https://www.biopreferred.gov/BioPreferred/faces/pages/DocumentBrowser.xhtml (Accessed 24 October 2018).

(6) Gallezot, P. Conversion of Biomass to Selected Chemical Products. *Chem. Soc. Rev.* **2012**, *41*, 1538–1558.

(7) World Economic Forum, Ellen MacArthur Foundation and McKinsey & Company. *The New Plastics Economy: Rethinking the Future of Plastics*, 2016.

(8) Luckachan, G. E.; Pillai, C. K. S. Biodegradable Polymers- A Review on Recent Trends and Emerging Perspectives. *J. Polym. Environ.* **2011**, *19*, 637–676.

(9) Otake, Y.; Kobayashi, T.; Asabe, H.; Murakami, N.; Ono, K. Biodegradation of Low-Density Polyethylene, Polystyrene, Polyvinyl Chloride, and Urea Formaldehyde Resin Buried under Soil for over 32 Years. *J. Appl. Polym. Sci.* **1995**, *56*, 1789–1796.

(10) Roy, P. K.; Hakkarainen, M.; Varma, I. K.; Albertsson, A. C. Degradable Polyethylene: Fantasy or Reality. *Environ. Sci. Technol.* **2011**, *45*, 4217–4227.

(11) Breulmann, M.; Künkel, A.; Philipp, S.; Reimer, V.; Siegenthaler, K. O.; Skupin, G.; Yamamoto, M. Polymers, Biodegradable. *Ullmann's Encycl. Ind. Chem.* **2009**, 266.

(12) Kale, G.; Kijchavengkul, T.; Auras, R.; Rubino, M.; Selke, S. E.; Singh, S. P. Compostability of Bioplastic Packaging Materials: An Overview. *Macromol. Biosci.* **2007**, *7*, 255–277.

(13) Taskila, S.; Ojamo, H. The Current Status and Future Expectations in Industrial Production of Lactic Acid by Lactic Acid Bacteria. In *Lactic Acid Bacteria - R & D for Food, Health and Livestock Purposes*; Kongo, M., Ed.; InTech, 2013; pp. 615–632.

(14) *Poly(Lactic Acid): Synthesis, Structures, Properties, Processing, and Applications*; Auras, R. A.; Lim, L.-T.; Selke, S. E. M.; Tsuji, H., Eds.; John Wiley & Sons, Inc.: Hoboken, NJ, USA, 2010.

(15) Tsuji, H. Poly(Lactide) Stereocomplexes: Formation, Structure, Properties, Degradation, and Applications. *Macromol. Biosci.* **2005**, *5*, 569–597.

(16) Jamshidi, K.; Hyon, S.-H.; Ikada, Y. Thermal Characterization of Polylactides. *Polymer* **1988**, *29*, 2229–2234.

(17) US Food and Drug Administration. Title 21. PART 175 - Indirect Food Additives: Adhesives and Components of Coatings, 2014.

(18) Kowalski, A.; Duda, A.; Penczek, S. Kinetics and Mechanism of Cyclic Esters Polymerization Initiated with Tin(II) Octoate. 3. † Polymerization of L ,L -Dilactide. *Macromolecules* **2000**, *33*, 7359–7370.

(19) Dechy-Cabaret, O.; Martin-Vaca, B.; Bourissou, D. Controlled Ring-Opening Polymerization of Lactide and Glycolide. *Chem. Rev.* **2004**, *104*, 6147–6175.

(20) Storey, R. F.; Sherman, J. W. Kinetics and Mechanism of the Stannous Octoate-Catalyzed Bulk Polymerization of ε-Caprolactone. *Macromolecules* **2002**, *35*, 1504–1512.

(21) Kowalski, A.; Duda, A.; Penczek, S. Mechanism of Cyclic Ester Polymerization Initiated with Tin(II) Octoate. 2. Macromolecules Fitted with Tin(II) Alkoxide Species Observed Directly in MALDI−TOF Spectra. *Macromolecules* **2000**, *33*, 689–695.

(22) Stjerndahl, A.; Finne-Wistrand, A.; Albertsson, A.-C.; Bäckesjö, C. M.; Lindgren, U. Minimization of Residual Tin in the Controlled Sn(II)Octoate-Catalyzed Polymerization of ε-Caprolactone. *J. Biomed. Mater. Res. A* **2008**, *87*, 1086–1091.

(23) Albertsson, A.-C.; Varma, I. K. Recent Developments in Ring Opening Polymerization of Lactones for Biomedical Applications. *Biomacromolecules* **2003**, *4*, 1466–1486.

(24) Baimark, Y.; Molloy, R. Synthesis and Characterization of Poly (L-Lactide-Co-ε-Caprolactone) Copolymers: Effects of Stannous Octoate Initiator and Diethylene Glycol Coinitiator Concentrations. *Sci. Asia* **2004**, *30*, 327–334.

(25) Chabot, F.; Vert, M.; Chapelle, S.; Granger, P. Configurational Structures of Lactic Acid Stereocopolymers as Determined by 13C-{1H} N.M.R. *Polymer* **1983**, *24*, 53–59.

(26) Bero, M.; Kasperczyk, J.; Jedlinski, Z. J. Coordination Polymerization of Lactides, 1. Structure Determination of Obtained Polymers. *Die Makromol. Chemie* **1990**, *191*, 2287–2296.

(27) Kricheldorf, H. R.; Boettcher, C.; Tönnes, K.-U. Polylactones: 23. Polymerization of Racemic and Mesod,l-Lactide with Various Organotin Catalysts—stereochemical Aspects. *Polymer* **1992**, *33*, 2817–2824.

(28) Duda, A.; Kowalski, A.; Libiszowski, J.; Penczek, S. Thermodynamic and Kinetic Polymerizability of Cyclic Esters. *Macromol. Symp.* **2005**, *224*, 71–84.

(29) Duda, A.; Kowalski, A.; Penczek, S.; Uyama, H.; Kobayashi, S. Kinetics of the Ring-Opening Polymerization of 6-, 7-, 9-, 12-, 13-, 16-, and 17-Membered Lactones. Comparison of Chemical and Enzymatic Polymerizations. *Macromolecules* **2002**, *35*, 4266–4270.

(30) Dainton, F. S.; Ivin, K. J. Reversibility of the Propagation Reaction in Polymerization Processes and Its Manifestation in the Phenomenon of a ‘Ceiling Temperature.’ *Nature* **1948**, *162*, 705–707.

(31) Save, M.; Schappacher, M.; Soum, A. Controlled Ring-Opening Polymerization of Lactones and Lactides Initiated by Lanthanum Isopropoxide, 1. General Aspects and Kinetics. *Macromol. Chem. Phys.* **2002**, *203*, 889–899.

(32) Seefried, C. G.; Koleske, J. V. Lactone Polymers. VI. Glass-Transition Temperatures of Methyl-Substituted ε-Caprolactones and Polymer Blends. *J. Polym. Sci. Polym. Phys. Ed.* **1975**, *13*, 851–856.

(33) Trollsås, M.; Kelly, M. a.; Claesson, H.; Siemens, R.; Hedrick, J. L. Highly Branched Block Copolymers: Design, Synthesis, and Morphology. *Macromolecules* **1999**, *32*, 4917–4924.

(34) Zupancich, J. A.; Bates, F. S.; Hillmyer, M. A. Aqueous Dispersions of Poly(Ethylene Oxide)- b -Poly(γ-Methyl-ε-Caprolactone) Block Copolymers. *Macromolecules* **2006**, *39*, 4286–4288.

(35) Martello, M. T.; Hillmyer, M. A. Polylactide-Poly(6-Methyl-ε-Caprolactone)-Polylactide Thermoplastic Elastomers. *Macromolecules* **2011**, *44*, 8537–8545.

(36) Olsén, P.; Borke, T.; Odelius, K.; Albertsson, A.-C. ε-Decalactone: A Thermoresilient and Toughening Comonomer to Poly(L-Lactide). *Biomacromolecules* **2013**, *14*, 2883–2890.

(37) Shin, J.; Martello, M. T.; Shrestha, M.; Wissinger, J. E.; Tolman, W. B.; Hillmyer, M. A. Pressure-Sensitive Adhesives from Renewable Triblock Copolymers. *Macromolecules* **2011**, *44*, 87–94.

(38) De Hoe, G. X.; Zumstein, M. T.; Tiegs, B. J.; Brutman, J. P.; McNeill, K.; Sander, M.; Coates, G. W.; Hillmyer, M. A. Sustainable Polyester Elastomers from Lactones: Synthesis, Properties, and Enzymatic Hydrolyzability. *J. Am. Chem. Soc.* **2018**, *140*, 963–973.

(39) Bates, F. S.; Fredrickson, G. H. Block Copolymer Thermodynamics: Theory and Experiment. *Annu. Rev. Phys. Chem.* **1990**, *41*, 525–557.

(40) Holden, G.; Bishop, E. T.; Legge, N. R. Thermoplastic Elastomers. *J. Polym. Sci. Part C Polym. Symp.* **1969**, *26*, 37–57.

(41) *Handbook of Elastomers*; Bhowmick, A. K.; Stephens, H. L., Eds.; 2nd ed.; Mercel Dekker, Inc.: New York, 2001.

(42) *Thermoplastic Elastomers*; Holden, G.; Kricheldorf, H. R.; Quirk, R. P., Eds.; 3rd ed.; Hanser Gardner Publications, Inc.: Cincinnati, 2004.

(43) Xiong, M.; Schneiderman, D. K.; Bates, F. S.; Hillmyer, M. A.; Zhang, K. Scalable Production of Mechanically Tunable Block Polymers from Sugar. *Proc. Natl. Acad. Sci.* **2014**, *111*, 8357–8362.

(44) Wanamaker, C. L.; O'Leary, L. E.; Lynd, N. A.; Hillmyer, M. A.; Tolman, W. B.

Renewable-Resource Thermoplastic Elastomers Based on Polylactide and Polymenthide. *Biomacromolecules* **2007**, *8*, 3634–3640.

(45) Wanamaker, C. L.; Bluemle, M. J.; Pitet, L. M.; O'Leary, L. E.; Tolman, W. B.; Hillmyer, M. A. Consequences of Polylactide Stereochemistry on the Properties of Polylactide-Polymenthide-Polylactide Thermoplastic Elastomers. *Biomacromolecules* **2009**, *10*, 2904–2911.

(46) Andronova, N.; Albertsson, A.-C. Resilient Bioresorbable Copolymers Based on Trimethylene Carbonate, L-Lactide, and 1,5-Dioxepan-2-One. *Biomacromolecules* **2006**, *7*, 1489–1495.

(47) Tsuji, H.; Ikada, Y. Stereocomplex Formation between Enantiomeric Poly(Lactic Acid)s. XI. Mechanical Properties and Morphology of Solution-Cast Films. *Polymer* **1999**, *40*, 6699–6708.

(48) Dorgan, J. R.; Williams, J. S.; Lewis, D. N. Melt Rheology of Poly(Lactic Acid): Entanglement and Chain Architecture Effects. *J. Rheol.* **1999**, *43*, 1141.

(49) Schneiderman, D. K.; Hill, E. M.; Martello, M. T.; Hillmyer, M. A. Poly(Lactide)-Block- Poly (ε- Caprolactone- co -ε- Decalactone)- Block- Poly(Lactide) Copolymer Elastomers. *Polym. Chem.* **2015**, *6*, 3641–3651.

Chapter 2.

Entropically-driven macrolide polymerizations for the synthesis of copolymers using titanium isopropoxide [†]

[†] Reproduced in part with permission from Amador, A.; Watts, A.; Neitzel, A.; Hillmyer, M. A. Entropically-driven macrolide polymerizations for the synthesis of aliphatic polyester copolymers using titanium isopropoxide. Submitted for publication to Macromolecules. Unpublished work copyright 2019 American Chemical Society.

2.1 Introduction

Although plastics have provided significant improvements in our daily lives, there has been recent awareness of the significant sustainability and waste-management problems associated with single-use plastics.[1] Due to these challenges, renewable and biodegradable plastics such as aliphatic polyesters have attracted substantial research efforts to compete with petroleum-derived polymers.[2,3] For example, polylactide (PLA) is a commercially available aliphatic polyester that is renewable, biocompatible, and biodegradable.[4,5] Moreover, the properties of PLA can be modulated for a wide variety of applications through the synthesis of aliphatic polyester copolymers, e.g., poly(lactide-*co*-glycolide) (PLGA).[4]

Aliphatic polyester copolymers are typically synthesized through condensation polymerization or ring-opening transesterification (co)polymerization (ROTEP). Using a wide range of metallic, enzymatic, and organic catalysts in ROTEP provides control over polymer architecture, producing polymers with moderate dispersities and high molar masses.[6–9] The reactivity ratios between comonomers in ROTEP can impact the polymer structure (e.g., random, alternating, gradient, block),[10–15] and the use of highly active catalysts often promotes inter- and intramolecular transesterification, resulting in polymers with broad dispersities and reduced control over monomer sequence.[14,16] One well-studied example is the copolymerization of lactide and glycolide to yield PLGA.[17] Catalyst activity and selectivity impact the polymer composition, architecture, tacticity, and sequence of repeat units, ultimately impacting on the thermal, mechanical, and degradation properties of PLGA.[17,18]

In contrast to the polymerization of two separate lactone monomers to target polyester copolymers, an alternate strategy is to incorporate two different monomer fragments into a single monomer. Such cyclic esters can be polymerized using ROTEP to yield perfectly alternating copolymers, a notable example being the polymerization of 3-methylglycolide to yield poly(LA-*alt*-GA).[19] We aimed to expand the scope of available polyester copolymers through the synthesis and polymerization of heterocycles composed of two distinct monomer units.

We hypothesized that condensation of lactic acid (LA) and 3-hydroxypropionic acid (3HP) into a single cyclic diester would provide a suitable precursor to perfectly alternating poly(LA-*alt*-3HP) (Scheme 2.1a). P3HP is a semicrystalline polyester (T_m = 76 °C, T_g = −22 °C) and high molar mass samples exhibit high tensile strength and rigidity.[20,21] The thermal and mechanical properties of P3HP can be modulated through the synthesis of copolymers of 3HP with other hydroxyalkanoates (i.e. 3-hydroxybutyric acid, 3-hydroxyhexanoic acid, etc.), mainly produced through biofermentation.[22] Similarly, the poly(ether ester) poly(GA-*alt*-2MD) could be constructed from condensation of glycolic acid (GA) with 2-methyl-1,3-propanediol (2MD) (Scheme 2.1b).[23,24] Similar poly(ether esters) from 1,4-dioxepan-2-one and *p*-dioxanone are biocompatible and biodegradable, making them suitable for biomedical applications (e.g., degradable sutures).[25,26] However, further exploration into other poly(ether ester) structures are limited. The synthesis of heterocycles that incorporate multiple moieties is an underutilized approach to yield these desirable copolyesters and poly(ether ester)s.

Scheme 2.1.
Retrosynthesis of a) poly[(lactic acid)-*alt*-(3-hydroxypropionic acid)] and b) poly[(glycolic acid)-*alt*-(2-methyl-1,3-propanediol)].

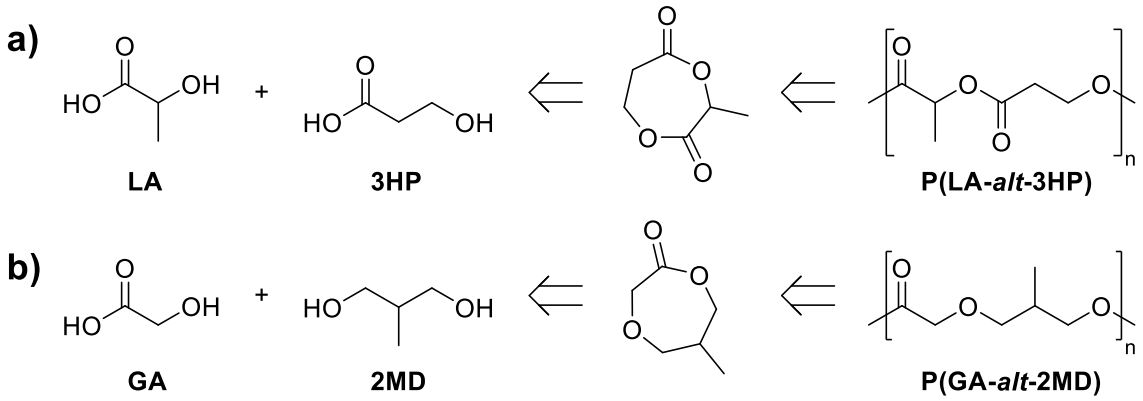

In this work, we report the controlled synthesis of P(LA-*stat*-3HP) and P(GA-*alt*-2MD) through entropically-driven ROTEP of two unprecedented cyclic monomers. Abundant and commodity chemicals were used to synthesize unstrained macrolides (≥ 12-membered lactones). These studies resulted in the discovery of Ti(O*i*-Pr)$_4$ as an inexpensive and highly efficient ROTEP catalyst for the polymerization of unstrained lactones: 14-membered macrolides, higher order cyclic oligomers (≥ 21-membered rings), and commercially-available ω-pentadecalactone. We further explore the impact of catalyst choice on the regioregularity in P(LA-*co*-3HP) as the thermal properties are highly dependent on the tacticity and regioregularity of this copolymer.

2.2 Results and discussion

The copolymer of LA and 3HP is of interest as the respective homopolymers are semicrystalline and the starting materials can be sourced from annually renewable feedstocks.[27] An isotactic, perfectly alternating copolymer P(LA-*alt*-3HP) was synthesized through a condensation polymerization using *N*,*N*-dimethylaminopyridinium *p*-toluenesulfonate (DPTS) and *N*,*N*-diisopropylcarbodiimide (DIC) (Scheme 2.2). This resulted in a brittle, semicrystalline polymer (T_g = 4 °C and T_m = 96 °C, Figure 2.1) with low molar mass (M_n = 2.6 kg mol^{-1}). High molar mass variants are expected to have higher T_g and T_m with improved mechanical properties. Due to the limitations of condensation polymerization, we set out to efficiently access this polymer with high molar mass through the ROTEP of a cyclic monomer that can be derived from LA and 3HP.

Scheme 2.2.
Synthesis of P(LA-*alt*-3HP) through condensation polymerization.

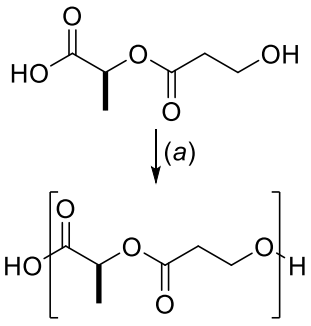

Conditions: (*a*) 20% DPTS, DIC (1.2 eq), CH_2Cl_2

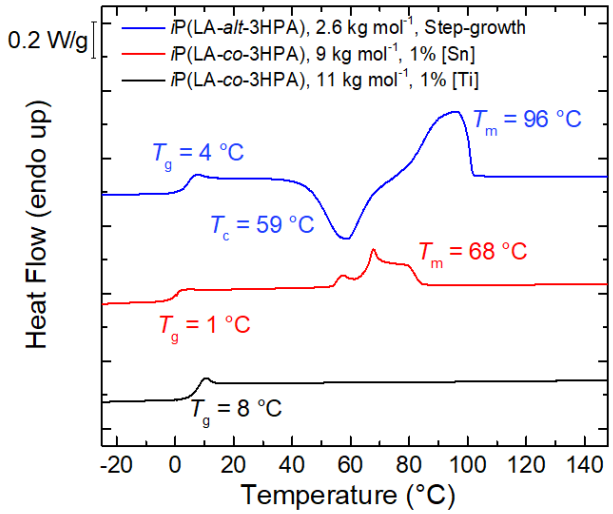

Figure 2.1.
DSC analysis of isotactic poly[((*S*)-lactic acid)-*co*-(3-hydroxypropionic acid)] synthesized using step-growth polymerization and ROTEP. The second heat cycle is reported for the step-growth polymer (blue) and titanium isopropoxide catalyzed polymer (black), heating at 10 °C min^{-1}. The $Sn(Oct)_2$ catalyzed polymerization did not exhibit a melting endotherm during the second heat, therefore the heat cycle after annealing the polymer at room temperature is reported.

Monomer Synthesis

Starting with abundant and commodity chemicals to synthesize the proposed 7-membered cyclic compounds (Scheme 2.1), dilute ring-closing reactions were used which resulted in the synthesis of higher order oligomers (dimers, trimers, etc.). The 14-membered cyclic tetraester (n = 1, **dLA-3HP**) and higher order oligomers (n ≥ 2, **nLA-3HP**) were formed through the cyclization of the linear precursor **3** under basic conditions, with no evidence of the formation of the 7-membered ring, 3-methyl-1,4-dioxepane-2,5-dione (**LA-3HP**) (Scheme 2.3). A *t*-butyl protected 3HP precursor **1** was readily synthesized *via* the conjugate addition between benzyl alcohol and *t*-butyl acrylate followed by hydrogenation. The resulting alcohol was acylated using the methyl-sulfonyl

ester of 2-hydroxypropanoyl chloride (***rac*-2** or **(*S*)-2**) and subsequently deprotected using trifluoroacetic acid to provide the linear precursor **3**. We observed high yields of a mixture of the dimer (n = 1, **dLA-3HP**) and higher order cyclic oligomers (n ≥ 2, **nLA-3HP**) (Figure 2.2). Using **(*S*)-2** provided access to enantiopure **(*R*,*R*)-dLA-3HP** (>99% *ee*, see experimental section). The isolated 14-membered diastereomers ***rac*-dLA-3HP** and ***meso*-dLA-3HP** were characterized by X-ray crystallography (Scheme 2.3, see Supplementary Information).

Scheme 2.3.
Synthesis of 14-membered cyclic tetraester (**dLA-3HP**) and higher order oligomers (**nLA-3HP**).

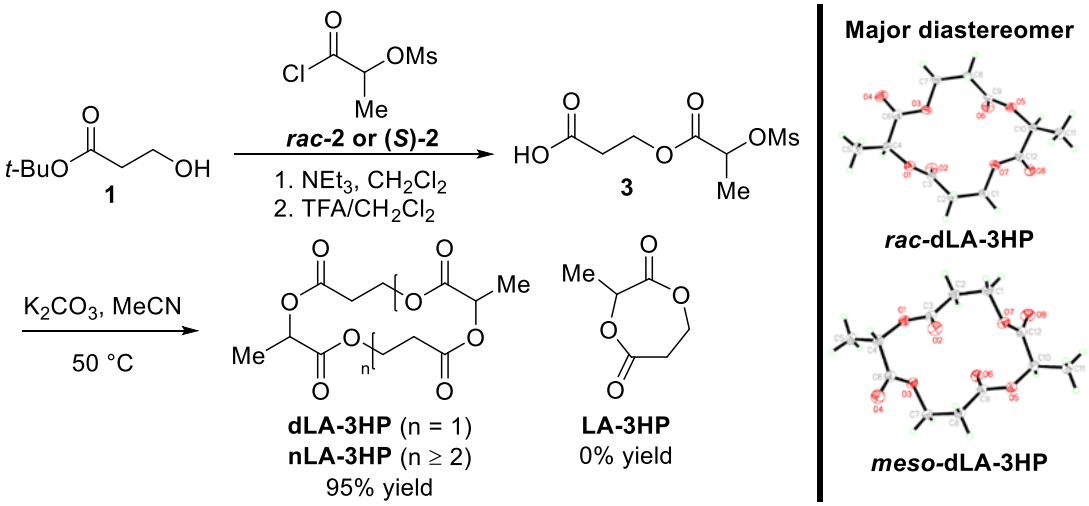

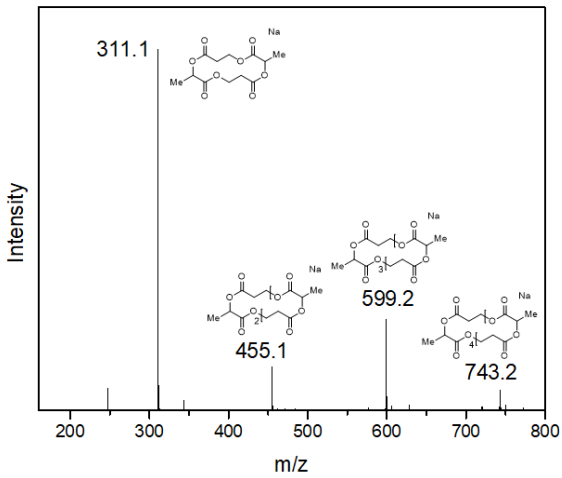

Figure 2.2.
ESI-MS results of a sample of dLA-3HP with higher order oligomers (n ≥ 2, nLA-3HP).

Similarly, the 14-membered cyclic diester (**dGA-2MD**) was formed with no evidence of the 7-membered lactone **GA-2MD** after cyclization of the hydroxy acid precursor **4** (Scheme 2.4). Reaction of sodiated 2-methyl-1,3-propanediol with sodium chloroacetate provided **4** after acidification, albeit in low yields (10%). Hydroxy acid **4** was then cyclized in the presence of catalytic tosylic acid and 4 Å molecular sieves providing **dGA-2MD** and the 21-membered cyclic triester (**tGA-2MD**) confirmed by high-resolution mass spectrometry and gas chromatography (Figure 2.4 and 2.5). The *meso*-compound was isolated through recrystallization and was characterized using X-ray crystallography (Scheme 2.4).

Scheme 2.4.
Synthesis of 14-membered cyclic diester (**dGA-2MD**) and 21-membered cyclic triester (**tGA-2MD**).

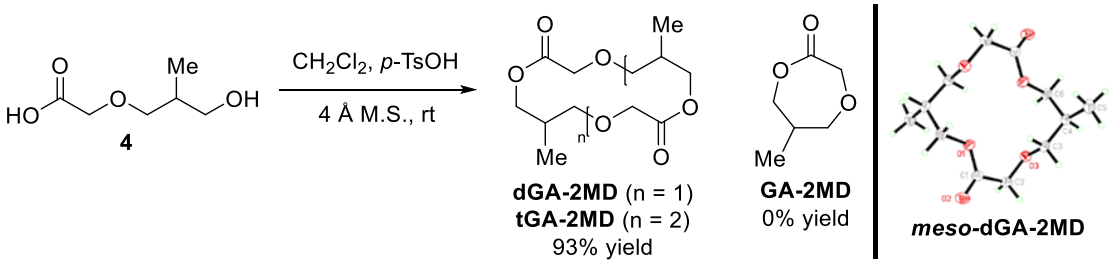

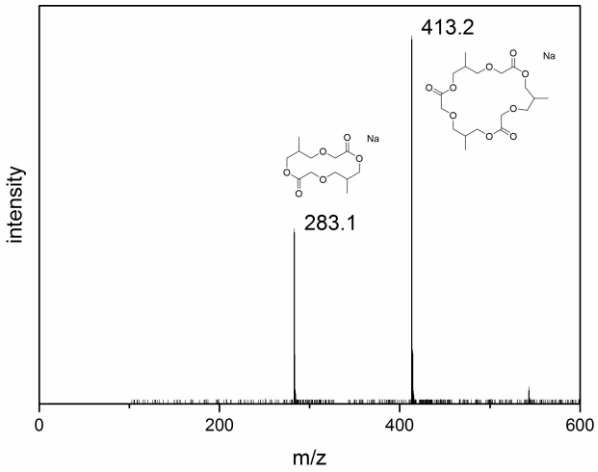

Figure 2.3.
ESI-MS results of a mixture of dGA-2MD and tGA-2MD.

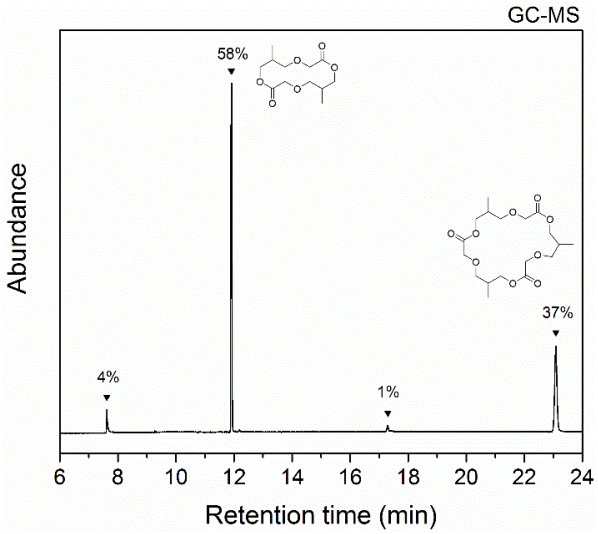

Figure 2.4.
Gas chromatograph of the mixture of dGA-2MD and tGA-2MD.

Using commercially available starting materials, we synthesized and isolated two 14-membered macrolides, **dLA-3HP** and **dGA-2MD**. Similar to other ring-closing reactions to form lactones, formation of 14-membered heterocycles and higher order cyclic oligomers dominated.[28,29] The 14-membered ring structures accommodate the *cis*-ester conformation with bond angles close to unstrained acyclic esters (Scheme 2.3 and 2.4).[30–32] These stable ester conformations and undistorted bond angles suggest that the ring-opening polymerizations will not be driven by relief of ring strain.

Polymer Synthesis

A variety of catalysts have been reported to be effective in the entropically-driven polymerization of macrolides.[33–41] First, we explored the use of 1,5,7-triazabicyclo[4.4.0]dec-5-ene (TBD) since it was the most active organocatalyst in the polymerization of ω-pentadecalactone (PDL), reaching high conversions at > 100 °C in days.[42] TBD was effective for the polymerization of **dGA-2MD** under similar reaction conditions, requiring long reaction times at elevated temperatures to achieve high conversions (Table 2.1). When used in the polymerization of ***rac*-dLA-3HP**, TBD provided minimal polymer formation at room temperature (Table 2.1). In the presence of TBD above 100 °C, the base-catalyzed E1cB elimination reaction in ***rac*-dLA-3HP** resulted in the formation of acrylate end groups as observed by ^{1}H NMR spectroscopy. (Figure 2.5). This elimination reaction is well precedented for β-acetoxy carbonyl compounds and results in decomposition of the monomer and likely fragmentation of the corresponding polymers.[43] A similar elimination reaction has been described in the

pyrolysis of P3HP to produce acrylic acid.[44] Due to these side reactions as well as the long reaction times required in TBD catalyzed polymerization of macrolides, other catalysts were explored.

Table 2.1.
Polymerization of macrolactones using TBD and Ti(O*i*-Pr)$_4$.

Monomer	Catalyst /initiator	$[M]_0/[I]_0$	$[M]_0$	Time	Conversion[a]	Yield[b]	M_n[c] (kg mol^{-1})	$Đ$[c]
dLA-3HP	Ti(O*i*-Pr)$_4$	100	3 M	24 h	98%	96%	12	1.7
dLA-3HP	TBD/BnOH	100	3 M	24 h	100%	0%		
dGA-2MD	Ti(O*i*-Pr)$_4$	400	3 M	30 min	94%	90%	31	1.7
dGA-2MD	TBD/BDM	80[d]	3 M	24 h	93%	90%	30[e]	1.7
ω-PDL	Ti(O*i*-Pr)$_4$	200	2 M	45 min	93%	90%	27[e]	1.7
ω-PDL	TBD/BnOH	200	Bulk	96 h	99%	NR	24	1.5

[a]Determined by ^{1}H NMR spectroscopy. [b]Isolated yield after precipitation into methanol. [c]Determined by THF SEC equipped with MALLS detector. [d]Using 1.25% TBD as catalyst and BnOH or BDM as initiator. [e]M_n determined by end-group analysis using ^{1}H NMR spectroscopy. NR = not reported

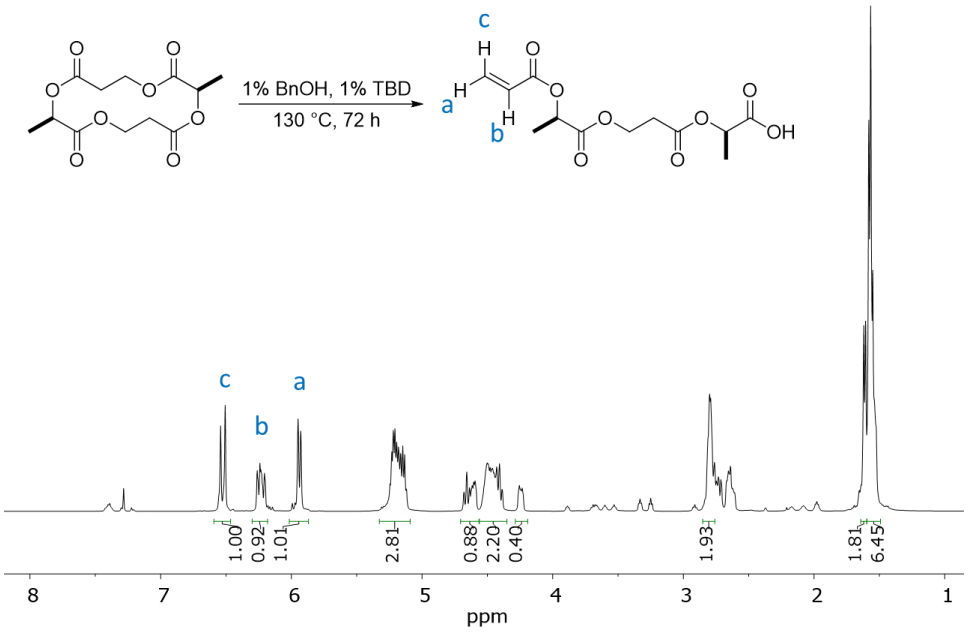

Figure 2.5.
Evidence for E1cB elimination using TBD as catalyst. New olefinic resonances consistent with acrylate byproducts can be seen in the ^{1}H NMR spectrum of the crude product, one possible product is shown in the scheme.

Lipases such as Novozyme 435 are well documented for entropically-driven polymerizations were also effective, though the conversion of ***rac*-dLA-3HP** did not proceed beyond 60%.[45–50] Coordination-insertion catalysts such as $Sn(Oct)_2$ and highly activated alkyl-zinc catalysts polymerized ***rac*-dLA-3HP**, albeit with low conversions and poor control over molar mass (Table 2.2).[28,51,52] Titanium isopropoxide Ti(O*i*-Pr)$_4$ proved to be a superior catalyst for the bulk polymerization of ***rac*-dLA-3HP** providing 98% conversion at 115 °C within 20 min (Table 2.2). This catalyst was also effective for the polymerization of macrolides **dGA-2MD** and PDL, all achieving high conversions within 1 h at 100 °C (Table 2.1). Titanium alkoxides are well-known catalysts for polycondensations and their use for the ring-opening polymerization of strained lactones have been extensively described.[53–57] However, we believe that Ti(O*i*-Pr)$_4$ has not been previously explored for polymerizations of macrolides.

Table 2.2.
Polymerization conditions for *rac*-dLA-3HP

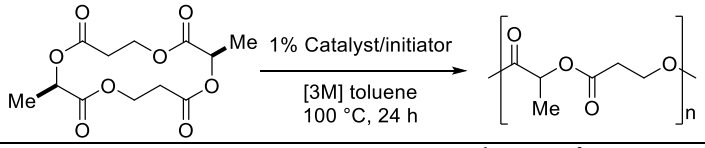

Catalyst/initiator	Conversion	Yield[a]	M_n (kDa)[b]	$Đ$[b]	T_g (°C)	T_m (°C)
TBD/BnOH	50%	0%				
TBD/BnOH[c]	0%					
$Sn(Oct)_2$/BnOH[d]	35%	30%	9.7	1.5	1	68
LZnEt/BnOH	65%	62%	9.6	1.4	ND	
Novozyme 435/BnOH[e]	55%	52%	3.8	1.2	ND	
Y(O*i*-Pr)$_3$	<5%	trace	ND	ND		
Ti(O*i*-Pr)$_4$	95%	92%	11	1.5	8	
Ti(O*i*-Pr)$_4$[f]	98%	96%	12	1.5	7	

[a]Determined by ^{1}H NMR spectroscopy using phenanthrene as internal standard. [b]Estimated by $CHCl_3$ SEC vs. polystyrene standards. [c]Reaction carried out at room temperature for 72 h. [d]Reaction carried out neat for 48 h at 120 °C. [e]10 wt% of Novozyme 435. [f]Reaction carried out neat for 20 minutes at 115 °C. ND = not detected.

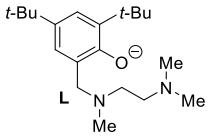

The impact of Ti(O*i*-Pr)$_4$ loading on the polymerization of ***rac*-dLA-3HP** and **dGA-2MD** is shown in Tables 2.3 and 2.4, respectively. Bulk polymerizations were carried out at elevated temperatures, above the melting point of monomer (**(*R,R*)-dLA-3HP** T_m = 130 °C, ***rac*-dLA-3HP** T_m = 110 °C, and **dGA-2MD** T_m = 86 °C), while polymerizations in toluene were carried out at 100 °C. Polymerization of **(*R,R*)-dLA-3HP** in the bulk > 130 °C resulted in significant yellow discoloration and decreased conversions, therefore only the solution polymerization of **(*R,R*)-dLA-3HP** is reported (Table 2.3). At the same monomer-to-catalysts loading $[M]_0/[Ti(O\textit{i}\text{-}Pr)_4]_0$ = 400, ***rac*-dLA-3HP** polymerization reaches similar conversions at 2 h in the bulk (115 °C) and 48 h in 3M toluene (100 °C). Polymerizations of **dGA-2MD** ($[M]_0/[Ti(O\textit{i}\text{-}Pr)_4]_0$ = 400) performed at the same temperature (100 °C) exhibit similar conversions at similar reaction times, 25 min in the bulk and 30 min in 3M toluene. The main difference between the bulk and solution polymerization is the observed molar mass of the product polymer (46 kg mol^{-1} and 31 kg mol^{-1}, respectively).

A wide range of molar masses are accessible with Ti(O*i*-Pr)$_4$; lower catalyst loading results in higher molar mass (Table 2.3 and 2.4). Titanium alkoxide catalysts are believed to initiate and catalyze polymerization of lactones through a coordination-insertion mechanism.[58] There is an upper limit in the monomer-to-catalyst ratio ($[M]_0/[Ti(O\textit{i}\text{-}Pr)_4]_0$ = 2000) as this concentration of catalyst results in a significant decrease in conversion and therefore lower molar mass compared to the other feed ratios. This is likely due to catalyst deactivation by minor impurities; at such low catalyst loadings any termination events will

Table 2.3.
Polymerization of dLA-3HP using Ti(O*i*-Pr)$_4$ with varying catalyst concentration

$[M]_0/[Ti(O\textit{i}\text{-}Pr)_4]_0$	$[M]_0$[a]	Time	Conversion[b]	Yield[c]	M_n[d] (kg/mol)	*N sites*/Ti[e]	$Đ$[d]	T_g[f] (°C)
25	5 M	10 min	98%	96%	2.9	2.4	1.8	
50	5 M	10 min	98%	95%	5.1	2.8	1.6	
100	5 M	20 min	98%	96%	12	2.4	1.5	7
200	5 M	30 min	88%	85%	19	2.7	1.4	
400	5 M	2 h	75%	73%	36	2.4	1.5	13
1000	5 M	7 d	54%	45%	51	3.0	1.5	9
2000	5 M	3 d	<10%	<10%	22[g]	2.6	1.3	
100	3 M	1.5 h	95%	92%	11	2.5	1.5	8
100[h]	3 M	1.5 h	95%	91%	11	2.5	1.5	9
400	3 M	48 h	84%	75%	36	2.7	1.4	13
400	3 M	48 h	85%	76%	35	2.8	1.4	13

Polymerizations were carried out at 115 °C in the bulk (5 M) and 100 °C in toluene solution (3 M). [a]Initial monomer concentration calculated from monomer density for bulk (5 M) and solution (3 M) polymerizations. [b]Determined by ^{1}H NMR spectroscopy. [c]Isolated yield after precipitation into methanol. [d]Determined by THF SEC equipped with MALLS detector, *dn/dc*=0.051. [e]Number of active sites per titanium center (*N sites*/Ti) calculated by ($[M]_0/[Ti(O\textit{i}\text{-}Pr)_4]_0$ × conversion × $MW_{monomer}$)/M_n. [f]Determined from the second heat cycle by DSC, heating at 10 °C min^{-1}. [g]Determined by $CHCl_3$ SEC using polystyrene standards.[h]Polymerization with (*R,R*)-dLA-3HP.

Table 2.4.
Polymerization of dGA-2MD using Ti(O*i*-Pr)$_4$ with varying catalyst concentration

$[M]_0/[Ti(O\textit{i}\text{-}Pr)_4]_0$	$[M]_0$	Time	Conversion[a]	Yield[b]	M_n[c] (kg/mol)	*N sites*/Ti[d]	$Đ$[c]	T_g[e] (°C)
50	Bulk	5 min	93%	87%	9.0	1.3	1.3	−32
100	Bulk	5 min	88%	71%	14	1.6	1.3	
400	Bulk	25 min	94%	91%	46	2.1	1.5	−30
1000	Bulk	90 min	80%	77%	70	3.0	1.7	−32
2000	Bulk	24 h	13%	12%	27	2.5	1.7	
100	3 M	5 min	94%	92%	7.8	3.1	1.6	
200	3 M	10 min	94%	91%	16	3.1	1.6	
400	3 M	30 min	93%	90%	31	3.1	1.7	

Polymerizations were carried out at 100 °C. [a]Determined by ^{1}H NMR spectroscopy. [b]Isolated yield after precipitation. [c]Determined by THF SEC equipped with MALLS detector, *dn/dc* = 0.062. [d]Number of active sites per titanium center (*N sites*/Ti) calculated by ($[M]_0/[Ti(O\textit{i}\text{-}Pr)_4]_0$ × conversion × $MW_{monomer}$)/M_n. [e]Determined from the second heat cycle by DSC, heating at 10 °C min^{-1}.

significantly reduce the concentration of active catalyst. As evidenced by ^{1}H NMR spectroscopy, the presence of a peak for isopropyl ester indicates the polymerization is initiated by insertion of the isopropyl group (Figure 2.6). End-group analysis from polymerization of **dGA-2MD** ($[M]_0/[Ti(O\textit{i}\text{-}Pr)_4]_0$ = 100) gives an estimate for M_n = 7.2 kg

mol^{-1}, yet SEC-MALLS indicates the molar mass is nearly twice that value, M_n = 14 kg mol^{-1}. The higher molar mass sample from polymerization of **dGA-2MD** ($[M]_0/[Ti(O\textit{i}\text{-}Pr)_4]_0$ = 1000) is in better agreement between the two characterization methods, M_n (^{1}H NMR) = 60 kg mol^{-1} and M_n (SEC) = 70 kg mol^{-1}. The inconsistency in the M_n for the low molar mass sample is likely a result of the increased error in molar mass determination by SEC-MALLS at low molar mass. Based on the molar masses determined by SEC-MALLS, the number of active sites per catalyst ranges from 1–3. Assuming all polymer chains have one isopropoxy end group, the molar masses obtained via SEC-MALLS indicate ~2–3 isopropoxide groups initiate polymerization of **dLA-3HP** and ~1–3 isopropoxide groups initiate polymerization of **dGA-2MD**.

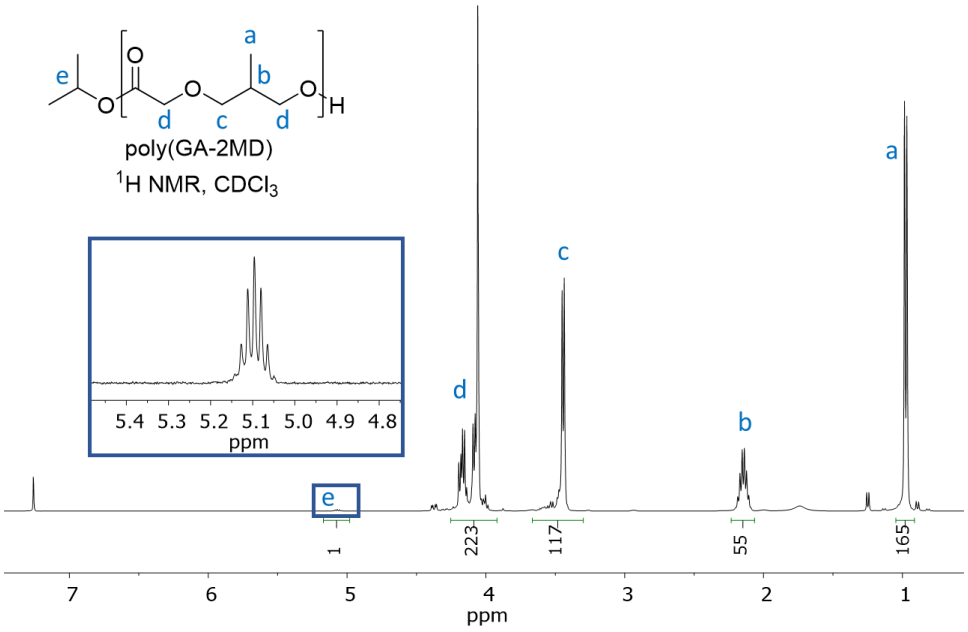

Figure 2.6.
Labeled ^{1}H NMR spectra of poly(GA-*alt*-2MD) from $[M]_0/[Ti(O\textit{i}\text{-}Pr)_4]_0$ = 100 in the bulk. The methine proton of the isopropyl group (e) is more downfield than expected for isopropoxide, isopropanol, $Ti(O\textit{i}\text{-}Pr)_4$, and isopropyl ether suggesting the formation of an alkyl ester.

Polymerizations with **(*R*,*R*)-dLA-3HP** were carried out in solution at 100 °C as described above. While the isotactic condensation polymer P(LA-*alt*-3HP) was found to be semicrystalline (T_m = 96 °C), the isotactic polymer obtained from ROTEP of **(*R*,*R*)-dLA-3HP** with Ti(O*i*-Pr)$_4$ was amorphous (Table 2.2). We believe this to be a consequence of the microstructure of the resulting polymers from polycondensation compared to ROTEP, see below.

Polymerization of larger macrolactones using Ti(O*i*-Pr)$_4$

Intrigued by the efficiency in which Ti(O*i*-Pr)$_4$ catalyzed the polymerization of 14-membered cyclic esters, we explored larger macrolides. The final step in the synthetic route for **dLA-3HP** results in ~6:1 ratio of the 14-membered macrolide (n = 1) to higher order cyclic oligomers (n ≥ 2). High-resolution mass spectrometry showed the presence of 21-, 28-, and 35-membered rings (Figure 2.2). These higher order oligomers were able to be isolated as a mixture by column chromatography. We subjected **dLA-3HP** and the isolated mixture of higher order cyclic oligomers to the polymerization conditions in the bulk at 115 °C with 2 mol% Ti(O*i*-Pr)$_4$ (Scheme 2.5). Both polymerizations reached high conversions within 10 min providing near-identical polymers (Figure 2.7).

Scheme 2.5.
Polymerization of dLA-3HP (n = 1) and the higher order cyclic oligomers (n ≥ 2)

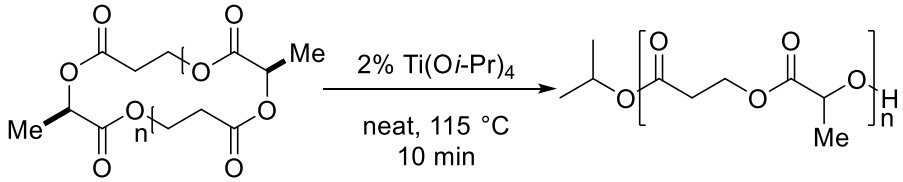

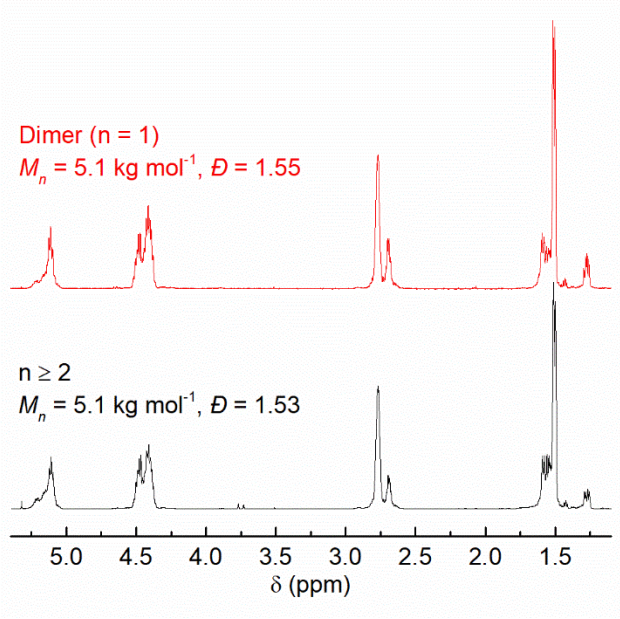

Figure 2.7.
^{1}H NMR spectra of P(LA-*co*-3HP) from the polymerization of **dLA-3HP** (n = 1) and higher order cyclic oligomers (n ≥ 2). Polymerizations were carried out with 2 mol% Ti(O*i*-Pr)$_4$ neat at 115 °C for 10 min.

Considering the high efficiency of Ti(O*i*-Pr)$_4$ in polymerizing ≥ 21-membered macrolide we were interested in the potential of this catalyst to polymerize PDL. Poly(PDL) (PPDL) has drawn significant interest from researchers as a potential sustainable replacement for linear low-density polyethylene.[59] Even at low loadings of Ti(O*i*-Pr)$_4$ (0.1 mol%), PDL can be efficiently polymerized in the bulk to provide moderate molar mass PPDL in 1 h (Scheme 2.6, Table 2.1). Notably, Ti(O*i*-Pr)$_4$ exhibits faster polymerization rates than many of the commercially available and tailored catalysts that have been reported in the literature for the polymerization of PDL and other macrolides.[53]

Scheme 2.6.
Polymerization of ω-pentadecalactone with Ti(O*i*-Pr)$_4$

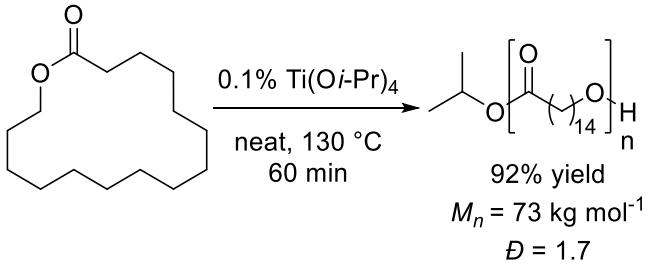

Kinetics and thermodynamics of macrolactone ROTEP using Ti(O*i*-Pr)$_4$

To further understand the polymerization of **dLA-3HP** and **dGA-2MD**, we studied the polymerization kinetics using Ti(O*i*-Pr)$_4$. Reactions were carried out in a 1 M toluene solution at 90 °C with 0.5 mol% Ti(O*i*-Pr)$_4$ to allow for the progress of the polymerization to be readily monitored. Aliquots taken during the reaction were analyzed by ^{1}H NMR spectroscopy and SEC. These polymerizations show first order kinetics with respect to monomer with an observed rate constant k_{obs} determined by an exponential fit of the decay curve (Figure 2.8 and 2.9). Interestingly, **dGA-2MD** polymerized approximately 40 times faster than **dLA-3HP** (k_{obs} = 0.075 min^{-1} and k_{obs} = 0.0018 min^{-1}, respectively). The position of the methyl substituent relative to the ester group has a significant impact on the rate of polymerization of the monomers.[60] These studies show molar mass increases linearly with conversion for both systems, consistent with a controlled polymerization (Figure 2.10). The dispersity values also increase with increasing conversion, indicative of increased transesterification.

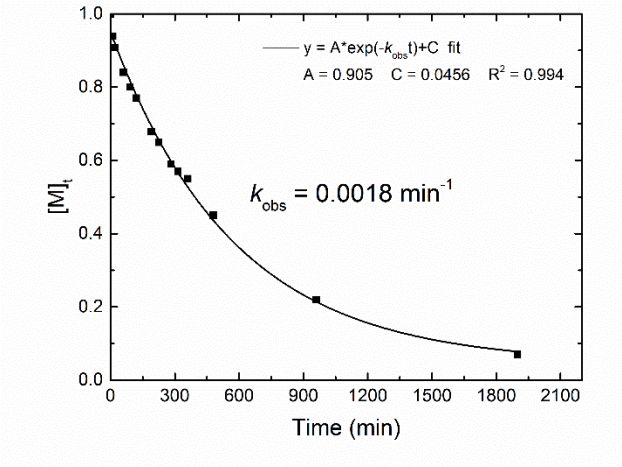

Figure 2.8.
Time course for polymerization of dLA-3HP with 0.5% Ti(O*i*-Pr)$_4$ in 1M toluene solution at 90 °C. An exponential fit of the decay curve is shown.

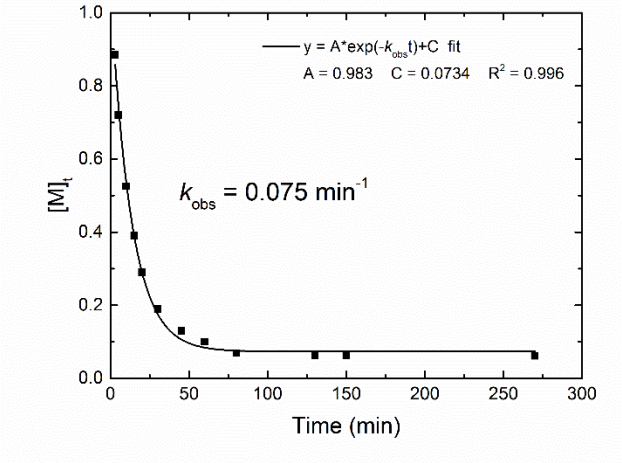

Figure 2.9.
Time course for polymerization of dGA-2MD with 0.5% Ti(O*i*-Pr)$_4$ in 1M toluene solution at 90 °C. An exponential fit of the decay curve is shown.

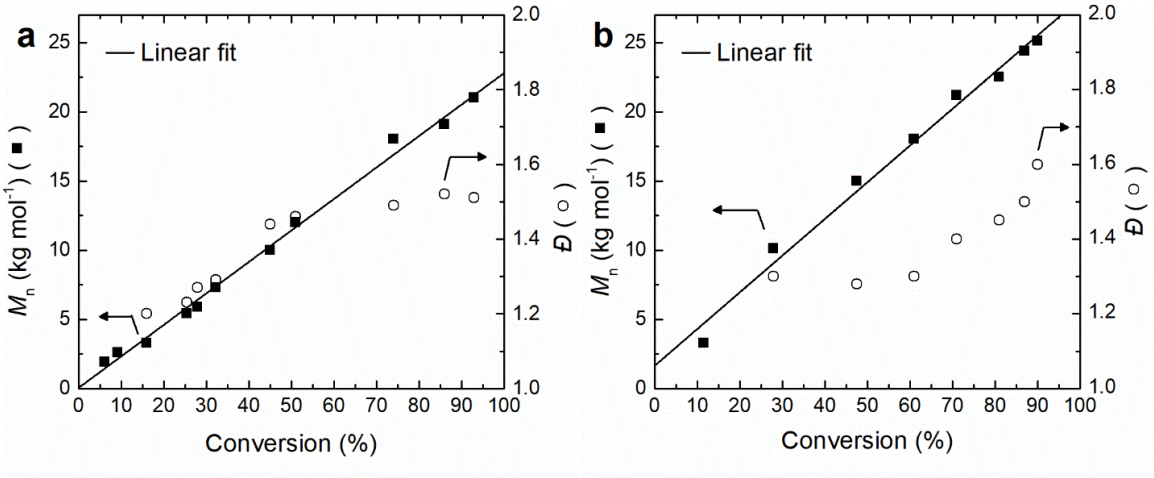

Figure 2.10.
Molar mass and dispersity as a function of conversion for the polymerization of a) dLA-3HP and b) dGA-2MD at 90 °C with 0.5 mol% Ti(Oi-Pr)$_4$ in toluene (1 M).

The thermodynamic parameters for the polymerization of each monomer were determined by van't Hoff analysis, where the equilibrium monomer concentration ($[M]_{eq}$) was measured at various temperatures, using the following equation:

$$\ln\left(\frac{[M]_{eq}}{[M]_{ss}}\right) = \frac{\Delta H_p^\circ}{RT} - \frac{\Delta S_p^\circ}{R} \qquad (2.1)$$

The $[M]_{eq}$ was determined using ^{1}H NMR spectroscopy and ln ($[M]_{eq}/[M]_{ss}$) was plotted as a function of inverse temperature (Figure 2.11). Reactions were carried out in triplicate over a range of temperatures at $[M]_{ss}$ = 1 M in toluene and 1 mol% Ti(O*i*-Pr)$_4$. One sample of each experiment was left to react and later analyzed to ensure that full equilibration had been achieved. The results of these experiments are shown in Figure 2.11 where the polymerization of **dLA-3HP** (ΔH_p° = 2.0 ± 0.4 kJ mol^{-1} and ΔS_p° = 27 ± 1.0 J mol^{-1} K^{-1}) and **dGA-2MD** (ΔH_p° = 0.5 ± 0.1 kJ mol^{-1} and ΔS_p° = 23 ± 0.3 J mol^{-1} K^{-1}) is endothermic and endoentropic. This indicates both polymerizations are entropically driven.[61]

Qualitatively, the increase in entropy upon polymerization is due to the increase in conformational freedom upon opening of the conformationally restricted macrocycle. This is contrary to typical ring-opening polymerizations which are driven forward by the release of ring-strain in the monomer ($\Delta H_p° < 0$).[62] These thermodynamic parameters are consistent with those reported for the polymerization of PDL ($\Delta H_p° = 3.0$ kJ mol^{-1} and $\Delta S_p° = 23$ J mol^{-1} K^{-1}) and 3-methyl-1,4-dioxane-2-one, a structural isomer of **dGA-2MD**, ($\Delta H_p° = 0.2$ kJ mol^{-1} and $\Delta S_p° = 16$ J mol^{-1} K^{-1}).[28,63]

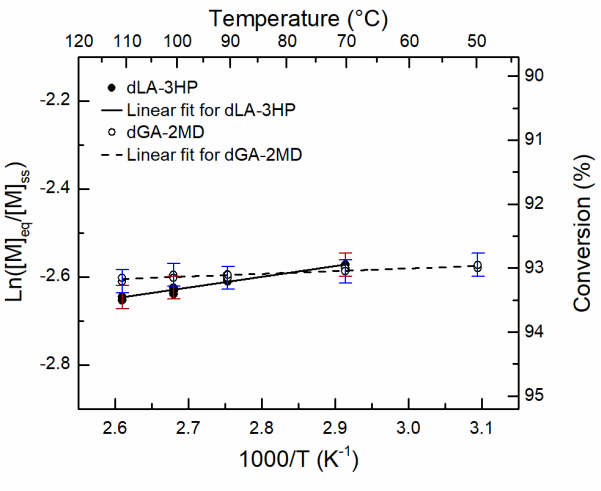

Figure 2.11.
van't Hoff analysis of the polymerization of dLA-3HP and dGA-2MD in toluene (1 M) and 1 mol% Ti(O*i*-Pr)$_4$.

Microstructure of P(LA-*co*-3HP)

The monomer **dLA-3HP** possesses two distinct ester moieties in the ring and can open at the LA ester or the 3HP ester (Scheme 2.7). If the ring-opening is chemoselective to one of those units and there is little transesterification to randomize the backbone, the reaction will yield the perfectly alternating copolymer P(LA-*alt*-3HP). Alternatively, if there is little chemoselectivity of the ring-opening step and/or there is significant

transesterification of the backbone, the product will be more consistent with a statistical copolymer P(LA-*stat*-3HP). Matrix-assisted laser desorption/ionization time of flight (MALDI-TOF) analysis revealed envelopes of mass peaks assigned to cyclic oligomers while linear polymer was not observed (Figure 2.12).[64] The mass peaks are separated by 72 g mol^{-1}, corresponding to the mass of either a LA fragment or 3HP fragment. This result indicates that intramolecular transesterification happens at both distinct ester moieties of the polymer chain.

Scheme 2.7.
Product of the ring-opening polymerization of **dLA-3HP**

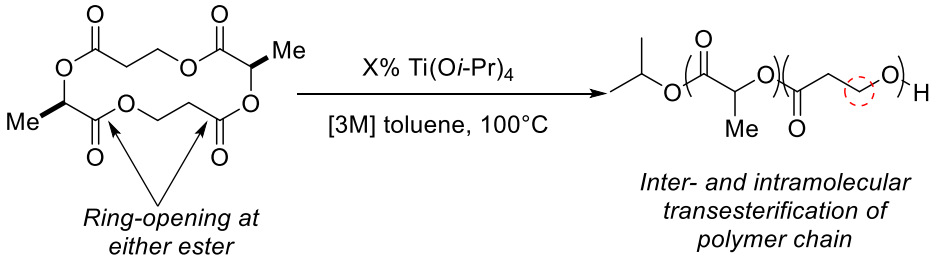

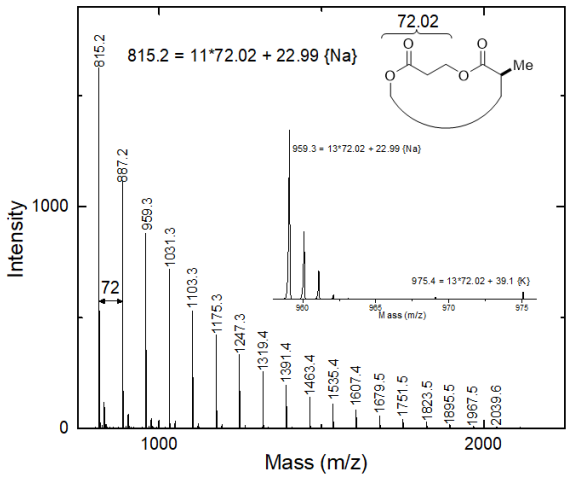

Figure 2.12.
MALDI-ToF analysis of 11 kg mol^{-1} polymer synthesized by ROTEP of dLA-3HP. Inset is an expanded view of the full spectrum showing envelope of peaks for 13-mer.

To study the microstructure of these polymers of **dLA-3HP** in more detail, we turned to carbon (^{13}C) NMR spectroscopy (Figure 2.13 and 2.14). The ^{13}C spectral region corresponding to the β-carbon of the 3HP fragment C_5 is shown in Figure 2.13. For reference, atactic (*a*P(LA-*alt*-3HP)) and isotactic (*i*P(LA-*alt*-3HP)) perfectly alternating copolymers of LA and 3HP were synthesized by condensation polymerization (Scheme 2.2, Figure 2.13, spectra a and b). Polymerization of **(*R,R*)-dLA-3HP** and ***rac*-dLA-3HP** for 1 h with Ti(O*i*-Pr)$_4$ produces a polymer that exhibits additional signals likely corresponding to different regio-triads and tetrads (Figure 2.13, spectra d and e). These differences become more pronounced when the polymerization of **(*R,R*)-dLA-3HP** is continued for 48 h, well beyond complete conversion of monomer (Figure 2.13, spectra f). This is due to continued transesterification that provides a statistical copolymer of LA and 3HP (*i*P(LA-*stat*-3HP)). Integration of these signals provides an estimate of the fraction of LA-3HP-LA (F_{LHL}) triads of 0.43 at 1 h and 0.14 at 48 h.[40,41,57] Interestingly, polymerizations of **(*R,R*)-dLA-3HP** with Sn(Oct)$_2$ were found to have a significantly higher degree of alternating character by ^1H and ^{13}C NMR spectroscopy (F_{LHL} = 0.72) (Figure 2.13, spectra c and Figure 2.14). This suggests that a more selective catalyst is required to efficiently produce perfectly alternating P(LA-alt-3HP) from **dLA-3HP**. The differences in the microstructure in ^1H and ^{13}C NMR spectroscopy indicate that both low regioselectivity of the initial ring-opening event as well as significant inter- and intramolecular transesterifications result in a low degree of alternating character for Ti(O*i*-Pr)$_4$ catalyzed polymerizations.[65]

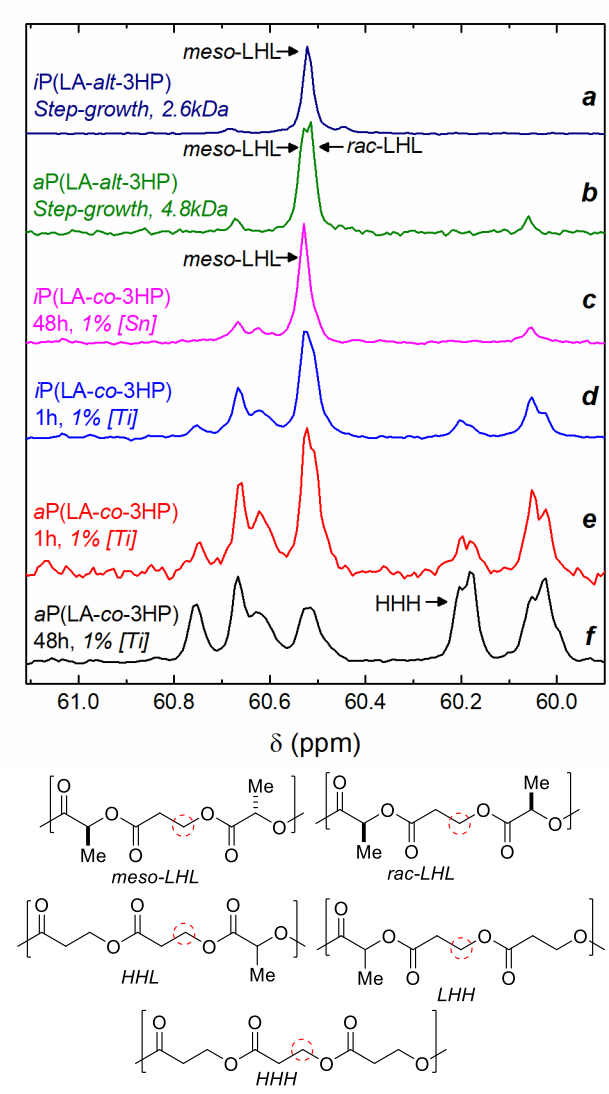

Figure 2.13.
^{13}C NMR analysis of P(LA-*co*-HP) within the 3HP β-carbon region, C_5 (circled), for determination of microstructure of copolymers resulting from condensation polymerization and ring-opening transesterification polymerization. Representative regio- and stereo-triads are shown.

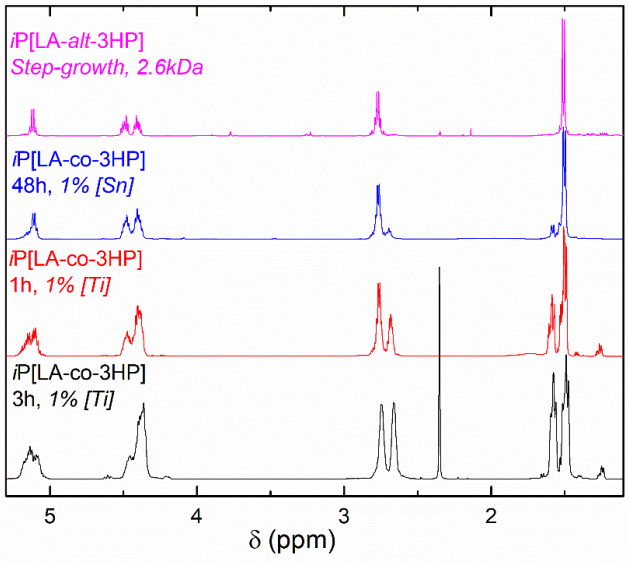

Figure 2.14.
Overlay of ^{1}H NMR spectra of *i*P(LA-*co*-3HP) polymers synthesized under different conditions.

Thermal characterization

Thermogravimetric analysis (TGA) and differential scanning calorimetry (DSC) were used to study the thermal stability and thermal transitions of several samples of each polymer (Figure 2.15). P(LA-*co*-3HP) and P(GA-*alt*-2MD) exhibit 5% mass loss by TGA at 213 °C and 230 °C, respectively. These are similar thermal decomposition temperatures to other aliphatic polyesters. P(GA-*alt*-2MD) is an amorphous polymer with no observed melting transition and a low T_g (−30 °C). This is close to the expected T_g of −25 °C, estimated using the Fox equation ($1/T_g = w_1/T_{g,1} + w_2/T_{g,2}$) using the T_g of the homopolymers PGA and P2MD (T_g = 45 °C and −62 °C, respectively) and the weight fractions w_{GA} and w_{2MD} in the copolymer.[66] P(LA-*stat*-3HP) obtained from the Ti(O*i*-Pr)$_4$ catalyzed polymerization of **(*R,R*)-dLA-3HP** or ***rac*-dLA-3HP** are amorphous, exhibiting T_g ranging from 7–13 °C. This agrees with the expected T_g of 13 °C, calculated using the

Fox equation from the T_g of the homopolymers P3HP and PLLA (T_g = −22 °C and 60 °C, respectively).[66]

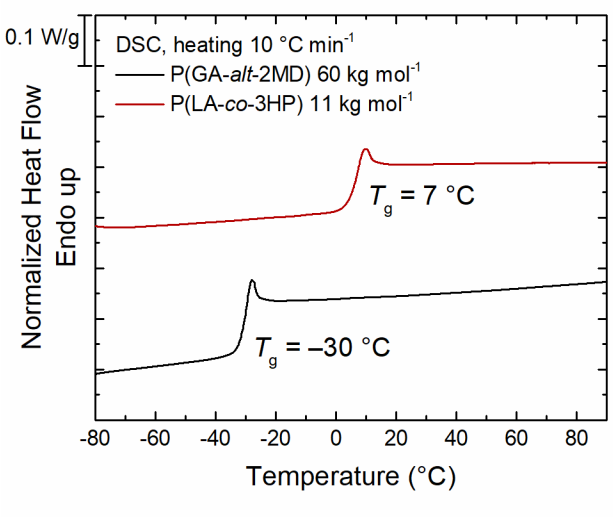

Figure 2.15.
DSC analysis of P(LA-*co*-3HP) and P(GA-*alt*-2MD), second heat at 10 °C min^{-1}.

In contrast to the amorphous polymers obtained from Ti(O*i*-Pr)$_4$ catalyzed ROTEP, the perfectly alternating isotactic polymer, *i*P(LA-*alt*-3HP), generated through condensation polymerization is semicrystalline with T_m = 96 °C (Scheme 2.2, Figure 2.1). This melting transition lies between the T_m of PLLA at 180 °C and the T_m of P3HP at 76 °C. The observed T_g of *i*P(LA-*alt*-3HP) is at 4 °C and is somewhat lower than the expected 13 °C, likely due to the low molar mass (2.4 kg mol^{-1}). The higher degree of alternating character from the polymerization of **(*R*,*R*)-dLA-3HP** with Sn(Oct)$_2$ resulted in a semicrystalline polymer, albeit with a lower T_m of 68 °C and a broad transition indicative of more than one crystalline polymorph (Figure 2.1). The degree of chemoselectivity of the catalyst used in the polymerization impacts the microstructure of P(LA-*co*-3HP), resulting in a broad range of thermal properties.

Rheological properties of P(LA-*co*-3HP)

High molar mass samples of amorphous P(LA-*co*-3HP) were relatively stiff at room temperature likely due to the proximity to the glass transition temperature. We studied the basic rheological properties of this copolymer (Figure 2.17). An entanglement molar mass (M_e) of 5.4 kg mol^{-1} was estimated from the plateau modulus of a 30 kg mol^{-1} sample of the copolymer. This is similar to the M_e observed in other aliphatic polyesters without methyl substituents.[60]

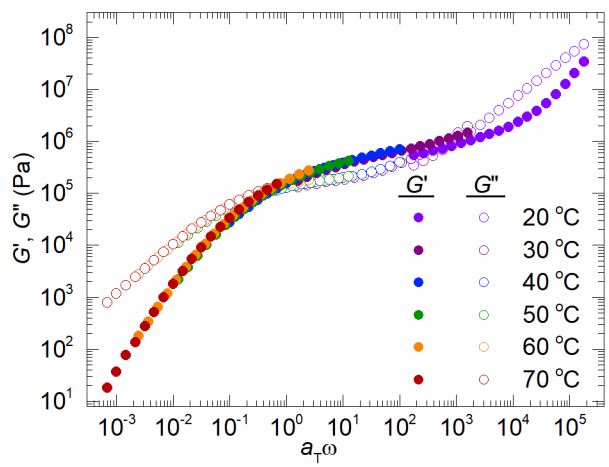

Figure 2.16.
Frequency sweeps in the linear viscoelastic region of 30 kg mol^{-1} P(LA-*co*-3HP) were shifted to construct this master curve. Entanglement molar mass (M_e) was determined using the plateau in the storage modulus where the loss tangent (tan δ) is at a minimum (M_e = 5.4 kg/mol).

2.3 Conclusions

We report the synthesis of two new macrolides which allow the efficient and selective synthesis of polyester copolymers. While the original goal of this study was to synthesize the 7-membered lactones, we observed the formation of 14-membered rings with excellent selectivity. In exploring polymerization conditions for these unstrained

cyclic monomers, we discovered that inexpensive and non-toxic Ti(O*i*-Pr)$_4$ proved to be a highly active polymerization catalyst. While Ti(O*i*-Pr)$_4$ has been extensively studied for the polymerization of strained lactones and condensation polymerization, it has not been reported as a catalyst in entropically-driven ROTEP of macrolides. Despite the unstrained nature of **dLA-3HP** and **dGA-2MD**, the polymerizations proceed rapidly and reach high conversions within reasonably short reaction times. Thermodynamic studies support the notion that the polymerization of both **dLA-3HP** and **dGA-2MD** are driven due to entropic factors. Furthermore, Ti(O*i*-Pr)$_4$ appears to be a highly efficient ROTEP catalyst regardless of the ring size showing excellent activity for the polymerization of 16-, 21-, 28-, and 35-membered macrolides. It is likely that this catalyst will allow the facile polymerization of other large lactones. The method to synthesize macrolides and polymerize them through active catalysts such as Ti(O*i*-Pr)$_4$ provide access to statistical and alternating copolymers through ROTEP.

2.4 Experimental Section

General considerations. All moisture sensitive compounds were handled in a nitrogen filled glovebox. Anhydrous toluene was obtained through a JC Meyer solvent drying system. Anhydrous dichloromethane was obtained by filtering through an activated alumina column. Ethyl lactate (98%), benzyl alcohol, sodium hydroxide, palladium on carbon (10%), triethylamine, potassium carbonate, acetonitrile, trifluoroacetic acid, Novozyme 435, *N*,*N*-diisopropylcarbodiimide, yttrium (III) isopropoxide, titanium (IV) isopropoxide (99.999% trace metals basis), *tert*-butyl acrylate, methanol, acetone, 2-

methyl-1,3-propanediol, sodium chloroacetate, sodium in kerosene, and *p*-toluenesulfonic acid were purchased from Sigma Aldrich without further purification. 1,5,7-Triazabicyclo[4.4.0]dec-5-ene (TBD) was sublimed two times under vacuum before storing in a nitrogen filled glove box. 1-chloro-1-oxopropan-2-yl methanesulfonate (**2**) was prepared as described previously in the literature.[67] Dimethylpyridinium *p*-toluenesulfonate was prepared as described previously by Moore *et al*.[68] The zinc catalyst reported by Williams et al. was obtained through Professor William Tolman.[69] Tin (II) octanoate ($Sn(oct)_2$) was distilled three times under vacuum (30–50 mtorr, 130–150°C) before storing in a nitrogen filled glove box. tert-butyl (*S*)-2-hydroxypropanoate was prepared as described previously in the literature.[70] ω-Pentadecalactone (PDL) was purified by distilling away from CaH_2 under reduced pressure (120 mtorr, 80 °C).

NMR spectra were recorded on a Bruker HD-500 spectrometer from solutions in deuterated solvent and chemical shifts in ppm were referenced to the solvent. Enantiomeric excesses were determined by chiral HPLC of pure monomer samples using an Agilent 1260 infinity system with Regis Technologies Inc (S,S) Whelk-O®-1-(S,S) 5 µm 100 Å, LC Column (250 x 4.6 mm) and HPLC grade isopropanol and hexane. Optical rotations were measured using a Rudolph Research Autopol III polarimeter at 25.8 °C in a cell with a 1 dm pathlength in $CDCl_3$. Mass spectrometry was performed with a Bruker BioTOF II ESI/TOF-MS (electrospray ionization, time-of-flight analyzer). GC-MS was collected using an Agilent 6890 GC equipped with a HP-5ms column (30 m x 0.25 mm) and Agilent 5973 MS detector. Matrix-assisted laser desorption ionization mass spectrometry (MALDI-MS) was performed on an AB-Sciex 5800 MALDI-TOF mass spectrometer.

Samples were deposited in a dithranol/sodium trifluoroacetate matrix. Internal calibration of the instrument was performed using PEO standards.

Unless stated otherwise, molar mass and dispersity were determined by size exclusion chromatography using either an (i) Agilent 1260 Infinity liquid chromatograph equipped with three Waters Styragel columns in series with a Wyatt DAWN Heleos II 18-angle laser light scattering detector and a Wyatt OPTILAB T-rEX refractive index detector in THF at 25 °C, with molar mass calculations assuming 100% mass recovery or (ii) Agilent 1100 series SEC with HP1047A refractive index detector using a $CHCl_3$ mobile phase at 35 °C through 3 Varian PLgel Mixed C columns at 1 mL min^{-1} and relative molar mass determined against polystyrene standards. Thermogravimetric analysis was conducted in air atmosphere using a TA instruments TGA Q500 heating at 10 °C min^{-1}. Thermal properties were obtained using a TA Instruments Discovery DSC. Samples were prepared in hermetically sealed pans and heated at 10 °C min^{-1} to 150 °C to erase thermal history, cooled to −85 °C, and data was collected from the second heat cycle. Using 8 mm parallel plates, TA Instruments Rheometric Series ARES instrument was used for dynamic mechanical thermal analysis (DMTA). Heating was controlled under nitrogen atmosphere, and the samples were equilibrated at the designated temperature for 10 minutes before testing.

***tert*-butyl 3-(benzyloxy)propanoate.** Reaction procedure was adapted from one previously described in the patent literature.[71] A 500 mL round bottom flask was charged with benzyl alcohol (135 g, 1.25 mmol) and *tert*-butyl acrylate (280 mL, 1.91 mmol). With vigorous stirring an aqueous solution of NaOH (5 g in 4 mL) was added dropwise. The

reaction mixture was then heated to 80 °C for 2 hours. After this time the reaction mixture was allowed to cool to room temperature and was then stirred overnight. The contents of the reaction flask were then transferred to a 1 L separatory funnel and diluted with EtOAc (200 mL) and H_2O (100 mL). The organic phase was isolated, dried over Na_2SO_4 and concentrated under reduced pressure to give the crude product. Unreacted benzyl alcohol and *tert*-butyl acrylate were then removed by distillation under reduced pressure to give provide the pure product as a colorless oil (178.8 g, 0.76 mmol, 60 % yield). ^{1}H NMR (400 MHz, Chloroform-d) δ 7.43 – 7.29 (m, 5H), 4.55 (s, 2H), 3.74 (t, J = 6.5 Hz, 2H), 2.55 (t, J = 6.5 Hz, 2H), 1.48 (s, 9H). HRMS (ESI) calculated for $[C_{14}H_{20}NaO_3]^+$ {M+Na} requires 259.1310, found 259.1303.

***tert*-butyl 3-hydroxypropanoate (1).** A 1 L round bottom flask with a large magnetic stir bar was charged with *tert*-butyl 3-(benzyloxy)propanoate (178.8 g, 0.76 mmol) and MeOH (500 mL). The flask was sealed with a rubber septum and sparged with N_2 (g) for 10 minutes. The reaction flask was then charged with Pd/C (10%, 15 g), the flask sealed and sparged with N_2(g) for an additional 5 minutes. The flask was then sparged with H_2 (g, balloon) for 1 hour. After this time the flask was placed under 1 atm of H_2 (g, balloon) and allowed to stir rapidly for 24 hours. After this time the reaction was determined to be finished by ^{1}H NMR analysis. The reaction mixture was then sparged for 15 minutes with N_2 (g). The Pd/C was then removed by vacuum filtration under a flow of nitrogen and the filter cake was washed several times with additional MeOH. The solvent was then removed under reduced pressure to provide the pure product as a colorless oil (110.8 g, 0.76 mmol, quant.). ^{1}H NMR (400 MHz, Chloroform-d) δ 3.84 (t, J = 5.6 Hz,

1H), 2.51 (t, J = 5.6 Hz, 1H), 1.49 (d, J = 1.1 Hz, 5H). ^{13}C NMR (126 MHz, Chloroform-d) δ 172.42, 81.18, 58.45, 37.93, 28.16. HRMS (ESI) calculated for $[C_7H_{14}NaO_3]^+$ {M+Na} requires 169.0841, found 169.0837.

3-(benzyloxy)propanoic acid. A 250 mL round bottom flask was charged with *tert*-butyl 3-(benzyloxy)propanoate (50.1 g, 0.21 mmol) and CH_2Cl_2 (100 mL). Trifluoroacetic acid (50 mL) was then added while stirring. The reaction mixture was allowed to stir at room temperature for 8 hours. After this time the volatiles were removed under reduced pressure to provide relatively pure 3-(benzyloxy)propanoic acid as a colorless oil (38.3g, 0.21 mmol, quant). ^{1}H NMR (500 MHz, Chloroform-d) δ 7.46 – 7.30 (m, 5H), 4.59 (s, 2H), 3.79 (t, J = 6.4 Hz, 2H), 2.70 (t, J = 6.4 Hz, 2H). 13C NMR (126 MHz, Chloroform-d) δ 177.41, 137.85, 128.47, 127.80, 127.79, 73.18, 67.01, 65.27, 34.96. HRMS (ESI) calculated for $[C_{10}H_{12}NaO_3]^+$ {M+Na} requires 203.0684, found 203.0679.

benzyl (*S*)-2-((3-(benzyloxy)propanoyl)oxy)propanoate. A flame-dried 1000 mL round bottom flask was charged with benzyl *(S)*-lactate (21 g, 0.12 mmol), 3-(benzyloxy)propanoic acid (22 g, 0.12 mmol), DMAP (18 g, 0.15 mmol), and CH_2Cl_2 (600 mL). EDC (28 g, 0.15mmol) was then added in portions as a solid. The reaction mixture was then sealed with a rubber septum, purged with N_2 (g), and stirred overnight. After this time the contents of the flask were transferred to a separatory funnel and the organics were washed with 2M HCl (×3). The organic layer was dried over Na_2SO_4 and concentrated under reduced pressure to give the product in sufficient purity for the next step in the reaction sequence (39.9 g, 0.12 mmol, 80% yield). ^{1}H NMR (500 MHz, Chloroform-d) δ 7.43 – 7.29 (m, 10H), 5.29 – 5.10 (m, 3H), 4.60 – 4.50 (m, 2H), 3.90 – 3.73 (m, 2H), 2.74

(t, J = 6.5 Hz, 2H), 1.53 (d, J = 7.1 Hz, 3H). ^{13}C NMR (126 MHz, Chloroform-d) δ 170.93, 170.59, 138.13, 135.41, 128.62, 128.40, 128.13, 127.69, 127.67, 73.11, 68.74, 66.98, 65.41, 53.53, 34.89, 16.90. HRMS (ESI) calculated for $[C_{20}H_{22}NaO_5]^+$ {M+Na} requires 365.1365, found 365.1354.

benzyl *rac*-2-((3-(benzyloxy)propanoyl)oxy)propanoate. Reaction was carried out as described for benzyl (*S*)-2-((3-(benzyloxy)propanoyl)oxy)propanoate using benzyl lactate (10 g, 0.057 mmol), 3-(benzyloxy)propanoic acid (10.5 g, 0.57 mmol), DMAP (8.6 g, 0.071 mmol), CH_2Cl_2 (285 mL), and EDC (13.3 g, 0.071 mmol) providing the product as a colorless oil (19 g, 0.057 mmol, 80% yield). Spectral data match those for benzyl (*S*)-2-((3-(benzyloxy)propanoyl)oxy)propanoate.

(*S*)-2-((3-hydroxypropanoyl)oxy)propanoic acid. A 500 mL round bottom flask was charged with benzyl (*S*)-2-((3-(benzyloxy)propanoyl)oxy)propanoate (14.23 g, 0.42 mmol) and EtOAc (250 mL). The flask was sealed with a rubber septum and sparged for 10 minutes with N_2 (g). After this time 10% Pd/C (2 g) was added in one portion as a solid. The reaction mixture was sparged for an additional 5 min with N_2 (g). After this time the reaction flask was fit with a balloon of hydrogen gas and sparged with the contents of the balloon (~30 min). The reaction flask was placed under 1 atm of H_2 (g) and stirred vigorously. Reaction progress was monitored by ^{1}H NMR analysis and stirred until complete consumption of the starting material was observed (~24 h). After this time the reaction mixture was sparged for 10 min with N_2 (g) and filtered washing the filter cake with additional EtOAc. The filtrate was then concentrated under reduced pressure to give the desired hydroxy acid as a colorless oil which was immediately carried on for

polymerization without further purification. ^{1}H NMR (500 MHz, Chloroform-d) δ 5.25 (q, J = 7.1 Hz, 1H), 4.04 – 3.87 (m, 2H), 2.77 – 2.58 (m, 2H), 1.59 (d, J = 7.1 Hz, 3H).

***rac*-2-((3-hydroxypropanoyl)oxy)propanoic acid.** Reaction was carried out as described above for (*S*)-2-((3-hydroxypropanoyl)oxy)propanoic acid using benzyl 2-((3-(benzyloxy)propanoyl)oxy)propanoate (2.2 g, 0.42 mmol), EtOAc (130 mL), and 10% Pd/C (553 mg) providing the product as a colorless oil that was carried on immediately (998 mg, 6.16 mmol, ~quant.). Spectral data match those for (*S*)-2-((3-hydroxypropanoyl)oxy)propanoic acid.

***i*P(LLA-*alt*-3HP).** A flame-dried 25 mL round bottom flask was charged with (*S*)-2-((3-hydroxypropanoyl)oxy)propanoic acid (662 mg, 4.08 mmol), DPTS (255 mg, 0.855 mmol), and CH_2Cl_2 (4 mL). The flask was sealed with a rubber septum, purged with N_2 (g), and cooled to 0 °C. DIC (773 mg, 6.1 mmol) was then added dropwise *via* syringe. The solution was then allowed to warm to room temperature and was stirred overnight. After this time the solution was diluted with addition CH_2Cl_2 and washed with 1M HCl. The organic layer was dried over Na_2SO_4 and concentrated under reduced pressure. The resulting polymer was purified by dissolving in a minimal amount of chloroform and precipitating into a 1:1 mixture of iPrOH/hexanes. After drying the pure polymer was obtained as an off-white powder (287 mg). $CHCl_3$ SEC, RI: M_n = 2.6 kg mol^{-1}, M_w = 3.7 kg mol^{-1}, $Đ$ = 1.4. ^{1}H NMR (500 MHz, Chloroform-d) δ 5.12 (q, J = 7.0 Hz, 1H), 4.49 (dt, J = 11.2, 6.4 Hz, 1H), 4.40 (dt, J = 11.4, 6.2 Hz, 1H), 2.83 – 2.71 (m, 2H), 1.51 (d, J = 7.1 Hz, 3H). ^{13}C NMR (126 MHz, Chloroform-d) δ 170.28, 169.78, 68.99, 60.53, 33.49, 16.90. $[\alpha]_D^{25.7}$ –29.0 (*c* 1.00, $CDCl_3$).

***a*P(LA-*alt*-3HP).** Polymerization was carried as described for *i*P(LLA-*alt*-3HP) using *rac*-2-((3-hydroxypropanoyl)oxy)propanoic acid (998 mg, 6.16 mmol), DPTS (378 mg, 1.28 mmol), CH_2Cl_2 (4 mL), and DIC (1.1 mg, 7.1 mmol) providing the polymer as a thick colorless amorphous oil (235 mg). $CHCl_3$ SEC, RI: M_n = 4.7 kg mol^{-1}, M_w = 5.6 kg mol^{-1}, $Đ$ = 1.2. ^{1}H NMR (500 MHz, Chloroform-d) δ 5.08 (p, J = 7.3, 5.8 Hz, 1H), 4.52 – 4.33 (m, 2H), 2.79 – 2.71 (m, 2H), 1.49 (d, J = 7.1, 1.5 Hz, 3H). ^{13}C NMR (126 MHz, Chloroform-d) δ 170.33, 170.31, 169.83, 69.01, 60.55, 60.53, 33.51, 16.91.

(*S*)-3-butoxy-3-oxopropyl 2-((methylsulfonyl)oxy)propanoate. A 3 L round bottom flask with magnetic stir bar was charged with *tert*-butyl 3-hydroxypropanoate (20.01 g, 0.14 mmol), triethylamine (28.8 mL, 0.21 mmol), and CH_2Cl_2. The reaction flask was sealed with a rubber septum, purged several times with N_2 (g) and cooled to 0 °C using an ice bath. (*S*)-1-chloro-1-oxopropan-2-yl methanesulfonate (28.1 g, 0.15 mmol) was then added dropwise by syringe. After stirring for 30 minutes at 0 °C the reaction mixture was allowed to warm to room temperature and stirred overnight. After this time the reaction mixture was quenched by addition of saturated aq. NH_4Cl and the contents of the flask were transferred to a large separatory funnel. The mixture was diluted with additional water and layers separated. The organic phase was washed with water, brine, dried over Na_2SO_4, and concentrated in vacuo to give the crude product in sufficient purity for the next step as a yellow to brown oil (38.8 g, 0.13 mmol, 95% yield). ^{1}H NMR (500 MHz, Chloroform-d) δ 5.14 (q, J = 7.0 Hz, 1H), 4.45 (ddt, J = 31.5, 11.8, 6.6 Hz, 2H), 3.17 (s, 3H), 2.62 (t, J = 6.2 Hz, 2H), 1.62 (d, J = 7.1 Hz, 3H), 1.48 (s, 9H). ^{13}C NMR (126 MHz, Chloroform-d) δ

169.40, 169.31, 81.41, 74.06, 61.57, 39.14, 34.79, 28.04, 18.36. HRMS (ESI) calculated for $[C_{11}H_{20}NaO_7S]^+$ {M+Na} requires 319.0827, found 319.0826.

***rac*-3-butoxy-3-oxopropyl 2-((methylsulfonyl)oxy)propanoate.** A 3 L round bottom flask with magnetic stir bar was charged with *tert*-butyl 3-hydroxypropanoate (43.72 g, 0.3 mmol), triethylamine (63 mL, 0.45 mmol), and CH_2Cl_2. The reaction flask was sealed with a rubber septum, purged several times with N_2 (g) and cooled to 0 °C using an ice bath. 1-chloro-1-oxopropan-2-yl methanesulfonate (61.4 g, 0.33 mmol) was then added dropwise by syringe. After stirring for 30 min at 0 °C the reaction mixture was allowed to warm to room temperature and stirred overnight. After this time the reaction mixture was quenched by addition of saturated aq. NH_4Cl and the contents of the flask were transferred to a large separatory funnel. The mixture was diluted with additional water and layers separated. The organic phase was washed with water, brine, dried over Na_2SO_4, and concentrated in vacuo to give the crude product in sufficient purity for the next step as a yellow to brown oil (85.1 g, 0.29 mmol, 96% yield). ^{1}H NMR (500 MHz, Chloroform-d) δ 5.14 (q, J = 7.0 Hz, 1H), 4.45 (ddt, J = 31.5, 11.8, 6.6 Hz, 2H), 3.17 (s, 3H), 2.62 (t, J = 6.2 Hz, 2H), 1.62 (d, J = 7.1 Hz, 3H), 1.48 (s, 9H). ^{13}C NMR (126 MHz, Chloroform-d) δ 169.40, 169.31, 81.41, 74.06, 61.57, 39.14, 34.79, 28.04, 18.36. HRMS (ESI) calculated for $[C_{11}H_{20}NaO_7S]^+$ {M+Na} requires 319.0827, found 319.0822.

***(S)*-3-((2-((methylsulfonyl)oxy)propanoyl)oxy)propanoic acid (3).** A 250 mL round bottom flask with a magnetic stir bar was charged with 3-butoxy-3-oxopropyl 2-((methylsulfonyl)oxy)propanoate (40.5 g, 0.14 mmol), CH_2Cl_2 (300 mL), and trifluoroacetic acid (70 mL, 90 mmol). The flask was then allowed to stir at room

temperature for 6 hours after which the reaction was determined to be finished by ^{1}H NMR analysis. The excess trifluoroacetic acid and CH_2Cl_2 were then removed in vacuo to provide the product in sufficient purity for the next step as a yellow to brown oil (31.8 g, 0.14 mmol, quant). ^{1}H NMR (400 MHz, Chloroform-d) δ 5.13 (q, J = 7.0 Hz, 1H), 4.56 – 4.43 (m, 2H), 3.15 (s, 3H), 2.81 (t, J = 6.1 Hz, 2H), 1.61 (d, J = 7.1 Hz, 3H). ^{13}C NMR (126 MHz, Chloroform-d) δ 176.42, 169.50, 73.88, 60.71, 39.09, 33.26, 18.25. HRMS (ESI) calculated for $[C_7H_{13}NaO_7S]^+$ {M+Na} requires 263.0201, found 263.0206.

***rac*-3-((2-((methylsulfonyl)oxy)propanoyl)oxy)propanoic acid (3).** A 500 mL round bottom flask with a magnetic stir bar was charged with 3-butoxy-3-oxopropyl 2-((methylsulfonyl)oxy)propanoate (88.6 g, 0.3 mmol), CH_2Cl_2 (300 mL), and trifluoroacetic acid (150 mL, 1.96 mmol). The flask was then allowed to stir at room temperature for 6 hours after which the reaction was determined to be finished by ^{1}H NMR analysis. The excess trifluoroacetic acid and CH_2Cl_2 were then removed in vacuo to provide the product in sufficient purity for the next step as a yellow to brown oil (71.8 g, 0.3 mmol, quant). ^{1}H NMR (400 MHz, Chloroform-d) δ 5.13 (q, J = 7.0 Hz, 1H), 4.56 – 4.43 (m, 2H), 3.15 (s, 3H), 2.81 (t, J = 6.1 Hz, 2H), 1.61 (d, J = 7.1 Hz, 3H). ^{13}C NMR (126 MHz, Chloroform-d) δ 176.42, 169.50, 73.88, 60.71, 39.09, 33.26, 18.25. HRMS (ESI) calculated for $[C_7H_{13}NaO_7S]^+$ {M+Na} requires 263.0201, found 263.0202.

(*R*,*R*)-3,10-dimethyl-1,4,8,11-tetraoxacyclotetradecane-2,5,9,12-tetraone ((*R*,*R*)-dLA-3HP). A dry 3 L round bottom flask with a magnetic stir bar was charged with K_2CO_3 (12.6 g, 0.09 mmol) and MeCN (0.8 L, anhydrous). The reaction flask was equipped with a 250 mL addition funnel and the reaction mixture was heated to 50 °C. A solution of

(*S*)-3-((2-((methylsulfonyl)oxy)propanoyl)oxy)propanoic acid (21.9 g, 0.046 mmol) in MeCN (100 mL) was transferred to the addition funnel and this solution was added dropwise to the reaction flask over the course of 12 h. After stirring for a total of 18 h the reaction mixture was allowed to cool to room temperature. The heterogeneous mixture was filtered through a pad of Celite and the filtrate was concentrated under reduced pressure to provide the crude product as a 5.5:1 mixture of 14-membered macrolactone to higher order oligomers. The crude product was taken up in acetone and filtered through a plug of silica. The filtrate was concentrated and the residue recrystallized from hot toluene (×2) to provide large crystals in ~10:1 d.r. The *meso* diastereomer could be isolated from the *rac* diastereomer by recrystallization from hot acetone. The crystalline product was then purified further in batches by sublimation (90 °C, 100 mtorr) to give *(R)*-dLA-HP as a white crystalline powder (10.2 g, 0.036 mmol, 80 % yield, 10:1 d.r). *(R)*-dLA-HP: ^{1}H NMR (500 MHz, Chloroform-d) δ 5.12 (q, J = 7.1 Hz, 2H), 4.64 (t, J = 10.8 Hz, 2H), 4.29 – 4.20 (m, 2H), 2.83 – 2.74 (m, 2H), 2.68 – 2.60 (m, 2H), 1.55 (d, J = 7.1 Hz, 6H). ^{13}C NMR (126 MHz, Chloroform-d) δ 170.25, 169.64, 69.40, 60.91, 33.03, 16.79. m.p 129 °C. HRMS (ESI) calculated for $[C_{12}H_{16}NaO_8]^+$ {M+Na} requires 311.0743, found 311.0739. $[\alpha]_D^{25.7}$ +38.3 (*c* 1.00, $CDCl_3$).

Scalemic: HPLC, Whelk-O®-1-(S,S) 5 µm 100 Å, 30% iPrOH/Hexane, 1 mL/min, 220 nm

Peak	Area (%)	Area	RT (min)	Height (mAU)
1	2.1081	59.427	9.15	2.75
2	97.892	2759.525	12.88	66.40
Total	100	2818.95		

***rac*-3,10-dimethyl-1,4,8,11-tetraoxacyclotetradecane-2,5,9,12-tetraone (*rac*-dLA-HP).** A dry 3 L round bottom flask with a magnetic stir bar was charged with K_2CO_3 (27.6 g, 0.2 mmol) and MeCN (1.75 L, anhydrous). The reaction flask was equipped with a 500 mL addition funnel and the reaction mixture was heated to 50 °C. A solution of 3-((2-((methylsulfonyl)oxy)propanoyl)oxy)propanoic acid (48.0 g, 0.1 mmol) in MeCN (250 mL) was transferred to the addition funnel and this solution was added dropwise to the reaction flask over the course of 12 h. After stirring for a total of 18 h the reaction mixture was allowed to cool to room temperature. The heterogeneous mixture was filtered through a pad of Celite and the filtrate was concentrated under reduced pressure to provide the crude product as a 5.5:1 mixture of 14-membered macrolactone to higher order oligomers. The crude product was taken up in acetone and filtered through a plug of silica. The filtrate was concentrated and the residue recrystallized from hot toluene (×2) to provide large crystals. The *meso*-diastereomer could be isolated from the *rac*-diastereomer by recrystallization from hot acetone. The crystalline product was then purified further in batches by sublimation (90 °C, 100 mtorr) to give dLA-HP as a white crystalline powder (22.4 g, 0.078 mmol, 78 % yield, 2:1 d.r). *rac*-dLA-HP: ^{1}H NMR (500 MHz, Chloroform-d) δ 5.12 (q, J = 7.1 Hz, 2H), 4.64 (t, J = 10.8 Hz, 2H), 4.29 – 4.20 (m, 2H), 2.83 – 2.74 (m, 2H), 2.68 – 2.60 (m, 2H), 1.55 (d, J = 7.1 Hz, 6H). ^{13}C NMR (126 MHz, Chloroform-d) δ 170.25, 169.64, 69.40, 60.91, 33.03, 16.79. m.p 110 °C. HRMS (ESI) calculated for $[C_{12}H_{16}NaO_8]^+$ {M+Na} requires 311.0743, found 311.0732. *meso*-dLA-HP: ^{1}H NMR (500 MHz, Chloroform-d) δ 5.19 (q, J = 7.0 Hz, 2H), 4.62 – 4.55 (m, 2H), 4.44 – 4.35 (m, 2H), 2.77 – 2.69 (m, 2H), 2.66 – 2.58 (m, 2H), 1.54 (d, J = 7.1 Hz, 6H). ^{13}C NMR (126

MHz, Chloroform-d) δ 170.03, 169.99, 69.37, 59.97, 33.51, 16.52. m.p 186 °C. HRMS (ESI) calculated for $[C_{12}H_{16}NaO_8]^+$ {M+Na} requires 311.0743, found 311.0745. The remaining residue in the sublimation apparatus was composed largely of higher order oligomers (trimers, tetramers, and pentamers by HRMS (ESI)). These can be further purified by flash column chromatography (1:3 acetone/hexanes) to give the collection of cyclic oligomers as a colorless oil (3.1 g, 10.8 % yield). ^{1}H NMR (500 MHz, Chloroform-d) δ 5.19 – 5.05 (m, 1H), 4.61 – 4.28 (m, 2H), 2.82 – 2.66 (m, 2H), 1.53 – 1.47 (m, 3H). ^{13}C NMR (126 MHz, Chloroform-d) δ 170.42, 170.36, 170.32, 170.30, 170.00, 169.73, 69.40, 69.32, 69.16, 69.12, 60.58, 60.52, 60.42, 33.45, 33.43, 33.41, 33.31, 16.89, 16.85, 16.84, 16.77. HRMS (ESI) calculated for $[C_{18}H_{24}NaO_{12}]^+$, $[C_{24}H_{32}NaO_{16}]^+$, or $[C_{30}H_{40}NaO_{20}]^+$ {M+Na} requires 455.1166, 599.1588, or 743.2011, found 455.1130, 599.1579, and 734.2014.

Racemic: HPLC, Whelk-O®-1-(S,S) 5 µm 100 Å, 30% iPrOH/Hexane, 1 mL/min, 220 nm

Peak	Area (%)	Area	RT (min)	Height (mAU)
1	5.124	218.396	9.127	10.08
2	47.526	2027.069	13.000	50.53
3	47.354	2019.714	14.971	35.52
Total	100	4265.179		

Sodium 2-(3-hydroxy-2-methylpropoxy)acetate (4). A 500 mL round bottom flask with a magnetic stir bar was charged with 2-methyl-1,3-propanediol (187 g, 2.1 mol) and heated to 70 °C. Small pieces of solid Na (11.1 g, 0.48 mol) rinsed in hexanes was added to the flask in small additions over 8 h. *(Safety note: Solid sodium (Na) metal is highly reactive and can spontaneously ignite in air. Additionally, hydrogen gas is highly flammable and evolves over the course of the reaction. Proper engineering controls and*

safety equipment is required.) After Na completely dissolved, the reaction was heated to 100 °C. Sodium chloroacetate (53.4 g, 0.46 mol) was added in 3–5 g increments with ~15 min between additions. After the last addition, the reaction was left to react at 100 °C overnight. After allowing to cool to room temperature, the mixture was diluted with MeOH (100 mL) and the reaction mixture was filtered. The solid NaCl was rinsed with MeOH. Sodium 2-(3-hydroxy-2-methylpropoxy)acetate was isolated by precipitating the filtrate in acetone (×3). The solid was collected and dried in vacuo to yield an off-white solid. ^{1}H NMR (500 MHz, D_2O) δ 3.91 (s, 1H), 3.63 – 3.37 (m, 3H), 2.23 (d, J = 1.1 Hz, 1H), 1.98 (h, J = 6.5 Hz, 1H), 0.92 (d, J = 7.0 Hz, 2H).

6,13-dimethyl-1,4,8,11-tetraoxacyclotetradecane-2,9-dione (dGA-2MD). Sodium 2-(3-hydroxy-2-methylpropoxy)acetate was dissolved in a minimal amount of water, cooled, then conc. HCl was added dropwise until pH 1. 2-(3-hydroxy-2-methylpropoxy)acetic acid (4.0 g, 27.0 mmol) was extracted into DCM, dried over $MgSO_4$, and concentrated to 100 mL. A 500 mL round bottom flask equipped with a stir bar, DCM (170 mL), *p*-TsOH (1.0 g, 5.4 mmol), 4 Å molecular sieves (5 g) was purged with nitrogen and the 2-(3-hydroxy-2-methylpropoxy)acetic acid solution was added dropwise. After the final addition, the reaction was left at room temperature for 24 h. Insoluble solids were removed by filtration. The filtrate was washed with saturated sodium bicarbonate then brine, dried over $MgSO_4$, filtered through basic alumina, and concentrated to yield crude product as a mixture of 14-membered macrolactone to higher order oligomers. The residue was recrystallized from hot toluene. The crystalline product was then purified further in batches by sublimation (90 °C, 100 mtorr) to give dGA-2MD as a white powder. The

remaining oily residue in the sublimation apparatus was composed largely of higher order oligomers. ^{1}H NMR (500 MHz, $CDCl_3$) δ 4.34 (ddd, J = 38.1, 10.8, 3.8 Hz, 1H), 4.22 – 3.95 (m, 3H), 3.64 – 3.42 (m, 2H), 2.14 (m, 1H), 0.98 (dd, J = 7.1, 3.3 Hz, 3H). ^{13}C NMR (126 MHz, $CDCl_3$) δ 171.02, 72.49, 72.30, 69.42, 69.36, 65.43, 65.36, 33.43, 33.17, 14.07, 13.98. HRMS (ESI) calculated for $[C_{12}H_{20}O_6Na]^+$ {M+Na} requires 283.1158, found 283.1150.

Polymerization of dGA-2MD. All polymerizations were set up in a nitrogen filled glove box using oven-dried vials equipped with a magnetic stir bar and sealed with a Teflon cap. The vial was charged with catalyst (TBD/BDM or Ti(O*i*-Pr)$_4$), with the amounts varied depending on desired molar mass. dGA-2MD was subsequently added to the vial, followed by toluene for solution polymerizations. The vial was sealed, brought out of the glove box and immersed in an oil bath preheated at 100 °C at the indicated times (Table 2.2 and 2.4). The vial was then cooled to room temperature then exposed to air. The polymer was purified by precipitation into cold methanol or hexanes from a minimal amount of toluene. The resulting polymer was dried overnight in vacuo. ^{1}H NMR (400 MHz, $CDCl_3$) δ 4.25 – 3.94 (m, 228H), 3.65 – 3.36 (m, 119H), 2.26 – 2.06 (m, J = 6.5 Hz, 58H), 0.98 (d, J = 6.9 Hz, 163H). (Ti(O*i*-Pr)$_4$ polymerization δ 5.06 (h, J = 6.2 Hz, 1H) and TBD/BDM polymerization δ 7.42 – 7.30 (m, 4H), 5.18 (s, 4H).) ^{13}C NMR (126 MHz, $CDCl_3$) δ 170.54, 73.59, 68.53, 66.71, 33.49, 14.08.

Polymerization of dLA-HP in bulk. All polymerizations were set up in a nitrogen filled glove box using oven-dried vials sealed with a Teflon cap. The amount of Ti(O*i*-Pr)$_4$ used for each polymerization varied depending on desired molar mass. In a representative

experiment: an oven-dried vial with a magnetic stir bar was charged first with Ti(O*i*-Pr)$_4$ (2.63 µL, 0.0087 mmol) followed by dLA-HP (1.00 g, 3.47 mmol). The vial was sealed, brought out of the glove box and immersed in an oil bath preheated at 115 °C for 24 h during which stirring stopped. The vial was then cooled to room temperature to provide the crude polymer. The polymer was purified by precipitation into cold isopropanol from a minimal amount of chloroform (×3). The resulting polymer was then dried overnight in a vacuum oven at 70 °C to give the pure polymer (731 mg, 71% yield). THF SEC-MALLS analysis, dn/dc = 0.051: M_n = 36 kg mol^{-1}, M_w = 54 kg mol^{-1}, $Đ$ = 1.5. ^{1}H NMR (500 MHz, Chloroform-d) δ 5.28 – 5.02 (m, 1H), 4.53 – 4.32 (m, 2H), 2.88 – 2.63 (m, 2H), 1.66 – 1.45 (m, 4H). ^{13}C NMR (126 MHz, CDCl3) δ 170.18, 170.16, 170.02, 169.89, 169.67, 69.24, 69.09, 68.86, 68.83, 68.71, 60.63, 60.54, 60.51, 60.40, 60.08, 59.93, 33.52, 33.44, 33.41, 33.37, 16.77.

Polymerization of dLA-HP in solution (3 M toluene): All polymerizations were set up in a nitrogen filled glove box in oven-dried vials with Teflon caps using anhydrous toluene. The amount of Ti(O*i*-Pr)$_4$ used for each polymerization varied depending on the desired molar mass. In a representative experiment: an oven-dried vial with a magnetic stir bar was charged sequentially with Ti(O*i*-Pr)$_4$ (5.27 µL, 0.017 mmol), (*R*,*R*)-dLA-3HP (500.1 mg, 1.74 mmol), and toluene (0.58 mL). The vial was sealed, brought out of the glove box and immersed in an oil bath preheated at 100 °C for 4 h during which the reaction mixture became very viscous and stirring slowed or stopped. The vial was then cooled to room temperature, opened to atmosphere, and the solvent removed under reduced pressure to provide the crude polymer. The polymer was purified by precipitation into cold

isopropanol from a minimal amount of chloroform (×3). The resulting polymer was then dried in a vacuum oven overnight at 70 °C to give the pure polymer (475.2 mg, 95 % yield). THF SEC-MALLS analysis, dn/dc = 0.051: M_n = 35 kg mol^{-1}, M_w = 49 kg mol^{-1}, $Đ$ = 1.4. The spectral data agree with those described above. $[\alpha]_D^{25.7}$ +33.0 (*c* 0.766, $CDCl_3$).

Polymerization of PDL. Polymerizations were set up in a nitrogen filled glovebox using Teflon capped pressure vessels. The amount of Ti(O*i*-Pr)$_4$ used varied depending on the desired molar mass. In a representative experiment: A 15 mL oven dried pressure vessel with a magnetic stir bar was charged with Ti(O*i*-Pr)$_4$ (4.56 µL, 4.37µmol) and PDL (3.70 g, 15.39 mmol). The pressure vessel was sealed, brought out of the glove box, and immersed in an oil bath preheated at 130 °C for one h during which stirring stopped. After this time the reaction vessel was cooled to room temperature and the crude polymer crystallized. The polymer was purified by precipitating a concentrated chloroform solution of the crude product into rapidly stirring methanol providing the pure polymer as a white semi-crystalline solid (3.42 g, 92 % yield). ^{1}H NMR end group analysis: M_n = 73.5 kg mol^{-1}. Spectral data match those reported previously in the literature. ^{1}H NMR (500 MHz, Chloroform-*d*) δ 5.02 (hept, *J* = 6.3 Hz, end-group), 4.07 (t, *J* = 6.8 Hz, 2H), 2.30 (t, *J* = 7.6 Hz, 2H), 1.68 – 1.57 (p, *J* = 7.0 Hz, 4H), 1.41 – 1.16 (m, 22H). ^{13}C NMR (126 MHz, Chloroform-*d*) δ 174.11, 64.52, 34.53, 29.77, 29.77 29.74, 29.67, 29.61, 29.42, 29.40, 29.31, 28.79, 26.07, 25.15.

Kinetics experiments. The kinetics experiments for each monomer were setup as described above for polymerizations in solution at a concentration of 1M in toluene with

0.5 mol% Ti(O*i*-Pr)$_4$ using a septum capped vial. In a typical experiment: in a nitrogen filled glove box an oven dried vial was charged with Ti(O*i*-Pr)$_4$ (0.005 mmol), monomer (1 mmol), and toluene (1 mL). The vial was sealed with a septum cap, removed from the glove box, and immersed in an oil bath preheated at 90 °C. Aliquots were removed at regular intervals using a clean dry syringe. Each aliquot was divided into two with the first portion being concentrated under reduced pressure and taken up in $CDCl_3$ for ^{1}H NMR analysis and the second portion being precipitated directly into cold isopropanol for characterization using $CHCl_3$ SEC. The overall conversion for dLA-HP was determined by comparing the integration of the β-methylene protons of the 3-HP fragment of the monomer with the same protons on the polymer backbone for which there was no signal overlap. The overall conversion for dGA-3MO was determined comparing the combined integrations of the δ-methine proton of dGA-3MO and P(GA-alt-3MO) with the isolated downfield ε-methylene protons of the monomer. Plotting $[M]_t$ vs. time and applying equation 2 to an exponential fit of the decay curve provides the observed rate constant k_{obs} for each monomer under these conditions. A plot of molecular weight vs. conversion for each monomer shows a linear correlation.

$$[M]_t = [M]_{eq} + A * e^{-kt} \tag{2.2}$$

Thermodynamics experiments. The thermodynamics experiments were set up in triplicate as described above for polymerizations in solution at a concentration of 1M in toluene with 1 mol% Ti(O*i*-Pr)$_4$ using oven-dried vials sealed with Teflon caps. A stock solution of Ti(*i*-OPr)$_4$ (0.01 M in toluene) was prepared in a nitrogen filled glove box in an

oven-dried vial by dissolving Ti(*i*-OPr)$_4$ (28.4 mg, 0.1 mmol) in toluene (10 mL). This stock solution was used for all thermodynamics experiments. In a typical experiment: in a nitrogen filled glove box three oven dried vials were each charged with monomer (0.34 mmol) and Ti(*i*-OPr)$_4$ stock solution (0.34 mL). The vials were then sealed, brought out of the glove box, and immersed in a pre-heated temperature-controlled oil bath for one week. After this time two of the vials were removed from the heating bath, concentrated under reduced pressure and taken up in $CDCl_3$ for ^{1}H NMR analysis. The third vial was allowed to react for an additional two days to ensure that no further conversion occurred. Equilibrium monomer concentration ($[M]_{eq}$) for each experiment was determined by comparing the integration of monomer proton signals to those of the polymer. The data were then plotted as $\ln([M]_{eq}/[M]_{ss})$ vs. 1/T. Applying equation 1 to a linear fit of each plot allowed for determination of the thermodynamic parameters.

2.5 References

(1) MacArthur, E. Beyond Plastic Waste. *Science* **2017**, *358*, 843–843.

(2) Albertsson, A.-C.; Hakkarainen, M. Designed to Degrade. *Science* **2017**, *358*, 872–873.

(3) Tong, R. New Chemistry in Functional Aliphatic Polyesters. *Ind. Eng. Chem. Res.* **2017**, *56*, 4207–4219.

(4) Poly(Lactic Acid): Synthesis, Structures, Properties, Processing, and Applications; Auras, R. A.; Lim, L.-T.; Selke, S. E. M.; Tsuji, H., Eds.; John Wiley & Sons, Inc.: Hoboken, NJ, USA, 2010.

(5) Luckachan, G. E.; Pillai, C. K. S. Biodegradable Polymers – A Review on Recent Trends and Emerging Perspectives. *J. Polym. Environ.* **2011**, *19*, 637–676.

(6) Wu, J.; Yu, T.; Chen, C.; Lin, C. Recent Developments in Main Group Metal Complexes Catalyzed/Initiated Polymerization of Lactides and Related Cyclic Esters. *Coord. Chem. Rev.* **2006**, *250*, 602–626.

(7) O'Keefe, B. J.; Hillmyer, M. A.; Tolman, W. B. Polymerization of Lactide and Related Cyclic Esters by Discrete Metal Complexes. *J. Chem. Soc. Dalt. Trans.* **2001**, 2215–2224.

(8) Dove, A. P. Organic Catalysis for Ring-Opening Polymerization. *ACS Macro Lett.* **2012**, *1*, 1409–1412.

(9) Duda, A.; Kowalski, A.; Penczek, S.; Uyama, H.; Kobayashi, S. Kinetics of the Ring-Opening Polymerization of 6-, 7-, 9-, 12-, 13-, 16-, and 17-Membered Lactones. Comparison of Chemical and Enzymatic Polymerizations. *Macromolecules* **2002**, *35*, 4266–4270.

(10) Penczek, S.; Cypryk, M.; Duda, A.; Kubisa, P.; Słomkowski, S. Living Ring-Opening Polymerizations of Heterocyclic Monomers. *Prog. Polym. Sci.* **2007**, *32*, 247–282.

(11) Kiesewetter, M. K.; Shin, E. J.; Hedrick, J. L.; Waymouth, R. M. Organocatalysis: Opportunities and Challenges for Polymer Synthesis. *Macromolecules* **2010**, *43*, 2093–2107.

(12) Hori, Y.; Hongo, H.; Hagiwara, T. Ring-Opening Copolymerization of (R)-β-Butyrolactone with Macrolide: A New Series of Poly(Hydroxyalkanoate)S. *Macromolecules* **1999**, *32*, 3537–3539.

(13) Kricheldorf, H. R.; Rost, S. Biodegradable Multiblock Copolyesters Prepared from ε-Caprolactone, L-Lactide, and Trimethylene Carbonate by Means of Bismuth Hexanoate. *Macromolecules* **2005**, *38*, 8220–8226.

(14) Kumar, A.; Kalra, B.; Dekhterman, A.; Gross, R. A. Efficient Ring-Opening Polymerization and Copolymerization of ε-Caprolactone and ω-Pentadecalactone Catalyzed by Candida Antartica Lipase B. *Macromolcules* **2000**, *33*, 6303–6309.

(15) Beckingham, B. S.; Sanoja, G. E.; Lynd, N. a. Simple and Accurate Determination of Reactivity Ratios Using a Nonterminal Model of Chain Copolymerization. *Macromolecules* **2015**, *48*, 6922–6930.

(16) Duda, A.; Penczek, S. Thermodynamics, Kinetics, and Mechanisms of Cyclic Esters Polymerization. In *Polymers from Renewable Resources*; Scholz, C.; Gross, R. A., Eds.; ACS Symposium Series; American Chemical Society: Washington, DC, 2001; Vol. 764, pp. 160–198.

(17) Dechy-Cabaret, O.; Martin-Vaca, B.; Bourissou, D. Controlled Ring-Opening Polymerization of Lactide and Glycolide. *Chem. Rev.* **2004**, *104*, 6147–6175.

(18) Stayshich, R. M.; Meyer, T. Y. New Insights into Poly(Lactic-co-Glycolic Acid) Microstructure: Using Repeating Sequence Copolymers to Decipher Complex NMR and Thermal Behavior. *J. Am. Chem. Soc.* **2010**, *132*, 10920–10934.

(19) Dong, C.; Qiu, K.; Gu, Z.; Feng, X. Synthesis of Poly(D,L-Lactic Acid-Alt-Glycolic Acid) from D,L-3-Methylglycolide. *J. Polym. Sci. Part A Polym. Chem.* **2000**, *38*, 4179–4184.

(20) Kumar, V.; Ashok, S.; Park, S. Recent Advances in Biological Production of 3-Hydroxypropionic Acid. *Biotechnol. Adv.* **2013**, *31*, 945–961.

(21) Zhang, D.; Hillmyer, M. A.; Tolman, W. B. A New Synthetic Route to Poly[3-Hydroxypropionic Acid] (P[3-HP]): Ring-Opening Polymerization of 3-HP Macrocyclic Esters. *Macromolecules* **2004**, *37*, 8198–8200.

(22) Andreeßen, B.; Steinbüchel, A. Biosynthesis and Biodegradation of 3-Hydroxypropionate-Containing Polyesters. *Appl. Environ. Microbiol.* **2010**, *76*, 4919–4925.

(23) Gilding, D. K.; Reed, A. M. Biodegradable Polymers for Use in Surgery-Polyglycolic/Poly(Lactic Acid) Homo- and Copolymers: 1. *Polymer* **1979**, *20*, 1459–1464.

(24) Riande, E.; De la Campa, J. G.; Guzman, J.; De Abajo, J. Ring-Opening Polymerization of 3-Methyloxetane: NMR Spectroscopy and Configurational Properties of the Polymer. *Macromolecules* **1984**, *17*, 1431–1436.

(25) Li, S.; Vert, M. Biodegradation of Aliphatic Polyesters. In *Degradable Polymers*; Scott, G., Ed.; Kluwer Academic Publishers, 2002; 71–131.

(26) Bechtold, K.; Hillmyer, M. A.; Tolman, W. B. Perfectly Alternating Copolymer of Lactic Acid and Ethylene Oxide as a Plasticizing Agent for Polylactide. *Macromolecules*, **2001**, *34*, 8641–8648.

(27) Gallezot, P. Catalytic Routes from Renewables to Fine Chemicals. *Catal. Today* **2007**, *121*, 76–91.

(28) Zhang, D.; Xu, J.; Alcazar-Roman, L.; Greenman, L.; Cramer, C. J.; Hillmyer, M. A.; Tolman, W. B. Isotactic Polymers with Alternating Lactic Acid and Oxetane Subunits from the Endoentropic Polymerization of a 14-Membered Ring. *Macromolecules* **2004**, *37*, 5274–5281.

(29) Mathisen, T.; Albertsson, A.-C. Polymerization of 1,5-Dioxepan-2-One. 1. Synthesis and Characterization of the Monomer 1,5-Dioxepan-2-One and Its Cyclic Dimer 1,5,8,12-Tetraoxacyclotetradecane-2,9-Dio. *Macromolecules* **1989**, *22*, 3838–3842.

(30) Nørskov-Lauritsen, L.; Bürgi, H.-B.; Hofmann, P.; Schmidt, H. R. Bond Angles in Lactones and Lactams. *Helv. Chim. Acta* **1985**, *68*, 76–82.

(31) Dale, J. Conformational Aspects of Many-Membered Rings. *Angew. Chemie Int. Ed. English* **1966**, *5*, 1000–1021.

(32) Keller, T. H.; Neeland, E. G.; Rettig, S.; Trotter, J.; Weiler, L. Conformational Analysis of 14-Membered Macrolides Using x-Ray Crystallography and Molecular Mechanics Calculations. *J. Am. Chem. Soc.* **1988**, *110*, 7858–7868.

(33) van der Meulen, I.; Gubbels, E.; Huijser, S.; Sablong, R.; Koning, C. E.; Heise, A.; Duchateau, R. Catalytic Ring-Opening Polymerization of Renewable Macrolactones to High Molecular Weight Polyethylene-like Polymers. *Macromolecules* **2011**, *44*, 4301–4305.

(34) Pepels, M. P. F.; Bouyahyi, M.; Heise, A.; Duchateau, R. Kinetic Investigation on the Catalytic Ring-Opening (Co)Polymerization of (Macro)Lactones Using Aluminum Salen Catalysts. *Macromolecules* **2013**, *46*, 4324–4334.

(35) Hodge, P. Entropically Driven Ring-Opening Polymerization of Strainless Organic Macrocycles. *Chem. Rev.* **2014**, *114*, 2278–2312.

(36) Pepels, M. P. F.; Souljé, P.; Peters, R.; Duchateau, R. Theoretical and Experimental Approach to Accurately Predict the Complex Molecular Weight Distribution in the Polymerization of Strainless Cyclic Esters. *Macromolecules* **2014**, *47*, 5542–5550.

(37) Wilson, J. A.; Hopkins, S. A.; Wright, P. M.; Dove, A. P. 'Immortal' Ring-Opening Polymerization of ω-Pentadecalactone by Mg(BHT) 2 (THF) 2. *Polym. Chem.* **2014**, *5*, 2691–2694.

(38) Pascual, A.; Sardon, H.; Veloso, A.; Ruipérez, F.; Mecerreyes, D. Organocatalyzed Synthesis of Aliphatic Polyesters from Ethylene Brassylate: A Cheap and Renewable Macrolactone. *ACS Macro Lett.* **2014**, *3*, 849–853.

(39) Jasinska-Walc, L.; Bouyahyi, M.; Rozanski, A.; Graf, R.; Hansen, M. R.; Duchateau, R. Synthetic Principles Determining Local Organization of Copolyesters Prepared from Lactones and Macrolactones. *Macromolecules* **2015**, *48*, 502–510.

(40) Pepels, M. P. F.; van der Sanden, F.; Gubbels, E.; Duchateau, R. Catalytic Ring-Opening (Co)Polymerization of Semiaromatic and Aliphatic (Macro)Lactones. *Macromolecules* **2016**, *49*, 4441–4451.

(41) Wang, B.; Pan, L.; Ma, Z.; Li, Y. Ring-Opening Polymerization with Lewis Pairs and Subsequent Nucleophilic Substitution: A Promising Strategy to Well-Defined Polyethylene-like Polyesters without Transesterification. *Macromolecules* **2018**, *51*, 836–845.

(42) Bouyahyi, M.; Pepels, M. P. F.; Heise, A.; Duchateau, R. ω-Pentandecalactone Polymerization and ω-Pentadecalactone/ε-Caprolactone Copolymerization Reactions Using Organic Catalysts. *Macromolecules* **2012**, *45*, 3356–3366.

(43) Ono, N.; Miyake, H.; Fujii, M.; Kaji, A. *Tet. Lett*. **1983**, *24*, 3477–3480.

(44) Mahoney, J. E. Acrylic Acid Production Methods. U.S. Application No. 15,247,833, August 25, 2016.

(45) Duda, A.; Kowalski, A.; Penczek, S.; Uyama, H.; Kobayashi, S. Kinetics of the Ring-Opening Polymerization of 6-, 7-, 9-, 12-, 13-, 16-, and 17-Membered Lactones. Comparison of Chemical and Enzymatic Polymerizations. *Macromolecules* **2002**, *35*, 4266–4270.

(46) van der Meulen, I.; de Geus, M.; Antheunis, H.; Deumens, R.; Joosten, E. A. J.; Koning, C. E.; Heise, A. Polymers from Functional Macrolactones as Potential Biomaterials: Enzymatic Ring Opening Polymerization, Biodegradation, and Biocompatibility. *Biomacromolecules* **2008**, *9*, 3404–3410.

(47) Witt, T.; Häußler, M.; Mecking, S. No Strain, No Gain? Enzymatic Ring-Opening Polymerization of Strainless Aliphatic Macrolactones. *Macromol. Rapid Commun.* **2017**, *38*, 1600638.

(48) Kumar, A.; Kalra, B.; Dekhterman, A.; Gross, R. A. Efficient Ring-Opening Polymerization and Copolymerization of ε-Caprolactone and ω-Pentadecalactone Catalyzed by Candida Antartica Lipase B. *Macromolecules* **2000**, *33*, 6303–6309.

(49) van der Mee, L.; Helmich, F.; de Bruijn, R.; Vekemans, J. A. J. M.; Palmans, A. R. A.; Meijer, E. W. Investigation of Lipase-Catalyzed Ring-Opening Polymerizations of Lactones with Various Ring Sizes: Kinetic Evaluation. *Macromolecules* **2006**, *39*, 5021–5027.

(50) Kobayashi, S.; Uyama, H.; Namekawa, S.; Hayakawa, H. Enzymatic Ring-Opening Polymerization and Copolymerization of 8-Octanolide by Lipase Catalyst. *Macromolecules* **1998**, *31*, 5655–5659.

(51) Slivniak, R.; Domb, A. J. Macrolactones and Polyesters from Ricinoleic Acid. *Biomacromolecules* **2005**, *6*, 1679–1688.

(52) Albertsson, A.-C.; Varma, I. K. Recent Developments in Ring Opening Polymerization of Lactones for Biomedical Applications. *Biomacromolecules* **2003**, *4*, 1466–1486.

(53) *Handbook of Ring-Opening Polymerization*; Dubois, P.; Coulembier, O.; Raquez, J.-M., Eds.; Wiley-VCH Verlag GmbH & Co. KGaA: Weinheim, Germany, 2009.

(54) Chuck, C. J.; Davidson, M. G.; Jones, M. D.; Kociok-, G.; Lunn, M. D.; Wu, S. Air-Stable Titanium Alkoxide Based Metal-Organic Framework as an Initiator for Ring-Opening Polymerization of Cyclic Esters. *Inorg. Chem.* **2006**, *45*.

(55) Le Roux, E. Recent Advances on Tailor-Made Titanium Catalysts for Biopolymer Synthesis. *Coord. Chem. Rev.* **2016**, *306*, 65–85.

(56) Kim, Y.; Jnaneshwara, G. K.; Verkade, J. G. Titanium Alkoxides as Initiators for the Controlled Polymerization of Lactide. *Inorg. Chem.* **2003**, *42*, 1437–1447.

(57) Durr, C. B.; Williams, C. K. New Coordination Modes for Modified Schiff Base Ti(IV) Complexes and Their Control over Lactone Ring-Opening Polymerization Activity. *Inorg. Chem.* **2018**, *57*, 14240–14248.

(58) Zing, J-B.; Srinivansan, M.; Li, Y-D.; Narayan, R.; Wang, Y-Z. *Journal of Polymer Science: Part A: Polymer Chemistry*, **2010**, *48*, 5885–5890

(59) de Geus, M.; van der Meulen, I.; Goderis, B.; van Hecke, K.; Dorschu, M.; van der Werff, H.; Koning, C. E.; Heise, A. Performance Polymers from Renewable Monomers: High Molecular Weight Poly(Pentadecalactone) for Fiber Applications. *Polym. Chem.* **2010**, *1*, 525–533.

(60) Schneiderman, D. K.; Hillmyer, M. A. Aliphatic Polyester Block Polymer Design. *Macromolecules* **2016**, *49*, 2419–2428.

(61) Myers, D.; Witt, T.; Cyriac, A.; Bown, M.; Mecking, S.; Williams, C. K. Ring Opening Polymerization of Macrolactones: High Conversions and Activities Using an Yttrium Catalyst. *Polym. Chem.* **2017**, *8*, 5780–5785.

(62) Olsén, P.; Odelius, K.; Albertsson, A. C. Thermodynamic Presynthetic Considerations for Ring-Opening Polymerization. *Biomacromolecules* **2016**, *17*, 699–709.

(63) Yevstropov, A. A.; Lebedev, B. V.; Kiparisova, Y. G. *Vysokomol. Soyed.*, **1983**, *A25*, 1679–1685.

(64) Li, Y.; Hoskins, J. N.; Sreerama, S. G.; Grayson, M. A.; Grayson, S. M. *Journal of Mass Spectrometry*, **2010**, *45*, 587–611

(65) Bouyahyi, M.; Duchateau, R. Metal-Based Catalysts for Controlled Ring-Opening Polymerization of Macrolactones: High Molecular Weight and Well-Defined Copolymer Architectures. *Macromolecules* **2014**, *47*, 517–524.

(66) Fox, T. G. Influence of Diluent and of Copolymer Composition on the Glass Temperature of a Polymer System. *Bull. Am. Phys. Soc.*, **1956**, *1*, 123.

(67) Yamauchi, T.; Hattori, K.; Nakao, K.; Tamaki, K. Preparation of 2-Arylpropanoates by the Reaction of 2-Hydroxypropiophenone Dimethyl Acetals with Sulfuryl Chloride in the Presence of an Amide or a Weak Base. *Bull. Chem. Soc. Jpn.* **1987**, *60*, 4015–4018.

(68) Moore, J. S., Stupp, S. I. Room Temperature Polyesterification. *Macromolecules*, **1990**, *23*, 65–70.

(69) Williams, C. K.; Breyfogle, L. E.; Choi, S. K.; Nam, W.; Young, V. G.; Hillmyer, M. A.; Tolman, W. B. A Highly Active Zinc Catalyst for the Controlled Polymerization of Lactide. *J. Am. Chem. Soc.* **2003**, *125*, 11350–11359.

(70) Schmidt, T.; Kirschnig, A. Total Synthesis of Carolactone, a Highly Potent Biofilm Inhibitor. *Angew. Chem. Int. Ed.* **2012**, *51*, 1063–1066.

(71) Eckhard, H. BASF AG. *Tert*-butylesters of substituted 3-hydroxyproponoic acid. DE Application No. 3925256A1, January 31, 1991.

Chapter 3.

Strong, resilient, and sustainable aliphatic polyester thermoplastic elastomers[†]

[†] Reproduced in part with permission from Watts, A.; Kurokawa, N.; Hillmyer, M.A. Strong, resilient, and sustainable aliphatic polyester thermoplastic elastomers. *Biomacromolecules* **2017**, *18*, 1845–1854. © 2017 American Chemical Society. View full text of this article at https://pubs.acs.org/articlesonrequest/AOR-ecN58T8ZvPdRzTNghrKJ

3.1 Introduction

As we experience the detrimental impacts of persistent plastics, there have been significant efforts to investigate methods to circumvent the negative consequences of our plastic society. The polymer industry relies heavily on the use of non-renewable feedstocks and the generation of non-degradable products. Though some of these materials synthesized can be efficiently recycled or harvested for energy, some estimates suggest that 40% of the produced plastic packaging end up in the landfill and 32% leak into the environment.[1] Expanding the implementation of green chemistry principles for polymer research is important for the future of plastics.[2,3] By designing practical approaches that employ safe, non-toxic chemicals while limiting waste and energy, useful materials from sustainable resources can be generated and implemented.

Thermoplastic elastomers (TPEs) include ABA triblock copolymers that are typically composed of polystyrene (PS) as the glassy A block and polyisoprene (PI) or polybutadiene (PB) (and hydrogenated variants) as the rubbery B block.[4] TPEs have hard (i.e., high glass transition and/or high melting temperature) A blocks in the minority fraction that microphase separate from the soft (i.e., low glass transition temperature) B block in the majority fraction, resulting in a physically cross-linked material. The hard end blocks, connected by rubbery midblocks that usually contain trapped entanglements, allow for the materials to exhibit high ultimate tensile strength (σ_B) and strain at break (ε_B). TPEs are used in a broad range of applications such as coatings, pressure sensitive adhesives, medical devices, and in automotive parts; the properties can range from hard plastics to soft rubbers depending on composition and architecture.[4] Styrenic TPEs (PS-TPEs) are

petroleum derived and are extensively used due to their versatile properties and low cost. PS-*block*-PB-*block*-PS (SBS) has comparable properties to vulcanized (i.e., chemically cross-linked) natural rubber and exceed the properties of styrene-butadiene rubber (SBR); TPEs exhibit ultimate tensile strengths up to 30 MPa and 800% strain at break.[4] The entanglement molar masses, glass transition temperatures, and the thermodynamic incompatibility between the rubbery block and the PS block all contribute to the properties exhibited in the resulting TPEs.[4-6]

Significant research efforts have utilized aliphatic polyesters, which provide inherent hydrolytic degradability to the material, as alternatives to styrenic TPEs.[7-12] Polylactide (PLA) has long been studied as a sustainable substitute for PS, and this has been extended to the utilization of PLA as the hard end blocks in TPEs. Performance of PLA-TPEs reported in literature depends on the tacticity of the PLA block and the identity of the rubbery midblock. Non-crystalline aliphatic polyester midblocks in PLA-containing TPEs reported in the literature include: poly(β-methyl-δ-valerolactone) (PβMVL),[13] poly(ε-caprolactone-co-δ-valerolactone),[14] poly(1,5-dioxepan-2-one),[15] poly(menthide) (PM),[16-18] poly(ε-methyl-ε-caprolactone) (PεMCL),[19] poly(ε-decalactone) (PDL),[20] and poly(ε-caprolactone-co-ε-decalactone) (PCD).[21] Other aliphatic polyesters such as poly(ε-caprolactone) (PCL), which is semicrystalline, and poly(ε-caprolactone-co-LLA), which can be amorphous or semicrystalline, have also been studied in PLA-TPEs.[22-25] These aliphatic polyester systems exhibit promising mechanical properties that rival PS-based TPEs. In fact, some of these low glass transition temperature (T_g) midblocks were

generated from renewable resources and thus are even more attractive from a sustainability standpoint.

PβMVL-based TPEs are among the highest performing aliphatic polyester examples, exceeding the mechanical properties of SBS in some cases.[13] From sustainable and economic standpoints, PβMVL is an attractive target as the soft segment in TPEs. However, the low ceiling temperature for the polymerization of βMVL can lead to significant levels of residual monomer present at equilibrium when using reaction conditions at or above room temperature for neat monomer.[26] This in turn necessitates the rigorous removal of catalyst or some post-modification to limit complications from depolymerization.[27] The polymerization of ε-caprolactone derivatives are more thermodynamically driven toward the formation of polymer and do not face the same issues of high equilibrium monomer concentration at typical melt polymerization temperatures.[28,29] For example, the melt polymerization of ε-caprolactone at 130 °C reaches an equilibrium conversion of ~99%, whereas the same polymerization of the constitutional isomer βMVL reaches an equilibrium conversion of 57%.[13,30]

Though polymerizations of substituted ε-caprolactones are thermodynamically favorable, the position of the substituents in the ε-position impacts the rates of polymerization. The position of the methyl substituent at the γ-position exhibits faster rates of polymerization than the substituent at the ε-position, in both enzymatic and metal-catalyzed polymerizations.[31] Moreover, the polymerization of γ-methyl-ε-caprolactone (γMCL) is known to be faster than γ-substituted ε-caprolactones with longer alkyl chains (ethyl, butyl, and propyl substituents).[32] The low glass transition temperature of PγMCL

(T_g = −61 °C) has motivated the use of this polymer in biomedical applications.[33-40] Combined, these attributes make PγMCL an interesting and desirable polymer to incorporate into PLA-TPEs. Moreover, γMCL can be synthesized through the Baeyer-Villiger oxidation of 4-methylcyclohexanone, a molecule that can ultimately be sourced from cresols. Although cresols exist in nature, the major sources of cresols are from petroleum products and coal tar.[41] Recent efforts that demonstrate the transformation of renewable feedstocks into cresols provide enticing and practical routes to sustainably sourced γMCL.[42-44] Two particularly attractive approaches that hold tremendous promise are shown in Scheme 3.1.

Scheme 3.1.
Proposed retro-synthetic analysis of the synthesis of γ-methyl-ε-caprolactone from renewable feedstocks.[42,43]

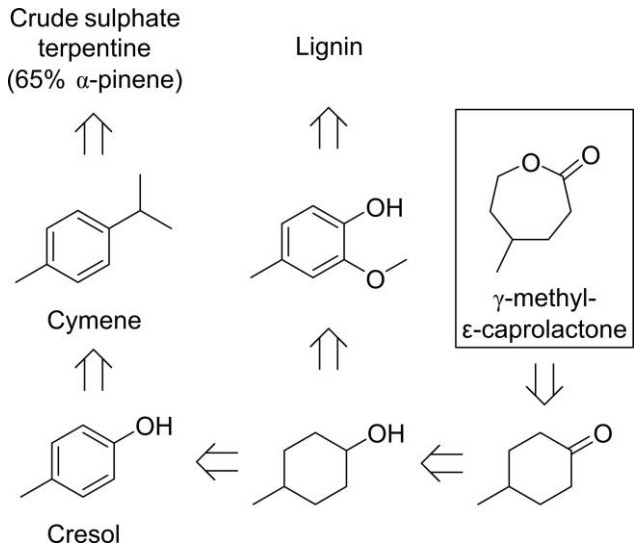

In this work, we report the use of PγMCL as the rubbery block in ABA triblock polymers with PLA as the end blocks to yield high performance PLA-TPEs. Furthermore,

we utilize the system PLA-*block*-PγMCL-*block*-PLA (LA-γMCL-LA) as a platform to better understand the effect of entanglements, microphase separation, and T_g in PLA-based TPEs. We also provide evidence for how crystallinity in the PLA end block improves mechanical properties. These results are compared to the properties and trends that have been studied in PS-based TPEs.

3.2 Results

To afford γMCL in high conversion with limited side-products, we employed a traditional Baeyer-Villiger oxidation using *meta*-chloroperoxybenzoic acid (*m*CPBA); alternatively, a green oxidant, Oxone®, can be used for this transformation.[18,19] After purification, the bulk polymerization of γMCL using a difunctional initiator, 1,4-benzenedimethanol (BDM), and the traditionally-utilized ring-opening transesterification polymerization catalyst $Sn(Oct)_2$ afforded an α,ω-hydroxy telechelic polymer (Scheme 3.2). The bulk ring-opening transesterification polymerization at 130 °C ($[\gamma MCL]_0$ = 7.95 M, $[BDM]_0$ = 0.051 M, and $[Sn(Oct)_2]_0$ = 0.016 M) was monitored over time by taking aliquots of the polymerization for analysis by ^1H NMR spectroscopy and size exclusion chromatography (SEC). The reaction reached 95% conversion after 1 h and near quantitative conversion (~99%) after 2 h (Figure 3.1a). Above 95% conversion, an increase in molar mass dispersity is evident due to intermolecular transesterification and/or equilibration phenomena, as described previously.[45,46] A linear relationship was observed between conversion and the molar mass of the polymer product (Figure 3.1b). The polymerization kinetics were first order in monomer, (Figure 3.1a, inset), however the

intercept appears to be positive, indicating the presence of polymer at t = 0 min. This is likely a result of the esterification reactions that occur at room temperature when the monomer, catalyst, and initiator are initially mixed;[47] the mixture of reagents at room temperature shows evidence of ring-opened γMCL and a shift in the benzylic protons by ^{1}H NMR spectroscopy (Figure 3.2). The pseudo first order rate constant averaged over three experiments at this concentration of $Sn(Oct)_2$ and at 130 °C is 0.050 min^{-1} (Figure 3.3). Assuming first order in catalyst concentration,[48] the average second order rate constant is 3.1 M^{-1} min^{-1}. The polymerization of γMCL catalyzed by $Sn(Oct)_2$ efficiently yields PγMCL with controlled molar mass and low dispersity.

Scheme 3.2.
Synthesis of PγMCL and LA-γMCL-LA.

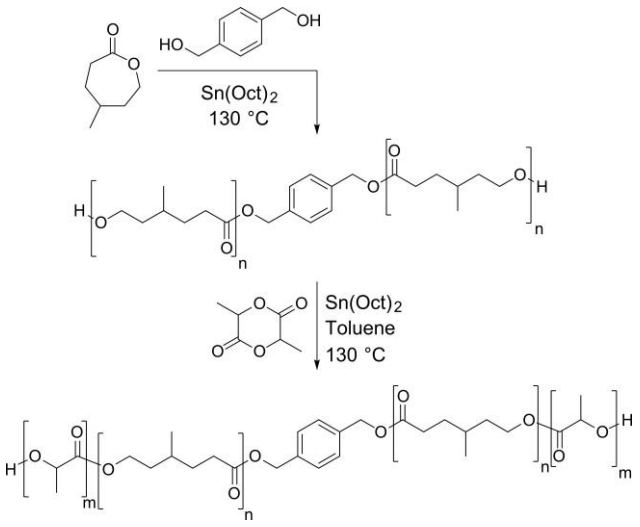

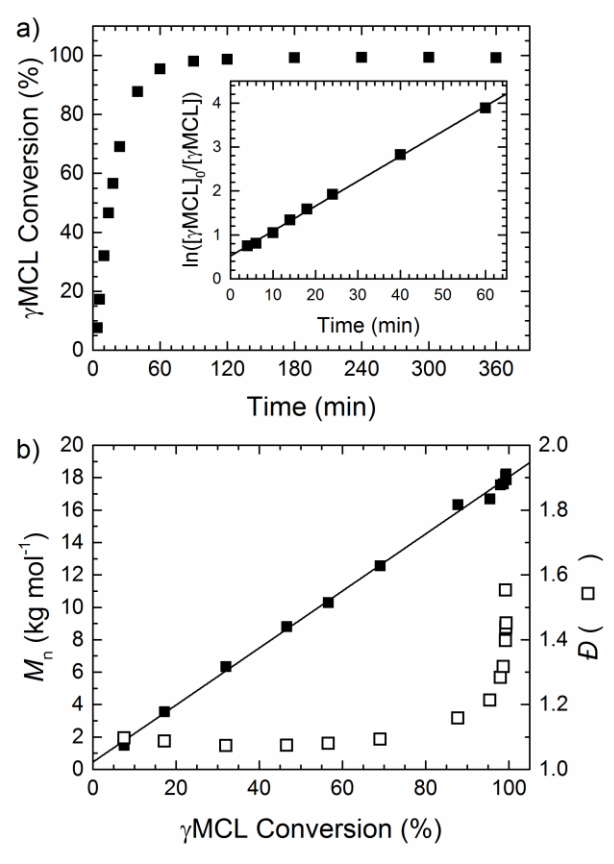

Figure 3.1.
Bulk polymerization of γMCL at 130 °C, $[\gamma MCL]_0$ = 7.96 M, $[BDM]_0$ = 0.051 M, $[Sn(Oct)_2]_0$ = 0.016 M. a) Conversion of γMCL determined by ^{1}H NMR spectroscopy as a function of time. The inset shows a linear fit of the kinetic data up to 60 min, where the reaction reaches 95% conversion. b) The molar mass (■) determined by end group analysis shows a linear relationship with conversion.

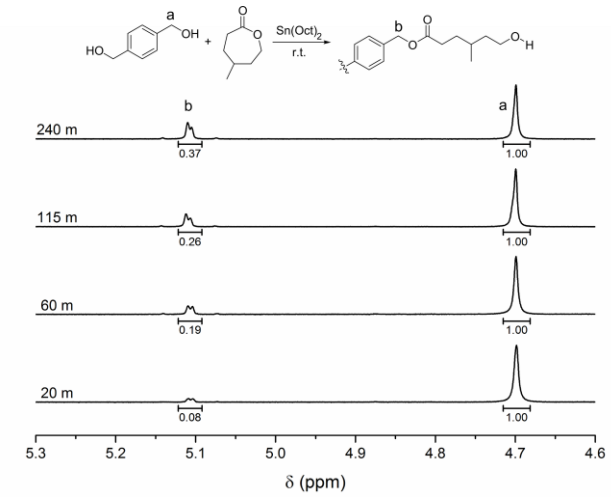

Figure 3.2.
Monomer, initiator and catalyst were combined and stirred at room temperature: $[\gamma MCL]_0$ = 7.96 M, $[BDM]_0$ = 0.051 M, $[Sn(Oct)_2]_0$ = 0.016 M. ^1H NMR spectra of the benzylic protons show room temperature esterification reactions between γMCL and benzene dimethanol noted by the shift from 4.7 ppm to 5.1 ppm.

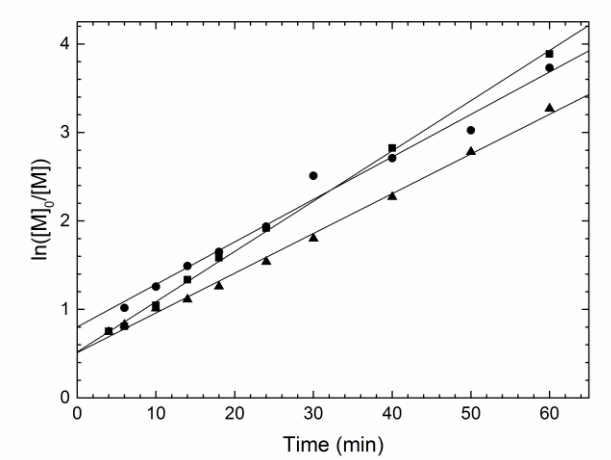

Figure 3.3.
Kinetic data was collected in triplicate for the bulk polymerization of γMCL. The linear fits provided the following rate constants k_{obs}(▲) = 0.045 ± 0.001 min^{-1} (R^2 = 0.995), k_{obs}(●) = 0.048 ± 0.002 min^{-1} (R^2 = 0.980), k_{obs}(■) = 0.057 ± 0.001 min^{-1} (R^2 = 0.998).

The polymerization of *rac*-lactide (known as D,L-(±)-lactide or LA) or (*S*,*S*)-lactide (known as L-(−)-lactide or LLA) from telechelic PγMCL catalyzed by $Sn(Oct)_2$ was carried out in toluene at 130 °C (Scheme 3.2). The SEC traces show the growth of the polymer

with no evidence of lower molar mass shoulders (representative data is shown Figure 3.4) and ^{1}H NMR spectroscopy shows a chemical shift of the end group (Section 3.5). Analysis of the PγMCL homopolymer via ^{13}C NMR spectroscopy indicates a distinct singlet in the carbonyl region that corresponds to a γMCL repeat unit adjacent to two γMCL units. In triblock copolymers, this PγMCL resonance remains unchanged with a second feature visible for PLA and PLLA in LA-γMCL-LA and LLA-γMCL-LLA samples, respectively (Figure 3.5).[49] The appearance of two features that correspond to the respective homopolymers indicates that highly pure blocks were formed with no evidence of transesterification between blocks.[18,19] A set of low molar mass volumetrically symmetric polymers with various molar masses were synthesized to determine the temperature dependent interaction parameter $\chi(T)$ while high molar mass polymers with various volume fractions of PLA were synthesized to study the mechanical properties for TPE applications. PLA-TPEs with PγMCL as the midblock were easily synthesized utilizing traditional polymerization catalyst and elevated temperature, providing control over molar mass and composition with low dispersity.

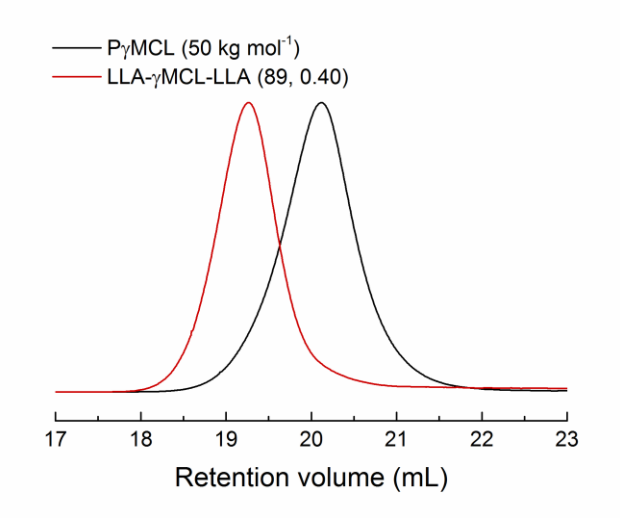

Figure 3.4.
Overlay of chloroform SEC traces for triblock polymers from 50 kg mol^{-1} PγMCL.

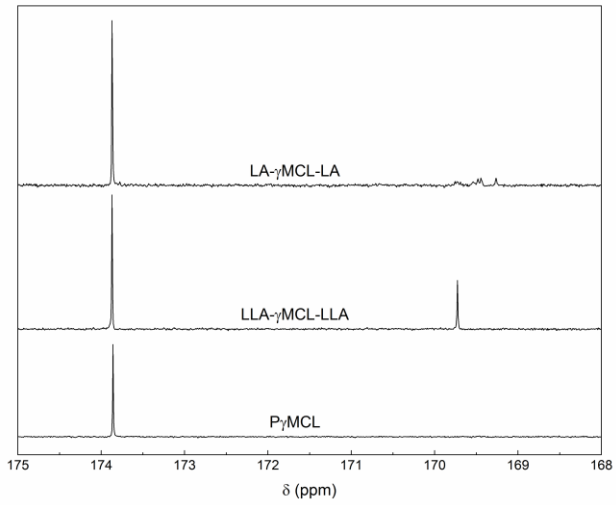

Figure 3.5.
^{13}C NMR spectra of the carbonyl carbon region showing a distinct singlet at 173.9 ppm for PγMCL, a singlet at 169.7 ppm for PLLA, and a multiplet at 169.5 ppm for PLA with no evidence of mixing between blocks due to the lack of other peaks in this region.

In a set of relatively low molar mass triblock samples, two glass transitions were observed by differential scanning calorimetry (DSC): one for the PγMCL block (−58 to −55 °C) and one for the PLA blocks (35 to 45 °C) (Table 3.1). The observed glass transition

temperature for PLA is lower than of the high molar mass homopolymer, likely due to the low molar mass of the PLA blocks. Small-angle X-ray scattering (SAXS) patterns of low molar mass polymers show long-range order and the samples with equivalent volume fractions of each block show reflections for lamellar morphology (Figure 3.6). Room temperature SAXS patterns and the evidence of two glass-transition temperatures corroborate the triblock polymers are microphase separated.

Table 3.1
Summary of symmetric (f_{LA} ~ 0.5) block polymers.

Sample ID ($M_{n,total}$, f_{LA})	$M_{n,P\gamma MCL}$[a] (kg mol-1)	$M_{n,PLA}$[a] (kg/mol)	$M_{n,total}$[a] (kg/mol)	f_{LA}[b]	$Đ$[c]	$T_{g,P\gamma MCL}$[d] (°C)	$T_{g,PLA}$[d] (°C)	T_{ODT}[e] (°C)
LA-γMCL-LA (20A, 0.49)	9.2	11	20	0.49	1.15	–55	36	84
LA-γMCL-LA (20B, 0.49)	9.3	11	20	0.49	1.14	–57	37	92
LA-γMCL-LA (23, 0.49)	10	12	23	0.49	1.17	–56	40	113
LA-γMCL-LA (27, 0.49)	12	14	27	0.49	1.25	–56	44	138
LA-γMCL-LA (27, 0.51)	12	15	27	0.51	1.16	–58	37	140
LA-γMCL-LA (30, 0.51)	13	17	30	0.51	1.20	–57	45	165

[a] determined using end-group analysis of ^{1}H NMR; [b] calculated using ρ_{PLA} = 1.25 g cm^{-3} and $\rho_{P\gamma MCL}$ = 1.037 g cm^{-3} at 25 °C; [c] chloroform SEC analysis with PS standards; [d] determined as the midpoint of the inflection on second heating at 10 °C min^{-1} in a DSC; [e] determined from the precipitous drop in DMTA heating at 1 °C min^{-1}.

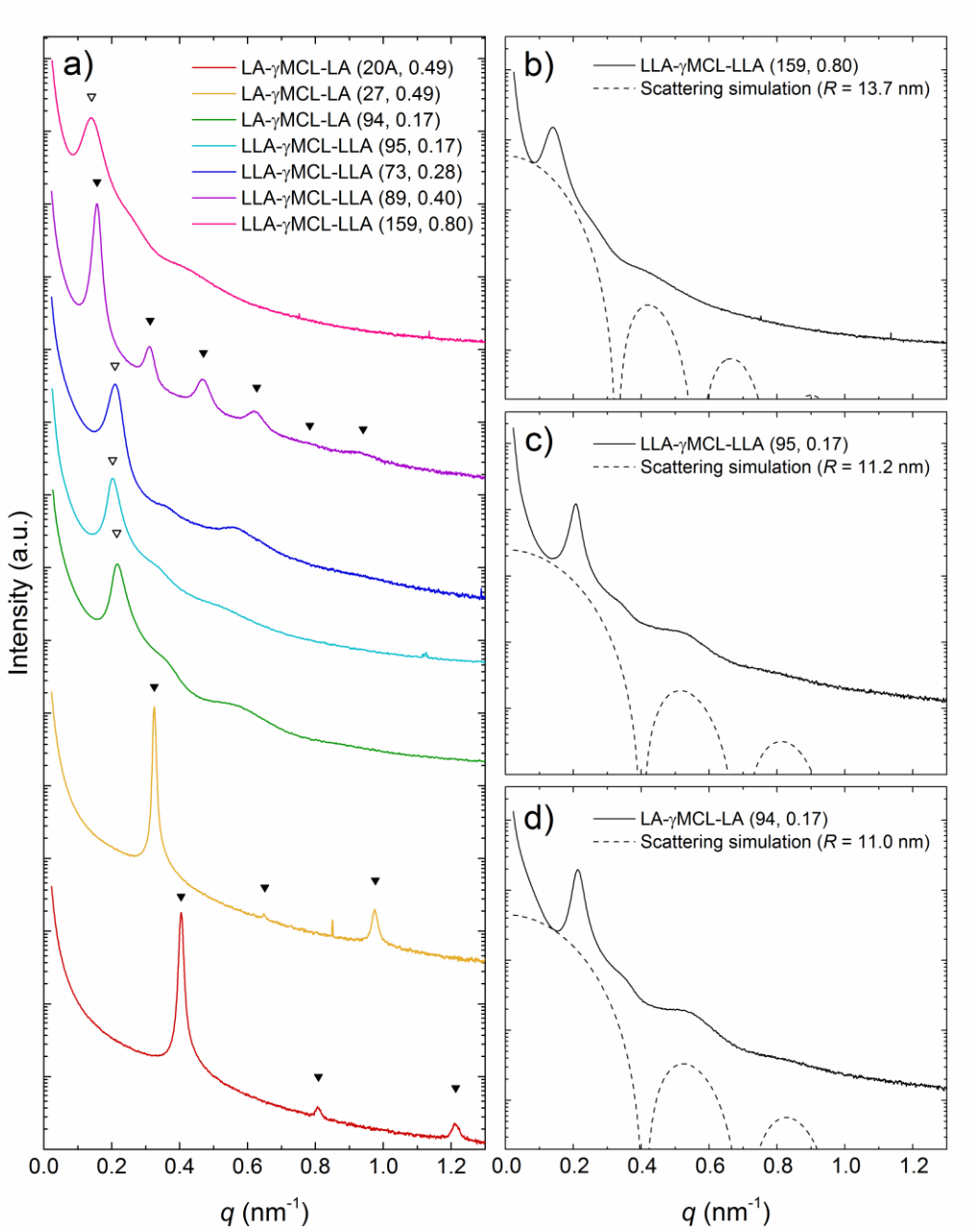

Figure 3.6.

a) Room temperature SAXS patterns, filled triangles indicate the expected peaks for lamellar morphology and open triangles indicate the principle peak. b-d) SAXS patterns of the indicated sample (solid line) with the simulated spherical form factor (dashed line):

$$P(q) = \left(\frac{3}{(qR)^3}\right)^2 (\sin qR - qR\cos qR)^2$$

Triblock polymers of low molar mass and equivalent volume fractions of PLA and PγMCL were melt-pressed at 70–110 °C to obtain uniform disks for dynamic mechanical thermal analysis (DMTA) experiments. A sample was placed between two 25 mm diameter parallel plates and the storage modulus was monitored while heating at 1 °C min^{-1} and oscillating at 1 rad s^{-1}. The order-disorder transition temperature T_{ODT} is evident by the precipitous drop in modulus (Figure 3.7 and Figure 3.8). Dynamic frequency sweeps below and above the ODT demonstrate that this drop in modulus is a result of the ODT (Figure 3.9 and Figure 3.10). We report results from both LA-γMCL-LA (20A, 0.49) and LA-γMCL-LA (20B, 0.49), though the samples appear to be the identical, as they exhibit a different T_{ODT} due to the slight difference in molar mass. A triblock polymer LA-γMCL-LA (27, 0.51) was also analyzed with temperature controlled SAXS, heating through the order-disorder transition, corroborating the results observed using DMTA (Figure 3.7). Plotting χ as a function of T^{-1} obtained from DMTA experiments, the temperature dependent interaction parameter $\chi(T)$ given in equation 3.1 was determined (Figure 3.8), using $(\chi N)_{ODT}$ = 17.996 and a reference volume of 118 $Å^3$ to calculate the degree of polymerization N.[50]

$$\chi(T) = \frac{51.6 \pm 2.1}{T} - (0.07 \pm 0.01) \tag{3.1}$$

The ODTs for the samples in Table 1 were observed above the T_g of PLA and below the temperature where 5% mass is lost in the sample ($T_{d,5\%}$ ~ 260 °C).

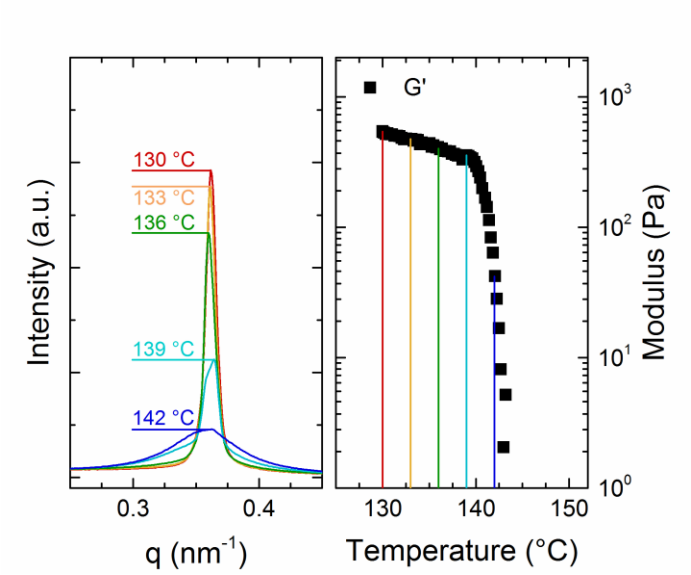

Figure 3.7.
SAXS analysis (left) and DMTA (right) upon heating showing ODT for LA-γMCL-LA (27, 0.51). For SAXS analysis, a sample was heated to the designated temperature, annealed 2 min, then analyzed. The decrease in the sharpness and intensity of the principle peak indicate the ODT at approximately 140 °C. The same polymer was subjected to DMTA where the ODT is indicated by the precipitous drop, also around 140 °C, in modulus upon heating at 1 °C min^{-1} in 25 mm plates with ω = 1 rad s^{-1} and 1% strain.

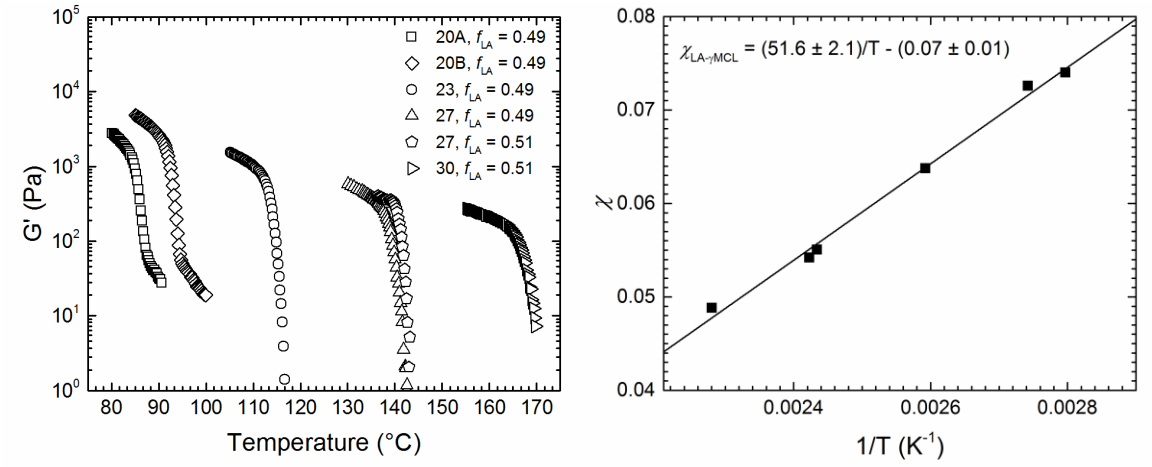

Figure 3.8.
Left: Order-disorder transitions for polymers with f_{LA} = 0.49–0.51, determined by temperature sweep, ODT determined by the precipitous drop in modulus upon heating at 1 °C min^{-1} in 25 mm plates with ω = 1 rad s^{-1} and 1% strain. Right: χ determined from

$(\chi N)_{ODT}$ = 17.996 for triblock polymers with equal volume fraction of the two blocks. The linear fit provides the relationship between the interaction parameter and temperature.

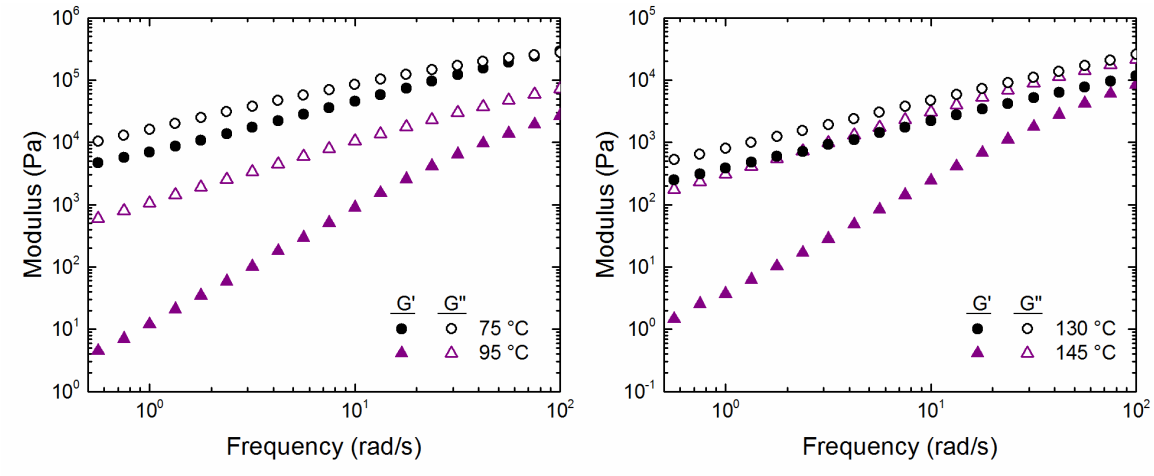

Figure 3.9.
Dynamic frequency sweeps above (purple) and below (black) the order-disorder transition temperature. LA-γMCL-LA (20A, 0.49) at 75 °C exhibits a power-law relationship $G' \sim \omega^{0.7}$ and $G'' \sim \omega^{0.7}$ while $G' \sim \omega^{1.8}$ $G'' \sim \omega^{1.0}$ at 95 °C (left). LA-γMCL-LA (27, 0.51) at 130 °C exhibits the power-law relationships $G' \sim \omega^{0.7}$ and $G'' \sim \omega^{0.8}$ while $G' \sim \omega^{1.7}$ $G'' \sim \omega^{1.0}$ at 95 °C (right).

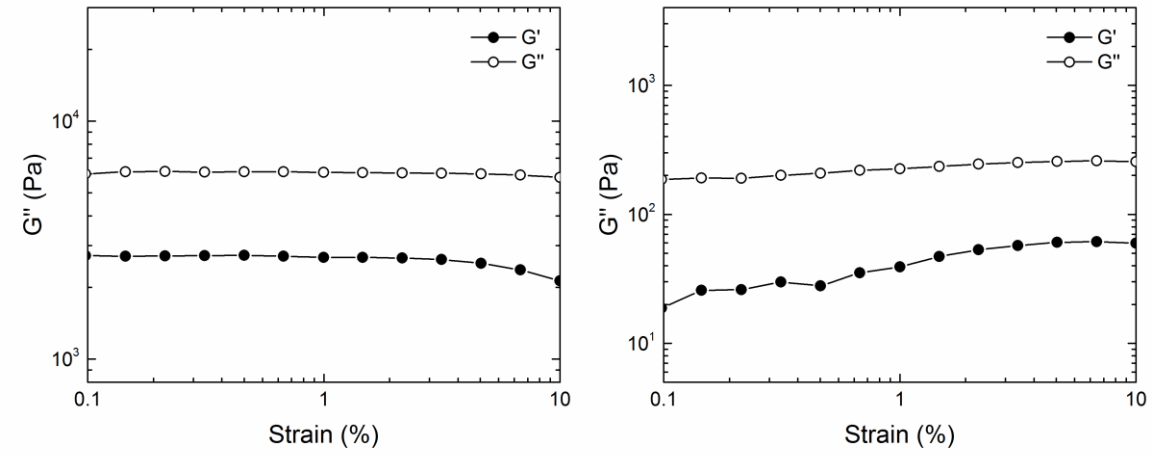

Figure 3.10.
Dynamic strain sweeps near the order-disorder transition demonstrating linear response within the strain % used of LA-γMCL-LA (20A, 0.49) at 83 °C (left) and LA-γMCL-LA (27, 0.49) at 140 °C (right).

To demonstrate the versatile properties of these new triblock polymers with PLLA end blocks and PγMCL midblock, the mechanical properties were determined for polymers with volume fractions of PLLA 0.08 to 0.80 (Table 3.2). The polymers were melt-pressed at 180 °C, quenched, and cut into dog bone shapes yielding transparent and colorless samples. These bars were left to age for 1 day at RT then a minimum of 5 samples were tested under uniaxial extension at a rate of 50 mm min^{-1} until break. A representative set of data for each sample pulled to its breaking point is shown in Figure 3.11 and averaged results with the standard deviation are summarized in Table 3.2. The sample with the lowest composition of PLLA (f_{LLA} = 0.08) does not exhibit the strain-hardening behavior observed in the other samples, resulting in a low ultimate tensile strength due to the short PLA chains. Samples with f_{LLA} of 0.17 and 0.28 exhibit low Young's modulus values and high elongations at break, typical of elastomeric behavior. These samples strain-harden, resulting in impressive average ultimate tensile strengths of 31 and 35 MPa, respectively. Cyclical extension of LLA-γMCL-LLA (159, 0.17) to 1000% strain and subsequent relaxation to 0% strain indicates that the strain-hardening behavior is irreversible; much less stress is required to deform this sample after the first cycle (Figure 3.12). Samples with a higher PLLA content (f_{LLA} = 0.80) exhibit high yield points and then plastic deformation. DSC analysis of tensile bars before and after testing show an increase in enthalpy of fusion upon the first heat corroborating strain-induced crystallization in the hard blocks (Figure 3.13). The jagged features seen in the stress-strain curve of LLA-γMCL-LLA (159, 0.80) were present through all five samples that were tested (Figure 3.14), likely a result of the irregularities apparent in the bars from processing. Based on

this sample set, the strain at break decreases as the mass fraction of PLLA increases. These samples with semicrystalline PLA, LLA-γMCL-LLA, exhibit excellent tensile properties, with high tensile strengths and elongations at break.

Table 3.2.
Summary of high molar mass triblock polymers with mechanical properties.

Sample ID ($M_{n,total}$, f_{LA})	$M_{n,PγMCL}$[a] (kg/mol)	$M_{n,PLA}$[a] (kg/mol)	$M_{n,total}$[a] (kg/mol)	f_{LA}[b]	$Đ$[c]	$T_{g,PγMCL}$[d] (°C)	$T_{g,PLA}$[d] (°C)	T_m[e] (°C)	E (MPa)[f]	$σ_B$ (MPa)[f]	$ε_B$ (%)[f]
LLA-γMCL-LLA (150, 0.08)	135	15	150	0.08	1.31	–60		159	2.2 ± 0.1	7.8 ± 0.5	1190 ± 60
LLA-γMCL-LLA (159, 0.17)	127	32	159	0.17	1.36	–59	47	162	4.0 ± 0.3	31 ± 4	1200 ± 30
LLA-γMCL-LLA (73, 0.28)	50	23	73	0.28	1.11	–59	52	163	13 ± 10	35 ± 3	895 ± 20
LLA-γMCL-LLA (89, 0.40)	50	40	89	0.40	1.07	–60	54	169	18 ± 10	37 ± 6	786 ± 90
LLA-γMCL-LLA (159, 0.80)	27	132	159	0.80	1.26	–65	56	175	1300 ± 30	42 ± 3	314 ± 20
LA-γMCL-LA (94, 0.17)	76	18	94	0.17	1.34	–60	42		4.8 ± 0.2	24 ± 2	1029 ± 20
LLA-γMCL-LLA (95, 0.17)	76	19	95	0.17	1.32	–59	47	162	3.6 ± 0.1	30 ± 4	988 ± 30

[a] determined using end-group analysis of ^{1}H NMR; [b] calculated using $ρ_{PLA}$ = 1.25 g cm^{-3} and $ρ_{PγMCL}$= 1.037 g cm^{-3} at 25 °C; [c] chloroform SEC analysis with PS standards; [d] determined as the midpoint of the inflection on second heat at 10 °C min^{-1} in a DSC; [e] determined as the peak temperature on second heat at 10 °C min^{-1} in a DSC; [f] determined from tensile testing to the break point of 5 samples extended at 50 mm min^{-1}.

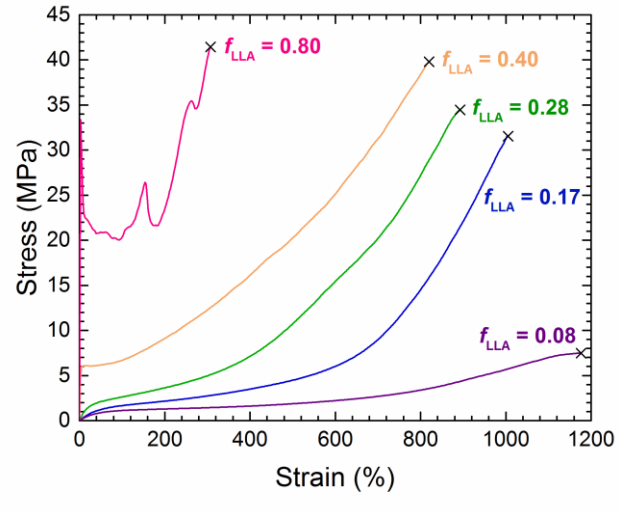

Figure 3.11.
Representative stress-strain curves of thermoplastic elastomers with varying fractions of PLLA, extended at 50 mm min^{-1}, with the break point indicated by ×.

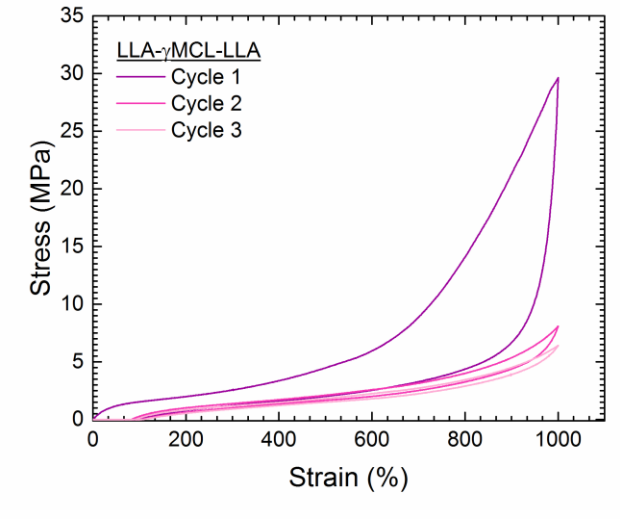

Figure 3.12.
Hysteresis experiments to 1000% strain of LLA-γMCL-LLA (f_{LLA} = 0.17) for 3 cycles extended at 50 mm min^{-1}.

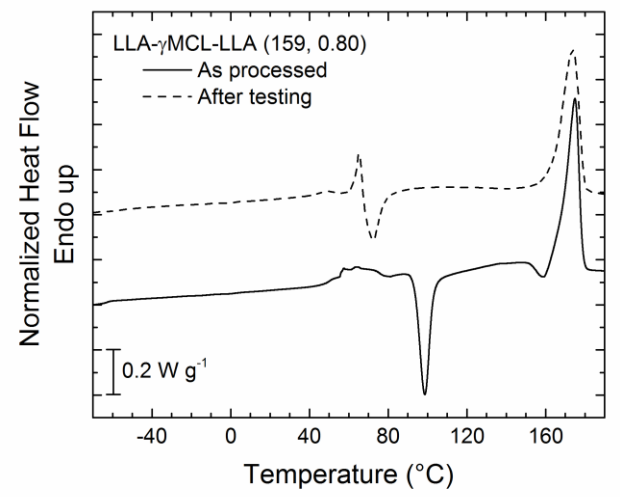

Figure 3.13.
First heat trace from DSC of LLA-γMCL-LLA (159, 0.80) as processed and after tensile testing, heating at 10 °C min^{-1}.

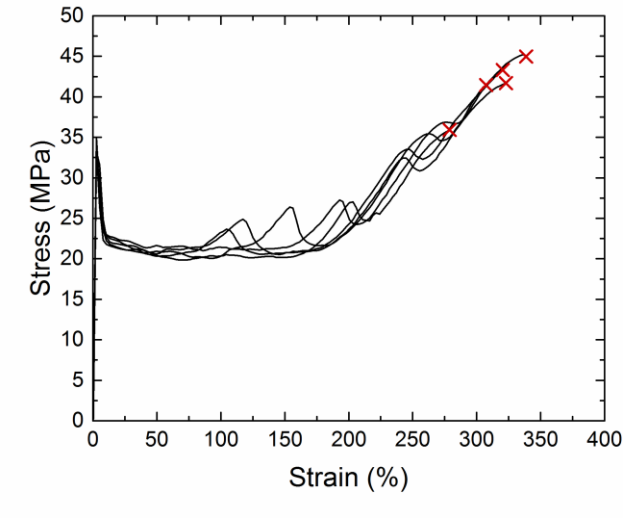

Figure 3.14.
Stress-strain curves for 5 samples of LLA-γMCL-LLA (159, 0.80), extended at 50 mm min^{-1} with the break point indicated by ×.

To study the effect of crystallinity in PLA on the mechanical properties of TPEs, block polymers of the same molar mass with a small volume fraction of PLA were synthesized. Polymerizing LA or LLA from 76 kg mol^{-1} PγMCL, a complementary pair of block polymers with atactic end blocks (LA-γMCL-LA) and isotactic end blocks (LLA-γMCL-LLA) were obtained with f_{LA} = 0.17 (Table 3.2). SAXS patterns of LA-γMCL-LA and LLA-γMCL-LLA with f_{LA} = 0.17 exhibit a principle scattering peak with broad secondary peaks (Figure 3.6). The morphology assignment is not definitive due to the lack of long range order, though the broad secondary peaks resemble spherical form-factor scattering.[51] Both block polymers exhibited glass transitions for PγMCL and PLA, and LLA-γMCL-LLA exhibited an additional melting transition by DSC at 162 °C with 21% crystallinity during the second heat.

Films of LA-γMCL-LA and LLA-γMCL-LLA with f_{LA} = 0.17 were subjected to extensional DMTA experiments, monitoring the modulus as a function of temperature (Figure 3.15). The glass transition, taken as the peak of tan δ, occurs at −59 °C for the PγMCL block and corroborates the glass transition temperature of PγMCL obtained from DSC (Table 3.2). Shin et al, and others, have analyzed the rubbery plateau of microphase separated block polymers to evaluate the entanglement molecular weight using the Guth-Smallwood approximation, which is based on the assumption that the spherical hard domains act like a filler in a rubber.[18,52] This approximation and the plateau modulus of LA-γMCL-LA with f_{LA} = 0.17 obtained using extensional DMTA was used to evaluate the entanglement molar mass for the PγMCL component via the following equation:

$$\boldsymbol{G_N}(\Phi) = \boldsymbol{G_N^0}\,(\mathbf{1} + \mathbf{2.5}\Phi + \mathbf{14.1}\Phi^{\mathbf{2}}) \tag{3.2}$$

where G_N^o is the plateau modulus of the PγMCL component and Φ is the volume fraction of PLA. Inserting the modulus measured $E(\Phi)$ = 5.6 × 10^6 Pa (Figure 5), and assuming there is minimal volume change upon deformation $E(\Phi) \approx 3G(\Phi)$, the plateau modulus G_N^o for PγMCL was determined to be 9.4 × 10^5 Pa. Using the Guth-Smallwood approximation with the assumption that the PLA domains are spherical hard domains acting as a filler in PγMCL rubber, the entanglement molar mass was calculated M_e = 2.8 kg mol^{-1}, which agrees with the entanglement molar mass M_e = 2.9 kg mol^{-1} obtained from the linear viscoelastic behavior of 92 kg mol^{-1} PγMCL (Section 3.5).[52] The rubbery plateau for both samples occurs at the same modulus, indicating that changing the crystalline nature of PLLA does not influence the stiffness of these TPEs. However, changing the end block affects the softening temperature indicated by a decrease in modulus; LA-γMCL-LA

begins to soften at the T_g of 45 °C while LLA-γMCL-LLA exhibits solid-like behavior up to 100 °C.

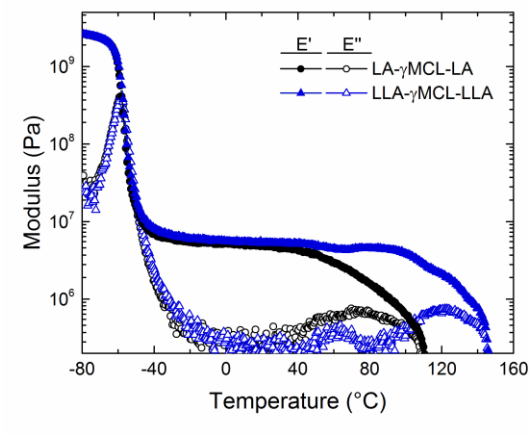

Figure 3.15.
Extensional DMTA of triblock polymers comparing the storage modulus (solid) and loss modulus (open) of LA-γMCL-LA (94, 0.17) (black) and LLA-γMCL-LLA (95, 0.17) (blue) heating at 5 °C min^{-1}.

LA-γMCL-LA exhibits high ultimate tensile strength of 24 MPa and LLA-γMCL-LLA exhibits an even higher strength (Figure 3.16, Table 3.3) consistent with similar studies.[13,16] The higher tensile strength in LLA-γMCL-LLA is a result of strain-induced crystallization in PLLA which enhances the strain-hardening behavior. These two elastomeric samples were subjected to cyclic loading of 300% strain at 50 mm min^{-1} for 10 cycles to explore their hysteresis behavior (Figure 3.17). There is some energy loss in the first cycle for LA-γMCL-LA and the stress at 300% continues to decrease in subsequent cycles. In contrast, LLA-γMCL-LLA exhibits much lower energy loss with a small decrease in stress at 300% in subsequent cycles. As the residual strain observed is dependent on the initial level of strain imposed, thus the ratio of residual strain to the subjected strain is reported. Hysteresis experiments were run in triplicate, providing a range

of residual strains for LA-γMCL-LA of 0.12-0.17 and LLA-γMCL-LLA of 0.06-0.07. In summary, the semicrystalline PLA end blocks impart higher temperature resistance and are more resilient than the samples with amorphous PLA end blocks.

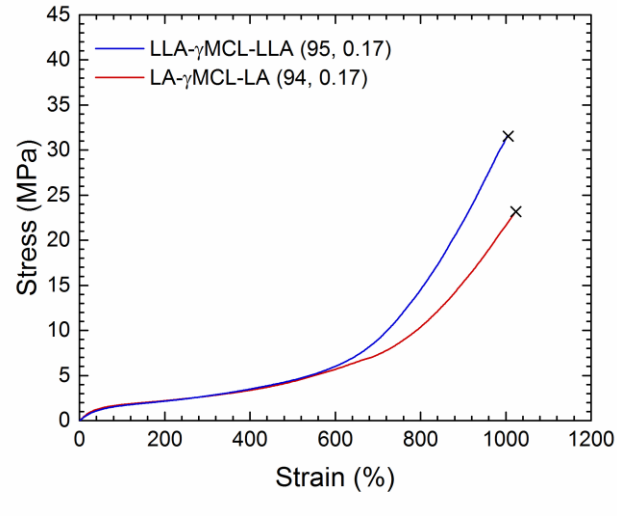

Figure 3.16.
Comparison of block polymers of PLA and PLLA with similar molar mass and composition. Representative stress-strain curves from five melt-pressed dog bones pulled at 50 mm min^{-1} to its break point ×.

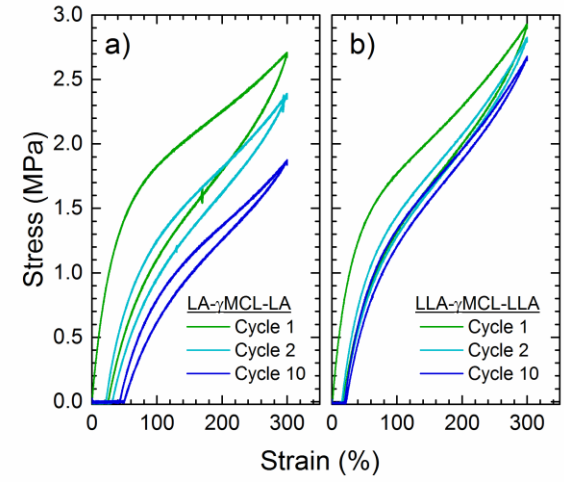

Figure 3.17.
Hysteresis of a) LA-γMCL-LA (94, 0.17) and b) LLA-γMCL-LLA (95, 0.17) of 10 cycles of 300% strain at 50 mm min^{-1}.

To further study the difference in permanent deformation observed in hysteresis experiments, LA-γMCL-LA and LLA-γMCL-LLA with f_{LA} = 0.17 were subjected to stress-relaxation experiments. A step-strain of 25% was imparted on the samples at various temperatures and the modulus was monitored over 3 h (Figure 3.18). Samples studied at 0 °C for LLA-γMCL-LLA and −40 °C for LA-γMCL-LA, show a small decrease in modulus with time. This is likely from the relaxation of the stressed amorphous PγMCL block which is above its T_g. At temperatures of 40 °C and above, both TPEs show a decrease in the normalized modulus to various amounts beyond the relaxation from PγMCL, where LA-γMCL-LA relaxes at a much faster rate than LLA-γMCL-LLA. Interestingly, LA-γMCL-LA exhibits significant stress relaxation at room temperature (T = 20 °C). The higher permanent deformation exhibited by amorphous PLA-TPEs when subjected to a step-strain corroborates the increased energy loss shown in hysteresis testing for the same samples.

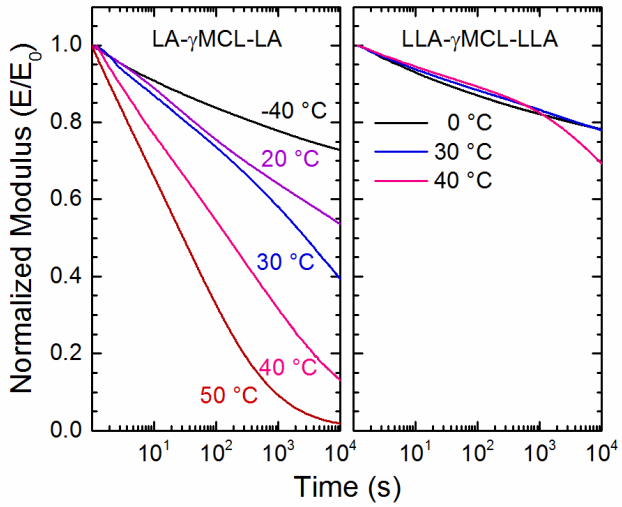

Figure 3.18.
Stress relaxation of LA-γMCL-LA (94, 0.17) and LLA-γMCL-LLA (95, 0.17). Samples were subjected to an instantaneous 25% strain at various temperatures and the modulus was monitored for three hours.

3.3 Discussion

The polymerizability of lactones has been a significant research topic as the size of the lactone, position of substituent, and size of substituent affect the thermodynamics and kinetics of polymerization.[30] A recent in-depth study demonstrated that the size of the lactone largely affects the thermodynamics of polymerization while the position and nature of the substituent largely affects the kinetics of polymerization.[26] The thermodynamic favorability to form polyesters from ε-caprolactones provides a synthetic advantage over δ-valerolactones. Of methyl-substituted ε-caprolactones that yield low-T_g polyesters, the kinetics of γMCL polymerization are significantly faster (95% conversion after 1 h) compared to εMCL (95% conversion after more than 3 h) under the same catalyst loading and reaction conditions.[19] The change in propagating group from secondary to primary alcohol, and a less sterically hindered ester, results in a significant increase in the rate of polymerization for γMCL.

The range of aliphatic polyester PLA-TPEs reported in literature provide us the opportunity to explore the key parameters that affect the mechanical properties in the resultant TPEs. However, because of the different sample preparation conditions and testing parameters used, quantitative comparisons can be challenging. Changing the ratio between blocks controls the morphology of the bulk material impacting the mechanical properties; an increase in PLLA content results in an increase in ultimate tensile strength and Young's modulus, and a decrease in elongation at break (Figure 3.11).[53] PγMCL incorporated as the minority component LLA-γMCL-LLA (159, 0.80) showed high modulus and high elongation at break for a majority PLLA sample, demonstrating PγMCL

acts as a toughening filler in PLLA when incorporated into a block polymer architecture. This result agrees with other reports that utilize block polymers, where the identity of the midblock impacts the toughness of the overall block polymer.[54] When block polymers demonstrate a spherical morphology, with glassy A blocks and rubbery B blocks, samples exhibit elastomeric behavior. A high performance PLA-TPE previously reported, LLA-βMVL-LLA (107, 0.32), exhibited $\sigma_B = 28 \pm 4$ MPa and $\varepsilon_B = 1720 \pm 140\%$.[13] We report a sample with a similar composition and lower overall molar mass, LLA-γMCL-LLA (72.9, 0.28), that exhibits a higher average ultimate tensile strength $\sigma_B = 35 \pm 3$ MPa albeit with lower elongation at break $\varepsilon_B = 895 \pm 20\%$. This increase in ultimate tensile strength and decrease in elongation at break has been observed in PS-TPEs, where SBS has higher strength and lower elongation in comparison to SIS.[4] This result has long been attributed to the differences in the midblock entanglement molar mass: $M_{e,PI} = 5.0$ kg mol^{-1} and $M_{e,PB} = 1.6$ kg mol^{-1}.[4] The same trend is seen in these PLA-TPEs where a decrease in entanglement molar mass provides high strength TPEs (Table 3.3). These data support the hypotheses that a lower entanglement molar mass leads to more trapped entanglements per volume in the rubbery midblock, which adds strength to the material.

Table 3.3.
Summary of the mechanical properties of PLA-TPEs with reports of the entanglement molar mass and the segment-segment interaction parameter.

PLA-TPE	$M_{n,total}$ (kg mol^{-1})	f_{LA}	E (MPa)	σ_B (MPa)	ε_B (%)	$M_{e,rubbery}$ (kg mol^{-1})	χ(140 °C)	Reference
LLA-γMCL-LLA	72.9	0.28	13 ± 9.9	35 ± 3	895 ± 20	2.9	0.055	This work
LLA-βMVL-LLA	107.2	0.32	5.9 ± 0.9	28 ± 4	1720 ± 140	4.3	0.036	13,26
LLA-M-LLA	41.8	0.34	1.5 ± 0.1	13.6 ± 1.4	900 ± 76	11-14	*NR*	16

LA-γMCL-LA	94	0.17	4.8 ± 0.2	24 ± 2	1030 ± 20	2.9	0.055	This work
LA-εMCL-LA	122	0.16	1.9 ± 0.1	10.2 ± 0.8	1880 ± 70	3.0	0.048	19,21
LA-CD-LA	104	0.17	1.5 ± 0.3	9.9 ± 0.6	2100 ± 100	3.9	0.041	21
LA-βMVL-LA	103.6	0.29	1.9 ± 0.6	9.0 ± 1.1	1790 ± 130	4.3	0.036	13,26
LA-D-LA	136	0.21	1.0 ± 0.1	4.5 ± 0.3	1600 ± 200	5.9	0.095	20,21

An increase in the segment-segment interaction parameter between blocks has also been shown to improve ultimate tensile strength and decrease elongation at break.[4] To further highlight this effect, a polymerization method that results in styrene repeat units in the rubbery midblock results in an imperfect block polymer that has a lower χ between blocks and leads to a decrease in material strength.[55] Ring-opening transesterification polymerization facilitates control over molar mass, however, side transesterification reactions can result in randomization of the chain and increased dispersity. Though these side reactions can be beneficial for the synthesis of random copolymers, such as poly(ε-caprolactone-*co*-LLA), it also means that when targeting an A-B-A architecture the A and B blocks can randomize, effectively reducing χ. The ^{13}C NMR spectra of polyester TPEs provide evidence for distinct blocks for TPEs reported in Table 3.3. When changing the midblock from PβMVL to PγMCL, there is an increase in χ, as well as a decrease in the entanglement molar mass, which contribute to the increase in tensile strength and decrease in elongation at break (Table 3.3).

LA-γMCL-LA demonstrates more than double the stress at break, albeit with a lower elongation at break compared to LA-εMCL-LA.[19] PγMCL and PεMCL have a very similar entanglement molar masses, $M_{e,P\gamma MCL}$ = 2.9 kg mol^{-1} and $M_{e,P\varepsilon MCL}$ = 3.0 kg mol^{-1}, thus the degree of entanglements do not explain this impact in the mechanical properties.[21]

Although the chemical nature of these polymers only differ by the change in the position of the methyl substituent, their segment-segment interaction parameter χ with PLA is slightly different (Table 3.3). As Martello et al. points out, the values reported for the tensile properties of LA-εMCL-LA are likely lower limits. Further studies to resolve these discrepancies are underway.

With a PγMCL midblock and f_{LA} = 0.17, the use of isotactic PLLA over atactic PLA improved the ultimate tensile stress by 7 MPa while maintaining an elongation at break of ~1000% (Table 3.2). Previous studies that directly compare the mechanical properties between PLA-TPEs with atactic PLA and isotactic PLLA also support this trend: PLLA end block TPEs exhibit significantly higher ultimate tensile strength while maintaining identical elongations at break.[13,16,56] TPEs have two types of physical cross-links: trapped entanglements in the rubbery domain and microphase separated glassy/semicrystalline domains. To avoid complications from crystallization breakout disrupting the microphase separated morphology, samples were quenched during processing. The trapped entanglements are dynamic and dictate the extensibility of the rubbery midblock, limiting the elongation at break for comparative samples.[6] Using the same rubbery midblock, the maximum tensile strength for a TPE system depends heavily on the nature of the hard end block, all other parameters being equal (molar mass, composition, and χ).

Impressively, LLA-γMCL-LLA exhibited half the residual strain when compared to the PLA counterpart, indicating PLLA-TPEs have lower permanent deformation after extension (Figure 3.17). The largest energy loss occurs in the first cycle of extension,

common for this class of compounds, which can be attributed to the alignment of the hard domains in the direction of extension or deformation of the domains themselves.[57,58] Subsequent cycles show stress softening, also known as the Mullins effect.[59] When extending LLA-γMCL-LLA to extreme elongations, 1000% strain, the strain-hardening behavior from strain-induced crystallization exhibited in the stress-strain curve is not reversible upon relaxation, only through reprocessing. Though, pre-straining the material does result in the ability to strain the material to the same elongation with less stress.

Stress relaxation studies indicate that the atactic PLA end blocks are soft enough at 20 °C to allow the TPEs to relax upon an applied stress (Figure 3.18). Similar studies on microphase separated SIS TPEs show a crossover temperature, where the behavior transitions from permanent to transient cross-links at 30 °C, significantly below the T_g of PS.[60] Above 30 °C, SIS TPEs under extension experience relaxation as a result of chain-pullout, wherein the PS chain slips out of the glassy domain which reduces the stress exhibited by the sample. The PLA chains in LA-γMCL-LA are likely experiencing similar chain-pullout near room temperature. The extent of chain-pullout increases closer to the glass transition temperature of PLA that consequently increases the rate at which stress is diminished. The temperature dependent χ also decreases as the system is heated. These more complex behaviors close to the T_g of PLA resulted in the failure of time-temperature superposition (TTS) for stress relaxation results.[61] This chain-pullout theory at moderate temperatures provides an explanation for the increased permanent deformation and lower ultimate tensile strengths observed in amorphous PLA-TPEs. In contrast, PLLA-TPEs show relaxation after long times (hours) when the temperature is near the glass transition

temperature of the PLLA blocks. We hypothesize that elastomers with PLLA exhibit lower permanent deformation due to the crystallinity in the hard domains that help prevent chain-pullout. Crystallinity is not the only method to reduce chain-pullout of the hard A block, as it can also be mitigated by utilizing star or multiblock architectures.[62,63]

3.4 Conclusion

We report the efficient and practical synthesis of an aliphatic polyester TPE system LA-γMCL-LA with precise control over molar mass with low dispersity. The high density of trapped entanglements in the rubbery midblock, dictated by the low entanglement molar mass of PγMCL, controls the extensibility of the TPE. The LA-γMCL-LA elastomers exhibit excellent mechanical properties, including the highest ultimate tensile strength reported to date for this class of materials. This is a result of the combination of high molar mass polymers, low entanglement molar mass of the rubbery block, and moderate incompatibility between the rubbery and glassy blocks. The permanent deformation seen in amorphous PLA-TPEs is likely a result of chain-pullout upon an applied stress and can be mitigated using semicrystalline PLA as the end block. Semicrystalline end blocks allow for a wider operating temperature window and even better mechanical performance; the ultimate tensile strength is higher and there is very little permanent deformation when compared to the amorphous PLA-TPE counterpart. This study demonstrates the key parameters that contribute to the mechanical strength seen in ABA block polymer TPEs and corroborates the behaviors observed in PS-TPEs. The properties observed in LA-

γMCL-LA TPEs expand our understanding for the design of high performance sustainable TPEs.

3.5 Experimental details

Materials

Chloroform, dichloromethane, methanol, and hexanes were obtained from Fisher Scientific and used without further purification. Lactide was generously provided by Altasorb (a subsidiary of Ortec, Inc). All other chemicals were used as received from Sigma-Aldrich unless otherwise specified. Lactide and 1,4-benzenedimethanol were recrystallized from toluene (x3), dried under vacuum for 48 h, and stored under inert atmosphere. $Sn(Oct)_2$ was distilled three times under vacuum with argon (30–50 mTorr, 130–150 °C) before storing under inert atmosphere. Anhydrous toluene was obtained through a JC Meyer solvent drying system.

Characterization

Bruker Avance III 500 was used for ^{1}H and ^{13}C NMR spectroscopy. Molar masses were calculated from end-group analysis. Thermal properties were obtained using a TA Instruments Discovery DSC. Samples were prepared in hermetically sealed pans and heated at 10 °C min^{-1} to 200 °C to erase any thermal history, cooled to −80 °C, and data was collected from the second heat cycle (unless otherwise indicated). Size exclusion chromatography was performed on an Agilent 1100 series SEC with HP1047A refractive index detector, using a chloroform mobile phase at 35 °C through 3 Varian PLgel Mixed C Columns at 1 ml min^{-1}. Relative molar mass was determined from a calibration curve

created using PS standards purchased from Polymer Laboratories. Polymer density was determined by making solutions of ethylene glycol and water to obtain solutions of varying density, and a bubble-free polymer sample was dropped in the solutions to determine if it would sink or float.

Triblock copolymers were placed between two Teflon sheets and melt-pressed at 70–180 °C for 3 minutes then quenched to room temperature using water cooling (~ 35 °C min^{-1}) through the hot press.[64] Dog-bone-shaped tensile bars were punched out resulting in samples with approximately 0.5 mm thickness, 3 mm gauge width, and 16 mm gauge length. Samples were tested to the point of break using Shimadzu Autograph AGS-X Tensile Tester and an extension rate of 50 mm min^{-1}. Using 25 mm parallel plates, TA Instruments Rheometric Series ARES instrument was used for dynamic mechanical thermal analysis (DMTA). Heating was controlled under nitrogen atmosphere, and the samples were equilibrated at the designated temperature for 10 minutes before testing. To determine order-disorder temperatures, the samples were heated at 1 °C min^{-1} while applying a 1% strain and 1 rad s^{-1}. Extensional DMTA and stress relaxation analysis were performed on a TA Instruments RSA-G2 in tension mode on rectangular polymer films with 0.5 mm thickness and 3 mm gauge width. DMTA experiments were conducted at a heating rate of 5 °C min^{-1} with an oscillating strain of 0.05% and angular frequency of 1 Hz. Stress relaxation analysis was conducted after an equilibration time of 10 min at the selected temperature by applying a step strain of 25% and measuring the modulus for 3 hours. Temperature control at 20 °C for LLA-γMCL-LLA was not able to be maintained over 3 hours and data was not collected. SAXS experiments were conducted at the DuPont-

Northwestern Dow Collaborative Access Team (DND-CAT) synchrotron research center 5-ID-D beamline of Advanced Photon Source at Argonne National Laboratory.

Dynamic mechanical analysis for M_e

Dynamic mechanical analysis of PγMCL (M_n = 91.8 kg mol^{-1}) was performed at various temperatures within the linear viscoelastic regime (Figure 3.19 and Figure 3.20). For this analysis, an oscillatory stress is applied to the material and the sinusoidal stress response is measured; this affords a complex modulus that is decoupled into the in-phase (G') and out-of-phase (G") components. The loss tangent (tan δ), or the ratio of the viscous modulus G" to the elastic modulus G', is also calculated. Horizontal shift factors (a_T) were determined by aligning the loss tangent curves and subsequently applied to each frequency sweep to generate a master curve via time-temperature superposition (Figure 3.21). The success of time-temperature superposition was evaluated by fitting the horizontal shift factors to the Williams-Landel-Ferry (WLF) equation:

$$\log(a_T) = \frac{C_1(T-T_r)}{C_2+(T-T_r)} \tag{3.3}$$

where a_T is the shift factor, C_1 and C_2 are empirically derived constants, T is the temperature of the measurement, and T_r is the reference temperature. The WLF fit agreed well with the horizontal shift factors obtained and the values of C_1 and C_2 were determined to be 4.6 and 150 °C, respectively. Using the data from the master curve, the entanglement molecular weight (M_e) was calculated via the following equation:

$$M_e = \frac{\rho RT}{G_N} \tag{3.4}$$

where ρ is the density, R is the universal gas constant, T is the temperature of reference, and G_N is the plateau modulus. The plateau modulus was defined as the point during the rubbery plateau where the loss tangent (tan δ) is at a minimum, as this corresponds to the point at which the elastic modulus is most dominant. Using this value, a reference temperature of 30 °C, and a measured density of 1.037 g cm^{-3}, the entanglement molar mass of PγMCL was determined to be 2.9 kg mol^{-1}. These calculations are using the Ferry equation that does not have the 4/5 prefactor.[65]

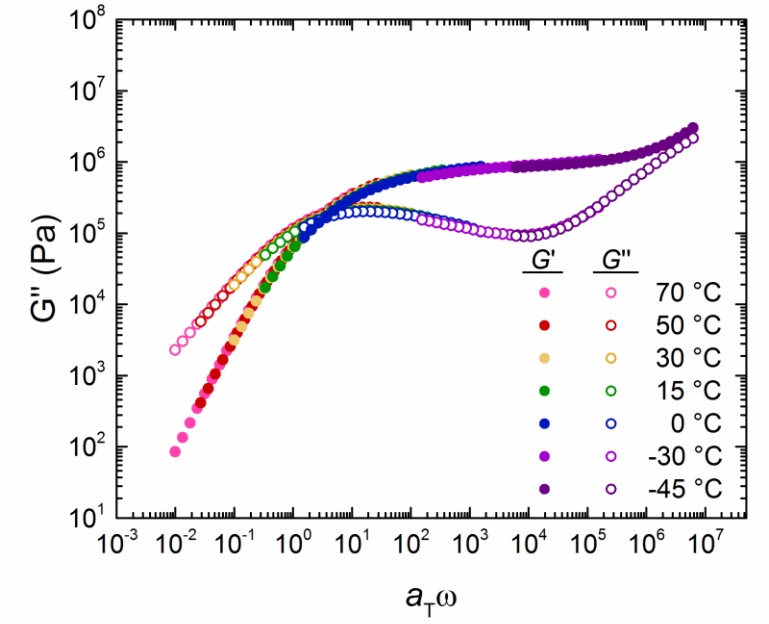

Figure 3.19.
A master curve of PγMCL generated from applying shift factors (a_T) to dynamic frequency sweep data obtained at various temperatures (reference temperature of 30 °C). The entanglement molar mass was determined using the plateau in the storage modulus, at the point where the loss tangent (tan δ) is at a minimum. (M_e = 2.9 kg/mol).

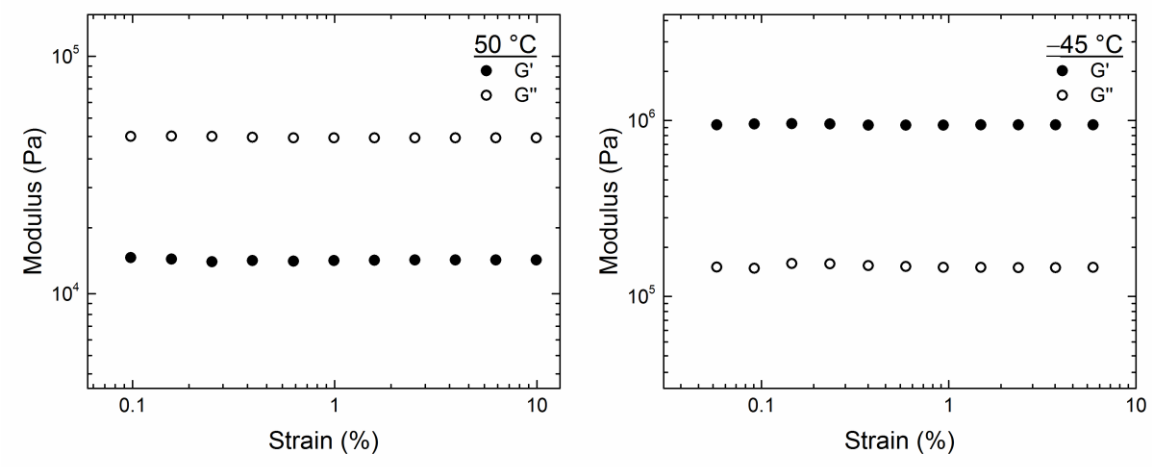

Figure 3.20.
Dynamic strain sweeps at 50 °C (left) and -45 °C (right).

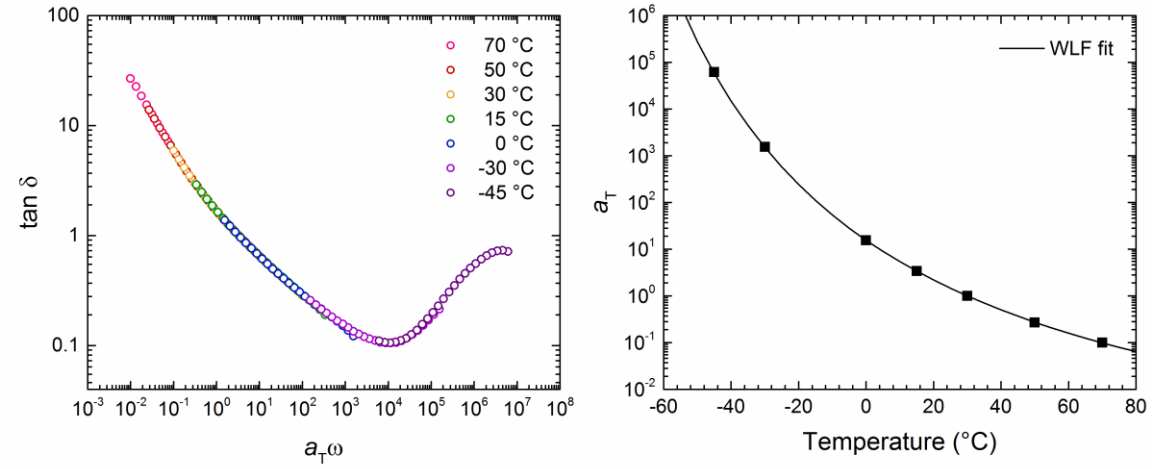

Figure 3.21.
The shift factors were determined by shifting the tan δ curves to align (left). Shift factor versus temperature are plotted and fit with the WLF equation (Equation 3.3) where C_1 = 4.8, C_2 = 150 °C and T_r = 30 °C (right).

γ-methyl-ε-caprolactone synthesis

In a typical reaction, *meta*-chloroperoxybenzoic acid (110 g of 77% *m*CPBA, 490 mmol) was dissolved in methylene chloride (1.6 L, 10% w/v). After removing water that phase separated by pipette, the solution was further dried over magnesium sulfate and

filtered into a round-bottom flask. The solution was cooled to 5 °C using a salt-ice bath and 4-methylcyclohexanone (50 g, 446 mmol) was added slowly such that the temperature was kept below 10 °C. The reaction was left to react while slowly warming up to room temperature, while *meta*-chlorobenzoic acid (*m*CBA) began to precipitate. After 4 hours, the reaction was cooled in an ice bath to 5 °C and the reaction mixture was filtered to remove precipitated *m*CBA. The reaction was then concentrated to half the volume, cooled, and filtered again. The solution collected was washed carefully with freshly prepared 10% aqueous sodium bisulfite, followed by saturated sodium bicarbonate. Once neutral, the solution was dried using brine and stirred over magnesium sulfate until dry. The product was then passed through a basic alumina plug and concentrated *in vacuo*. The product was isolated by fractional distillation under dynamic vacuum (200–1000 mTorr, 70–100 °C). The distilled product was dried over calcium hydride overnight and then distilled, this was repeated 2-3 times (70-80% yield).

^{1}H NMR (500 MHz, Chloroform-d) δ = 4.33 – 4.24 (m, 1 H), 4.24 – 4.13 (m, 1 H), 2.72 - 2.56 (m, 2 H), 2.00 – 1.85 (m, 2 H), 1.85 – 1.72 (m, 1 H), 1.56 – 1.44 (m, 1 H), 1.39 – 1.26 (m, 1 H), 1.00 (d, J = 7.0 Hz, 3 H)

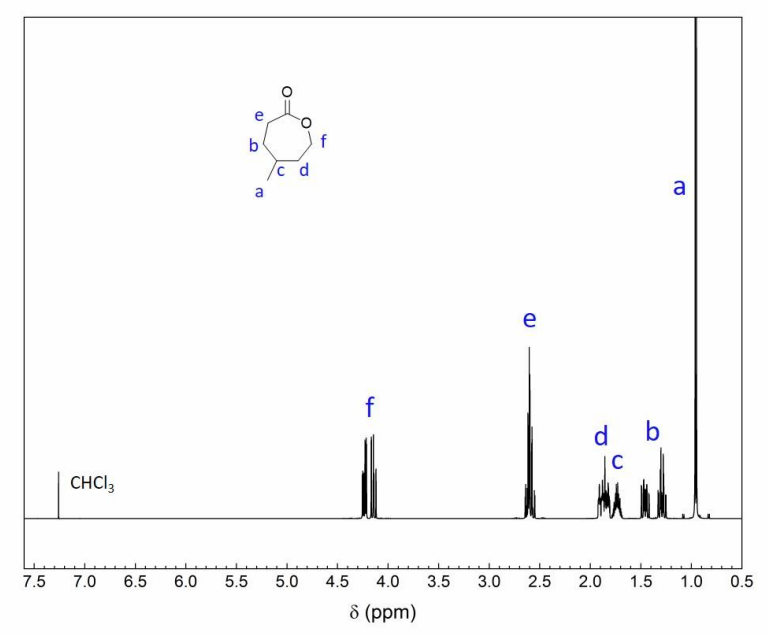

Figure 3.22.
^{1}H NMR spectra for γMCL in $CDCl_3$.

Polymer synthesis

γ-methyl-ε-caprolactone (10 g, 78 mmol), 1,4-benzenedimethanol (43 mg, 0.31 mmol), and $Sn(Oct)_2$ (32 mg, 0.078 mmol) were added to a pressure vessel under nitrogen atmosphere in a glove box. (Note: pressure vessels were inspected for imperfections before use and vessels were filled below the halfway point for all reactions.) The vessel was sealed, taken out of the glovebox, and placed in a 130 °C oil bath. After 1 hour, the vessel was cooled in an ice bath to stop the reaction. The clear, viscous polymer was dissolved in chloroform and precipitated into cold methanol (x1) then hexanes (x2). A clear, viscous liquid was collected by decanting the solvent and dried by blowing nitrogen over the sample for 1 hour then *in vacuo* for a minimum of 48 hours (93-96% yield).

PγMCL ^{1}H NMR (500 MHz, Chloroform-d) δ = 7.35 (s, 4 H), 5.11 (s, 4 H), 4.20 – 4.01 (m, 507 H), 3.76 – 3.62 (m, 5 H), 2.42 – 2.23 (m, 516 H), 1.74 – 1.62 (m, 561 H), 1.62 – 1.39 (m, 790 H), 0.97 – 0.87 (m, 780 H)

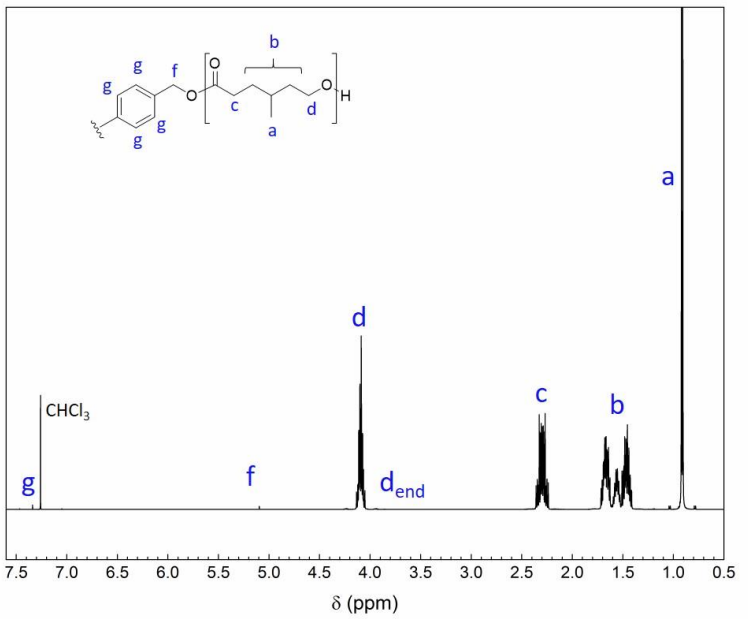

Figure 3.23.
^{1}H NMR spectra for PγMCL in $CDCl_3$.

PγMCL (3 g, 0.09 mmol), lactide (3.3 g, 23 mmol), $Sn(Oct)_2$ (8 mg, 0.02 mmol), and toluene (1 mol L^{-1} monomer in solvent) were added to a pressure vessel under nitrogen atmosphere in a glovebox. (Note: pressure vessels were inspected for imperfections before use and vessels were filled below the halfway point for all reactions.) The solution was left stirring overnight to ensure PγMCL was completely dissolved in toluene. The reaction vessel was submerged in a 130 °C oil bath for 90 min, then cooled using an ice bath. The polymer was dissolved in chloroform and precipitated into methanol (x3) then hexanes (x1). Polymers were dried *in vacuo* for a minimum of 48 h (80-88% yield).

LA-γMCL-LA ^{1}H NMR (500 MHz, Chloroform-d) δ = 7.35 (s, 4 H), 5.26 – 5.12 (m, 443 H), 4.36 (q, 2 H), 4.16 – 4.04 (m, 507 H), 2.40 – 2.22 (m, 516 H), 1.78 – 1.62 (m, 598 H), 1.62 – 1.40 (m, 2137 H), 0.97 – 0.86 (m, 770 H)

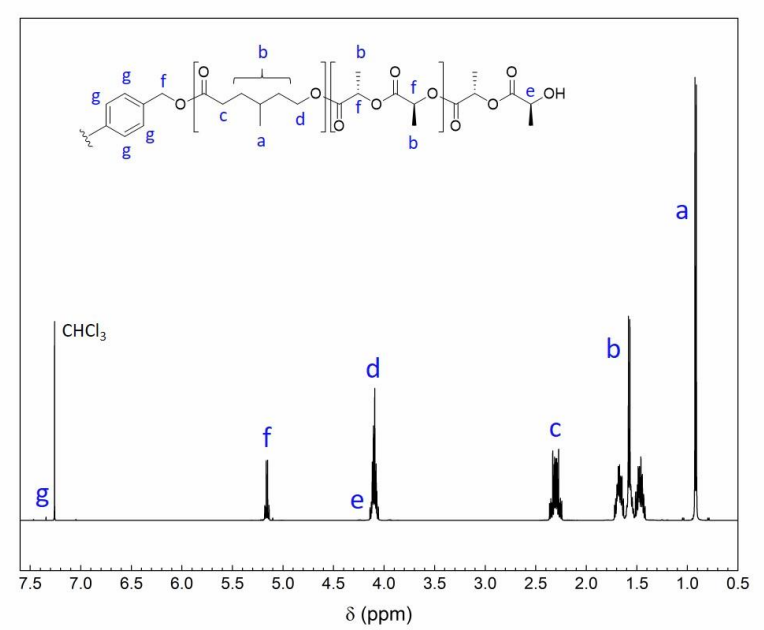

Figure 3.24.
^{1}H NMR spectra for LLA-γMCL-LLA in $CDCl_3$.

Polymerization kinetics

Polymerizations were assembled in 48 ml pressure vessels with a side arm adapter, under inert atmosphere in a glove box. The vessel was taken out of the glovebox and the side arm was purged of air by cycling with vacuum and argon (3x). The pressure vessel was then placed in an oil bath at 130 °C. The start time for the polymerization was taken to be the time when the vessel was lowered into the oil bath. Aliquots were taken at various time points by placing the system under positive pressure of argon, opening the reaction vessel, taking an aliquot, closing the reaction vessel, then closing the system to argon. The aliquots

were quenched by cooling to 0 °C and samples for ^{1}H NMR spectroscopy and SEC analysis were prepared.

3.6 References

(1) World Economic Forum, Ellen MacArthur Foundation, and McKinsey and Company. The New Plastics Economy: Rethinking the future of plastics. 2016, report. http://www.ellenmacarthurfoundation.org/publications

(2) Anastas, P.; Eghbali, N. Green Chemistry: Principles and Practice. *Chem. Soc. Rev.* **2010**, *39*, 301–312.

(3) Dubé, M. A.; Salehpour, S. Applying the Principles of Green Chemistry to Polymer Production Technology. *Macromol. React. Eng.* **2014**, *8*, 7–28.

(4) *Thermoplastic Elastomers*; Holden, G.; Kricheldorf, H. R.; Quirk, R. P., Eds.; 3rd ed.; Hanser Gardner Publications, Inc.: Cincinnati, 2004.

(5) Holden, G.; Bishop, E. T.; Legge, N. R. Thermoplastic Elastomers. *J. Polym. Sci. Part C Polym. Symp.* **1969**, *26*, 37–57.

(6) Tong, J.; Jerôme, R. Dependence of the Ultimate Tensile Strength of Thermoplastic Elastomers of the Triblock Type on the Molecular Weight between Chain Entanglements of the Central Block. *Macromolecules* **2000**, *33*, 1479–1481.

(7) Shin, J.; Kim, Y.-W.; Kim, G.-J. Sustainable Block Copolymer-Based Thermoplastic Elastomers. *Appl. Chem. Eng.* **2014**, *25*, 121–133.

(8) Hillmyer, M. A.; Tolman, W. B. Aliphatic Polyester Block Polymers: Renewable, Degradable, and Sustainable. *Acc. Chem. Res.* **2014**, *47*, 2390–2396.

(9) Pitt, C. G.; Gratzl, M. M.; Kimmel, G. L.; Surles, J.; Schindler, A. Aliphatic Polyesters II. The Degradation of Poly (D,L-lactide), Poly (ε-caprolactone), and Their Copolymers in Vivo. *Biomaterials* **1981**, *2*, 215−220.

(10) Loefgren, A.; Albertsson, A.-C.; Dubois, P.; Jerome, R.; Teyssie, P. Synthesis and Characterization of Biodegradable Homopolymers and Block Copolymers Based on 1,5-Dioxepan-2-One. *Macromolecules* **1994**, *27*, 5556–5562.

(11) Albertsson, A.-C.; Varma, I. K. Recent Developments in Ring Opening Polymerization of Lactones for Biomedical Applications. *Biomacromolecules* **2003**, *4*, 1466–1486.

(12) Cohn, D.; Hotovely Salomon, A. Designing Biodegradable Multiblock PCL/PLA Thermoplastic Elastomers. *Biomaterials* **2005**, *26*, 2297–2305.

(13) Xiong, M.; Schneiderman, D. K.; Bates, F. S.; Hillmyer, M. A.; Zhang, K. Scalable Production of Mechanically Tunable Block Polymers from Sugar. *Proc. Natl. Acad. Sci.* **2014**, *111*, 8357–8362.

(14) Huang, Y.; Chang, R.; Han, L.; Shan, G.; Bao, Y.; Pan, P. ABA-Type Thermoplastic Elastomers Composed of Poly(ε-Caprolactone-co-δ-Valerolactone) Soft Midblock and Polymorphic Poly(Lactic Acid) Hard End Blocks. *ACS Sustain. Chem. Eng.* **2016**, *4*, 121–128.

(15) Ryner, M.; Albertsson, A.-C. Resorbable and Highly Elastic Block Copolymers from 1,5-Dioxepan-2-One and L-Lactide with Controlled Tensile Properties and Hydrophilicity. *Biomacromolecules* **2002**, *3*, 601–608.

(16) Wanamaker, C. L.; Bluemle, M. J.; Pitet, L. M.; O'Leary, L. E.; Tolman, W. B.; Hillmyer, M. A. Consequences of Polylactide Stereochemistry on the Properties of Polylactide-Polymenthide-Polylactide Thermoplastic Elastomers. *Biomacromolecules* **2009**, *10*, 2904–2911.

(17) Wanamaker, C. L.; O'Leary, L. E.; Lynd, N. A.; Hillmyer, M. A.; Tolman, W. B. Renewable-Resource Thermoplastic Elastomers Based on Polylactide and Polymenthide. *Biomacromolecules* **2007**, *8*, 3634–3640.

(18) Shin, J.; Martello, M. T.; Shrestha, M.; Wissinger, J. E.; Tolman, W. B.; Hillmyer, M. A. Pressure-Sensitive Adhesives from Renewable Triblock Copolymers. *Macromolecules* **2011**, *44*, 87–94.

(19) Martello, M. T.; Hillmyer, M. A. Polylactide-Poly(6-Methyl-ε-Caprolactone)-Polylactide Thermoplastic Elastomers. *Macromolecules* **2011**, *44*, 8537–8545.

(20) Martello, M. T.; Schneiderman, D. K.; Hillmyer, M. A. Synthesis and Melt Processing of Sustainable Poly(ε-Decalactone)-Block-Poly(Lactide) Multiblock Thermoplastic Elastomers. *ACS Sustain. Chem. Eng.* **2014**, *2*, 2519–2526.

(21) Schneiderman, D. K.; Hill, E. M.; Martello, M. T.; Hillmyer, M. A. Poly(Lactide)-Block-Poly(ε-Caprolactone-co-ε-Decalactone)-Block-Poly(Lactide) Copolymer Elastomers. *Polym. Chem.* **2015**, *6*, 3641–3651.

(22) Cohn, D.; Hotovely Salomon, A. Designing Biodegradable Multiblock PCL/PLA Thermoplastic Elastomers. *Biomaterials* **2005**, *26*, 2297–2305.

(23) Kong, J. F.; Lipik, V.; Abadie, M. J. M.; Roshan Deen, G.; Venkatraman, S. S. Characterization and Degradation of Elastomeric Four-Armed Star Copolymers Based on Caprolactone and L-Lactide. *J. Biomed. Mater. Res. Part A* **2012**, *100A*, 3436–3445.

(24) Kong, J. F.; Lipik, V.; Abadie, M. J.; Deen, G. R.; Venkatraman, S. S. Biodegradable Elastomers Based on ABA Triblocks: Influence of End-Block Crystallinity on Elastomeric Character. *Polym. Int.* **2012**, *61*, 43–50.

(25) Nakayama, Y.; Aihara, K.; Yamanishi, H.; Fukuoka, H.; Tanaka, R.; Cai, Z.; Shiono, T. Synthesis of Biodegradable Thermoplastic Elastomers from ε-Caprolactone and Lactide. *J. Polym. Sci. Part A Polym. Chem.* **2015**, *53*, 489–495.

(26) Schneiderman, D. K.; Hillmyer, M. A. Aliphatic Polyester Block Polymer Design. *Macromolecules* **2016**, *49*, 2419–2428.

(27) Brutman, J. P.; De Hoe, G. X.; Schneiderman, D. K.; Le, T. N.; Hillmyer, M. A. Renewable, Degradable, and Chemically Recyclable Cross-Linked Elastomers. *Ind. Eng. Chem. Res.* **2016**, *55*, 11097–11106.

(28) Martello, M. T.; Burns, A.; Hillmyer, M. Bulk Ring-Opening Transesterification Polymerization of the Renewable δ-Decalactone Using an Organocatalyst. *ACS Macro Lett.* **2012**, *1*, 131–135.

(29) Olsén, P.; Borke, T.; Odelius, K.; Albertsson, A.-C. ε-Decalactone: A Thermoresilient and Toughening Comonomer to poly(L-Lactide). *Biomacromolecules* **2013**, *14*, 2883–2890.

(30) Olsén, P.; Odelius, K.; Albertsson, A.-C. Thermodynamic Presynthetic Considerations for Ring-Opening Polymerization. *Biomacromolecules* **2016**, *17*, 699–709.

(31) Breteler, M. R. T.; Zhong, Z.; Dijkstra, P. J.; Palmans, A. R. A.; Peeters, J.; Feijen, J. Ring-Opening Polymerization of Substituted Ɛ-Caprolactones with a Chiral (Salen) AlOiPr Complex. *J. Polym. Sci. Part A Polym. Chem.* **2007**, *45*, 429–436.

(32) Peeters, J. W.; van Leeuwen, O.; Palmans, A. R. A.; Meijer, E. W. Lipase-Catalyzed Ring-Opening Polymerizations of 4-Substituted ε-Caprolactones: Mechanistic Considerations. *Macromolecules* **2005**, *38*, 5587–5592.

(33) Seefried, C. G.; Koleske, J. V. Lactone Polymers. VI. Glass-Transition Temperatures of Methyl-Substituted ε-Caprolactones and Polymer Blends. *J. Polym. Sci. Polym. Phys. Ed.* **1975**, *13*, 851–856.

(34) Xiao, Y.; Cummins, D.; Palmans, A. R. A.; Koning, C. E.; Heise, A. Synthesis of Biodegradable Chiral Polyesters by Asymmetric Enzymatic Polymerization and Their Formulation into Microspheres. *Soft Matter* **2008**, *4*, 593–599.

(35) Zupancich, J. A.; Bates, F. S.; Hillmyer, M. A. Aqueous Dispersions of Poly(Ethylene Oxide)-b-Poly(γ-Methyl-ε-Caprolactone) Block Copolymers. *Macromolecules* **2006**, *39*, 4286–4288.

(36) Chen, M.; Zhang, Y.; Zhou, Y.; Zhang, Y.; Lang, M.; Ye, Z.; Tan, W. S. Pendant Small Functional Groups on Poly(ε-Caprolactone) Substrate Modulate Adhesion, Proliferation and Differentiation of Human Mesenchymal Stem Cells. *Colloids Surfaces B Biointerfaces* **2015**, *134*, 322–331.

(37) Lee, R.; Huang, Y.; Chen, W. Synthesis and Characterization of Temperature-Sensitive Block Copolymers from Poly(N-isopropylacrylamide) and 4-Methyl-ε-Caprolactone or 4-Phenyl-ε-Caprolactone. *J. Appl. Polym. Sci.* **2010**, *118*, 1634–1642.

(38) Lee, R.-S.; Hung, C.-B.; Huang, Y.; Chen, W. Synthesis and Characterization of Amphiphilic Block Copolymers from Poly(Ethylene Glycol)Methyl Ether and 4-Methyl-ε-Caprolactone or 4-Phenyl-ε-Caprolactone. *Polymer* **2007**, *48*, 2605–2612.

(39) Rainbolt, E. A.; Washington, K. E.; Biewer, M. C.; Stefan, M. C. Recent Developments in Micellar Drug Carriers Featuring Substituted Poly(ε-Caprolactone)s. *Polym. Chem.* **2015**, *6*, 2369–2381.

(40) Vangeyte, P.; Jérôme, R. Amphiphilic Block Copolymers of High-Molecular-Weight Poly(Ethylene Oxide) and Either ε-Caprolactone or γ-Methyl-ε-Caprolactone: Synthesis and Characterization. *J. Polym. Sci. Part A Polym. Chem.* **2004**, *42*, 1132–1142.

(41) Fiege, H. Cresols and Xylenols. In *Ullmann's Encyclopedia of Industrial Chemistry*; Wiley-VCH Verlag GmbH & Co. KGaA: Weinheim, Germany, 2000; 419–461.

(42) Roberge, D. M.; Buhl, D.; Niederer, J. P. M.; Hölderich, W. F. Catalytic Aspects in the Transformation of Pinenes to p-Cymene. *Appl. Catal. A Gen.* **2001**, *215*, 111–124.

(43) Linnekoski, J. A.; Asikainen, M.; Heikkinen, H.; Kaila, R. K.; Räsänen, J.; Laitinen, A.; Harlin, A. Production of p-Cymene from Crude Sulphate Turpentine with Commercial Zeolite Catalyst Using a Continuous Fixed Bed Reactor. *Org. Process Res. Dev.* **2014**, *18*, 1468–1475.

(44) Schutyser, W.; Van Den Bosch, S.; Dijkmans, J.; Turner, S.; Meledina, M.; Van Tendeloo, G.; Debecker, D. P.; Sels, B. F. Selective Nickel-Catalyzed Conversion of Model and Lignin-Derived Phenolic Compounds to Cyclohexanone-Based Polymer Building Blocks. *Chem. Sus. Chem.* **2015**, *8*, 1805–1818.

(45) Albertsson, A.-C.; Varma, I. K. Recent Developments in Ring Opening Polymerization of Lactones for Biomedical Applications. *Biomacromolecules* **2003**, *4*, 1466–1486.

(46) Martello, M. T.; Burns, A.; Hillmyer, M. Bulk Ring-Opening Transesterification Polymerization of the Renewable δ-Decalactone Using an Organocatalyst. *ACS Macro Lett.* **2012**, *1*, 131–135.

(47) Kricheldorf, H. R.; Kreiser-Saunders, I.; Stricker, A. Polylactones 48. SnOct2-Initiated Polymerizations of Lactide: A Mechanistic Study. *Macromolecules* **2000**, *33*, 702–709.

(48) Witzke, D. R.; Narayan, R.; Kolstad, J. J. Reversible Kinetics and Thermodynamics of the Homopolymerization of L-Lactide with 2-Ethylhexanoic Acid Tin(II) Salt. *Macromolecules* **1997**, *30*, 7075–7085.

(49) In't Veld, P. J. A.; Velner, E. M.; Van De Witte, P.; Hamhuis, J.; Dijkstra, P. J.; Feijen, J. Melt Block Copolymerization of ε-Caprolactone and L-Lactide. *J. Polym. Sci. Part A Polym. Chem.* **1997**, *35*, 219–226.

(50) Wu, L.; Cochran, E. W.; Lodge, T. P.; Bates, F. S. Consequences of Block Number on the Order-Disorder Transition and Viscoelastic Properties of Linear (AB)N Multiblock Copolymers. *Macromolecules* **2004**, *37*, 3360–3368.

(51) Frick, E. M.; Zalusky, A. S.; Hillmyer, M. A. Characterization of Polylactide-b-Polyisoprene-b-Polylactide Thermoplastic Elastomers. *Biomacromolecules* **2003**, *4*, 216–223.

(52) Guth, E. Theory of Filler Reinforcement. *J. Appl. Phys.* **1945**, *16*, 20–25.

(53) Honeker, C. C.; Thomas, E. L. Impact of Morphological Orientation in Determining Mechanical Properties in Triblock Copolymer Systems. *Chem. Mater.* **1996**, *8*, 1702–1714.

(54) Olsén, P.; Borke, T.; Odelius, K.; Albertsson, A.-C. ε-Decalactone: A Thermoresilient and Toughening Comonomer to poly(L-Lactide). *Biomacromolecules* **2013**, *14*, 2883–2890.

(55) Cunningham, R. E.; Auerbach, M.; Floyd, W. J. Preparation and Stress–strain Properties of SBS and SIS Block Polymers Made with Dilithium Initiators. *J. Appl. Polym. Sci.* **1972**, *16*, 163–173.

(56) Zhang, Z.; Grijpma, D. W.; Feijen, J. Triblock Copolymers Based on 1,3-Trimethylene Carbonate and Lactide as Biodegradable Thermoplastic Elastomers. *Macromol. Chem. Phys.* **2004**, *205*, 867–875.

(57) Zhao, Y.; Ning, N.; Hu, X.; Li, Y.; Chen, F.; Fu, Q. Processing Temperature Dependent Mechanical Response of a Thermoplastic Elastomer with Low Hard Segment. *Polymer* **2012**, *53*, 4310–4317.

(58) Tomita, S.; Lei, L.; Urushihara, Y.; Kuwamoto, S.; Matsushita, T.; Sakamoto, N.; Sasaki, S.; Sakurai, S. Strain-Induced Deformation of Glassy Spherical Microdomains in Elastomeric Triblock Copolymer Films: Simultaneous Measurements of a Stress–Strain Curve with 2D-SAXS Patterns. *Macromolecules* **2017**, *50*, 677–686.

(59) Payne, A. R. Hysteresis in Rubber Vulcanizates. *J. Polym. Sci. Polym. Symp.* **2007**, *48*, 169–196.

(60) Hotta, A.; Clarke, S. M.; Terentjev, E. M. Stress Relaxation in Transient Networks of Symmetric Triblock Styrene-Isoprene-Styrene Copolymer. *Macromolecules* **2002**, *35*, 271–277.

(61) Han, C. D.; Baek, D. M.; Kim, J. K.; Ogawa, T.; Sakamoto, N.; Hashimoto, T. Effect of Volume Fraction on the Order-Disorder Transition in Low Molecular Weight Polystyrene-Block-Polyisoprene Copolymers. 1. Order-Disorder Transition Temperature Determined by Rheological Measurements. *Macromolecules* **1995**, *28*, 5043–5062.

(62) Burns, A. B.; Register, R. A. Mechanical Properties of Star Block Polymer Thermoplastic Elastomers with Glassy and Crystalline End Blocks. *Macromolecules* **2016**, *49*, 9521–9530.

(63) Matsumiya, Y.; Watanabe, H.; Takano, A.; Takahashi, Y. Uniaxial Extensional Behavior of (SIS)P-Type Multiblock Copolymer Systems: Structural Origin of High Extensibility. *Macromolecules* **2013**, *46*, 2681–2695.

(64) Panthani, T. R.; Bates, F. S. Crystallization and Mechanical Properties of Poly(L-Lactide)-Based Rubbery/Semicrystalline Multiblock Copolymers. *Macromolecules* **2015**, *48*, 4529–4540.

(65) Fetters, L. J.; Lohse, D. J.; Milner, S. T.; Graessley, W. W. Packing Length Influence in Linear Polymer Melts on the Entanglement, Critical, and Reptation Molecular Weights. *Macromolecules* **1999**, *32*, 6847–6851.

Chapter 4.

Aliphatic polyester thermoplastic elastomers containing hydrogen-bonding ureidopyrimidinone endgroups

4.1 Introduction

Thermoplastic elastomers (TPEs) are characterized by their high strength, tunable modulus, and resilience that makes them suitable for applications ranging from footwear to automotive products.[1] ABA triblock polymers display these elastomeric properties as a result of microphase separation with the glassy A block making up the minority component and the rubbery B block as the matrix. Styrenic TPEs such as polystyrene-*b*-polyisoprene-*b*-polystyrene (SIS) and polystyrene-*b*-polybutadiene-*b*-polystyrene (SBS) are ubiquitous largely due to their versatile and broad property profiles. Significant efforts have been made to utilize annually renewable feedstocks and degradable polymers (e.g., polylactide (PLA) block polymers) as sustainable TPE alternatives to SIS and SBS.[2–4] An aliphatic polyester TPE candidate, PLA-*b*-poly(γ-methyl-ε-caprolactone)-*b*-PLA (LML), reported in our previous work exhibits comparable stress-strain behavior to styrenic TPEs.[5] However, one major limitation in the amorphous LML system is the relatively high level of stress relaxation that occurs at moderate temperatures.

TPEs are known to exhibit some creep, stress relaxation, and hysteresis upon deformation, impacting their long-term mechanical performance.[6-10] The rubbery network in TPEs deforms and rearranges under an applied force (compression or extension) through chain segment motion and slippage of entanglements. The glassy hard domains also undergo displacement and rearrangement, leading to domain deformation and even rupture under enough stress.[11-14] Chain pullout, where chains from the A endblock are forced into the B domain upon deformation, can occur when the system is near the glass transition temperature of the A block ($T_{g,A}$) and/or when the polymers are not well-segregated. Chain

pullout leads to creep (irrecoverable deformation when subjected to a constant stress) and stress relaxation (reduction in restoring force when subjected to a constant strain) in TPEs, limiting their broad utility. There have been many attempts to improve the mechanical properties and mitigate these deleterious effects in TPEs. Some examples include employing various non-linear block architectures,[15-17] chemically crosslinking the rubbery matrix,[18] and chain extension to make -$(AB)_n$- multiblock polymers.[19-23] However, these methods do not change the intrinsic properties of a particular block polymer system such as a low Flory-Huggins interaction parameter χ between the constituent segments and/or the highest T_g being near the use temperature.

Supramolecular polymer materials exhibit useful thermoplastic and self-healing properties for coating and viscosity-modifying applications.[24-28] Ureidopyrimidinone (UPy), a quadruple hydrogen-bonding moiety, has been widely-studied in polymers due to its strong and reversible self-dimerization behavior (Figure 4.1a).[29] Association and dissociation of UPy groups is an equilibrium exchange reaction; dimers dissociate followed by random recombination as detected by NMR spectroscopy.[30] The dissociation rate constant k_d (in this specific case the sum of the forward and reverse rate constants of a model UPy dimer exchange equilibrium: UPy–UPy ⇌ UPy–UPy') is impacted by the polarity of the environment; the UPy-UPy half-life ($t_{1/2} = \ln(2)/k_d$) at 300 K is 1.2 s in toluene-d_8, 0.08 s in $CDCl_3$, and 0.05 s in a mixture of $CDCl_3$ and water.[30] This UPy exchange behavior in UPy-functionalized polymers can be observed using shear rheology: at short times UPy dimers act as physical crosslinks, while at long times UPy dimers dissociate and recombine with another partner to relax stress.[31,32] Dimerized UPy groups

have been shown to laterally aggregate through physical π-π stacking and dipole-dipole interactions to form UPy nanofibers (~7 nm diameter).[33] The substituents on the UPy moiety impact lateral π-π stacking, e.g., bulky substituents result in little to no fiber formation.[34] Hydrogen-bonding linkers connecting the UPy group to the polymer provides added support for lateral stacking (Figure 4.1b); a urethane linkage between UPy and poly(ethylene butylene) results in short UPy fibers with a melting transition ($T_{m,UPy}$) at 45 °C while a urea linkage results in longer UPy fibers with a $T_{m,UPy}$ at 129 °C.[26] Nanofiber formation is also dependent on thermal history (e.g., annealing increases UPy nanofiber length) and concentration of UPy groups (e.g., spherical aggregates have been observed at low UPy concentration while long fibers form at high UPy concentration).[35] Thermoplastic behavior is observed when aggregates and dimers can dissociate upon heating or in the presence of solvent.[36-38]

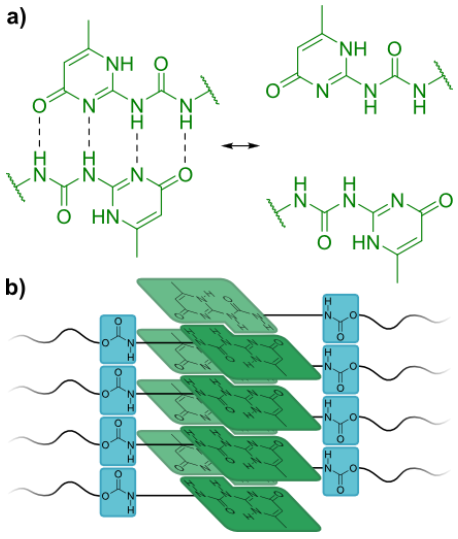

Figure 4.1.
Illustration of a) reversible quadruple hydrogen-bonding of ureidopyrimidinone (UPy) and b) lateral stacking of hydrogen-bonded UPy groups (green) supported by additional hydrogen-bonding of urethane linkers (blue).

Mechanical performance of supramolecular UPy-based TPEs has been found to be dependent on both bulk polymer properties and UPy aggregation behavior. Aggregates of UPy dimers in UPy-telechelic polymers are necessary to provide a multi-junction point for network formation. When UPy dimerizes but does not aggregate to a large extent in amorphous, low-T_g polymers, samples behave like high molar mass polymers rather than crosslinked networks.[26,39] Since the association/dissociation of UPy groups are supramolecular in nature, the nanofibers and dimers can reshuffle under stress resulting in useful self-healing properties.[27] However, the long-term mechanical performance with respect to creep, stress relaxation, and hysteresis suffers. Desirable elastomeric behavior is observed when UPy moieties are combined with polymers that exhibit other physical network forming properties (e.g., crystallization and microphase separation).[39]

The combination of microphase separated block polymers and supramolecular interactions results in complex hybrid materials. AB and ABA block polymers with supramolecular moieties in the rubbery B domains exhibit self-healing properties as the rubbery B block can reorganize after damage.[40,41] ABA block polymers with telechelic hydrogen-bonding moieties yield supramolecular -$(AB)_n$- multiblock polymers that exhibit shape memory behavior and are tougher than the comparative unfunctionalized derivatives.[42–46] PLA block polymers with UPy endgroups have been shown to exhibit higher softening temperatures (~100 °C) compared to the inherent T_g of PLA (~40 °C).[43] Shape-memory behavior has also been observed in these supramolecular TPEs as temporary shapes can be set above the T_g of PLA and below the thermal transition attributed to UPy dissociation.[42–45,47] The chain segment mobility is reduced in UPy-

telechelic PLA block polymers, manifesting in slower aging of PLA and suppressed crystallization of poly((*S*,*S*)-lactide) (PLLA).[42,46,47] Adding UPy endgroups to PLA-*b*-polybutadiene-*b*-PLA (LBL, containing 82–100 wt% PLA) resulted in increased toughness, attributed to a higher amount of crazing during plastic deformation in UPy-telechelic samples.[46]

In this work, we combine the hydrogen-bonding UPy group with LML TPEs to yield supramolecular multiblock elastomers with the aim of mitigating undesirable stress relaxation.[5] We focus on systems of moderate molar masses (34 kg mol^{-1}) that are more processable but mechanically inferior compared to their high performing, high molar mass variants.[5] We hypothesize that end-functionalizing the PLA blocks with UPy groups will reduce chain pullout from these domains through intermolecular H-bonding interactions. We first investigated the properties of telechelic UPy-functionalized poly(γ-methyl-ε-caprolactone) (PMCL) as a benchmark. The thermal properties of UPy-functionalized LML were compared to unfunctionalized LML through differential scanning calorimetry (DSC) and dynamic mechanical thermal analysis (DMTA) experiments. Uniaxial extension tests were utilized to assess the impact of UPy group incorporation on LML tensile properties. We also show semicrystalline block polymers PLLA-*b*-PMCL-*b*-PLLA (LLMLL) and UPy–LLMLL–UPy exhibit more complex thermal behavior. We demonstrate the tensile properties are influenced by the thermal history and overall degree of crystallinity of these semicrystalline TPEs. Finally, hysteresis and stress relaxation studies demonstrate the impact of UPy groups on the long-term behavior of functionalized LML and LLMLL TPEs.

4.2 Results and Discussion

Low-T_g aliphatic polyesters including polycaprolactone (PCL), polyvalerolactone (PVL), and PMCL with UPy endgroups have previously been reported.[36,48–51] UPy-functionalized semicrystalline polyesters PCL, PVL, and P(CL-*co*-VL) exhibit elastomeric properties with relatively low strain at break ($\leq$ 31%).[49] While UPy-functionalized PMCL (UPy–PMCL–UPy) has been reported in the literature, the results are limited to high temperature (70–130 °C) rheological properties.[50] The results by van Beek and coworkers demonstrate the formation of crystalline UPy fibers in UPy–PMCL$_{3.9k}$–UPy (M_n = 3.9 kg mol^{-1}) that melt at 40 °C with a melting enthalpy ΔH_m of 5.8 J g^{-1}.[50] Yet, room temperature mechanical properties of UPy–PMCL–UPy have not been reported. Although the $T_{m,UPy}$ is relatively low, the presence of UPy fibers at room temperature seems promising and may result in room temperature elastomeric behavior.[26]

To explore this possibility, we prepared two UPy-functionalized telechelic PMCL samples UPy–PMCL$_{11k}$–UPy (M_n = 11 kg mol^{-1}, Table 4.1, entry 2) and UPy–PMCL$_{26k}$–UPy (M_n = 26 kg mol^{-1}, Table 4.1, entry 4) (Scheme 4.1). Compression molding of these samples at 60 °C produced transparent, colorless films. DMTA of these samples showed rubbery plateaus above the T_g of PMCL at E' = 2 MPa (Figure 4.2a). The effective molar mass between crosslinks ($M_{x,eff}$) was calculated to be 3.8 kg mol^{-1}, consistent with the molar mass between entanglements (M_e) reported for PMCL homopolymer (2.9–4.6 kg mol^{-1}).[5,52] The rubbery plateau modulus between –50 and 30 °C was largely independent of temperature and concentration of UPy groups (4.9 wt % in UPy–PMCL$_{11k}$–UPy and 1.7 wt

% in UPy–PMCL$_{26k}$–UPy). These DTMA results indicate the low strain mechanical properties of UPy–PMCL–UPy are likely dominated by the entanglements in PMCL. The samples soften around 30 °C for UPy–PMCL$_{11k}$–UPy and 40 °C for UPy–PMCL$_{26k}$–UPy, close to the expected value of $T_{m,UPy}$ at 40 °C.[50] Unfunctionalized PMCL$_{26k}$ softens near −30 °C, indicating the UPy aggregates in UPy–PMCL–UPy support a rubbery network up to 30–40 °C (Figure 4.2b). DSC results corroborate the T_g of PMCL observed by DMTA, yet no melting endotherm was observed by DSC for the putative UPy aggregates near 40 °C (Figure 4.2c). The absence of a melting endotherm in DSC could be due to the lack of significant lateral stacking of UPy groups in UPy–PMCL$_{11k}$–UPy and UPy–PMCL$_{26k}$–UPy.[35]

Scheme 4.1.
Reaction conditions for end-functionalization of α,ω-hydroxy telechelic polymers with UPy–NCO.

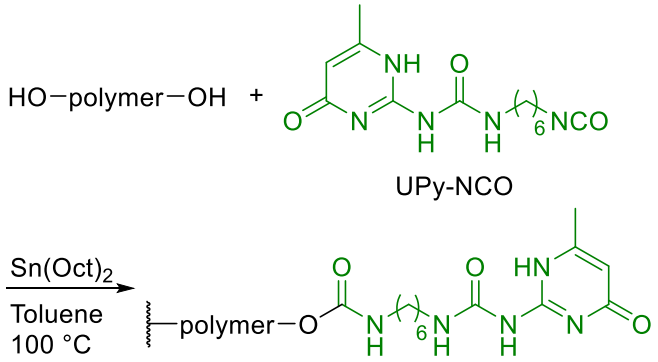

Table 4.1.
Summary of molecular and thermal properties of polymers and their UPy-functionalized counterparts.

Entry	Polymer	$M_{n,total}$[a] (kg mol^{-1})	$f_{(L)LA}$[a]	w_{UPy}[a]	$M_{n,total}$[b] (kg mol^{-1})	$Đ$[b]	$T_{g,PMCL}$[c] (°C)	$T_{g,PLA}$[c] (°C)	$T_{m,PLLA}$[c] (°C)	$T_{m,UPy}$[c] (°C)	$T_{d,5\%}$[d] (°C)
1	$PMCL_{11k}$	11			14	1.11	−63				244
2	UPy-$PMCL_{11k}$-UPy	12		0.049	15	1.16	−57			ND	272
3	$PMCL_{26k}$	26			30	1.14	−60				269
4	UPy–$PMCL_{26k}$–UPy	26		0.017	32	1.19	−58			ND	277
5	LML (34, 0.19)	34	0.19		39	1.09	−56	ND			227
6	UPy–LML–UPy	34	0.19	0.013	41	1.07	−57	ND		88	250
7	LLMLL (34, 0.19)	34	0.19		33	1.10	−57	ND	138		244
8	UPy–LLMLL–UPy	34	0.19	0.013	45	1.04	−56	ND	134	ND	263

a) Analysis by ^{1}H NMR spectroscopy; b) SEC in THF with MALLS; c) second heat in DSC, heating at 10 °C min^{-1}; d) temperature at 5% mass loss by TGA under nitrogen atmosphere, heating at 10 °C min^{-1}. ND = not detected.

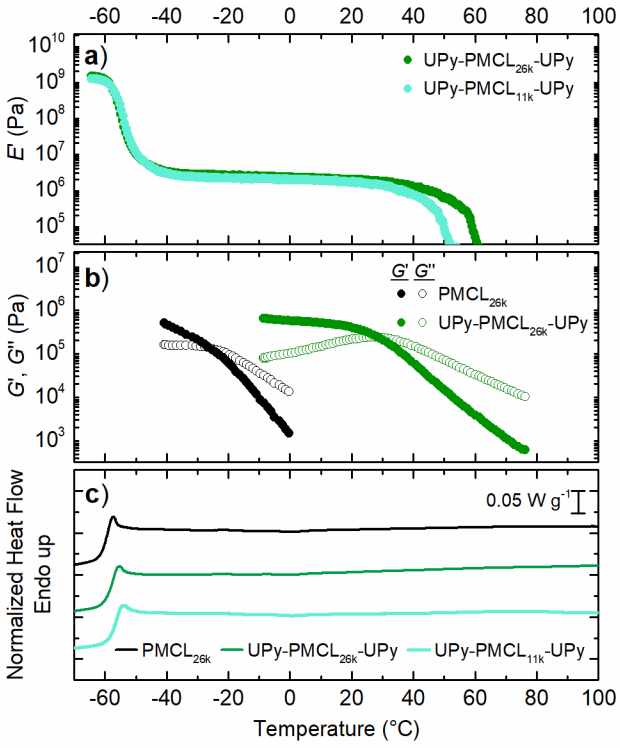

Figure 4.2.
a) DMTA in extension of UPy–$PMCL_{11k}$–UPy and UPy–$PMCL_{26k}$–UPy upon heating at 5 °C min^{-1} at 1 Hz and 0.05% strain, b) DTMA in shear of $PMCL_{26k}$ and UPy–$PMCL_{26k}$–UPy, heating 5 °C min^{-1} at 1 rad s^{-1} and 1% strain, and c) DSC upon heating at 10 °C min^{-1} (bottom).

UPy aggregation in UPy–PMCL–UPy is evident by the plateau modulus in DMTA that extends well above the softening temperature for unfunctionalized PMCL. However, the UPy aggregates are apparently not extensive enough to give UPy–PMCL–UPy elastomeric character in and of itself. Qualitatively, UPy–PMCL–UPy flowed and conformed to the shape of the storage container over long times, days, at room temperature. When films were loaded in the tensile tester and extended, the polymer would draw and thin, behaving like soft chewing gum. Although the force to break UPy nanofibers has not been quantified, it is estimated that less energy is required to break up aggregates/nanofibers than UPy dimers.[53,54] Upon extension of UPy-telechelic networks, UPy aggregates/nanofibers begin to fragment as polymer chains become oriented and further extension leads to UPy dissociation.[53] The alignment of the polymer chains at this point can lead to strain-induced crystallization, resulting in strain-hardening behavior and elastomeric properties.[39,49,53] This strain induced crystallization provides UPy-functionalized semicrystalline polyesters PCL, PVL, and P(CL-*co*-VL) their elastomeric properties.[49] However, UPy–PMCL–UPy does not exhibit strain-induced crystallization behavior and exhibits permanent deformation upon extension.[26] We conclude that UPy–PMCL–UPy networks did not exhibit appreciable mechanical integrity at room temperature due to the lack of other network-forming features (i.e., crystallization or microphase separation) thus we moved on to exploring the incorporation of UPy groups into PMCL-containing block polymers.[39,49,53]

Polylactide-b-poly(γ-methyl-ε-caprolactone)-b-polylactide with UPy end groups

High molar mass LML with M_n = 94 kg mol^{-1} and f_{LA} = 0.17 (LML (94, 0.17) is characterized by excellent elastomeric properties with high strength and high extensibility.[5] In this work, low molar mass samples were targeted to achieve a low order-disorder transition temperature (T_{ODT}), providing TPEs that would require lower processing temperatures. Triblock polymer, LML (34, 0.19) (Table 4.1, entry 5), and the corresponding UPy-functionalized derivative, UPy–LML–UPy (Table 4.1, entry 6), were synthesized as reported previously (Scheme 4.1).[5,36]

LML and UPy–LML–UPy are microphase separated at room temperature, exhibiting a principal scattering peak q^* with a higher order shoulder at $\sqrt{3}q^*$ in small-angle X-ray scattering (SAXS, Figure 4.3). The principal domain spacing in UPy–LML–UPy ($d = 2\pi/q^*$ = 17.5 nm) is slightly larger than in LML (d = 16.8 nm), possibly due to the UPy endgroups contributing to increased chain length and/or fractionation of the polymer during purification of UPy–LML–UPy. Although an order-disorder transition (ODT) was not observed as a distinct transition and thus a discrete T_{ODT} was not able to be determined, we posit that these samples are disordered at elevated temperature. The intensity I_m of the principal scattering peak q^* of LML (34, 0.19) and UPy–LML–UPy decreases upon heating until no peak is observed at 100 °C (Figure 4.4). The higher order shoulder at $\sqrt{3}q^*$ is no longer observed between 53 °C and 70 °C, typically indicative of an ODT, yet a discontinuous decrease in intensity was not observed (Figure 4.4c).[55] A clear ODT was also not observed using DMTA as samples did not exhibit a precipitous drop in modulus (Figure 4.5).[56] There is a change in slope near 60 °C, and we note terminal flow

behavior, $G' \sim \omega^2$ and $G'' \sim \omega^1$, at 70 °C in LML (34, 0.19), indicating this sample should be readily processable above 70 °C (Figure 4.5).

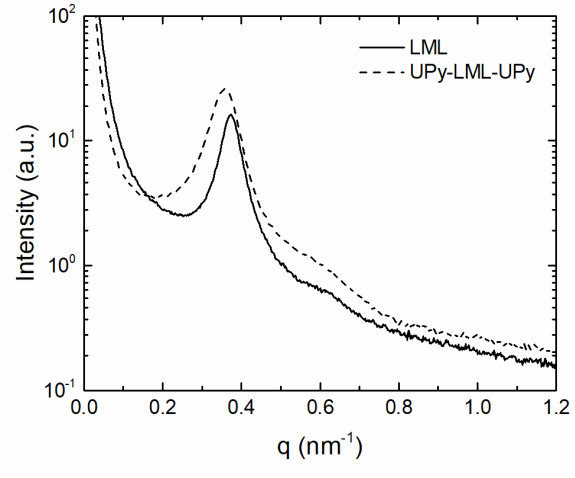

Figure 4.3.
Room temperature SAXS patterns of LML (34, 0.19) and UPy–LML–UPy. Samples were prepared by compression molding at 100 °C and cooling rapidly to room temperature.

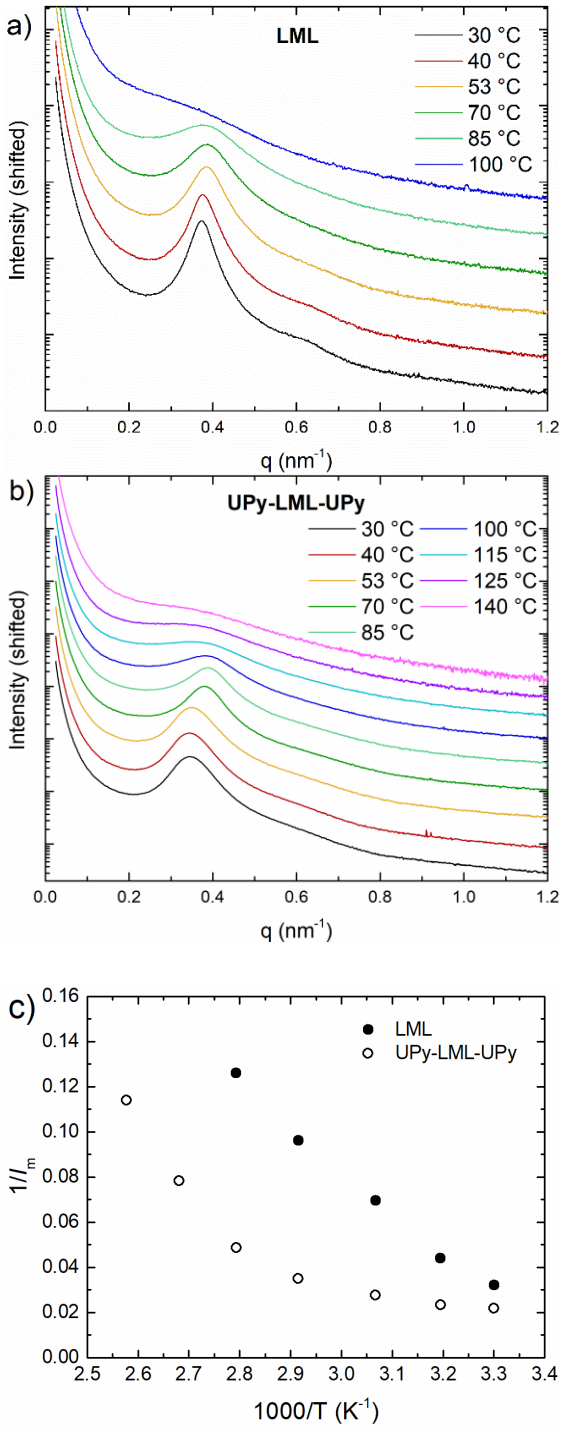

Figure 4.4.
SAXS profiles of a) LML (34, 0.19) and b) UPy–LML–UPy after annealing at the indicated temperature for 2 min. c) The inverse peak intensity of q^* is plotted as a function of 1000/T (K^{-1}).

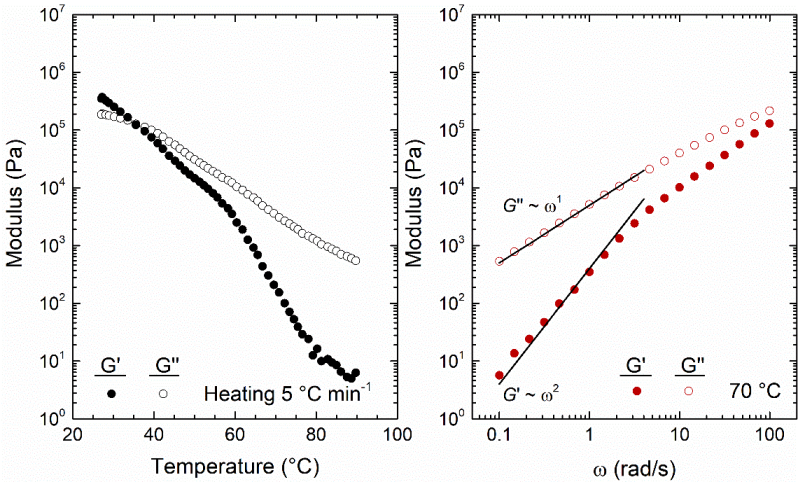

Figure 4.5.
Shear modulus of LML (34, 0.19) heating at 5 °C min^{-1} (1% strain, 1 rad s^{-1}) on the left. Frequency sweep of LML at 70 °C in the linear viscoelastic regime.

The thermal properties of the samples were characterized using DSC (Figure 4.6). The glass transition for PMCL occurs at −56 °C and there is broad sloping baseline near the expected T_g of PLA by DSC. Using the Fox equation, we approximate that the PMCL matrix could contain up to 6 wt % PLA.[57] The low overall molar mass results in lower segregation strength χN that could lead to some degree of mixing between blocks. This is in contrast to high molar mass LML (94, 0.17) that exhibits identical $T_{g,PMCL}$ in PMCL and LML (94, 0.17) as well as a distinct $T_{g,PLA}$ near 45 °C, indicating there is negligible PLA/PMCL mixing.[5] In addition to the thermal transitions observed in LML (34, 0.19), UPy–LML–UPy exhibits a small endothermic transition near 88 °C (ΔH_m = 0.8 J g^{-1}). This additional thermal transition is attributed to the melting of UPy aggregates in the PLA domain.[37]

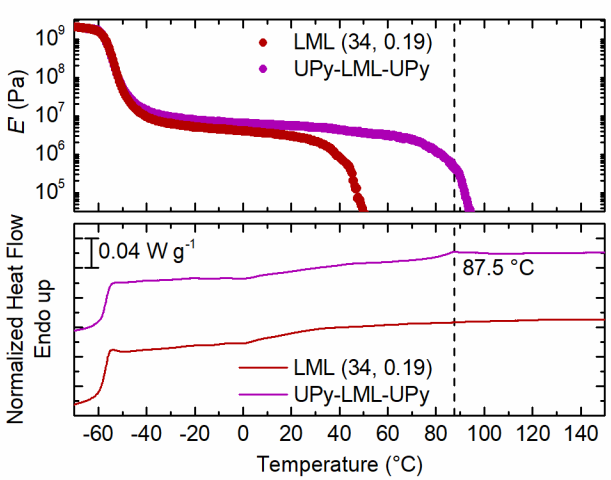

Figure 4.6.
Thermal properties of LML (34, 0.19) and UPy-LML-UPy analyzed by DMTA in tension upon heating at 5 °C min^{-1} (top, 1 Hz, 0.05% strain) and DSC upon heating at 20 °C min^{-1} (bottom).

The modulus of compression molded films in uniaxial extension was measured as a function of temperature (Figure 4.6). Both samples exhibit a nearly identical drop in modulus near −55 °C due to the glass transition of PMCL. The modulus in the rubbery plateau region for both LML and UPy–LML–UPy are similar, E' ≈ 3 MPa and 5 MPa, respectively. The plateau modulus is dominated by entanglements in the PMCL block with PLA domains acting as solid fillers, thus the higher value as compared to PMCL homopolymer (Figure 4.2).[5] LML (34, 0.19) softens near 45 °C, at the expected T_g of PLA (Figure 4.5). UPy–LML–UPy maintains this plateau modulus up to 80 °C after which the modulus decreases significantly, corroborating the $T_{m,UPy}$ observed by DSC.[58] Interestingly, this drop in modulus occurs at a higher temperature than in UPy–PMCL–UPy (30–40 °C).[26] Based on previous literature, we posit that the differences between the PLA and PMCL repeat unit adjacent to the urethane group could impact the stacking of

UPy groups, leading to the difference in softening temperature observed in DMTA for UPy–LML–UPy and UPy–PMCL–UPy.

TPE mechanical performance is highly dependent on molar mass; lower molar mass results in less entangled polymers in both the glassy and rubbery domains as well as lower segregation strength χN between blocks. With a low molar mass sample such as LML (34, 0.19), we expected the tensile properties to be inferior to the high molar mass variants based on our experience with these and related aliphatic polyester block polymers.[21,59] To determine the ultimate tensile properties of triblock polymers, samples were compression molded into films and cut into dog-bone shaped tensile bars. LML (34, 0.19) exhibited strain softening behavior (Figure 4.7) with relatively low modulus and low stress at break (E = 1.7 ± 0.1 MPa and σ_b = 0.11 ± 0.01 MPa, respectively). LML (34, 0.19) samples were drawn upon extension and thinned until they broke around 850% elongation. These properties are very different from high molar mass LML (94. 0.17) that exhibited strain hardening behavior and broke around 25 MPa and 1000% strain.[5] This dependence of tensile properties on molar mass agrees with previous studies on styrenic TPEs.[1,60] The low χN and the lack of PLA entanglements ($M_{n,PLA}$ = 4 kg mol^{-1}) in low molar mass LML (34, 0.19) likely results in chain pullout from the PLA domains, leading to ductile failure at low stresses.

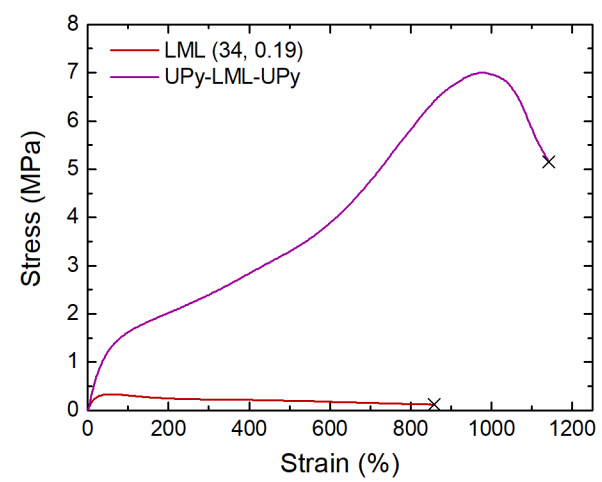

Figure 4.7.
Representative stress-strain curve for LML (34, 0.19) and UPy–LML–UPy extending at 50 mm min^{-1} up to its break point indicated by ×.

The tensile properties in the parent LML (34, 0.19) were dramatically improved by end-functionalizing with UPy groups. UPy–LML–UPy samples exhibited much higher modulus, ultimate tensile strength, and elongation at break (E = 3.7 ± 0.2 MPa, σ_b = 5.4 ± 0.3 MPa, ε_b = 1133 ± 25%) as compared to LML (Figure 4.7). Similar improvements in stress-strain behavior were observed when low molar mass triblock polymers were chain extended to make multiblock polymers.[21] Strain hardening behavior is observed in UPy–LML–UPy upon extension leading to stress whitening near 1000%.[46,61,62] Optical images of the UPy–LML–UPy films after testing show small cracks perpendicular to the direction of extension, indicating stress whitening is a result of hole formation possibly due to crazing (Figure 4.8). The difference between LML (34, 0.19) and UPy–LML–UPy tensile properties is consistent with distinct failure mechanisms.[47,63] Based on previous reports on the strength of UPy dimers and UPy stacks, the observed improvements in mechanical properties are likely not directly due to the UPy aggregates/dimers withstanding the forces

applied.[53,54] Rather, the synergistic combination of the microphase separated structure and UPy aggregates in the PLA domain contribute to the improved mechanical properties. We hypothesize that the aggregation of UPy groups reduces chain pullout from the PLA domain during extension. The force is then distributed to the PMCL matrix and the intact PLA domains, ultimately leading in PLA domain deformation and rupture at higher elongation and stress.[64] The above experiments demonstrate that we can achieve significant improvements in TPE properties by end-functionalizing underperforming LML block polymers with UPy groups. We next explored the influence of end block crystallinity on the properties of these UPy-functionalized TPEs.

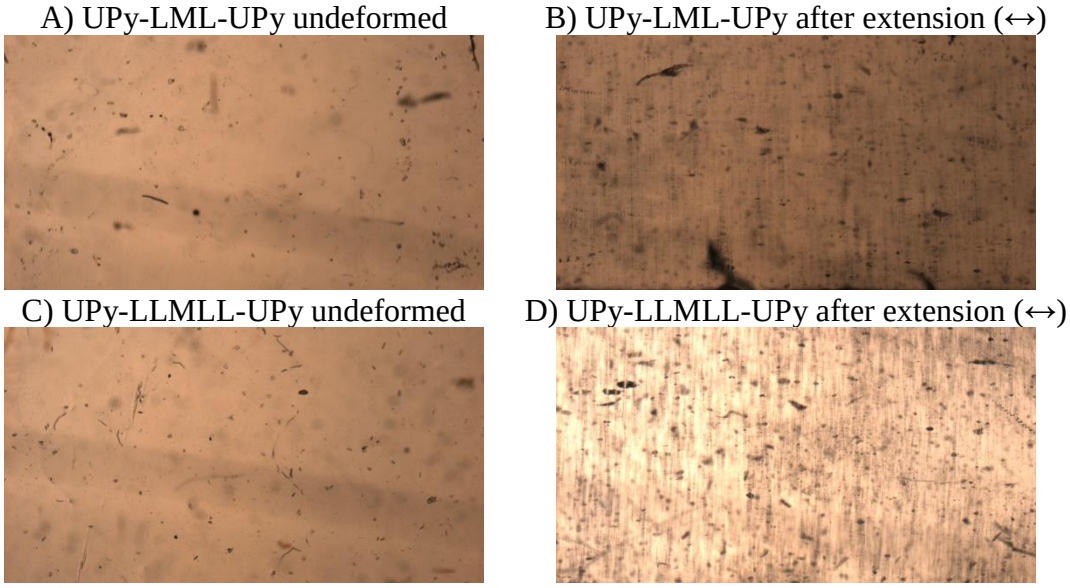

Figure 4.8.
Optical microscopy images of before (A,C) and after (B,D) tensile testing.

Poly((S,S)-lactide)-b-poly(γ-methyl-ε-caprolactone)-b-poly((S,S)-lactide) with UPy end groups

Low molar mass semicrystalline analogues LLMLL (34, 0.19) (Table 4.1, entry 7) and UPy–LLMLL–UPy (Table 4.1, entry 8) were synthesized as discussed above (Scheme 4.1).[5,36] DSC traces of LLMLL (34, 0.19) and UPy–LLMLL–UPy demonstrate the PLLA blocks can crystallize in both samples with T_c values near 100 °C and T_m values near 135 °C (Figure 4.9). Although there is no discernable melting transition for UPy aggregates, enthalpies ΔH_c and ΔH_m in UPy–LLMLL–UPy are smaller in magnitude than those for LLMLL (34, 0.19). These results support suppressed crystallinity in UPy-functionalized PLLA derivatives that could be due to reduced chain segment mobility of the PLLA end block.[42,67]

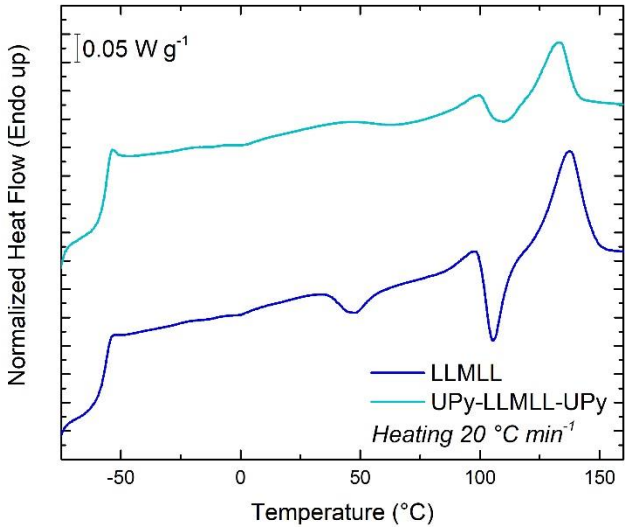

Figure 4.9.
Vertically shifted DSC traces of LLMLL (T_c = 106 °C, ΔH_c = 3.3 J g^{-1} and T_m = 137 °C, ΔH_m = 8.2 J g^{-1}) and UPy-LLMLL-UPy (T_c = 109 °C with ΔH_c = 1.5 J g^{-1} and T_m = 134 °C with ΔH_m = 3.7 J g^{-1}) during the second heat while heating at 20 °C min^{-1}.

Based on the lack of a principal scattering peak at 100 °C in the amorphous LML (34, 0.19) sample (SAXS, Figure 4.4), we estimated that LLMLL (34, 0.19) will also be disordered at 100 °C which is below the PLLA crystallization temperature for this sample (T_c = 106 °C).[51] This indicates the potential for crystalline breakout where crystalline lamellae dominate the morphology when crystallization is not confined within microphase separated PLLA domains.[51–53] To explore this possibility, LLMLL (34, 0.19) and UPy–LLMLL–UPy were processed in three ways to better understand the impact of processing history on mechanical and thermal properties; samples were (i) melt-processed (MP) at 160 °C and quenched rapidly to limit crystallization (LLMLL^{MP} and UPy-LLMLL-UPy^{MP}), (ii) melt-processed at 160 °C, quenched rapidly, then cold-crystallized at 80 °C (MP*) in a weakly segregated state to promote crystallization (LLMLL^{MP*} and UPy-LLMLL-UPy^{MP*}), and (iii) solvent-cast (SC) from dichloromethane and annealed at 40 °C (LLMLL^{SC} and UPy-LLMLL-UPy^{SC}) for comparison. LLMLL^{SC} was the only sample to appear opaque indicating some level of crystalline breakout. Transparent films were produced for all other samples.

SAXS patterns of the processed films are shown in Figure 4.10. LLMLL^{MP} exhibits a broad principal scattering peak near 0.34 nm^{-1} (d = 18.5 nm), comparable to the domain spacing in the amorphous LML (34, 0.19), quenched from the disordered melt at 100 °C (Figure 4.9). This is consistent with vitrification of the melt morphology in LLMLL^{MP} when cooled rapidly to below the T_g. The LLMLL^{MP} SAXS pattern does not exhibit any higher order reflections due to the putative disordered state of the samples at 160 °C. In contrast, LLMLL^{MP*} and LLMLL^{SC} exhibit dramatically increased principal domain

spacings of 37.2 nm and 27.8 nm, respectively. This is likely a result of PLLA crystallites dominating the morphology of the films. LLMLL^{SC} exhibits a higher order reflection at 2q*, indicative of lamellar morphology. The increased domain spacing, the higher order peak at 2q*, and the opaque appearance of LLMLL^{SC} indicate that a lamellar crystalline morphology dominates the structure in the film due to crystalline breakout.[65]

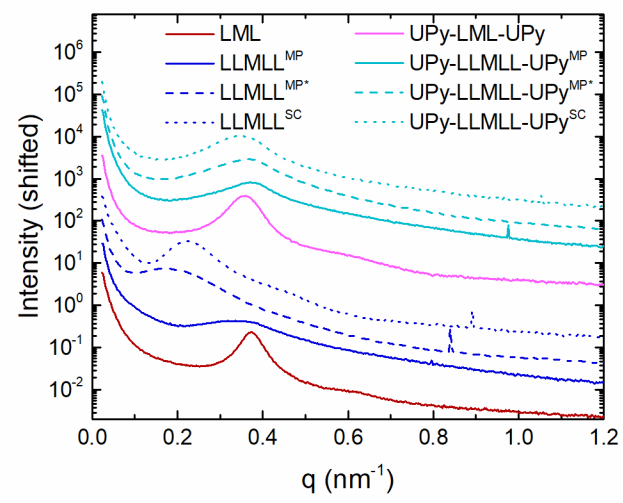

Figure 4.10.
SAXS of samples LLMLL (34, 0.19) and UPy–LLMLL–UPy after processing, vertically shifted for clarity.

SAXS patterns of semicrystalline derivatives with UPy endgroups exhibit a principal scattering peak 0.345–0.372 nm^{-1} (d = 16.9–18.7 nm) with no higher order reflections (Figure 4.10). The domain spacing is similar to that observed in the non-crystalline UPy–LML–UPy derivative, d = 17.5 nm. In fact, UPy–LLMLL–UPy SAXS patterns are essentially independent of the three different processing conditions MP, MP*, and SC (Figure 4.10) indicating there is no evidence by SAXS that crystallization disrupts

the morphology of the UPy–LLMLL–UPy films. The presence of UPy endgroups in LLMLL seems to mitigate crystalline breakout under the described processing conditions (compare $LLMLL^{SC}$ with clear crystalline break out and $UPy–LLMLL–UPy^{SC}$ in Figure 4.10).

The thermal properties of processed films were characterized using DSC (Figure 4.11) and the degree of crystallinity Φ was calculated using the following equation:[66]

$$\Phi = \Delta H_m/(\Delta H_m^{\infty} \times w_{LLA})$$

Where $\Delta H_m^{\infty} = 93$ J/g for an infinite PLLA crystal and w_{LLA} is the weight fraction of PLLA in the block polymer. $LLMLL^{MP}$ exhibits the lowest degree of crystallinity ($\Phi = 0.16$) with a T_m at 135 °C, indicating rapid cooling from the melt prevents significant formation of PLLA crystallites. The degree of crystallinity was enhanced to $\Phi = 0.32$ by cold-crystallizing the samples at 80 °C ($LLMLL^{MP*}$). $LLMLL^{SC}$, the sample with the higher order peak at $2q^*$ likely a consequence of crystalline breakout (SAXS, Figure 4.10), exhibited the highest degree of crystallinity with $\Phi = 0.42$.

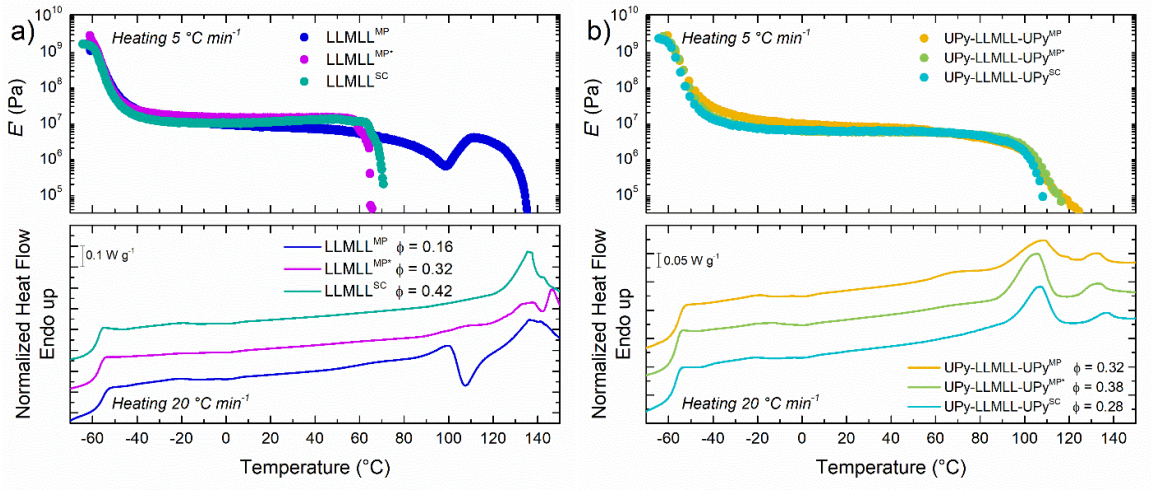

Figure 4.11.
Thermal properties of (a) LLMLL (34, 0.19) and (b) UPy–LLMLL–UPy analyzed by DMTA in tension upon heating at 5 °C min^{-1} (top, 1 Hz, 0.05% strain) and DSC upon heating at 20 °C min^{-1} (bottom).

In the UPy–LLMLL–UPy samples, two PLLA melting endotherms centered at 107 °C and 135 °C were observed (Figure 4.11). Work by Bao and coworkers argue that less stable PLLA crystallites are preferentially formed in the presence of UPy groups, resulting in lower temperature melting endotherms.[67] We observe more pronounced melting endotherms at 107 °C in UPy–LLMLL–UPy, indicating less stable PLLA crystallites are more dominant in these samples. For simplicity, the degree of crystallinity Φ was calculated as described above by adding the enthalpies of both melting transitions and using the enthalpy of fusion for pure PLLA ΔH_m^{∞} = 93 J/g. Contrary to the unfunctionalized examples, the solvent-cast UPy–LLMLL–UPy sample exhibits the lowest degree of crystallinity (UPy–LLMLL–UPy^{SC} Φ = 0.28) among the series. The degree of crystallinity in UPy–LLMLL–UPy^{MP} (Φ = 0.32) was somewhat enhanced by annealing the sample (UPy–LLMLL–UPy^{MP*} Φ = 0.38). The different sample processing histories resulted in

different degrees of crystallinity, yet the PLLA crystallites in UPy–LLMLL–UPy seem to remain confined in MP, MP* and SC samples as SAXS patterns do not indicate any dramatic changes in morphology (Figure 4.10).

DMTA was used characterize the mechanical properties of the samples as a function of temperature (Figure 4.10). The modulus drops near −55 °C due to the PMCL glass transition and the rubbery plateau modulus is consistent across all samples, E' = 7–13 MPa. $LLMLL^{MP}$ maintains the plateau upon heating, undergoing a melting then crystallization event near 100 °C indicated by the recoverable dip in modulus. The modulus then drops precipitously near 135 °C due to melting of PLLA crystallites. This was further corroborated using shear rheology (Figure 4.12a). Unlike $LLMLL^{MP}$ which maintains a plateau modulus upon heating, $LLMLL^{MP*}$ and $LLMLL^{SC}$ both undergo brittle fracture during testing, leading to the apparent precipitous drop in modulus at 60 °C. This early fracture indicates the mechanical properties are compromised in $LLMLL^{MP*}$ and $LLMLL^{SC}$ samples, likely a result of some crystal breakout in these lower-molar-mass and weakly segregated semicrystalline block polymers under these processing conditions.

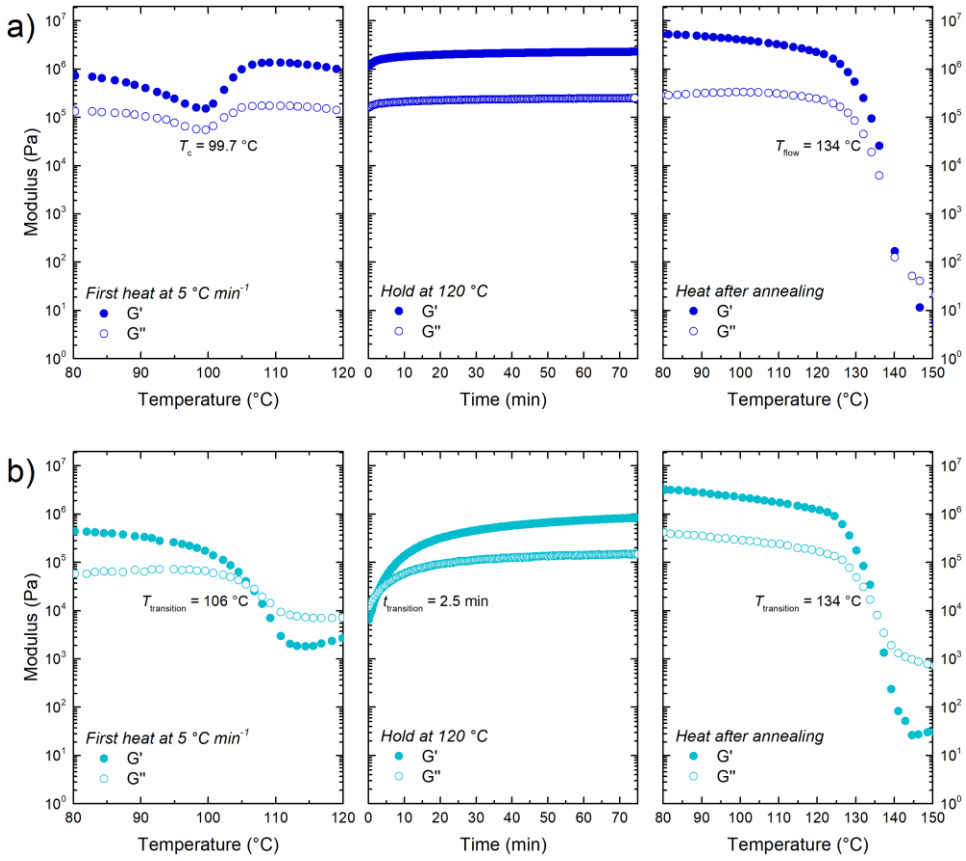

Figure 4.12.
Shear rheology experiments in 8 mm diameter parallel plates, at 1% strain and 1 rad/s frequency, heating at 5 °C min^{-1}. An 8 mm diameter sample was cut from a film of (a) LLMLL^{MP} and (b) UPy-LLMLL-UPy^{SC}. The sample was loaded while maintaining an axial force to establish contact between the parallel plates and the sample during the first heat (left). Immediately after 120 °C was reached, the modulus was monitored as a function of time (middle). After annealing the sample, the sample was cooled and then heated again (right).

All UPy–LLMLL–UPy samples exhibit a decrease in modulus near 100 °C, corresponding with the melting transition at 107 °C observed in DSC (Figure 4.11b). These data further demonstrate that the temperature dependent mechanical properties of UPy–LLMLL–UPy are independent of processing conditions (MP, MP*, and SC). Shear rheology experiments were used to demonstrate that crystallization in UPy–LLMLL–UPy

can be promoted through annealing at 120 °C, resulting in formation of PLLA crystallites that melt at 134 °C (Figure 4.12b). Comparing the shear rheology results of LMLL (34, 0.19) and UPy–LLMLL–UPy indicates that crystallization is slower in UPy–LLMLL–UPy, again consistent with reduced chain segment mobility.

The stress-strain behavior of UPy–LLMLL–UPy is drastically improved compared to LLMLL (34, 0.19) (Figure 4.13, Table 4.2). LLMLL^{MP} (Table 4.2, entry 3) does not exhibit strain hardening behavior, breaking at σ_b = 2.5 ± 0.1 MPa and ε_b = 486 ± 21%. Enhanced crystallinity in LLMLL^{MP*} (Table 4.2, entry 4) and LLMLL^{SC} (Table 4.2, entry 5) results in lower strain at break and higher modulus. This is consistent with crystalline breakout dominating the microstructure; the samples exhibit increased stiffness and lower strain at break.[54,55]

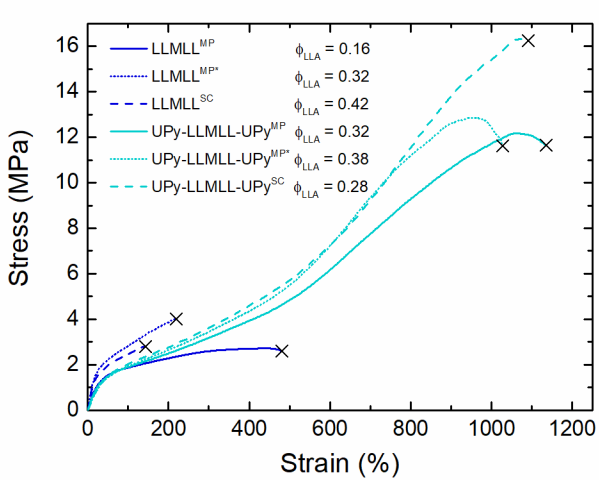

Figure 4.13.
Representative stress-strain curve for polymers extending at 50 mm min^{-1} up to its break point indicated by ×.

Table 4.2.
Summary of ultimate tensile properties, recovery, and crystallinity of LLMLL and UPy-LLMLL-UPy.

Entry	Polymer	E^a (MPa)	$\sigma_B{}^a$ (MPa)	$\varepsilon_B{}^a$ (%)	Toughness[a] (MJ/m^3)	Residual strain[b] (%)	Strain recovery[c] (%)	$\Delta H_m{}^d$ (J/g)	Φ_C
1	LML	1.7 ± 0.1	0.11 ± 0.01	870 ± 40	1.8 ± 0.1	NT	NT		
2	UPy–LML–UPy	3.7 ± 0.2	5.4 ± 0.3	1130 ± 30	46 ± 2	50 – 52	74 – 75		
3	$LLMLL^{MP}$	5.1 ± 0.2	2.5 ± 0.1	490 ± 20	11 ± 1	30 – 31	84 – 85	3.4	0.16
4	$LLMLL^{MP*}$	11 ± 1	4.0 ± 0.3	220 ± 30	6.3 ± 1.1	NT	NT	7.0	0.32
5	$LLMLL^{SC}$	10 ± 1	2.9 ± 0.3	150 ± 30	3.2 ± 0.9	NT	NT	9.1	0.42
6	UPy–LLMLL–UPy^{MP}	5.4 ± 0.3	13 ± 1	1140 ± 40	79 ± 7	19 – 20	89 – 90	6.9	0.32
7	UPy–LLMLL–UPy^{MP*}	4.2 ± 0.3	11 ± 1	1080 ± 90	69 ± 4	14 – 20	90 – 93	8.3	0.38
8	UPy–LLMLL–UPy^{SC}	4.1 ± 0.3	16 ± 1	1020 ± 90	80 ± 6	11 – 13	93 – 94	6.2	0.28

a) Average values and standard deviations are reported for tensile tests of 5 samples extended at 50 mm min^{-1}, toughness was calculated as area under the stress-strain curve. b) The residual strain is the percent strain where the sample exhibits zero stress after the 10^{th} extension cycle. c) Strain recovery calculated by taking 100×(200%-residual strain)/200%. d) area under the melting endotherm during the first heat in DSC, heating at 20 °C min^{-1}. NT = not tested.

The different processing conditions do not significantly impact the stress-strain behavior of UPy-functionalized TPEs as the thermal properties and microstructure are similar across samples. UPy–LLMLL–UPy films exhibit strain hardening behavior, leading to stress whitening in the sample near 1000% strain with a subsequent downturn in the stress strain curve. Figure 4.8 shows optical microscopy images that show lines perpendicular to the direction of extension, indicative of crazing. TEM micrographs of the gauge area of these samples after extension show UPy-LLMLL-UPy exhibits < 1 μm voids while UPy–LML–UPy exhibits large > 1 μm voids (Figure 4.14). This indicates that the increased tensile toughness in UPy-functionalized TPEs is a result of deformation mechanisms that result in void formation.

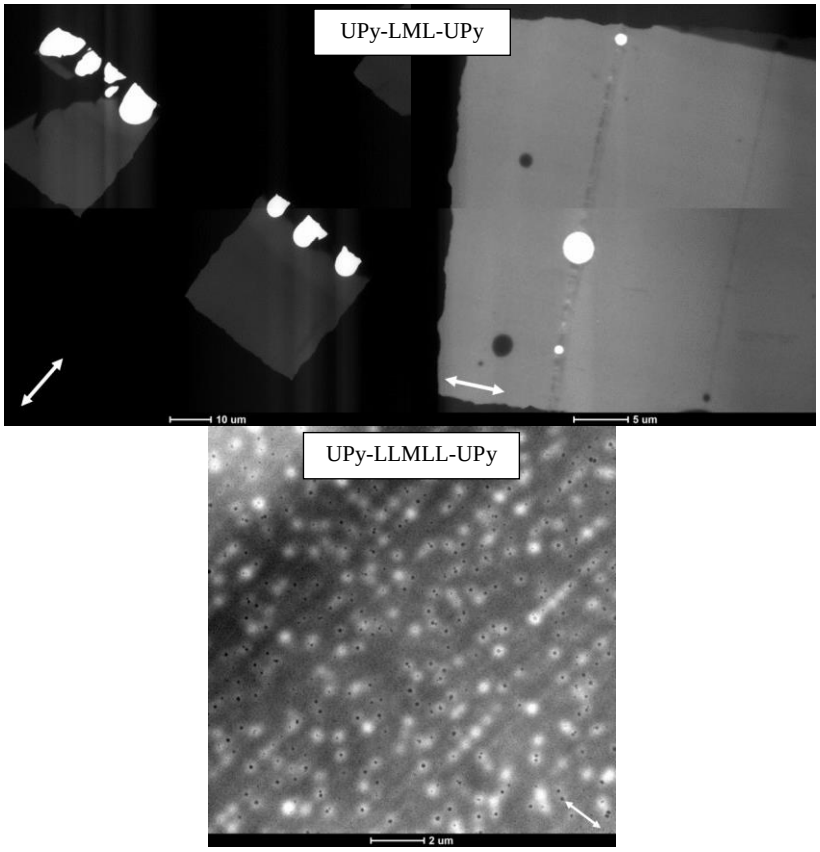

Figure 4.14.
TEM of tensile bar gauge area after tensile testing, stained with RuO_4. White arrows on images indicate the direction of extension for these samples.

Hysteresis and stress relaxation experiments

The samples were subjected to hysteresis experiments by extending and retracting cyclically to 200% strain (less than half of the strain at break of $LLMLL^{MP}$) at 50 mm min^{-1} for 10 cycles (Figure 4.15). The residual strain (strain when material exhibits zero stress after 10 cycles) and the strain recovery (recovered strain as a percentage of the applied 200% strain after 10 cycles) are reported (Table 4.2). Due to the low strain at break observed in $LLMLL^{MP*}$ and $LLMLL^{SC}$, the samples were not able to withstand the 200% strain without failure and thus the recovery properties are not reported. Also, LML (34,

0.19) exhibits permanent deformation upon extension and thus could not be tested. In contrast, non-crystalline UPy–LML–UPy results in elastomeric properties with 74% strain recovery (Table 4.2, entry 2). Likewise, semicrystalline LLMLL^{MP} exhibits elastomeric properties with 84% recovery (Table 4.2, entry 3). By end-functionalizing LLMLL with UPy groups, the recovery increases to 90% or greater and the solvent-cast samples UPy–LLMLL–UPy^{SC} exhibit the highest recovery at 94% (Table 4.2, entry 8). The addition of UPy groups results in significant improvement in both the tensile properties and the elastomeric properties of both LML and LLMLL.

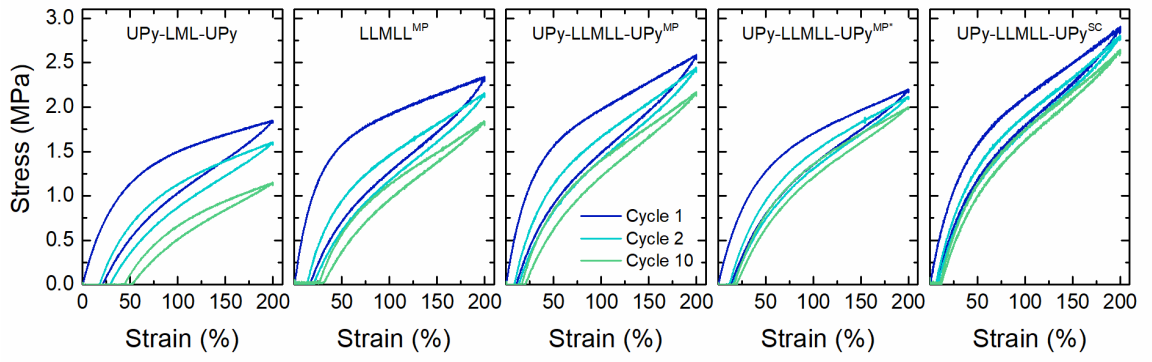

Figure 4.15.
Samples were extended to 200% strain cyclically at 50 mm min^{-1} for 10 cycles. Cycles 1, 2 and 10 are plotted for samples tested.

To explore the impact of UPy groups on stress relaxation, we compared the behavior of LML (34, 0.19) and UPy–LML–UPy under constant strain. Samples were equilibrated at the designated temperature for 10 min, rapidly extended to 25% strain and the stress was monitored over 3 h (Figure 4.16). The stress relaxation behavior in these TPEs does not follow a single exponential decay with a single characteristic relaxation energy (i.e., as in chemical exchange in vitrimers or chemical degradation in vulcanized

rubber).[68] Instead, these data fit a phenomenological stretched exponential function, also known as the Kohlrausch-Williams-Watts (KWW) model:

$$E'(T) = C \times \exp(-(t/\tau_{fit})^{\alpha}) \text{ with } 0 < \alpha \leq 1$$

where α is a measure of the distribution of relaxation times and τ_{fit} is the temperature-dependent KWW relaxation time.[69,70] The stress relaxation of the TPEs reported in this work were fit to this function, floating all three parameters C, τ_{fit}, and α (Figure 4.17, Table 4.3).[69,71] Qualitatively, the shape of the stress relaxation curve changes between −30 °C (black) and −10 °C (blue) for LML (34, 0.19) and between 0 °C (green) and 10 °C (orange) in UPy–LML–UPy. This change in shape of the stress relaxation curves also correlate to the change in the KWW fit (Table 4.3), possibly indicating a change in the molecular mobility of the polymers between these temperatures.[69]

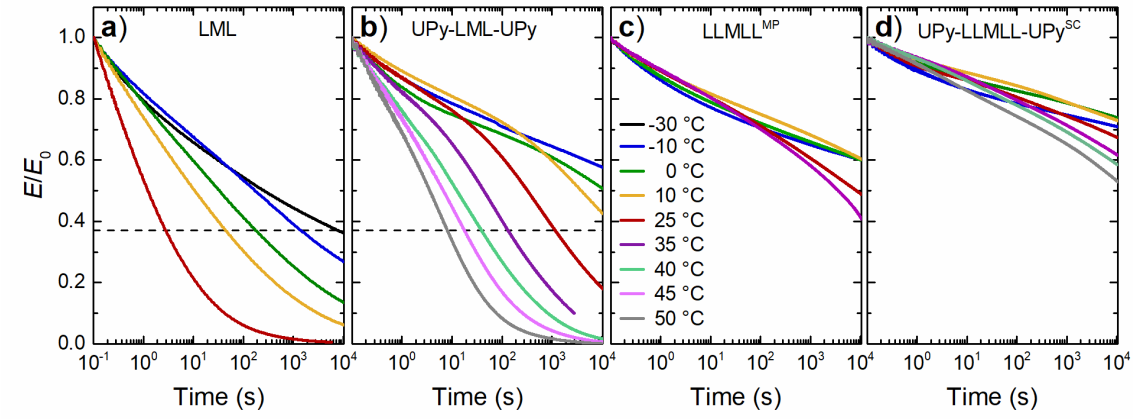

Figure 4.16.
Stress relaxation of thermoplastic elastomers at the indicated temperatures, held at 25% strain for 3 h. Dashed line at 1/*e* of E_0.

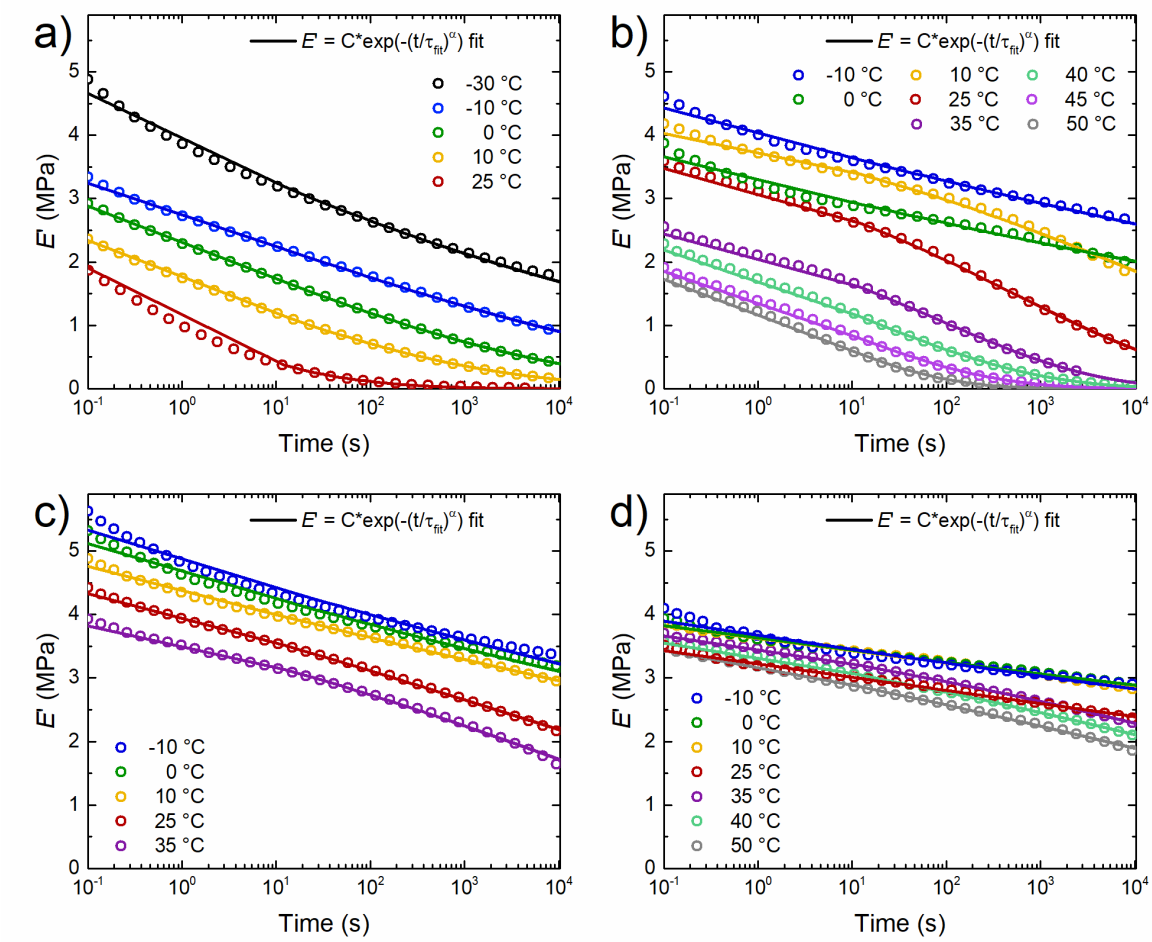

Figure 4.17.
Stress relaxation data (scatter) collected for a) LML, b) UPy–LML–UPy, c) $LLMLL^{MP}$, and d) UPy–LLMLL–UPy^{SC} at the indicated temperatures holding 25% step strain. The data were fit to the stretched exponential decay (line) for all curves (Levenberg-Marquardt algorithm, a least-squares fitting method, using 500 iterations and a tolerance of 10^{-9}). The fitting parameters and R^2 values are reported in Table S1.

Table 4.3.
Fitting parameters for the stretched exponential fit

$$E' = C \times \exp(-(t/\tau_{fit})^{\alpha}) \text{ with } 0 < \alpha \leq 1$$

using the Levenberg-Marquardt algorithm, a least-squares fitting method, using 500 iterations and a tolerance of 10^{-9}. Highlighted in red are fits that did not converge within these restrictions or had a standard error larger than the parameter value. These data highlighted in red were omitted when estimating τ^* for the Arrhenius analysis.

LML (34, 0.19)

Temperature (°C)	C (MPa)	τ_{fit} (s)	α	R^2	Fit converged
−30	49.9 ± 10.4	$7.4 \times 10^{-14} \pm 0.3 \times 10^{-14}$	0.0309 ± 0.0024	0.9964	No
−10	7.05 ± 0.11	2.0 ± 0.4	0.0846 ± 0.0011	0.9992	Yes
0	6.19 ± 0.04	1.1 ± 0.1	0.111 ± 0.001	0.9999	Yes
10	5.68 ± 0.02	0.26 ± 0.01	0.123 ± 0.001	0.9999	Yes
25	8.81 ± 0.14	0.0055 ± 0.0005	0.151 ± 0.001	0.9999	Yes

UPy–LML–UPy

Temperature (°C)	C (MPa)	τ_{fit} (s)	α	R^2	Fit converged
−10	24.7 ± 6.4	$9.3 \times 10^{-12} \pm 0.8 \times 10^{-12}$	0.0234 ± 0.0031	0.9928	No
0	19.7 ± 6.3	$2.4 \times 10^{-10} \pm 0.2 \times 10^{-10}$	0.0263 ± 0.0043	0.9863	No
10	4.75 ± 0.04	15200 ± 600	0.151 ± 0.003	0.9937	Yes
25	4.12 ± 0.01	464 ± 11	0.211 ± 0.002	0.9987	Yes
35	2.92 ± 0.01	85.9 ± 0.7	0.259 ± 0.001	0.9993	Yes
40	3.09 ± 0.01	12.1 ± 0.1	0.226 ± 0.001	0.9997	Yes
45	2.69 ± 0.01	5.51 ± 0.07	0.251 ± 0.001	0.9996	Yes
50	2.51 ± 0.01	2.95 ± 0.04	0.295 ± 0.001	0.9995	Yes

LLMLL (34, 0.19)

Temperature (°C)	C (MPa)	τ_{fit} (s)	α	R^2	Fit converged
−10	37.2 ± 21.3	$3.59 \times 10^{-16} \pm 0.85 \times 10^{-16}$	0.0200 ± 0.0053	0.9793	No
0	36.5 ± 7.4	$1.12 \times 10^{-16} \pm 9.54 \times 10^{-16}$	0.0196 ± 0.0019	0.9899	No
10	19.1 ± 1.2	$2.53 \times 10^{-7} \pm 5.84 \times 10^{-7}$	0.0255 ± 0.0010	0.9968	No
25	6.59 ± 0.03	3140 ± 170	0.0838 ± 0.0005	0.9990	Yes
35	4.83 ± 0.02	7800 ± 170	0.130 ± 0.001	0.9978	Yes

UPy–LLMLL–UPy

Temperature (°C)	C (MPa)	τ_{fit} (s)	α	R^2	Fit converged
−10	19.5 ± 6.8	$1.01 \times 10^{-14} \pm 0.20 \times 10^{-14}$	0.016 ± 0.003	0.9700	No
0	29.7 ± 11.4	$1.58 \times 10^{-29} \pm 0.51 \times 10^{-29}$	0.011 ± 0.002	0.9884	No
10	7.80 ± 0.26	7600 ± 8300	0.030 ± 0.001	0.9957	Yes
25	8.40 ± 0.41	4.38 ± 7.36	0.029 ± 0.001	0.9941	Yes
35	4.64 ± 0.01	377000 ± 3000	0.096 ± 0.001	0.9997	Yes
40	4.69 ± 0.01	113000 ± 1000	0.092 ± 0.001	0.9997	Yes
50	4.97 ± 0.02	15100 ± 700	0.083 ± 0.001	0.9988	Yes

LML (94, 0.17)					
Temperature (°C)	C (MPa)	τ_{fit} (s)	α	R^2	Fit converged
−40	25.6 ± 14.7	$2.81 \times 10^{-17} \pm 0.72 \times 10^{-17}$	0.019 ± 0.005	0.9643	No
20	5.96 ± 0.07	690 ± 100	0.079 ± 0.001	0.9980	Yes
30	3.57 ± 0.01	7960 ± 20	0.20 ± 0.01	0.9997	Yes
40	3.13 ± 0.01	126 ± 1	0.20 ± 0.01	0.9997	Yes
50	3.79 ± 0.01	5.47 ± 0.12	0.21 ± 0.01	0.9996	Yes

As a benchmark, LLMLL (95, 0.17) that we reported previously exhibited the least amount of stress relaxation at 30 °C, relaxing only 20% of the applied stress after 3 h (10^4 s).[5] Qualitatively, the low molar mass variants studied in this work exhibit significantly more stress relaxation; LML (34, 0.19) at 25 °C (Figure 4.16a, red curve) relaxes the applied stress completely within 3 h. We posit that this is due to chain pullout of the PLA block from the hard domains.[6–8,10] End-functionalizing this low molar mass TPE with UPy groups (UPy–LML–UPy) results in less stress relaxation, but 80% of the original stress is still lost after 3 h at 25 °C (Figure 4.16b, red curve) These stress relaxation results indicate segmental motion of amorphous PLA with UPy endgroups is slower compared to the unfunctionalized derivatives at any given temperature.

The Arrhenius model has been used to describe the segmental relaxation of a polymer below T_g and TPEs between $T_{g,B}$ and $T_{g,A}$.[8,72] The Arrhenius temperature dependence of stress relaxation can be described by the following relationship:[8]

$$\tau^*(T) = \tau_0 e^{E_a/RT}$$

where τ* is the time required for the material to relax to a designated percent of the initial value (typically 37% or 50%), τ_0 is a preexponential constant, E_a is the activation energy, R is the gas constant, and T is the temperature of the experiment. When the normalized

modulus reached 1/*e* (or 0.368) during the 3 h experiment, $T \geq -10$ °C for LML (34, 0.19) and ≥ 25 °C for UPy–LML–UPy, the τ^* was plotted as a function of inverse absolute temperature (Figure 4.18, red and pink data). The stress relaxation activation energies as determined through the Arrhenius relationship are comparable: E_a = 121 ± 8 kJ mol^{-1} for LML and 132 ± 4 kJ mol^{-1} for UPy–LML–UPy. These E_a values are similar to those observed in SIS, 113 kJ mol^{-1}, and SBS, 84 kJ mol^{-1}.[8] The main difference is the relaxation time at any given temperature: τ^*(23 °C) = 3.2 s for LML and τ^*(23 °C) = 1.5×10^3 s (or 25 min) for UPy–LML–UPy, and this is reflected by the difference between the preexponential constant. As a result, trapping the endblocks by adding UPy associating groups to the PLA termini increases the relaxation time by a factor of nearly 500 at room temperature.

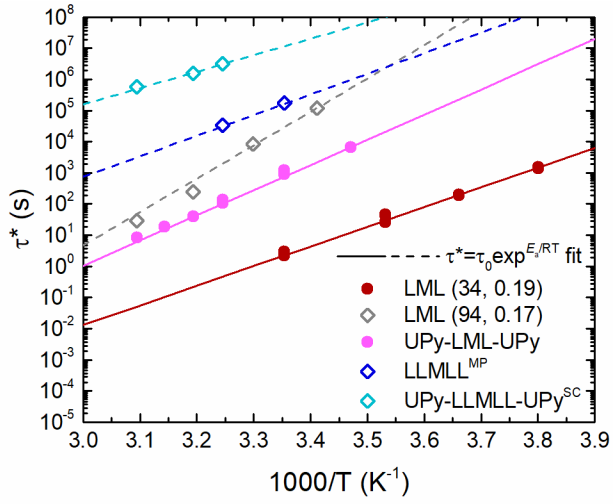

Figure 4.18.
Fit of the stress relaxation time (τ*), taken as the time to reach a normalized stress of 1/*e*, as a function of temperature.

For semicrystalline derivatives, $LLMLL^{MP}$ and $UPy–LLMLL–UPy^{SC}$, the experimental stress relaxation curves did not reach E_0/e during the 3 h experiment. Unfortunately, stress relaxation experiments were limited to 35 °C for $LLMLL^{MP}$ and 50 °C for $UPy–LLMLL–UPy^{SC}$ as tests above these temperatures resulted in fractured samples during testing. By using the fitted stretched exponential function (Figure 4.17, Table 4.3), the τ^* was estimated for curves that exhibited stress relaxation with an Arrhenius temperature dependence: ≥ 25 °C for $LLMLL^{MP}$ and ≥ 35 °C for $UPy–LLMLL–UPy^{SC}$ (Figure 4.18, open symbols). The stress relaxation activation energies were similar to those reported above for the amorphous derivatives: E_a = 127 kJ mol^{-1} for $LLMLL^{MP}$ and 101 ± 11 kJ mol^{-1} for $UPy–LLMLL–UPy^{SC}$ (Figure 4.18, blue and aqua data). The relaxation time τ^*(23 °C) = 2.4×10^5 s (or 66 h) for $LLMLL^{MP}$ is 70-fold smaller than in $UPy–LLMLL–UPy^{SC}$ (τ^*(23 °C) = 1.6×10^7 s or 181 days). The use of semicrystalline PLLA endblocks with UPy endgroups result in TPEs that have very long stress relaxation times, with τ^* @ 23 °C that is 4-orders of magnitude greater than in non-crystalline UPy–LML–UPy.

The original aim of this work was to utilize UPy groups to reduce chain pullout in LML TPEs. When comparing between the low molar mass amorphous derivatives, LML (34, 0.19) and UPy–LML–UPy, UPy endgroups effectively reduced chain pullout as stress relaxation was sufficiently slower. For comparison, we fit the experimental stress relaxation data of high molar mass LML (94, 0.17) reported in our previous work to the stretched exponential function (Figure 4.19, Table 4.3).[5] The extrapolated τ^* values for the stress relaxation curves between 20 °C and 50 °C are plotted in Figure 4.18 (gray, open symbols). These τ^*s were fit to the Arrhenius relationship to provide estimates of E_a = 205

± 7 kJ mol^{-1} and τ*(23 °C) = 5.4×10^4 s (or 15 h) for LML (94, 0.17). We suspect that the higher E_a of stress relaxation in LML (94, 0.17) compared to the low molar mass derivatives is a result of a stronger segregation strength χN due to the overall increase in molar mass; higher energy barrier for chain pullout in the high molar mass system. Furthermore, the timescales at which the stress relaxation occurs is 35 times slower in LML (94, 0.17) compared to the low molar mass UPy–LML–UPy at room temperature. We expect that end functionalizing high molar mass LML samples with UPy we could further reduce the rate of stress relaxation.

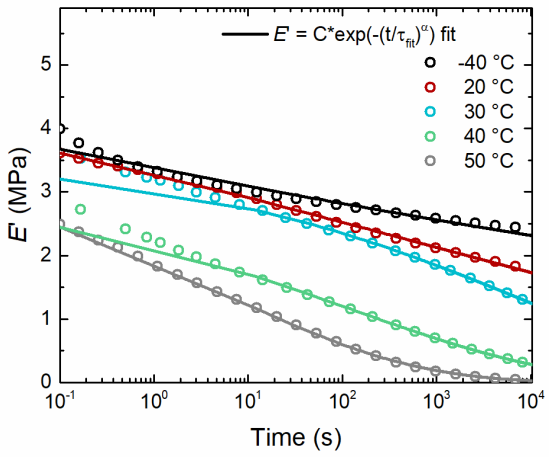

Figure 4.19.
Stress relaxation data (scatter) reported in Watts et al. for LML (94, 0.17) at the indicated temperatures holding 25% step strain.[5] The data was fit to the stretched exponential decay (line) for all curves (Levenberg-Marquardt algorithm, a least-squares fitting method, using 500 iterations and a tolerance of 10^{-9}). The fitting parameters and R^2 values are reported in Table 4.3.

4.3 Conclusions

As expected, ABA triblock polymer LML (34, 0.19) exhibits less impressive ultimate tensile properties compared to the high molar mass derivatives reported in our

previous work.[5] LML (34, 0.19) is microphase separated at room temperature and thermal properties indicate some degree of mixing between blocks due to the low molar mass. The unentangled PLA endblocks (4 kg mol^{-1}) and the low segregation strength contribute to the lack of mechanical integrity in LML. The addition of UPy endgroups to the parent LML (34, 0.19) drastically improves the mechanical properties, leading to a 25-fold increase in toughness. Unlike the parent LML (34, 0.19), UPy–LML–UPy exhibits elastomeric behavior with 74% strain recovery. Terminating poor-performing LML block polymers with UPy groups resulted in drastic improvements to the mechanical and thermal properties of these low molar mass TPEs.

The thermal and mechanical properties of semicrystalline LLMLL (34, 0.19) derivatives are impacted by the processing conditions (MP, MP*, and SC) used in preparing films. When crystallinity was enhanced in these low molar mass derivatives through annealing ($LLMLL^{MP*}$) or solvent-casting ($LLMLL^{SC}$), the samples exhibited morphology changes indicative of crystalline breakout leading to higher modulus and reduced strain at break. When crystallization was inhibited by rapidly cooling the sample below the $T_{g,PLA}$ from the melt state, $LLMLL^{MP}$, films exhibited elastomeric properties with 84% recovery. Adding UPy endgroups to LLMLL resulted in a system that was less sensitive to thermal history as the microstructure did not change and crystalline breakout was not observed between MP, MP*, and SC treatments. These UPy-functionalized semicrystalline TPEs exhibited strain hardening behavior, resulting in a 7-fold increase in toughness compared to the parent LLMLL (34, 0.19) samples. The addition of UPy endgroups improves the mechanical and thermal properties of LLMLL TPEs.

Using stress relaxation experiments, we were able to estimate the amount of time it would take for the applied stress to relax upon initial loading at room temperature, τ^*(23 °C). Stress relaxation in LML-based TPEs sorted from fastest to slowest is LML (34, 0.19) > UPy–LML–UPy > LML (94, 0.17) > LLMLL^{MP} (34, 0.19) > UPy–LLMLL–UPy^{SC}. Stress relaxation in LML (34, 0.19) occurs on the order of seconds, correlating to the permanent deformation observed during tensile testing experiments. By adding UPy endgroups, UPy–LML–UPy, the relaxation time is increased by a factor of 500 compared to the parent LML (34, 0.19). Although UPy–LML–UPy exhibits elastomeric behavior, there is some degree of permanent deformation as only 74% strain recovery is observed. Even with a drastic increase in the τ^*(23 °C), there is still sufficient stress relaxation that occurs at room temperature leading to permanent deformation. We estimated τ^*(23 °C) for our previously reported high molar mass LML (94, 0.17) to be on the scale of hours. Although LML (94, 0.17) reported in our previous work exhibits less stress relaxation than LML (34, 0.19) and UPy–LML–UPy at fixed time and temperature, we demonstrate that adding UPy endgroups to low molar mass LML (34, 0.19) mitigates chain pullout resulting in slower stress relaxation.

When PLLA crystallization is confined within the microphase separated structure in LLMLL^{MP}, the samples exhibit slow stress relaxation at room temperature with τ^*(23 °C) = 66 h. The estimate of τ^*(23 °C) for UPy–LLMLL–UPy^{SC} indicates that it will take nearly half a year for the material to relax (1/*e*) the original stress at room temperature. Hysteresis testing revealed that UPy–LLMLL–UPy TPEs exhibit 90–94% strain recovery, indicating there is very little permanent deformation that occurs during these hysteresis

experiments. The combination of semicrystalline PLLA endblocks with UPy endgroups sufficiently reduces the amount of permanent deformation as stress relaxation is slow. Chain pullout is mitigated by using semicrystalline PLLA with UPy endgroups in LML-based TPEs.

4.4 Experimental details

Materials. Chloroform, dichloromethane, methanol, and hexanes were obtained from Fisher Scientific and used without further purification. Lactide was generously provided by Altasorb (a subsidiary of Ortec, Inc). All other chemicals were used as received from Sigma-Aldrich unless otherwise specified. Lactide and 1,4-benzenedimethanol were recrystallized from toluene (x3), dried under vacuum for 48 h, and stored inert atmosphere. $Sn(Oct)_2$ was distilled three times under vacuum with argon (30–50 mTorr, 130–150 °C) before storing under inert atmosphere. Anhydrous toluene was obtained through a JC Meyer solvent drying system.

Characterization. Bruker Avance III 500 was used for ^{1}H and ^{13}C NMR spectroscopy. Molar mass by ^{1}H NMR spectroscopy was calculated from end-group analysis. Size exclusion chromatography was performed in THF at 25 °C using Agilent 1260 Infinity liquid chromatograph system equipped with three Waters Styragel columns in series with a Wyatt DAWN Heleos II 18-angle laser light scattering detector and a Wyatt OPTILAB T-rEX refractive index detector. Molar mass was determined from light scattering results assuming 100% mass recovery. The FT-IR spectra were obtained on a Bruker Alpha Platinum spectrometer equipped with a diamond crystal in attenuated total

reflection (ATR) mode at a resolution of 4 cm^{-1} and 32 scans were obtained for each spectrum. Thermogravimetric analysis was carried out in nitrogen atmosphere using TA Instruments Q500 Analyzer. Thermal properties were obtained using a TA Instruments Discovery DSC. Samples were prepared in hermetically sealed pans and cooled to −80 °C. Samples were then heated at 5, 10, or 20 °C min^{-1} to 180 °C (first heat), cooled to −80 °C, and heated to 180 °C again (second heat).

To compression mold polymers, dry samples were placed between two Teflon sheets with a 0.5 mm stainless steel spacer, melt-pressed at 60–180 °C for 3-6 minutes, then quenched to room temperature using water cooling (~ 35 °C min^{-1}) through the hot press. Dog-bone-shaped tensile bars were punched out resulting in samples with approximately 0.5 mm thickness, 3 mm gauge width, and 16 mm gauge length. Samples were tested to the point of break using Shimadzu Autograph AGS-X Tensile Tester and an extension rate of 50 mm min^{-1}. Using 8 mm parallel plates, TA Instruments Rheometric Series ARES instrument was used for dynamic mechanical thermal analysis (DMTA). Heating was controlled under nitrogen atmosphere, and the samples were equilibrated at the designated temperature for 10 minutes before testing. Extensional DMTA and stress relaxation analysis were performed on a TA Instruments RSA-G2 in tension mode on rectangular polymer films with 0.5 mm thickness and 3 mm gauge width. DMTA experiments were conducted at a heating rate of 5 °C min^{-1} with an oscillating strain of 0.05% and angular frequency of 1 Hz. Stress relaxation analysis was conducted after an equilibration time of 10 min at the selected temperature by applying a step strain of 25% and measuring the modulus for 3 hours. SAXS experiments were conducted either on at

the DuPont-Northwestern Dow Collaborative Access Team (DND-CAT) synchrotron research center 5-ID-D beamline of Advanced Photon Source at Argonne National Laboratory.

Polymer synthesis. PMCL, and LML, LLMLL, and UPy-NCO were synthesized and purified as previously reported.[5,36] α,ω-hydroxy telechelic polymers (1 equiv.) were reacted with UPy-NCO (4.2 equiv.) with catalytic amounts of $Sn(Oct)_2$ in toluene. The reaction was carried out at 100 °C for 1–4 h. The reaction was cooled, diluted with acetone and unreacted UPy–NCO was removed as a solid during filtration. The filtrate was precipitated into methanol and precipitated a second time into hexanes. The UPy-functionalized polymers were dried in vacuo.

4.5 References

(1) *Thermoplastic Elastomers*; Holden, G.; Kricheldorf, H. R.; Quirk, R. P., Eds.; 3rd ed.; Hanser Gardner Publications, Inc.: Cincinnati, 2004.

(2) Shin, J.; Kim, Y.-W.; Kim, G.-J. Sustainable Block Copolymer-Based Thermoplastic Elastomers. *Appl. Chem. Eng.* **2014**, *25*, 121–133.

(3) Hillmyer, M. A.; Tolman, W. B. Aliphatic Polyester Block Polymers: Renewable, Degradable, and Sustainable. *Acc. Chem. Res.* **2014**, *47*, 2390–2396.

(4) Zhu, Y.; Romain, C.; Williams, C. K. Sustainable Polymers from Renewable Resources. *Nature* **2016**, *540*, 354–362.

(5) Watts, A.; Kurokawa, N.; Hillmyer, M. A. Strong, Resilient, and Sustainable Aliphatic Polyester Thermoplastic Elastomers. *Biomacromolecules* **2017**, *18*, 1845–1854.

(6) Hsiue, G. -H; Wu, G. -W. The Stress Relaxation of the Thermoplastic Elastomer (SBS Type). *J. Appl. Polym. Sci.* **1980**, *25*, 2119–2121.

(7) Hsiue, G.; Chen, D.; Liew, Y.-K. Stress Relaxation and the Domain Structure of Thermoplastic Elastomer. *J. Appl. Polym. Sci.* **1988**, *35*, 995–1002.

(8) Wu, G.-W.; Hsiue, G.-H.; Yang, J.-S. Stress Relaxation in Poly(Styrene-Butadiene-Styrene) and Poly(Styrene-Isoprene-Styrene) Triblock Copolymers and Their Derivatives. *Mater. Chem. Phys.* **1994**, *37*, 191–196.

(9) Gwo-Wen, W.; Ging-Ho, H.; Jin-Sheng, Y. Stress Relaxation Behavior of Low Epoxidized Poly(Styrene-b-Butadiene-b-Styrene) Triblock Copolymers. *Mater. Chem. Phys.* **1994**, *39*, 29–33.

(10) Spaans, R. D.; Williams, M. C. Nonlinear Viscoelasticity of ABA Block Copolymer Melts: Stress Relaxation and Recovery. *Ind. Eng. Chem. Res.* **1995**, *34*, 3496–3507.

(11) Gent, A. N. Relaxation Processes in Vulcanized Rubber. *J. Appl. Polym. Sci.* **1962**, *VI*, 442–448.

(12) Fukumori, K.; Kurauchi, T.; Kamigaito, O. Pulsed NMR Study of Elastomeric Block Copolymer under Deformation. *J. Appl. Polym. Sci.* **1989**, *38*, 1313–1334.

(13) Sato, T.; Watanabe, H.; Osaki, K. Rheological and Dielectric Behavior of a Styrene−Isoprene−Styrene Triblock Copolymer in n -Tetradecane. 1. Rubbery−Plastic−Viscous Transition. *Macromolecules* **1996**, *29*, 6231–6239.

(14) Bergström, J. S.; Boyce, M. C. Constitutive Modeling of the Large Strain Time-Dependent Behavior of Elastomers. *J. Mech. Phys. Solids* **1998**, *46*, 931–954.

(15) Lynd, N. A.; Oyerokun, F. T.; O'Donoghue, D. L.; Handlin, D. L.; Fredrickson, G. H. Design of Soft and Strong Thermoplastic Elastomers Based on Nonlinear Block Copolymer Architectures Using Self-Consistent-Field Theory. *Macromolecules* **2010**, *43*, 3479–3486.

(16) Burns, A. B.; Register, R. A. Mechanical Properties of Star Block Polymer Thermoplastic Elastomers with Glassy and Crystalline End Blocks. *Macromolecules* **2016**, *49*, 9521–9530.

(17) Kan, H.-C.; Ferry, J. D.; Fetters, L. J. Rubber Networks Containing Unattached Macromolecules. 5. Stress Relaxation in Styrene-Butadiene-Styrene Block Copolymer with Unattached Linear and Star Polybutadienes. *Macromolecules* **1980**, *13*, 1571–1577.

(18) Singh, N. K.; Lesser, A. J. A Physical and Mechanical Study of Prestressed Competitive Double Network Thermoplastic Elastomers. *Macromolecules* **2011**, *44*, 1480–1490.

(19) Lee, I.; Panthani, T. R.; Bates, F. S. Sustainable Poly(Lactide-b-Butadiene) Multiblock Copolymers with Enhanced Mechanical Properties. *Macromolecules* **2013**, *46*, 7387–7398.

(20) Panthani, T. R.; Bates, F. S. Crystallization and Mechanical Properties of Poly(L-Lactide)-Based Rubbery/Semicrystalline Multiblock Copolymers. *Macromolecules* **2015**, *48*, 4529–4540.

(21) Martello, M. T.; Schneiderman, D. K.; Hillmyer, M. A. Synthesis and Melt Processing of Sustainable Poly(ε-Decalactone)-block-Poly(Lactide) Multiblock Thermoplastic Elastomers. *ACS Sustain. Chem. Eng.* **2014**, *2*, 2519–2526.

(22) Zhu, Y.; Radlauer, M. R.; Schneiderman, D. K.; Shaffer, M. S. P.; Hillmyer, M. A.; Williams, C. K. Multiblock Polyesters Demonstrating High Elasticity and Shape Memory Effects. *Macromolecules* **2018**, *51*, 2466–2475.

(23) Gardella, L.; Cavallo, D.; Colonna, S.; Fina, A.; Monticelli, O. Novel Poly(l-Lactide)/Poly(d-Lactide)/Poly(Tetrahydrofuran) Multiblock Copolymers with a Controlled Architecture: Synthesis and Characterization. *J. Polym. Sci. Part A Polym. Chem.* **2014**, *52*, 3269–3282.

(24) Brunsveld, L.; Folmer, B. J. B.; Meijer, E. W.; Sijbesma, R. P. Supramolecular Polymers. *Chem. Rev.* **2001**, *101*, 4071–4098.

(25) Bosman, A. W.; Sijbesma, R. P.; Meijer, E. W. Supramolecular Polymers at Work. *Mater. Today* **2004**, *7*, 34–39.

(26) Kautz, H.; van Beek, D. J. M.; Sijbesma, R. P.; Meijer, E. W. Cooperative End-to-End and Lateral Hydrogen-Bonding Motifs in Supramolecular Thermoplastic Elastomers. *Macromolecules* **2006**, *39*, 4265–4267.

(27) *Supramolecular Polymer Networks and Gels*; Seiffert, S., Ed.; Advances in Polymer Science; Springer International Publishing: Cham, 2015; Vol. 268.

(28) *Self-Healing Materials*; Hager, M. D.; van der Zwaag, S.; Schubert, U. S., Eds.; Springer International Publishing: Cham, 2016; Vol. 273.

(29) Beijer, F. H.; Sijbesma, R. P.; Kooijman, H.; Spek, A. L.; Meijer, E. W. Strong Dimerization of Ureidopyrimidones via Quadruple Hydrogen Bonding. *J. Am. Chem. Soc.* **1998**, *120*, 6761–6769.

(30) Söntjens, S. H. M.; Sijbesma, R. P.; Van Genderen, M. H. P.; Meijer, E. W. Stability and Lifetime of Quadruply Hydrogen Bonded 2-Ureido-4[1H]-Pyrimidinone Dimers. *J. Am. Chem. Soc.* **2000**, *122*, 7487–7493.

(31) Feldman, K. E.; Kade, M. J.; Meijer, E. W.; Hawker, C. J.; Kramer, E. J. Model Transient Networks from Strongly Hydrogen-Bonded Polymers. *Macromolecules* **2009**, *42*, 9072–9081.

(32) Rubinstein, M.; Semenov, A. N. Dynamics of Entangled Solutions of Associating Polymers. *Macromolecules* **2001**, *34*, 1058–1068.

(33) Hutin, M.; Burakowska-Meise, E.; Appel, W. P. J.; Dankers, P. Y. W.; Meijer, E. W. From Molecular Structure to Macromolecular Organization: Keys to Design Supramolecular Biomaterials. *Macromolecules* **2013**, *46*, 8528–8537.

(34) Appel, W. P. J.; Portale, G.; Wisse, E.; Dankers, P. Y. W.; Meijer, E. W. Aggregation of Ureido-Pyrimidinone Supramolecular Thermoplastic Elastomers into Nanofibers: A Kinetic Analysis. *Macromolecules* **2011**, *44*, 6776–6784.

(35) Botterhuis, N. E.; van Beek, D. J. M.; van Gemert, G. M. L.; Bosman, A. W.; Sijbesma, R. P. Self-Assembly and Morphology of Polydimethylsiloxane Supramolecular Thermoplastic Elastomers. *J. Polym. Sci. Part A Polym. Chem.* **2008**, *46*, 3877–3885.

(36) Folmer, B. J. B.; Sijbesma, R. P.; Versteegen, R. M.; Van Der Rijt, J. A. J.; Meijer, E. W. Supramolecular Polymer Materials: Chain Extension of Telechelic Polymers Using a Reactive Hydrogen-Bonding Synthon. *Adv. Mater.* **2000**, *12*, 874–878.

(37) Yamauchi, K.; Kanomata, A.; Inoue, T.; Long, T. E. Thermoreversible Polyesters Consisting of Multiple Hydrogen Bonding (MHB). *Macromolecules* **2004**, *37*, 3519–3522.

(38) Bertrand, A.; Lortie, F.; Bernard, J. Routes to Hydrogen Bonding Chain-End Functionalized Polymers. *Macromol. Rapid Commun.* **2012**, *33*, 2062–2091.

(39) Kajita, T.; Noro, A.; Matsushita, Y. Design and Properties of Supramolecular Elastomers. *Polymer* **2017**, *128*, 297–310.

(40) Hentschel, J.; Kushner, A. M.; Ziller, J.; Guan, Z. Self-Healing Supramolecular Block Copolymers. *Angew. Chemie* **2012**, *124*, 10713–10717.

(41) Hayashi, M.; Noro, A.; Matsushita, Y. Highly Extensible Supramolecular Elastomers with Large Stress Generation Capability Originating from Multiple Hydrogen Bonds on the Long Soft Network Strands. *Macromol. Rapid Commun.* **2016**, *37*, 678–684.

(42) Chang, R.; Shan, G.; Bao, Y.; Pan, P. Enhancement of Crystallizability and Control of Mechanical and Shape-Memory Properties for Amorphous Enantiopure Supramolecular Copolymers via Stereocomplexation. *Macromolecules* **2015**, *48*, 7872–7881.

(43) Chang, R.; Huang, Y.; Shan, G.; Bao, Y.; Yun, X.; Dong, T.; Pan, P. Alternating Poly(Lactic Acid)/Poly(Ethylene-Co-Butylene) Supramolecular Multiblock Copolymers with Tunable Shape Memory and Self-Healing Properties. *Polym. Chem.* **2015**, *6*, 5899–5910

(44) Jing, Z.; Shi, X.; Zhang, G.; Gu, J. Synthesis and Properties of Poly(Lactide)/Poly(ε-Caprolactone) Multiblock Supramolecular Polymers Bonded by the Self-Complementary Quadruple Hydrogen Bonding. *Polymer* **2017**, *121*, 124–136.

(45) Shi, X.; Jing, Z.; Zhang, G.; Xu, Y.; Yao, Y. Fully Bio-Based Poly(ε-Capolactone)/Poly(Lactide) Alternating Multiblock Supramolecular Polymers: Synthesis, Crystallization Behavior, and Properties. *J. Appl. Polym. Sci.* **2017**, *134*, 1–12.

(46) Delgado, P. A.; Hillmyer, M. A. Combining Block Copolymers and Hydrogen Bonding for Poly(Lactide) Toughening. *RSC Adv.* **2014**, *4*, 13266–13273.

(47) Jing, Z.; Shi, X.; Zhang, G. Synthesis and Properties of Biodegradable Supramolecular Polymers Based on Polylactide- Block -Poly(δ -Valerolactone)- Block -Polylactide Triblock Copolymers. *Polym. Int.* **2017**, *66*, 1487–1497.

(48) van Beek, D. J. M.; Peters, G. M. W.; Sijbesma, R. P. Rheological Behavior of a Quadruple Hydrogen-Bonded Suprarmolecular Polyester. *Mater. Technol.* **2005**, 433–434.

(49) van Beek, D. J. M.; Gillissen, M. A. J.; van As, B. A. C.; Palmans, A. R. A.; Sijbesma, R. P. Supramolecular Copolyesters with Tunable Properties. *Macromolecules* **2007**, *40*, 6340–6348.

(50) van Beek, D. J. M.; Spiering, A. J. H.; Peters, G. W. M.; te Nijenhuis, K.; Sijbesma, R. P. Unidirectional Dimerization and Stacking of Ureidopyrimidinone End Groups in Polycaprolactone Supramolecular Polymers. *Macromolecules* **2007**, *40*, 8464–8475.

(51) Wietor, J. L.; Van Beek, D. J. M.; Peters, G. W.; Mendes, E.; Sijbesma, R. P. Effects of Branching and Crystallization on Rheology of Polycaprolactone Supramolecular Polymers with Ureidopyrimidinone End Groups. *Macromolecules* **2011**, *44*, 1211–1219.

(52) De Hoe, G. X.; Zumstein, M. T.; Tiegs, B. J.; Brutman, J. P.; McNeill, K.; Sander, M.; Coates, G. W.; Hillmyer, M. A. Sustainable Polyester Elastomers from Lactones: Synthesis, Properties, and Enzymatic Hydrolyzability. *J. Am. Chem. Soc.* **2018**, *140*, 963–973.

(53) Chen, Y.; Zhang, H.; Fang, X.; Lin, Y.; Xu, Y.; Weng, W. Mechanical Activation of Mechanophore Enhanced by Strong Hydrogen Bonding Interactions. *ACS Macro Lett.* **2014**, *3*, 141–145.

(54) Guan, Z.; Roland, J. T.; Bai, J. Z.; Ma, S. X.; McIntire, T. M.; Nguyen, M. Modular Domain Structure: A Biomimetic Strategy for Advanced Polymeric Materials. *J. Am. Chem. Soc.* **2004**, *126*, 2058–2065.

(55) Bates, F. S.; Rosedale, J. H.; Fredrickson, G. H. Fluctuation Effects in a Symmetric Diblock Copolymer near the Order-Disorder Transition. *J. Chem. Phys.* **1990**, *92*, 6255–6270.

(56) Han, C. D.; Baek, D. M.; Kim, J. K.; Ogawa, T.; Sakamoto, N.; Hashimoto, T. Effect of Volume Fraction on the Order-Disorder Transition in Low Molecular Weight Polystyrene-Block-Polyisoprene Copolymers. 1. Order-Disorder Transition Temperature Determined by Rheological Measurements. *Macromolecules* **1995**, *28*, 5043–5062.

(57) Fox, T. G. Influence of Diluent and of Copolymer Composition on the Glass Temperature of a Polymer System. *Bull. Am. Phys. Soc.* **1956**, *1*, 123.

(58) Dimopoulos, A.; Wietor, J. L.; Wübbenhorst, M.; Napolitano, S.; Van Benthem, R. A. T. M.; De With, G.; Sijbesma, R. P. Enhanced Mechanical Relaxation below the Glass

Transition Temperature in Partially Supramolecular Networks. *Macromolecules* **2010**, *43*, 8664–8669.

(59) Wanamaker, C. L.; O'Leary, L. E.; Lynd, N. A.; Hillmyer, M. A.; Tolman, W. B. Renewable-Resource Thermoplastic Elastomers Based on Polylactide and Polymenthide. *Biomacromolecules* **2007**, *8*, 3634–3640.

(60) Chen, Y.-D. M.; Cohen, R. E. The Influence of Molecular Weight on the Large Deformation Behavior of SBS Triblock Copolymer Elastomers. *J. Appl. Polym. Sci.* **1977**, *21*, 629–643.

(61) Spurr, O. K.; Niegisch, W. D. Stress Crazing of Some Amorphous Thermoplastics. *J. Appl. Polym. Sci.* **1962**, *6*, 585–599.

(62) Kambour, R. P. A Review of Crazing and Fracture in Thermoplastics. *J. Polym. Sci. Macromol. Rev.* **1973**, *7*, 1–154.

(63) Parker, A. J.; Rottler, J. Molecular Mechanisms of Plastic Deformation in Sphere-Forming Thermoplastic Elastomers. *Macromolecules* **2015**, *48*, 8253–8261.

(64) Parker, A. J.; Rottler, J. Molecular Mechanisms of Plastic Deformation in Sphere-Forming Thermoplastic Elastomers. *Macromolecules* **2015**, *48*, 8253–8261.

(65) Nagarajan, S.; Gowd, E. B. Cold Crystallization of PDMS and PLLA in Poly(L-Lactide-b-Dimethylsiloxane-b- L-Lactide) Triblock Copolymer and Their Effect on Nanostructure Morphology. *Macromolecules* **2015**, *48*, 5367–5377.

(66) Fisher, E. W.; Sterzel, H. J.; Wegner, G. *Kolloid Z. Z. Polym.* **1973**, *251*, 980–990.

(67) Bao, J.; Chang, X.; Xie, Q.; Yu, C.; Shan, G.; Bao, Y.; Pan, P. Preferential Formation of β-Form Crystals and Temperature-Dependent Polymorphic Structure in Supramolecular Poly(l-Lactic Acid) Bonded by Multiple Hydrogen Bonds. *Macromolecules* **2017**, *50*, 8619–8630.

(68) Meng, F.; Pritchard, R. H.; Terentjev, E. M. Stress Relaxation, Dynamics, and Plasticity of Transient Polymer Networks. *Macromolecules* **2016**, *49*, 2843–2852.

(69) Baeurle, S. a.; Hotta, A.; Gusev, A. a. A New Semi-Phenomenological Approach to Predict the Stress Relaxation Behavior of Thermoplastic Elastomers. *Polymer* **2005**, *46*, 4344–4354.

(70) Chung, S. H.; Stevens, J. R. Time-dependent Correlation and the Evaluation of the Stretched Exponential or Kohlrausch–Williams–Watts Function. *Am. J. Phys.* **1991**, *59*, 1024–1030.

(71) Hotta, A.; Clarke, S. M.; Terentjev, E. M. Stress Relaxation in Transient Networks of Symmetric Triblock Styrene−Isoprene−Styrene Copolymer. *Macromolecules* **2002**, *35*, 271–277.

(72) O'Connell, P. A.; McKenna, G. B. Arrhenius-Type Temperature Dependence of the Segmental Relaxation below Tg. *J. Chem. Phys.* **1999**, *110*, 11054–11060.

Chapter 5.

Controlled chain walking for the synthesis of thermoplastic polyolefin elastomers: synthesis, structure, and properties[†]

[†] Reproduced in part with permission from O'Connor; K. S.; Watts, A.; Vaidaya, T.; LaPointe, A. M.; Hillmyer, M. A.; Coates, G. W. Controlled chain walking for the synthesis of thermoplastic polyolefin elastomers: synthesis, structure, and properties. *Macromolecules* **2016**, *49*, 6743–6751.

5.1 Introduction

Elastomers are an extremely important class of polymeric materials with commercial applications spanning tires, rubbers, clothing, and insulators.[1] Typical thermoset elastomers, such as vulcanized rubber, are amorphous polymers that have been chemically crosslinked.[2] These crosslinks provide excellent mechanical properties, allowing for nearly perfect elastic recovery after strain-induced deformation, though they result in materials that are not easily recycled, reprocessed, or reused.[3] Thermoplastic elastomers (TPEs) are a desirable alternative to thermoset materials because they contain physical crosslinks that can similarly resist strain-induced deformation, while maintaining the ability to be reprocessed.[45] Elasticity of TPEs is derived from a polymer microstructure containing alternating hard segments with either high melting points (T_m) or high glass transition temperatures (T_g) and soft, low T_g segments. The soft segments elongate upon strain-induced deformation, while the hard segments create anchoring points needed for elastic recovery.[4] Typically, at least two glassy or semicrystalline segments and one amorphous segment are required to achieve good elastic behavior, so ABA triblock or $(AB)_n$ multiblock copolymer architectures are generally targeted.[6,7,8]

Polystyrene is commonly used as the hard segment with rubbery polydienes as the soft segment in commercial triblock TPEs, which are synthesized via living anionic polymerization. Although this robust system can access materials with predictable molar mass and narrow molar mass distributions,[9,10] there has been increasing interest in exploring new systems capable of incorporating different feedstocks from styrene and dienes, monomers primarily derived from fossil fuel sources.[11,12] TPEs derived entirely

from olefinic feedstocks, specifically ethylene and α-olefins, represent an attractive alternative to styrene-based materials due to the high abundance, low cost, and potential biorenewability of the monomers. Ethylene can be renewably sourced through the dehydration of bioethanol,[13] whereas α-olefins can be renewably accessed through ethylene oligomerization[14] and ethenolysis of fatty acids.[15] Anionic polymerization cannot efficiently enchain ethylene and α-olefins, however, so a different polymerization strategy is required.

There are a number of methods known for generating elastic materials from olefinic building blocks. In 2006, Dow Chemical Company developed a remarkable chain-shuttling strategy for synthesizing multiblock TPEs from ethylene and α-olefins.[16] In this one-pot procedure, two catalysts with different α-olefin affinities individually operate to polymerize ethylene or copolymerize ethylene and 1-octene. A shuttling agent transfers the growing polymer chains between catalysts, giving an $(AB)_n$ multiblock copolymer with alternating semicrystalline and amorphous segments. This commercial technology is capable of synthesizing TPEs, but the ability to study the effects of number and size of blocks on elastic properties is challenging with this catalyst platform. Another methodology for the generation of polyolefin elastomers was recently developed by Coates and coworkers involving the synthesis of elastomeric graft copolymers. In this system, a hafnium catalyst is utilized to incorporate semicrystalline allyl-terminated polypropylene macromonomers into an amorphous ethylene/1-octene copolymer backbone.[1718] The resulting graft materials exhibit exceptional tensile properties and elastic recovery; however, the synthesis of the graft copolymers requires a two-step polymerization process.

Group IV metallocene complexes were some of the earliest examples used to access TPEs from olefins, specifically propylene, through living coordination polymerization, with the capability of controlling molar mass and block structure. Coates and Waymouth developed an oscillating zirconocene catalyst that changes its geometry during the course of the polymerization, generating multiblock copolymers consisting of alternating isotactic and atactic polypropylene segments.[19] Sita and co-workers developed a zirconocene catalyst that changes polymerization behavior by adjusting the stoichiometry of the borate activator, allowing access to alternating hard–soft block structures.[20] The materials synthesized through these systems have elastic properties at room temperature, but their elasticity suffers below the T_g of the soft atactic polypropylene segment (~0 °C), thereby limiting low temperature applications. Propylene-based materials with lower T_g's can be synthesized using late transition metal catalysts. A chiral nickel α-diimine complex was shown to produce well-defined elastomeric materials from propylene by adjusting the temperature over the course of the polymerization.[21] Reactions performed at low temperatures produced highly crystalline isotactic polypropylene, whereas elevated temperatures produced a microstructure resembling an ethylene/propylene copolymer, which has a lower T_g (−44 °C) than atactic polypropylene.

The difference in polymer microstructure obtained between the zirconocene and nickel α-diimine complexes can be explained by a phenomenon known as "chain walking". This process, common to late transition metal catalysts, involves rapid β-hydride elimination and reinsertion into the propagating polymer chain, which can position the active catalyst at numerous sites along the polymer backbone (Scheme 5.1). Insertion of

monomer off the backbone produces branches of various lengths, a property that has been reported to modulate with monomer concentration and reaction temperature.[22] Since the seminal discovery of α-diimine nickel complexes for olefin polymerization over two decades ago,[23] many studies have been performed to better understand the chain walking polymerization mechanism for both ethylene and α-olefins.[24,25,26] One of the earliest nickel complexes developed by Brookhart and coworkers (**1**, Scheme 5.1) generally gave highly branched, amorphous polymers from ethylene, but more linear materials could be accessed high pressures and low temperatures. For the polymerization of α-olefins, a chain straightening phenomenon can occur, where 2,1-insertion followed by complete chain walking to the ω-position of the growing polymer chain before subsequent monomer insertion (ω-1 enchainment) leads to linear regions of polyethylene (Scheme 5.1). Reaction conditions such as temperature and concentration of α-olefin have shown to affect the rates of chain walking relative to insertion, allowing access to various polymer structures.[27] The regiochemistry of insertion is critical for optimal chain straightening, as 1,2-insertion and complete chain walking before subsequent insertion (ω-2 enchainment) will install a methyl group on the polymer backbone, decreasing crystallinity of the polymer. Various ligand structures have been explored to control the regiochemistry of α-olefin insertion. Wu and co-workers demonstrated precise control over the regiochemistry of 1-hexene insertion by modifying the ligand structure of a nickel amine–imine complex, accessing both a 1,2-selective complex which produces amorphous polymer and a 2,1-selective complex which produces semicrystalline polymer (T_m = 107 °C).[28] Chen and coworkers also developed an interesting aminopyridyl nickel complex which exhibits significant 2,1-

insertion and complete chain walking of α-olefins to yield semicrystalline materials with high melting temperatures (T_m = 105.5 °C).[29]

Scheme 5.1.
Modes of enchainment for ethylene and α-olefins by α-diimine nickel complexes

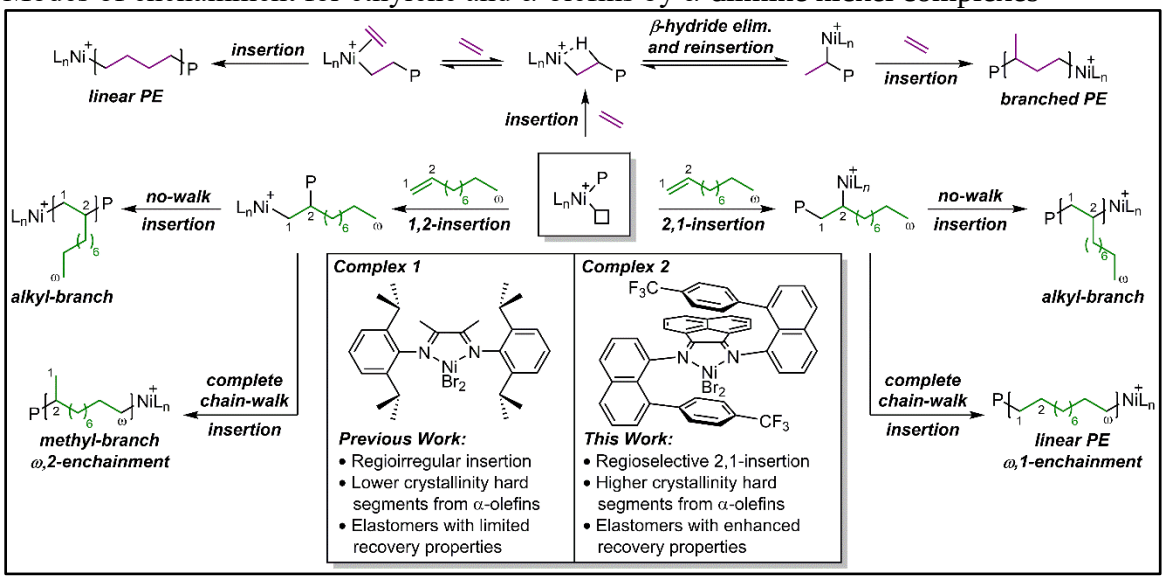

With precise control over regiochemistry of insertion and chain walking, nickel complexes can create TPEs with α-olefin semicrystalline blocks and ethylene amorphous blocks. This methodology is intriguing because it forms the hard segments using α-olefins, which are much more commonly used to introduce branching and decrease crystallinity in early metal systems. Brookhart and co-workers reported the first triblock copolymer using this methodology, with 1-octadecene and ethylene at low temperatures.[30] These materials were empirically described as elastic, but no further characterization of mechanical properties was reported. Ricci and co-workers recently employed the same approach to synthesize triblock copolymers from 1-dodecene and ethylene at room temperature[31] to give materials with strain at break values approaching 1000%. Despite these impressive strain values, the resulting polymers suffered from significant permanent deformations

after stretching (~35% recovery after 10 cycles of 300% strain). These materials were synthesized using complex **1**, which exhibits regiorandom insertion of α-olefins, thus decreasing the degree of crystallinity in the hard segments. Coates and Daugulis recently reported an arylnaphthyl-α-diimine Ni(II) sandwich complex (**2**, Scheme 5.1) which exhibits regioselective 2,1-insertion and complete chain walking of 1-decene at room temperature, giving polymers with low dispersities ($Đ$ = 1.2) and competitive thermal properties (T_m = 106 °C).[32] A similar nickel sandwich complex has previously been reported[33] to give highly branched amorphous materials from low pressures of ethylene. We hypothesized that we could combine the outstanding chain straightening of 1-decene with the facile chain walking of ethylene using complex **2** to synthesize block copolymers in a controlled manner with improved T_m and crystallinity in the hard regions, allowing access to thermoplastic elastomers with improved mechanical properties.

Herein, we report the one-pot synthesis of thermoplastic elastomer block copolymers by polymerizing 1-decene to form hard blocks with high crystallinity and ethylene to form soft blocks with low crystallinity using complex **2**. A variety of block structures ranging from a diblock up to a heptablock copolymer were synthesized. Statistical copolymers of ethylene and 1-decene were also synthesized for comparison. The effects of the architecture as well as the ratio of hard to soft segments are discussed. The mechanical properties of these copolymers were explored by subjecting samples to uniaxial tension until failure and hysteresis step cycle tests. The creep behavior was also analyzed to demonstrate the resilience of the materials.

5.2 Results and Discussion

Complex **2** was selected for the synthesis of block copolymer TPEs due to its ability of producing highly linear materials from α-olefins and branched materials from ethylene in a controlled and facile manner (Figure 5.1). 1-Decene was chosen as the α-olefin because there are multiple renewable pathways for accessing this monomer, and it has previously been shown to give highly crystalline materials using complex **2**. Complex **2** (and other α-diimine nickel complexes) is known to polymerize longer chain α-olefins, such as 1-octadecene, and access materials with higher melting temperatures than those found using shorter chain α-olefins. Varying the length of the α-olefins could potentially modulate the properties of the resulting materials. However, since 1-decene can be accessed renewably not only through bioethylene oligomerization but also the ethenolysis of fatty acids, we chose to focus our studies using 1-decene as the hard segment. A sample of chain straightened 1-decene was prepared and the mechanical properties were tested to determine the behavior of the hard block. Figure 5.2 shows that the hard block does not behave as an elastomer, demonstrating a high Young's modulus and plastic deformation with no elastic recovery.

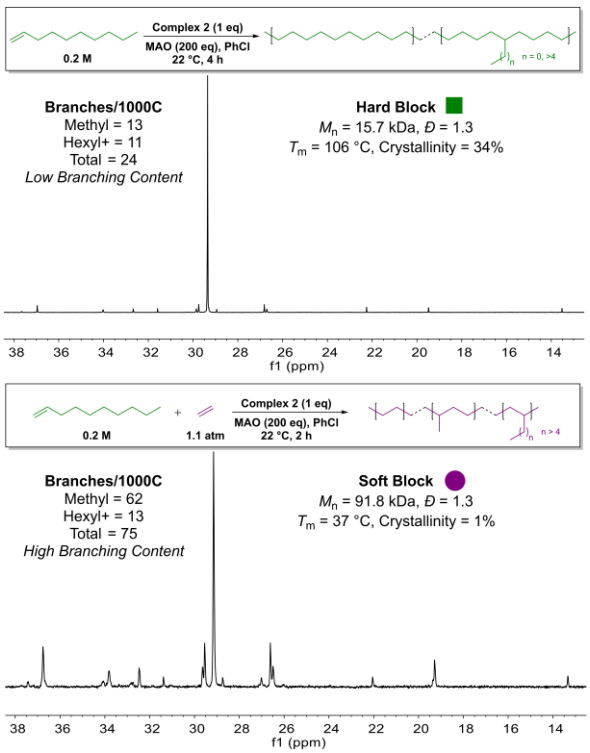

Figure 5.1.
^{13}C NMR spectra of a representative hard block from 1-decene (top) and soft block from ethylene/1-decene (bottom) using complex **2**.

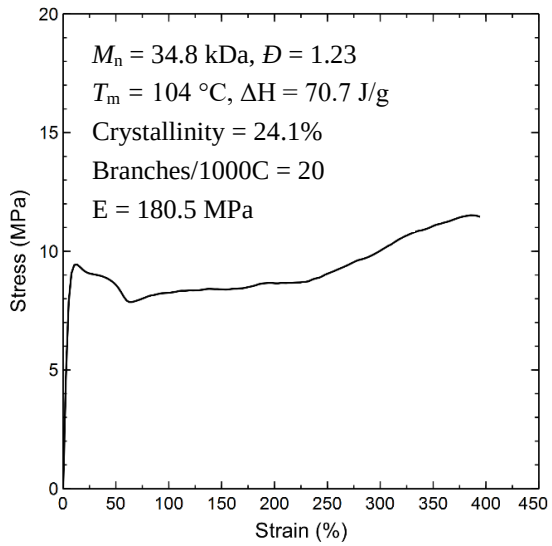

Figure 5.2.
Stress-strain behavior of hard block from 1-decene.

Triblock architectures were synthesized by first polymerizing 1-decene at low concentrations using **2** activated with methylaluminoxane (MAO) to generate the initial hard block. Aliquots were taken after the growth of each block to analyze molar mass and thermal properties (Section 5.4). A dilute solution of 1-decene was necessary to maximize chain straightening for high T_m and crystallinity.[32] After the appropriate amount of time, ethylene was pressurized directly into the reaction vessel to grow the subsequent soft block. Because of the faster polymerization rate of ethylene compared to 1-decene and the low concentration of α-olefin present in the reaction mixture, 1-decene consumption was negligible during the polymerization of ethylene.[30] After growing the soft block to the intended length, excess ethylene was exchanged with a nitrogen atmosphere. In the absence of ethylene, 1-decene polymerization resumed, generating the next hard block. This strategy is convenient because it does not require complete consumption of 1-decene before adding ethylene, unlike other sequential addition strategies which generally require full consumption of initial monomer before adding the next monomer to access well-defined blocks.

ABA triblock copolymers grown in toluene demonstrated modest control of molar mass, with dispersities ranging from 1.4 to 1.6 (Table 5.1, entries 1–4). Polymer molar masses were kept relatively constant, while the ratio of hard segments incorporated was varied (Table 5.1, entries 1–3). A lower molar mass sample was also synthesized for comparison (Table 5.1, entry 4). Gel permeation chromatography (GPC) traces displayed a clear shift in molar mass distribution for each aliquot, which was indicative of successful

block copolymer growth (Figure 5.3). The dispersity after growth of the first 1-decene block was generally low $Đ$ = 1.2–1.3, though broadening was observed during the polymerization of the ethylene block. This broadening was likely due to chain transfer reactions with trace trimethylaluminum present from the MAO activator,[34] or from associative chain transfer of the growing polymer chain via ethylene. These undesired chain transfer events can be mitigated by performing the polymerization in the more polar solvent chlorobenzene, producing materials with better control over molar mass and lower dispersities of 1.3 (Table 5.1, entries 5–6). It appears the additional polarity of chlorobenzene compared to toluene has a beneficial effect on the ion pair of complex **2** and MAO in limiting chain transfer, though the exact mechanism is unclear. Detailed studies on ion pairing in late transition metal complexes are limited, but ion pairing in early transition metal complexes are well documented. For zirconium metallocene complexes, the nature of the ion pair can affect catalyst activity and stability as well as polymer molecular weight, tacticity, and branching content.[35] Samples with higher molar mass exhibited a shoulder in the molar mass distribution (Figure 5.3, right). While we cannot confirm the cause for this second distribution, we suspect that a low pressure of ethylene coupled with increasing viscosity of the reaction mixture causes a heterogeneity in the overall ethylene concentration in solution, which may generate two distributions. At lower molar masses (lower viscosity), the distributions are unimodal (Figure 5.3, left).

Table 5.1.
Effect of Solvent and Hard Content on Synthesis and Mechanical Properties of Triblock Copolymers[a]

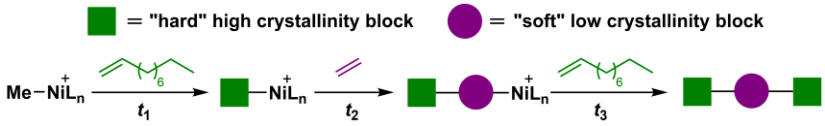

entry	solvent	block lengths[b] (kDa)	M_n total[b] (kDa)	$Đ$[b]	wt. % of hard blocks[c]	T_m[d] (°C)	X[d] (%)	ε[e] (%)	σ[e] (MPa)	E[f] (MPa)	SR[g] (%)
1	PhMe	5–90–5	100	1.4	10	40, 89	1.1	630 ± 10	12.8 ± 1.1	8.1 ± 0.7	77
2	PhMe	12–95–10	117	1.5	19	42, 99	4.2	640 ± 50	18.1 ± 2.2	16.5 ± 1.2	72
3	PhMe	22–73–18	113	1.6	35	98	6.6	670 ± 10	29.7 ± 2.5	26.0 ± 1.5	61
4	PhMe	14–43–17	74	1.5	42	99	6.9	750 ± 10	23.3 ± 2.6	38.4 ± 1.3	59
5	PhCl	14–66–11	91	1.3	27	23, 97	3.0	680 ± 30	19.8 ± 3.2	9.8 ± 0.2	85
6[h]	PhCl	13–53–12	78	1.3	32	25, 98	4.6	710 ± 10	23.9 ± 1.1	14.4 ± 0.3	80

[a]Polymerization conditions: [**2**] = 5.7 mM in PhCl, [MAO] / [**2**] = 200, [1-decene] = 0.1 M, ethylene pressure = 1.1 atm, solvent = 72 mL, 22 °C. [b]Determined using gel permeation chromatography (GPC) in 1,2,4-trichlorobenzene at 150 °C vs polyethylene standards. [c]Wt. % of hard blocks = ($\Sigma M_{n,hard}/M_{n,total}$). [d]Determined using differential scanning calorimetry (DSC), melting endotherm of second heat. Crystallinity (X) was calculated using the reference enthalpy of fusion (293.6 J g^{-1}) for fully crystalline polyethylene. [e]Strain at break, ε, and stress at break, σ, determined at fracture using uniaxial tensile test. [f]Young's modulus, E, is the initial slope of the stress vs strain curve in the linear region ($0 < \varepsilon < 0.05$) and was calculated from the average of at least 5 monotonic curves. [g]Strain recovery, SR, determined by a 300% strain step cycle test using equation $100(\varepsilon_a - \varepsilon_r)/\varepsilon_a$, where ε_a = applied strain and ε_r = strain at zero load after 10th cycle. [h][1-decene] = 0.2 M.

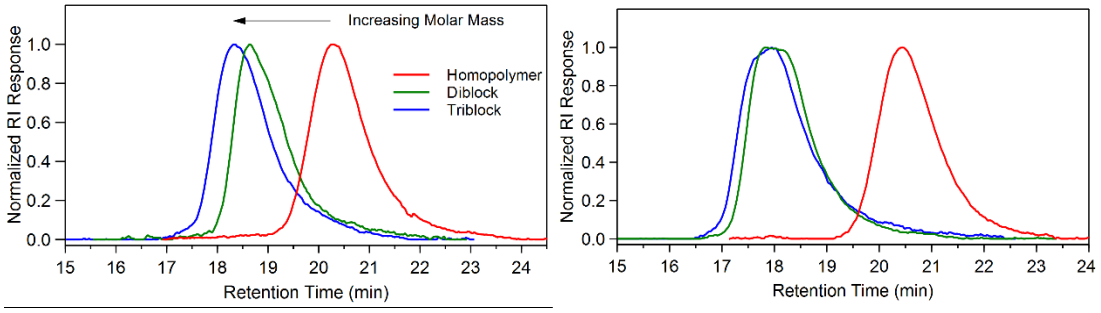

Figure 5.3
GPC trace of successive blocks of a triblock copolymer. Left: Table 5.1, entry 4. Right: Table 5.1, entry 2.

Utilizing differential scanning calorimetry (DSC), the thermal transitions were analyzed for each aliquot of every elastomer sample (Figure 5.4, Section 5.4). The hard

block from 1-decene (red) was highly crystalline, displaying melting temperatures ≥106 °C for samples above 10 kDa and crystallinities ≥30%. The maximum T_m of the 1-decene hard block measures at 106 °C, but a smaller endotherm can be observed at 95 °C. We suspect this endotherm is due to branching defects in the hard block, possibly from the melting of long side chains. Hard block samples with molar masses below 10 kDa exhibited broader and lower T_m's (103 °C, entry 1). The degree of crystallinity and the melting temperature in the sample decreased after growth of the second block, consistent with the branched polyethylene block inhibiting some crystallization of the chain straightened 1-decene block. The final triblock sample (blue) exhibited a similar T_m and slightly enhanced crystallinity in comparison to the diblock, which is consistent with enchaining more hard segment. For triblock samples with higher ethylene incorporation, a lower melting endotherm can be observed from 30–60 °C (Table 5.1, entries 1 and 2). This melting endotherm suggested that the soft polyethylene segment is not completely amorphous but possesses regions of crystallinity. This lower melting endotherm could also be seen in triblock copolymers synthesized in chlorobenzene (Table 5.1, entries 5 and 6) at a lower melting range of 20–45 °C. These polymers have highly crystalline regions from the chain straightened 1-decene end blocks connected by a slightly crystalline (~1%) polyethylene midblock, providing an architecture suitable for TPEs.

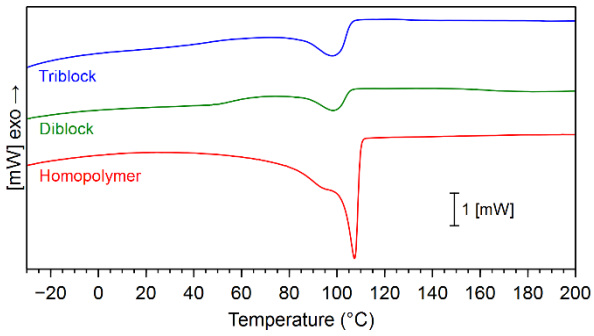

Figure 5.4
Representative DSC analysis of polymers at successive stages of a triblock copolymer (Table 5.1, entry 4). Melting endotherms from second heating cycles are reported heating at 10 °C min^{-1}.

Polymer films were melt-pressed at 110 °C under a pressure of 5.2 MPa for 15 min and cooled at a rate of ~6 °C/min to 22 °C. These films were subsequently cut into tensile bars for analysis of mechanical properties. Tensile strength was measured for all elastomer samples and Figure 5.5 shows representative tensile strength curves for entries 1–3 (Table 5.1). The slope of the tensile strength curve increases on approach to break, suggesting strain hardening.[36] These samples exhibited strain at break values ranging from 630 to 670%, a property that did not vary considerably by adjusting the ratio of hard content in the triblock copolymer. The lower molar mass sample (Table 5.1, entry 4) experienced somewhat higher elongations at break (750%). Stress at break and Young's modulus, however, showed an increase with increasing hard content in the triblock copolymer (Figure 5.5), indicating that increasing hard content increases ultimate tensile strength and tensile toughness of the material. The sample with the lowest hard content (Table 5.1, entry 1, 10%) showed stress at break values of 13 MPa and a Young's modulus of 8.1 MPa. The sample with 35% hard content (Table 5.1, entry 3) showed stress at break values of 30 MPa

and a Young's modulus of 26 MPa. Triblock copolymers grown in chlorobenzene (Table 5.1, entries 5 and 6) display slightly elevated strain at break values (680–710%), comparable stress at break values (20–24 MPa), and lower Young's moduli (9.8–14.4 MPa) than samples grown in toluene of similar hard content (Table 5.1, entry 3).

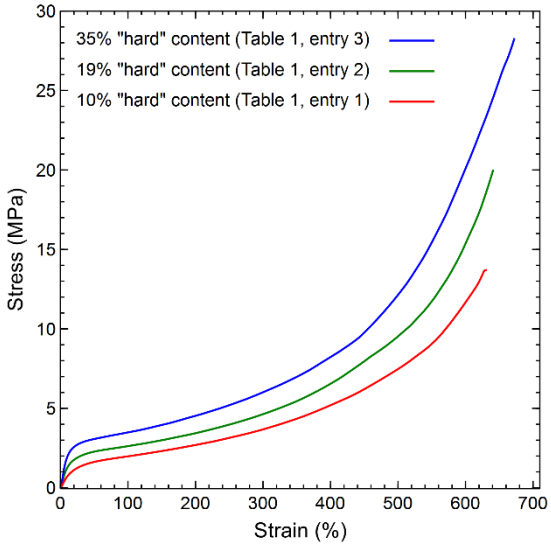

Figure 5.5.
Representative tensile strength curves for triblock copolymers with increasing hard content (Table 5.1, entries 1–3).

Polymer samples were also subjected to hysteresis testing where each sample was extended to 300% strain over 10 cycles to determine the elastic recovery. This was calculated by comparing the strain recovered after cycle 10 to the tensile bar's original length (Table 5.1). The first cycle resulted in the most significant amount of permanent deformation, followed by minimal deformation on subsequent cycles (Figure 5.6). For samples grown in toluene, as the crystallinity of the material increased, the amount of permanent deformation also increased. Entry 1 (10% hard content) showed an elastic strain recovery of 77% compared to entry 3 (35% hard content), which only showed a strain

recovery of 61%. For samples grown in chlorobenzene (entries 5 and 6), recoveries were substantially improved (80–85%) compared to toluene-grown samples of similar soft content. We suspected that the reduced T_m and crystallinity of the soft block observed for samples synthesized in chlorobenzene compared to toluene improve the recovery properties. It is known that elastomers such as vulcanized rubber can experience strain-induced crystallization after deformation,[37] where soft segments can align and crystallize. Samples with less crystallinity in the soft blocks could potentially exhibit less strain-induced crystallization, giving materials with improved elastic recovery. Further experimentation is necessary to confirm strain-induced crystallization, but initial DSC studies comparing unstrained and strained samples show a change of the melting endotherm in the low melting region which supports this possibility (Section 0). We also cannot rule out the possibility that triblock copolymers grown in toluene have a greater amount of diblock copolymer side product than samples grown in chlorobenzene due to increased chain transfer events during the course of the polymerization, which could have a detrimental effect on elastic recovery.

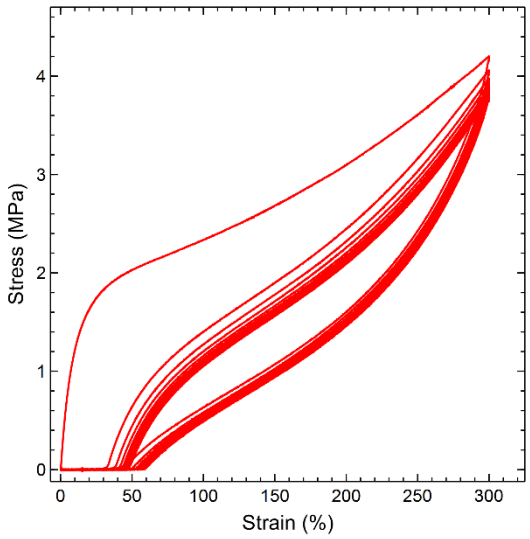

Figure 5.6.
Plot of hysteresis experiment for a representative triblock copolymer (Table 5.1, entry 6). Ten cycles at 300% strain were performed.

Since higher order block copolymers have been shown to exhibit improved mechanical properties compared to triblock copolymers,[38,39] we subsequently targeted pentablock and heptablock structures. To successfully access these materials, three parameters were adjusted. First, all polymerizations were carried out in chlorobenzene to maintain the molar mass control necessary to achieve these structures. Second, the concentration of 1-decene was increased from 0.1 to 0.2 M in order to reproducibly complete the synthesis. Growing the final hard block was prohibitively challenging at 0.1 M, likely due to increased viscosity and low free monomer concentration at the end of polymerization. This issue was originally circumvented by injecting additional 1-decene for the growth of the final block (Table 5.2, entry 1), but this procedure requires estimating the amount of 1-decene consumed in the reaction to add the correct amount of monomer to return the concentration to 0.1 M. Third, the individual block sizes for the hard and soft

segments were decreased in comparison to the triblock copolymers in order to maintain the same overall molar mass. Attempts were made to access polymer molar masses above 120 kDa but were ultimately unsuccessful due to the high viscosity of the solution and precipitation of the growing polymer chain. With these modifications, pentablock and heptablock structures were successfully synthesized with hard content varying from 24% to 42% (Table 5.2, Section 5.4). Overall molar masses ranged from 83 to 117 kDa, with a relatively constant $Đ$ of 1.3 maintained throughout the majority of the polymerization, until the final block, where a slight broadening from 1.3 to 1.4 occurred (Figure 5.7). DSC showed similar trends to the triblock structures, where the high hard block T_m decreased sharply after addition of the soft block (Figure 5.8). As previously observed with the triblock copolymers, the crystallinity of each aliquot increased slightly with the enchainment of 1-decene and decreased slightly with the enchainment of ethylene/1-decene throughout the polymerization (Section 5.4). The sample synthesized as described in Table 5.2, entry 4 was an exception to this trend, where crystallinity did not predictably change between enchaining hard and soft segments. For the heptablock copolymer, the overall crystallinity and melting temperature were lower than expected considering the amount of 1-decene incorporation, suggesting that the individual lengths of the hard blocks are more important than the overall incorporation of hard content in terms of increasing T_m and crystallinity.

Table 5.2
Synthesis and Characterization of Higher Order Block Copolymers[a]

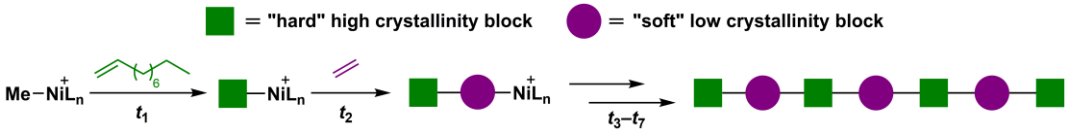

entry	block lengths[b] (kDa)	M_n total[b] (kDa)	$Đ$[b]	wt. % of hard blocks[c]	T_m[d] (°C)	X[d] (%)	ε[e] (%)	σ[e] (MPa)	E[f] (MPa)	SR[g] (%)
1[h]	11–40–6–42–17	117	1.4	29	24, 98	5.6	630 ± 20	29.1 ± 1.9	18.6 ± 0.3	77
2	9–48–9–33–8	107	1.4	24	25, 94	2.8	570 ± 10	16.9 ± 1.3	10.2 ± 0.4	80
3	16–43–19–25–14	116	1.4	42	22, 96	4.4	620 ± 10	19.8 ± 0.6	14.2 ± 0.1	78
4	6–18–11–20–10–12–6	83	1.4	40	91	2.0	670 ± 40	28.8 ± 6.0	14.9 ± 0.7	80

[a]Polymerization conditions: [**2**] = 5.7 mM in PhCl, [MAO] / [**2**] = 200, [1-decene] = 0.2 M, ethylene pressure = 1.1 atm, PhCl = 72 mL, 22 °C. [b]Determined using gel permeation chromatography (GPC) in 1,2,4-trichlorobenzene at 150 °C vs polyethylene standards. [c]Wt. % of 1-decene = ($\Sigma M_{n,hard}/M_{n,total}$). [d]Determined using differential scanning calorimetry (DSC), melting endotherm of second heat. Crystallinity (X) was calculated using the reference enthalpy of fusion (293.6 J g^{-1}) for fully crystalline polyethylene. [e]Strain at break, ε, and stress at break, σ, determined at fracture using uniaxial tensile test. [f]Young's modulus, E, is the initial slope of the nominal stress vs nominal strain curve in the linear region ($0 < \varepsilon < 0.05$) and was calculated from the average of 5 monotonic curves. [g]Strain recovery, SR, determined by a 300% strain step cycle test using equation $100(\varepsilon_a - \varepsilon_r)/\varepsilon_a$, where ε_a = applied strain and ε_r = strain at zero load after 10th cycle. [h][1-decene] = 0.1 M.

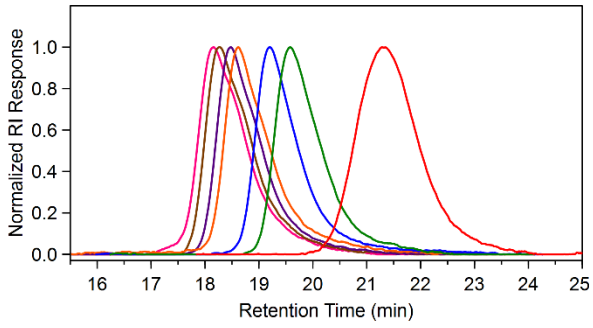

Figure 5.7.
Representative GPC trace of successive blocks of a heptablock copolymer (Table 5.2, entry 4).

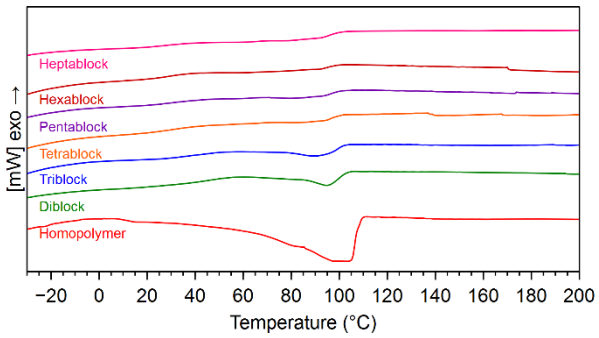

Figure 5.8.
Representative DSC analysis of polymers at successive stages of a heptablock copolymer (Table 5.2, entry 4). Melting endotherms from second heating cycles are reported heating at 10 °C min^{-1}.

The mechanical properties of these higher order block copolymers were tested and compared to the original triblock samples. Interestingly, these materials (Table 5.2, entries 1–3) generally exhibited similar mechanical properties to the triblock copolymers in terms of tensile strength and elastic recovery (Table 5.1, entries 5–6). One particular pentablock structure (Table 5.2, entry 2) even exhibited slightly lower strain at break values compared to the triblock copolymers. This is potentially due to the short length of the soft segments, reducing the amount the polymer chain can extend, resulting in lower strain at break values.

To understand how a soft segment with a low degree of crystallinity contributes to the elastic properties of the resulting TPEs, AB diblock copolymers consisting of one hard and one soft segment were synthesized and their mechanical properties were tested. Diblock copolymers were grown in both toluene and chlorobenzene with hard ratios of 10–30% for comparison to their triblock counterparts (Table 5.3). After performing tensile strength and hysteresis experiments, we were surprised to observe that all samples exhibited elastic properties (Figure 5.9). While the diblock copolymers (Table 5.3, entries

1–3) exhibited similar stress at break and elastic recovery values compared to the triblock copolymers of similar molar mass and hard content, they displayed higher elongation at break values than the previously tested copolymers (780–970%). We observed consistent trends for the triblock and diblock samples; materials grown in chlorobenzene experienced higher strain at break values than samples grown in toluene when controlling for molar mass and hard content, and elastic recovery suffered as the ratio of hard content increased (Table 5.3, entries 2–3).

Table 5.3.
Synthesis and Characterization of Diblock and Statistical Copolymers[a]

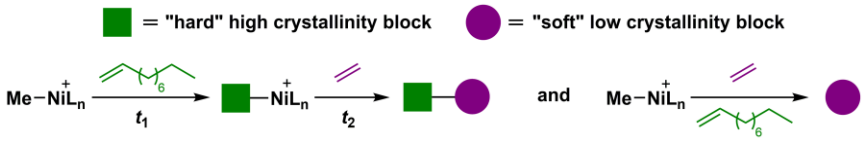

entry	solvent	block lengths[b] (kDa)	M_n total[b] (kDa)	$Đ$[b]	wt. % of hard blocks[c]	T_m[d] (°C)	X[d] (%)	ε[e] (%)	σ[e] (MPa)	E[f] (MPa)	SR[g] (%)
1[h]	PhMe	14–115	128	1.5	11	50, 97	3.1	780 ± 10	19.2 ± 1.8	9.8 ± 0.2	70
2	PhCl	15–107	122	1.4	10	36, 97	3.6	870 ± 10	26.1 ± 1.1	8.6 ± 0.2	78
3	PhCl	25–59	84	1.3	30	100	5.4	970 ± 40	24.4 ± 1.8	18.0 ± 0.2	58
4	PhMe	102	102	1.3	n/a	49	2.2	1100 ± 20	17.6 ± 2.2	5.9 ± 0.3	66
5	PhCl	102	102	1.2	n/a	41	1.4	1120 ± 30	11.6 ± 1.7	3.8 ± 0.2	77

[a]Polymerization conditions: [**2**] = 5.7 mM in PhCl, [MAO] / [**2**] = 200, [1-decene] = 0.2 M, ethylene pressure = 1.1 atm, solvent = 72 mL, 22 °C. [b]Determined using gel permeation chromatography (GPC) in 1,2,4-trichlorobenzene at 150 °C vs polyethylene standards. [c]Wt. % of hard blocks = ($\Sigma M_{n,hard}/M_{n,total}$). [d]Determined using differential scanning calorimetry (DSC), melting endotherm of second heat. Crystallinity (X) was calculated using the reference enthalpy of fusion (293.6 J g^{-1}) for fully crystalline polyethylene. [e]Strain at break, ε, and stress at break, σ, determined at fracture using uniaxial tensile test. [f]Young's modulus, E, is the initial slope of the nominal stress vs nominal strain curve in the linear region ($0 < \varepsilon < 0.05$) and was calculated from the average of 5 monotonic curves. [g]Strain recovery, SR, determined by a 300% strain step cycle test using equation $100(\varepsilon_a - \varepsilon_r)/\varepsilon_a$, where ε_a = applied strain and ε_r = strain at zero load after 10th cycle. [h][1-decene] = 0.1 M.

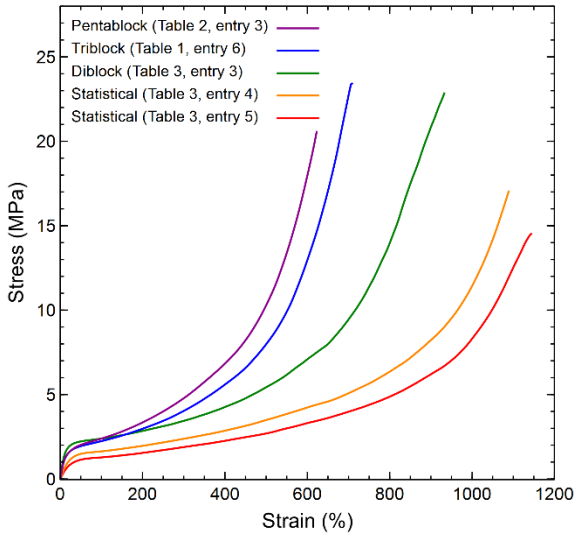

Figure 5.9.
Representative tensile strength curves for various block architectures, from pentablock to statistical copolymers.

These results indicated that the crystalline regions of the soft block contribute to the elastic behavior of the diblock copolymers by providing sufficient anchoring domains. Therefore, statistical copolymers of ethylene and 1-decene were synthesized to study materials with compositions mimicking that of the soft blocks in the TPE samples (Table 5.3, entries 4–5). Since 1-decene consumption was negligible, the resulting materials are essentially homopolymers of ethylene. These materials had narrow dispersities (1.2–1.3) and exhibited low T_m's (42–49 °C) with low levels of crystallinity (1.4–2.2%). The mechanical properties were surprisingly impressive as the elongations were upwards of 1100% (Table 5.3, entry 5, in chlorobenzene), longer than any of the block copolymer samples. This is an underestimate of the true strain at break for the sample as the samples broke near the grips as opposed to the gauge area of the tensile bar. Two tensile bars tested

broke in the gauge area at elongations beyond 1300% before break. These samples were omitted from the average calculations, but they are likely more indicative of the true properties of this material. It appeared that block architecture had a significant detrimental effect on the maximum elongation possible. As the number of blocks decreased, the maximum strain at break increased (Figure 5.9). The Young's moduli were also lower than the other samples (3.8 and 5.9 MPa). Most surprisingly, the statistical copolymer samples displayed comparable elastic recovery to all other materials tested. The statistical copolymer grown in toluene exhibited lower elastic recovery (66%) than the statistical copolymer grown in chlorobenzene (77%), corresponding to differences in the crystallinity of the soft segment as previously observed.

To explain why all of the polymers synthesized, regardless of block architecture, behaved as elastomers, we posit that the crystalline regions of the soft block are significant enough to act as physical cross-links, allowing elastic recovery to occur. To test this hypothesis, the creep behavior of these polymers was studied. Samples with various architectures were elongated to 300% strain and kept at a constant stress for 3 h (Figure 5.10, Section 0). We suspect that elasticity in these materials is derived not from phase separation of the individual blocks into well-ordered structures, but rather crystallizable domains embedded in an amorphous matrix behaving as anchoring units.[40,41] If low melting crystallites are responsible for the elastic recovery seen in diblock and statistical copolymers, then a constant force could disrupt these interactions and pull the polymer chains apart. Conversely, triblock and pentablock copolymers with the conventional hard–soft–hard architecture have larger proportions of crystalline domains that should better

resist strain-induced deformation. The results of the creep experiment support our hypothesis, showing that higher numbers of blocks result in less deformation under constant force conditions (Figure 5.10) after 3 h. Statistical copolymers (Table 5.3, entries 4–5) resulted in the greatest deformation over time, particularly the sample grown in chlorobenzene (entry 5), which has the lowest crystallinity. The diblock copolymer (Table 5.3, entry 3) experienced improved resistance to creep compared to the statistical copolymers, but triblock (Table 5.1, entry 6) and pentablock copolymers (Table 5.2, entry 3) exhibited the least amount of deformation. Since both the triblock and pentablock structures displayed virtually the same amount of creep over the given time, it appears that again no benefit was gained through the synthesis of higher order multiblocks. These results show that although all samples generated with this catalyst system behave as elastomers, materials with two or more hard blocks are better suited for performance applications, as diblock and statistical copolymers more rapidly lose elasticity over longer periods of extension.

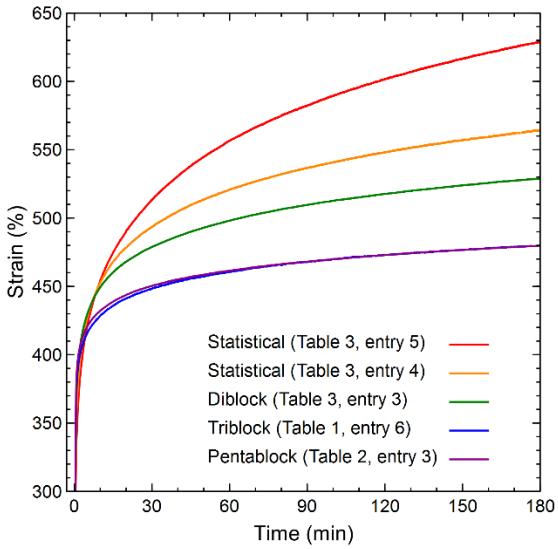

Figure 5.10.
Creep results for various block architectures, from pentablock to statistical copolymers. Samples were strained to 300% and held at constant force over a period of 3 hours. The change in strain over time is reported.

5.3 Conclusion

We report a chain walking strategy for the synthesis of thermoplastic elastomer block copolymers from inexpensive, potentially biorenewable feedstocks, where 1-decene is utilized as the hard segment and ethylene is utilized as the soft segment. Modest control of molar mass can be maintained by growing these samples in toluene, yielding triblock copolymers with mechanical properties that can be modulated by varying the ratio of the hard and soft blocks. Switching the solvent to chlorobenzene was pivotal for accessing improved triblock materials with low $Đ$ (1.3), high elongations before break (680–710%), low Young's moduli (9.8–14.4 MPa), and improved elastic recovery (80–85%). This additional control of block length allowed for higher order block copolymers to be

synthesized, which displayed similar mechanical properties to triblock copolymers, albeit with lower overall elongations before break (570–630%). Diblock and statistical copolymers were synthesized and exhibited comparable elastic properties to triblock and pentablock copolymers, with even higher elongations before break (780–1120%). By performing a creep experiment, which maintained a constant force and measured change in strain over time, we observed that samples with higher numbers of blocks (triblock, pentablock) were more resistant to deformation compared to samples with lower numbers of blocks (diblock, statistical).

Our system allows access to a variety of elastic materials with tunable properties that can be modulated based on block architecture and ratio of hard content. Materials with lower numbers of blocks can elongate further before breaking, but elasticity is lost under sustained force. Conversely, materials with increased hard content are stronger but also show a decrease in elastic recovery. The TPEs accessed by our system have the best mechanical properties to date when using α-olefins as the hard segments and ethylene as the soft segments, as well as comparable properties to other ethylene/1-octene block and statistical copolymers.[42] Promisingly, these materials have similar tensile strength and elastic recovery values to Dow's commercial olefin block copolymers. However, chemically cross-linked materials such as vulcanized rubber are still dominant in terms of their near perfect elastic recovery. Further catalyst optimization has the potential to improve upon the elastic recovery of the reported materials by modulating the chain walking process to obtain more crystalline hard segments and completely amorphous soft segments. In order to realize this goal, mechanistic studies of complex **2** and other related

nickel species are currently in progress. This system demonstrates great promise due to the low cost and accessibility of the monomer feedstocks along with the sustainability and reusability of the resulting materials.

5.4 Experimental details

Materials

Acenapthenequinone (Sigma), triphenyl phosphite (Sigma), zinc chloride (Strem), nickel bromide dimethoxyethane adduct (Strem), palladium acetate (Acros), 1-napthylamine (AK Scientific), silver acetate (AK Scientific), potassium hydroxide (Macron), acetic acid (Macron), 2-picolinic acid (Alfa Aesar), potassium oxalate (Alfa Aesar), 4-iodobenzotrifluoride (Oakwood Chemical) and pyridine (Fisher Scientific) were used as received.

Anhydrous chlorobenzene was purchased from Sigma Aldrich, sparged with nitrogen for 40 minutes and stored over activated 4 Å molecular sieves. 1-Decene was purchased from Acros Chemicals (95% purity), distilled and stored over activated 4 Å molecular sieves prior to use. Ethylene was from Airgas, Inc. Methylaluminoxane (MAO) was purchased from Albemarle Corporation (30 wt% in toluene) and dried by removing volatiles (toluene and trace trialkylaluminum) under vacuum and heating at 40 °C for at least 8 hours. Anhydrous toluene, hexanes, and dichloromethane (HPLC) were purchased from Fisher Scientific, sparged with nitrogen for 40 minutes, and purified over solvent columns. NMR solvents were purchased from Cambridge Isotope Laboratories and stored over activated 4 Å molecular sieves.

General considerations

Air and/or moisture sensitive compounds were manipulated under an atmosphere of nitrogen using standard schlenk techniques or an MBraun Labmaster glovebox. Flash column chromatography was performed using silica gel (particle size 40–64 μm, 230–400 mesh).

The ^{1}H NMR, $^{13}C\{^{1}H\}$ NMR spectra were recorded on Varian INOVA 500, Varian INOVA 600, or Varian INOVA 400 using the residual non-deuterated solvent signal as a reference. Polymers were analyzed using quantitative ^{1}H and ^{13}C NMR spectroscopy in $Cl_2CDCDCl_2$ (d_2-TCE) at 135 °C. $Cr(acac)_3$ (acac=acetylacetonate) from Sigma Aldrich was added for quantitative ^{13}C NMR analysis of select samples (0.1 M in d_2-TCE). MestReNova software was used to process the NMR spectra. Branches per 1000 carbons were determined by ^{1}H NMR for the final block copolymer of each sample, as well as select aliquots.

High temperature gel permeation chromatography (GPC) was performed on Agilent PL-GPC 220 equipped with a refractive index (RI) detector and three PL-Gel Mixed B columns. GPC columns were eluted at 1.0 mL/min with 1,2,4-trichlorobenzene (TCB) containing 0.01 wt. % di-*tert*-butylhydroxytoluene (BHT) at 150 °C. The samples were prepared in TCB (with BHT) at a concentration of 1.0 mg/mL and heated at 150 °C for at least 1 hour prior to injection. GPC data calibration was done with monomodal polyethylene standards from Polymer Standards Service. GPC traces are plotted where lower retention time signifies higher molecular weight (block size increases from right to left). The refractive index (RI) of each aliquot was normalized to 1.0.

Differential scanning calorimetry (DSC) measurements were performed on Mettler-Toledo Polymer DSC instrument equipped with an automated sampler. Polymer samples in crimped aluminum pans were analyzed under nitrogen at a heating rate of 10 °C/min from -70 to 200°C. STARe software was used to process the collected data and melting points (T_m) were obtained and reported from the second heating run. DSC traces of the second heat of each aliquot are plotted. Sample crystallinity (X) was calculated using the reference enthalpy ($\Delta H_m^0 = 293.6$ J g^{-1}) for fully crystalline polyethylene: $[(\Delta H_m - \Delta H_c) / \Delta H_m^0] \times 100$. The glass transition temperature (T_g) for each block could not be visualized over the given temperature range (-70 to 200 °C), which is consistent with polyethylene possessing a very low T_g.[43]

Casting Polymer Films

All polymer samples were melt-casted using a Carver Press hot plate. Each sample was loaded into a rectangular stainless-steel mold (92 mm x 30 mm x 0.5 mm) sandwiched between two Mylar sheets and two stainless steel sheets and pressed under a pressure of ~52 MPa at 110 °C for 15 minutes. At this pressure, the sample was cooled to 22 °C at a rate of 6 °C/min over a period of 20 minutes. The rectangular film was removed from the mold and excess polymer around the edges was removed with a razor blade. The film was subsequently cut into tensile bars using a stainless-steel polymer die (gauge length = 16 mm, gauge width = 3 mm, gauge thickness = 0.6 mm) to give polymer bars which were rubbery, clear and easy to handle.

Complex 2 synthesis

Complex **2** was synthesized according to literature procedures.[32] The resulting dark red crystals were stored in a vial inside a glovebox and crushed into a fine powder immediately before use.

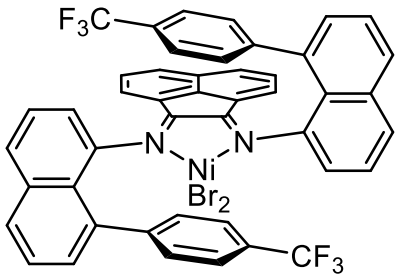

Complex 2

General Polymerization Scheme (Synthesis of Block Copolymers)

All polymerizations were set up in a MBraun Labmaster glovebox. An oven-dried 200 mL Fisher-Porter bottle (Andrews Glass) equipped with a magnetic stir bar was charged with d-MAO (200 eq, 6.79 mmol), solvent (72 mL of toluene or chlorobenzene) and 1-decene (0.1 M, 1.6 mL or 0.2 M, 3.2 mL). The vessel was sealed with a Swagelok reactor head. Complex **2** (1 eq, 34.1 μmol) was dissolved in chlorobenzene (6 mL) and drawn into a gas tight syringe equipped with a stainless steel needle, then sealed at the tip using a rubber septum. The vessel and syringe were removed from the glovebox. The vessel was submerged in a water bath, connected to a nitrogen inlet and pressurized to 20 psig (1.4 atm). Under this pressure, the catalyst solution was injected. The polymerization was run for the appropriate time to grow the first hard block from 1-decene. An aliquot was removed (8 mL) and precipitated into acidic methanol (5 % HCl v/v, ~50 ml) for future analysis. The nitrogen atmosphere was then exchanged with ethylene (16 psig, 1.1 atm) by

cycling ethylene into the bottle and releasing pressure through the top valve via a syringe needle inserted through a rubber septum at least 3 times. The ethylene inlet was left open for a given amount of time to grow the soft block, after which the ethylene atmosphere was replaced with nitrogen by cycling nitrogen into the bottle and releasing pressure through the top valve at least 8 times. An aliquot was removed (3 mL) and precipitated into acidic methanol for analysis future analysis. For triblock copolymers, the polymerization was quenched after the given time by reducing pressure through the top valve and injecting 10 mL of methanol into the vessel with vigorous stirring. The polymer solution was then precipitated into a solution of acidic methanol (5 % HCl v/v ~500 mL) and stirred for at least 4 hours. All polymers were filtered, washed with methanol and dried under vacuum at 45 °C until constant weight. For higher order block copolymers, additional cycles were repeated until the desired block architecture was achieved. Additional data tables are included for each sample (Table 5.4–Table 5.16). Yield of polymer is determined from the aliquot removed during the polymerization.

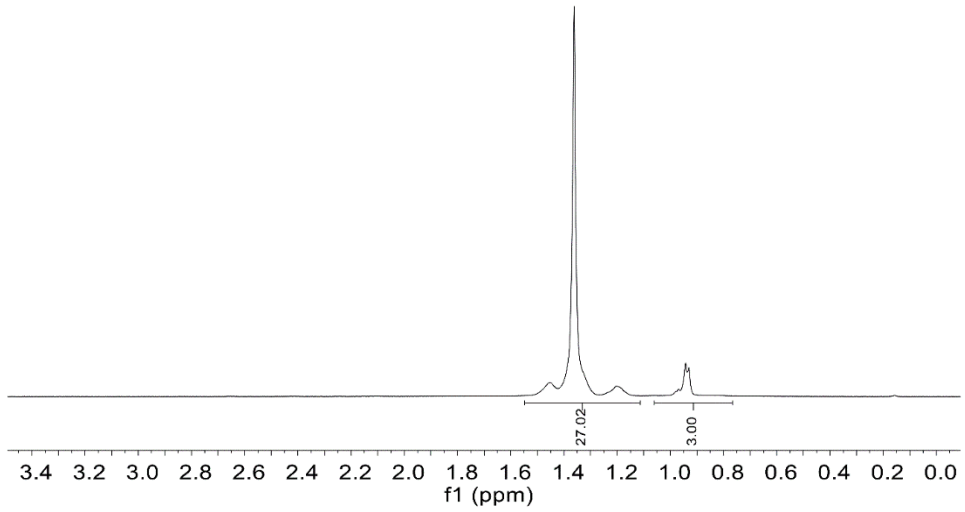

Figure 5.11.
^{1}H NMR of Representative Block Copolymer (Table 5.2, Entry 1)

Table 5.4.
Triblock Copolymer Data (Table 5.1, Entry 1)

Sample	**Time (h)**	**Yield (g)**	M_n **(kDa)**	$Đ$	T_m **(°C)**	**ΔH (J/g)**	X **(%)**	**Branches/ 1000C**
Homopolymer	2.0	0.014	4.9	1.28	101	103.0	35.1	n/d
Diblock	0.8	0.048	94.4	1.34	43, 89	3.1, 1.4	1.0, 0.5	n/d
Triblock	4.5	1.64	99.2	1.42	40, 89	1.9, 1.2	0.6, 0.4	69

Table 5.5.
Triblock Copolymer Data (Table 5.1, Entry 2)

Sample	**Time (h)**	**Yield (g)**	M_n **(kDa)**	$Đ$	T_m **(°C)**	**ΔH (J/g)**	X **(%)**	**Branches/ 1000C**
Homopolymer	5.5	0.014	12.1	1.32	108	106.0	36.1	n/d
Diblock	0.8	0.060	107.1	1.36	46, 97	4.1, 7.7	1.4, 2.6	n/d
Triblock	16.5	2.08	116.9	1.42	42, 99	1.8, 10.6	0.6, 3.6	65

Table 5.6.
Triblock Copolymer Data (Table 5.1, Entry 3)

Sample	**Time (h)**	**Yield (g)**	M_n **(kDa)**	$Đ$	T_m **(°C)**	**ΔH (J/g)**	X **(%)**	**Branches/ 1000C**
Homopolymer	15.0	0.031	22.1	1.34	107	90.6	30.9	n/d
Diblock	0.9	0.062	95.4	1.48	40, 97	0.9, 11.4	0.3, 3.9	n/d
Triblock*	33.0	2.49	113.2	1.55	98	19.4	6.6	57

*Additional 1-decene (0.81 mL) was injected via gas-tight syringe into reaction in order to have enough free monomer to complete the polymerization.

Table 5.7.
Triblock Copolymer Data (Table 5.1, Entry 4)

Sample	Time (h)	Yield (g)	M_n (kDa)	$Đ$	T_m (°C)	ΔH (J/g)	X (%)	Branches/ 1000C
Homopolymer	7.5	0.010	14.0	1.30	107	114.8	39.1	n/d
Diblock	0.5	0.023	56.7	1.29	51, 99	2.3, 17.2	0.8 5.8	n/d
Triblock	24.0	1.34	73.9	1.38	99	20.4	6.9	60

Table 5.8.
Triblock Copolymer Data (Table 5.1, Entry 5)

Polymer	Time (h)	Yield (g)	M_n (kDa)	$Đ$	T_m (°C)	ΔH (J/g)	X (%)	Branches/ 1000C
Homopolymer	7.0	0.041	13.7	1.29	108	114.8	39.1	n/d
Diblock	1.0	0.113	79.9	1.30	27, 98	2.0, 7.1	0.7, 2.4	n/d
Triblock	20.0	2.38	91.2	1.31	23, 97	1.2, 7.6	0.4, 2.6	74

Table 5.9.
Triblock Copolymer Data (Table 5.1, Entry 6)

Polymer	Time (h)	Yield (g)	M_n (kDa)	$Đ$	T_m (°C)	ΔH (J/g)	X (%)	Branches/ 1000C
Homopolymer	3.0	0.028	13.4	1.29	106	93.6	31.8	n/d
Diblock	0.8	0.071	66.3	1.29	30, 99	1.3, 9.7	0.4, 3.3	n/d
Triblock	5.0	2.39	78.1	1.31	25, 98	0.6, 12.9	0.2, 4.4	70

Table 5.10.
Pentablock Copolymer Data (Table 5.2, Entry 1)

Sample	Time (h)	Yield (g)	M_n (kDa)	$Đ$	T_m (°C)	ΔH (J/g)	X (%)	Branches/ 1000C
Homopolymer	6.0	0.017	11.2	1.32	107	103.9	35.3	n/d
Diblock	0.7	0.053	51.6	1.24	28, 99	0.9, 11.5	0.3 3.9	n/d
Triblock	14.5	0.040	57.7	1.32	24, 100	0.6, 16.6	5.9	n/d
Tetrablock	0.7	0.080	99.9	1.35	25, 96	1.6, 12.5	4.8	n/d
Pentablock*	14.5	3.25	117.0	1.38	24, 98	1.2, 15.2	5.6	65

*Additional 1-decene (1.0 mL) was injected via gas-tight syringe into reaction

Table 5.11.
Pentablock Copolymer Data (Table 5.2, Entry 2)

Sample	Time (h)	Yield (g)	M_n (kDa)	$Đ$	T_m (°C)	ΔH (J/g)	X (%)	Branches/ 1000C
Homopolymer	2.0	0.022	9.1	1.34	105	113.2	38.6	n/d
Diblock	0.7	0.070	56.9	1.36	37, 96	3.0, 7.5	3.6	n/d
Triblock	3.0	0.080	65.8	1.38	32, 96	2.1, 9.1	3.8	n/d
Tetrablock	0.7	0.106	99.0	1.34	28, 93	1.1, 5.3	2.2	n/d
Pentablock	5.0	2.97	106.5	1.39	25, 94	1.8, 6.4	2.8	68

Table 5.12.
Pentablock Copolymer Data (Table 5.2, Entry 3)

Sample	Time (h)	Yield (g)	M_n (kDa)	$Đ$	T_m (°C)	ΔH (J/g)	X (%)	Branches/ 1000C
Homopolymer	4.0	0.052	15.7	1.31	106	99.3	33.8	24
Diblock	0.7	0.069	58.6	1.31	30, 100	0.8, 14.4	5.2	n/d
Triblock	6.0	0.068	77.4	1.27	100	15.0	5.1	n/d
Tetrablock	0.7	0.076	102.2	1.40	23, 98	1.3, 11.7	4.4	n/d
Pentablock	10.0	3.24	116.4	1.40	22, 96	1.2, 12.5	4.7	64

Table 5.13.
Heptablock Copolymer Data (Table 5.2, Entry 4)

Sample	Time (h)	Yield (g)	M_n (kDa)	$Đ$	T_m (°C)	ΔH (J/g)	X (%)	Branches/ 1000C
Homopolymer	1.5	0.011	5.6	1.33	103	109.0	37.1	n/d
Diblock	0.3	0.029	23.9	1.30	41, 95	1.4, 12.5	4.7	n/d
Triblock	2.0	0.028	35.2	1.26	33, 91	1.2, 9.5	3.6	n/d
Tetrablock	0.3	0.044	55.1	1.32	93	6.2	2.1	n/d
Pentablock	3.0	0.063	64.7	1.29	92	5.5	1.9	n/d
Hexablock	0.4	0.064	77.0	1.29	92	3.6	1.2	n/d
Heptablock	6.0	2.32	82.8	1.37	91	5.8	2.0	65

Table 5.14.
Diblock Copolymer Data (Table 5.3, Entry 1)

Sample	Time (h)	Yield (g)	M_n (kDa)	$Đ$	T_m (°C)	ΔH (J/g)	X (%)	Branches/ 1000C
Homopolymer	7.5	0.016	13.8	1.22	107	105.1	35.8	n/d
Diblock	0.7	2.54	128.4	1.50	50, 97	3.3, 5.9	1.1, 2.0	70

Table 5.15.
Diblock Copolymer Data (Table 5.3, Entry 2)

Sample	Time (h)	Yield (g)	M_n (kDa)	$Đ$	T_m (°C)	ΔH (J/g)	X (%)	Branches/ 1000C
Homopolymer	3.5	0.020	15.2	1.27	106	118.5	40.4	n/d
Diblock	1.5	2.43	121.9	1.38	36, 97	4.0, 6.5	1.4, 2.2	72

Table 5.16.
Diblock Copolymer Data (Table 5.3, Entry 3)

Sample	Time (h)	Yield (g)	M_n (kDa)	$Đ$	T_m (°C)	ΔH (J/g)	X (%)	Branches/ 1000C
Homopolymer	8.0	0.032	26.6	1.22	106	106.0	36.1	n/d
Diblock	0.3	1.93	85.2	1.27	100	16.0	5.4	62

Synthesis of Statistical Copolymers

An oven-dried 200 mL Fisher-Porter bottle equipped with a magnetic stir bar was charged with MAO (200 eq, 6.79 mmol), appropriate solvent (72 mL of toluene or chlorobenzene) and 1-decene (0.2 M, 3.2 mL). Complex 2 was dissolved in chlorobenzene (6 mL) and drawn into a gas tight syringe equipped with a stainless-steel needle, sealed at the tip using a rubber septum. The vessel and syringe were removed from the glovebox. The vessel was submerged in a water bath and connected to an ethylene inlet (1.1 atm), cycling 3 times to exchange the nitrogen environment. While open to ethylene, the catalyst was immediately injected into the reaction vessel. After the desired polymerization time, the pressure was reduced through the top valve and the reaction mixture was quenched with methanol (10 mL) under vigorous stirring. The polymer solution was precipitated into acidic methanol (5% HCl v/v, ~500 mL), and stirred for at least 4 hours. The resulting polymers were filtered, washed with methanol and dried in vacuo until constant weight. Additional data tables are included for each sample (Table 5.17–Table 5.19). Yield of polymer is determined from the aliquot removed during the polymerization.

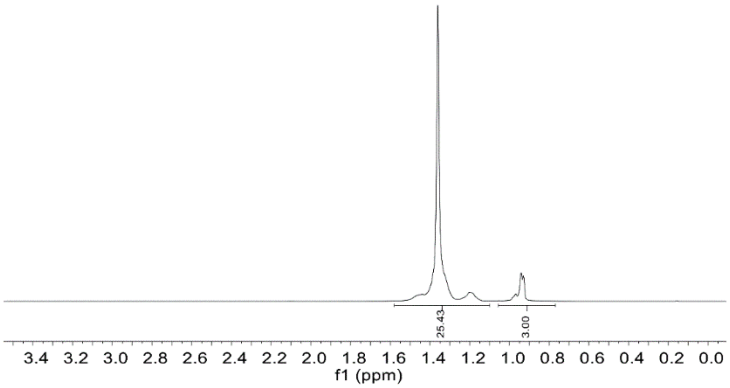

Figure 5.12.
^{1}H NMR of Representative Statistical Copolymer (Table 2, Entry 4)

Table 5.17.
Statistical Copolymer Data (Table 5.3, Entry 4)

Sample	Time (h)	Yield (g)	M_n (kDa)	$Đ$	T_m (°C)	ΔH (J/g)	X (%)	Branches/ 1000C
Statistical	1.0	2.33	102	1.3	49	6.4	2.2	72

Table 5.18.
Statistical Copolymer Data (Table 5.3, Entry 5)

Sample	Time (h)	Yield (g)	M_n (kDa)	$Đ$	T_m (°C)	ΔH (J/g)	X (%)	Branches/ 1000C
Statistical	2.0	3.44	102	1.2	41	4.0	1.4	83

Ethylene Homopolymerization

A polymer sample was prepared using complex **2** in chlorobenzene with identical conditions to the statistical copolymer synthesis, except 1-decene was **not** included. The resulting polymer has similar properties compared to the statistical copolymer, suggesting negligible 1-decene incorporation for the copolymerization of 1-decene and ethylene.

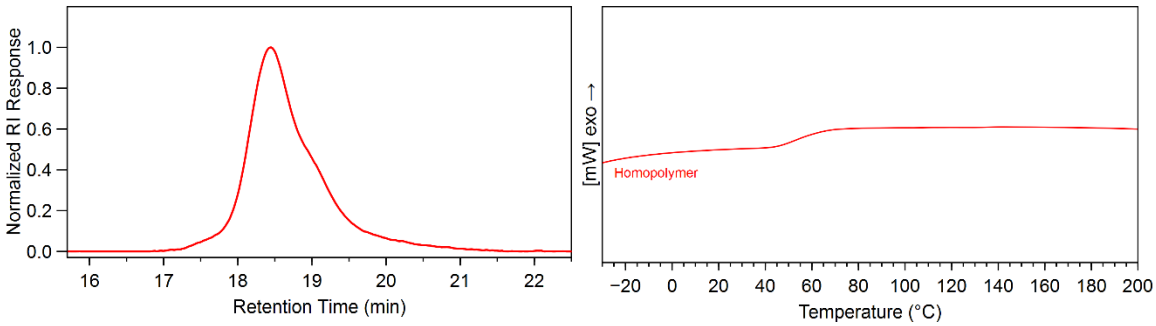

Figure 5.13.
GPC trace (left) and DSC analysis (right) of homopolymer.

Table 5.19.
Homopolymer Data

Sample	Time (h)	Yield (g)	M_n (kDa)	$Đ$	T_m (°C)	ΔH (J/g)	X (%)	Branches/ 1000C
Homopolymer	1.5	2.11	125	1.28	46	4.9	1.7	77

Mechanical properties and additional experiments

Mechanical studies were performed using a Shimadzu Autograph AGS-X Series tensile tester. For tensile strength and hysteresis experiments, a crosshead velocity of 50 mm/min was used for each sample. For tensile strength experiments, tensile bars were elongated until break. At least five tensile bars were tested for each individual sample. For hysteresis experiments, tensile bars were cycled ten times to 300% strain. Three tensile bars were tested for each individual sample.

A creep experiment was performed on samples with various block architectures in order to probe their resistance to permanent deformation. Tensile bars were elongated to 300% strain and held at a constant stress (Table 5.20) over a period of three hours. The change in strain over time was monitored. Individual samples required different levels of stress in order to achieve the initial 300% strain.

Table 5.20.
Constant stress chosen for each sample at which the material exhibited 300 % strain.

Sample (Solvent)	Stress (MPa)
Statistical (PhCl)	1.8
Statistical (PhMe)	2.4
Diblock (PhCl)	4.0
Triblock (PhCl)	4.5
Pentablock (PhCl)	5.8

An additional creep experiment was performed where samples were subjected to the same constant force (1.8N) over a period of three hours, monitoring change in strain over time (Figure 5.14). A similar trend was found under these conditions, where lower

block structures (diblock) deformed more rapidly than higher block structures (pentablock).

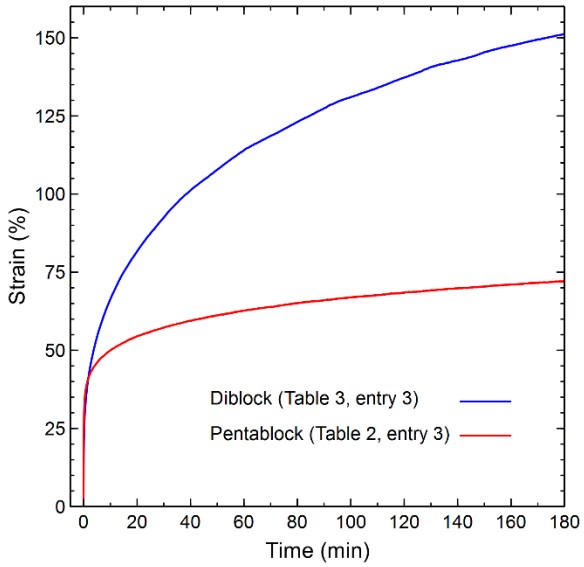

Figure 5.14.
Creep Experiment at Constant Force for Diblock and Pentablock Copolymers

Two samples were further analyzed to determine the dependence of hysteresis rate on elastic return properties. A representative triblock (Table 5.1, Entry 6) and statistical (Table 5.3, Entry 5) copolymer were stretched to 300% strain at 5 mm/min over 10 cycles (compared to 50 mm/min). It was determined that hysteresis rate does not have a significant effect on elastic return properties over this range (Figure 5.15 and Figure 5.16).

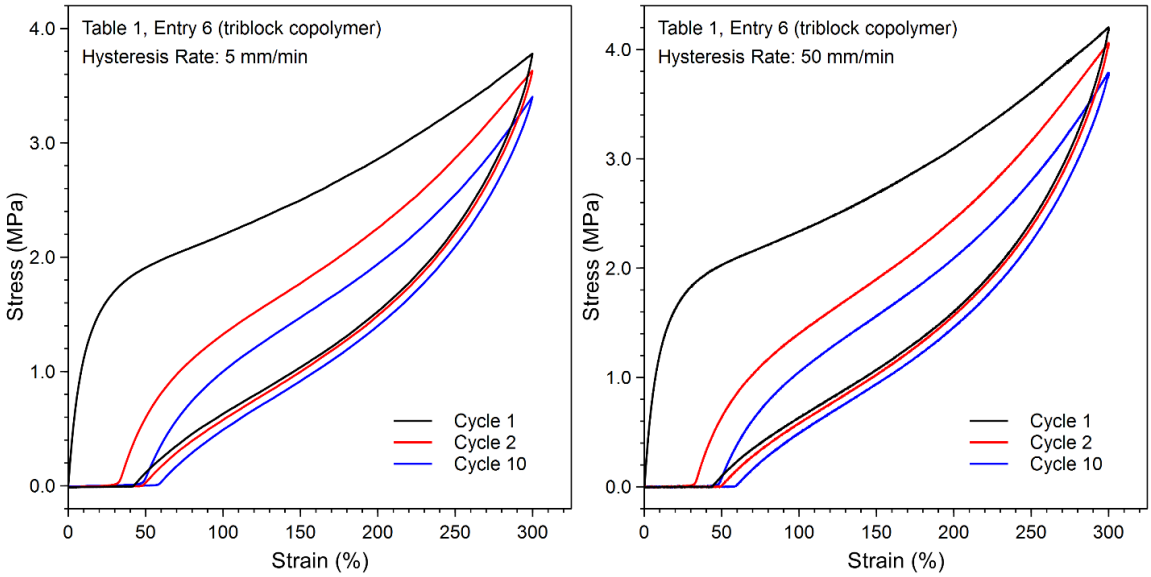

Figure 5.15.
Hysteresis Curves at Fast and Slow Elongation Rates for Triblock Copolymer

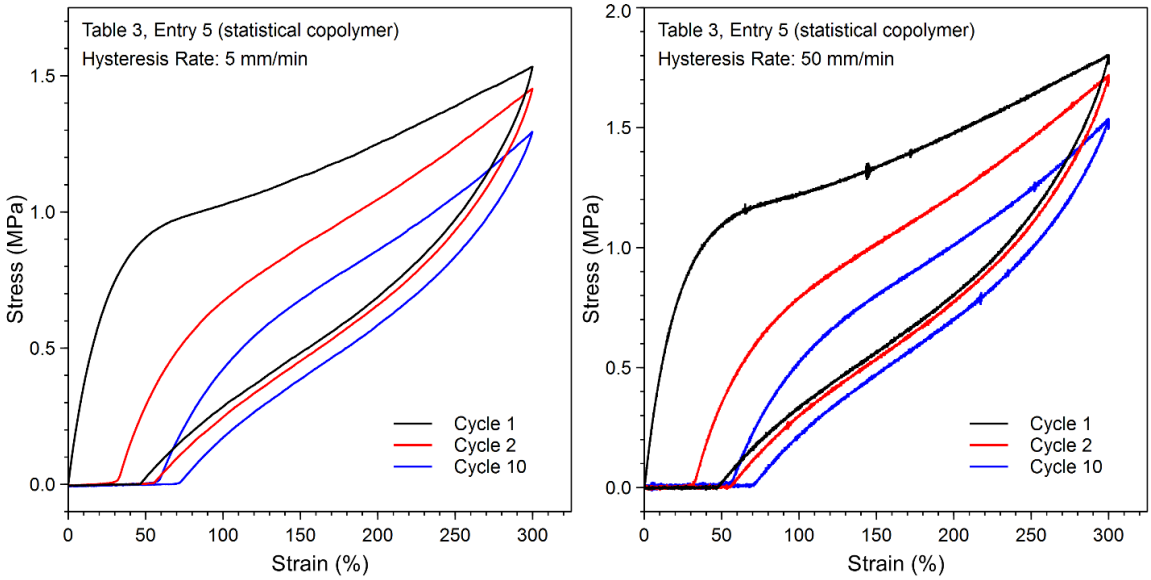

Figure 5.16.
Hysteresis Curves at Fast and Slow Elongation Rates for Statistical Copolymer

Determination of Branching in Polymer Samples

The number of branches per 1000 carbons (branches/1000C) for each final sample was determined using ^{1}H NMR as demonstrated by Rieger et. al.[44] using the following equation:

$$\text{total branching/1000C} = \frac{\frac{1}{3} I_{CH_3}}{\frac{\left(I_{CH_2} - \left(\frac{1}{3} I_{CH_3}\right)\right)}{2} + \frac{1}{3} I_{CH_3}} \times 1000$$

Select samples were analyzed by quantitative ^{13}C NMR in order to determine the specific branching distribution. Signals were assigned based on previous literature reports.[32,45] All signals were integrated, setting the total integral value to 1000. Branching distributions were calculated based on the follow simplified equations below. Branching numbers determined between ^{1}H NMR and ^{13}C NMR are in agreement.

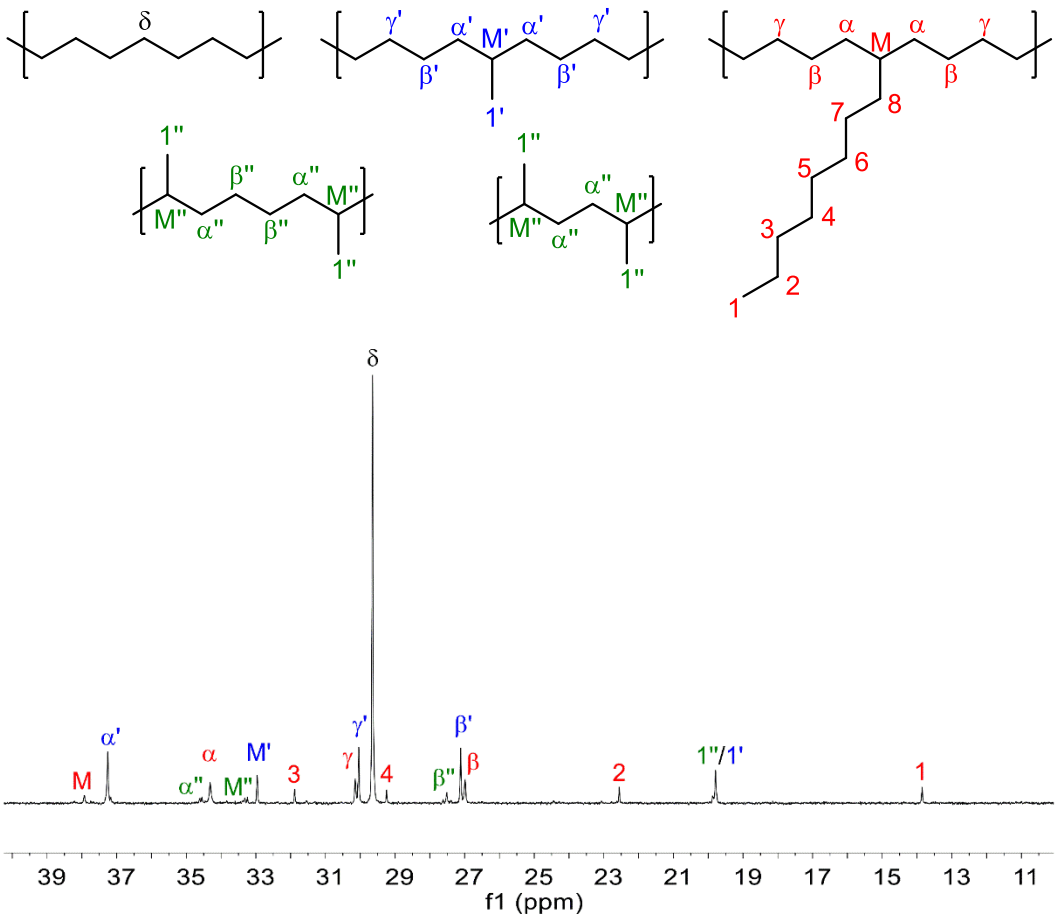

Figure 5.17.
^{13}C NMR Assignment of a Representative Copolymer (Table 1, Entry 6)

Table 5.21.
^{13}C NMR Assignment of a Representative Copolymer (Table 1, Entry 6)

Signal Number	Chem. Shift (ppm)	Assignment
1	13.33	1 ($1B_n$)
2	19.27	1' ($1B_1$)
3	19.33	1" ($1B_1$)
4	22.03	2 ($2B_n$)
5	26.46	β (βB_n)
6	26.59	β' (βB_1)
7	26.99	β" (1,6-β'B_n)
8	28.72	4 ($4B_n$)
9	29.12	δ, 5, 6 (σB_{1-n})
10	29.52	γ' (γB_1)
11	29.62	γ (γB_{2-n})
12	31.36	3 ($3B_n$)
13	32.44	M' (brB_1)
14	32.76	M" (1,4/6-brB_1)
15	33.79	α (αB_n)
16	34.06	α" (1,4/6-α'B_n)
17	36.73	α' (αB_1)
18	37.41	M (brB_{3-n})

Methyl = $I_{1'} + I_{1''}$

Hexyl and above = $I_2 + I_3 / 2$

Branches/1000C (via ^{13}C NMR)
Methyl = 50
Ethyl = 0
Propyl = 0
Butyl = 0
≥Hexyl = 12
Total = 62
Total (via ^{1}H NMR) = 70

Evidence of Strain-Induced Crystallization by DSC Analysis

Two tensile bars cut from the same film (Table 5.3, entry 4) were analyzed and compared by DSC. One bar was left unstrained, while the other bar was rapidly stretched

to ~300% strain and relaxed approximately 15 times over the course of 30 seconds. A piece of the center gauge from each bar was cut using a razor blade and subjected to DSC measurements. The first heating traces were compared since we were specifically interested in sample history (strained vs unstrained). The unstrained sample shows a single major melting endotherm at 43 °C, while the strained sample shows broadening, with two identifiable endotherms at 39 °C and 46 °C. These results suggest that the crystallinity of the material changes after strain-induced deformation, potentially due to strain-induced crystallization. Further studies need to be performed in order to better characterize this phenomenon.

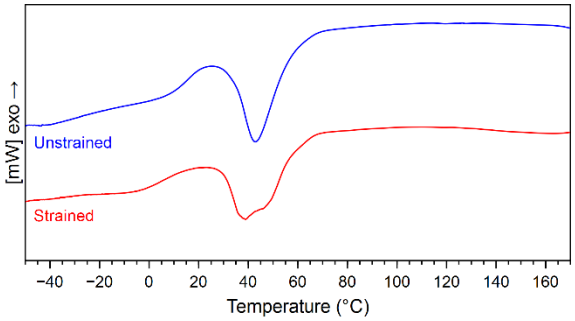

Figure 5.18.
DSC analysis of the first hear before and after extension of entry 4 (Table 5.3)

Table 5.22.
Thermal properties before and after extension

Sample	T_m **(°C)**	**ΔH (J/g)**
Table 5.3, entry 4 (unstrained)	43	22.1
Table 5.3, entry 4 (strained)	39, 46	21.8

5.5 References

(1) Craver, C.; Carraher, C.; Applied Polymer Science: 21st Century, Elsevier Science, Oxford, 2000.

(2) Akiba, M.; Hashim, A. S. Vulcanization and Crosslinking in Elastomers. *Prog. Polym. Sci.* **1997**, *22*, 475–521.

(3) Adhikari, B.; De, D.; Maiti, S. Reclamation and Recycling of Waste Rubber. *Prog. Polym. Sci.* **2000**, *25*, 909–948.

(4) Holden, G.; Kricheldorf, H. R.; Quirk, R. P. Thermoplastic Elastomers, 3rd ed.; Hanser Publishers: Munich, 2004.

(5) Brobny, J.G. Handbook of Thermoplastic Elastomers; William Andrews: New York, 2007.

(6) Koo, C. M.; Hillmyer, M. A.; Bates, F. S. Structure and Properties of Semicrystalline–Rubbery Multiblock Copolymers. *Macromolecules* **2006**, *39*, 667–677.

(7) Schneiderman, D. K.; Hill, E. M.; Martello, M. T.; Hillmyer, M. A. Poly(lactide)-*block*-poly(ε-caprolactone-co-ε-decalactone)-*block*-poly(lactide) Copolymer Elastomers. *Polym. Chem.* **2015**, *6*, 3641–3651.

(8) Ocando, C.; Fernández, R.; Tercjak, A.; Mondragon, I.; Eceiza, A. Nanostructured Thermoplastic Elastomers Based on SBS Triblock Copolymer Stiffening with Low Contents of Epoxy System. Morphological Behavior and Mechanical Properties. *Macromolecules* **2013**, *46*, 3444–3451.

(9) Hirao, A.; Goseki, R.; Ishizone, T. Advances in Living Anionic Polymerization: From Functional Monomers, Polymerization Systems, to Macromolecular Architectures. *Macromolecules* **2014**, *47*, 1883–1905.

(10) Morton, M.; McGrath, J. E.; Juliano, P. C. Structure–Property Relationships for Styrene–Diene Thermoplastic Elastomers. *J. Polym. Sci., Part C: Polym. Symp.* **1969**, *26*, 99–115.

(11) Weisz, P. B. Basic Choices and Constraints on Long-Term Energy Supplies. *Physics Today* **2004**, *57*, 47–52.

(12) Robertson, M. L; Hillmyer, M. A.; Mortamet, A. -C.; Ryan, A. J. Biorenewable Multiphase Polymers. *MRS Bull.* **2010**, *35*, 194–200.

(13) Takahara, I.; Saito, M.; Inaba, M.; Murata, K. Dehydration of Ethanol into Ethylene over Solid Acid Catalysts. *Catal. Lett.* **2005**, *105*, 249−252.

(14) Small, B. L.; Brookhart, M. Iron-Based Catalysts with Exceptionally High Activities and Selectivities for Oligomerization of Ethylene to Linear α-Olefins. *J. Am. Chem. Soc.* **1998**, *120*, 7143–7144.

(15) Thomas, R. M.; Keitz, B. K.; Champagne, T. M.; Grubbs, R. H. Highly Selective Ruthenium Catalysts for Ethenolysis. *J. Am. Chem. Soc.* **2011**, *133*, 7490−7496.

(16) Arriola, D. J.; Carnahan, E. M.; Hustad, P. D.; Kuhlman, R. L.; Wenzel, T. T. Catalytic Production of Olefin Block Copolymers via Chain Shuttling Polymerization. *Science* **2006**, *312*, 714−719.

(17) Ohtaki, H.; Deplace, F.; Vo, G. D.; LaPointe, A. M.; Shimizu, F.; Sugano, T.; Kramer, E. J.; Fredrickson, G. H.; Coates, G. W. Allyl-Terminated Polypropylene Macromonomers: A Route to Polyolefin Elastomers with Excellent Elastic Behavior. *Macromolecules* **2015**, *48*, 7489–7494.

(18) Ohtaki, H; Shimizu, F; Coates, G. W.; Fredrickson, G. H. Thermoplastic Elastomer Compositions with High Mechanical Strength and their Manufacture. *PCT Int. Appl.* WO 2013061974 A1 20130502, 2013.

(19) Coates, G. W.; Waymouth, R. M. Oscillating Stereocontrol: A Strategy for the Synthesis of Thermoplastic Elastomeric Polypropylene. *Science* **1995**, *267*, 217−219.

(20) Harney, M. B.; Zhang, Y.; Sita, L. R. Discrete, Multiblock Isotactic–Atactic Stereoblock Polypropene Microstructures of Differing Block Architectures through Programmable Stereomodulated Living Ziegler–Natta Polymerization. *Angew. Chem. Int. Ed.* **2006**, *45*, 2400−2404.

(21) Rose, J. M.; Deplace, F.; Lynd, N. A.; Wang, Z.; Hotta, A.; Lobkovsky, E. B.; Kramer, E. J.; Coates, G. W. C2-Symmetric Ni(II) α-Diimines Featuring Cumyl-Derived Ligands: Synthesis of Improved Elastomeric Regioblock Polypropylene. *Macromolecules* **2008**, *41*, 9548−9555.

(22) Subramanyam, U.; Sivaram, S. Synthesis and Characterization of Poly(higher-α-olefins) with a Nickel(α-diimine)/Methylaluminoxane Catalyst System: Effect of Chain Running on the Polymer Properties. *J. Polym. Sci., Part A: Polym. Chem.* **2007**, *45*, 191−210.

(23) Johnson, L. K.; Killian, C. M.; Brookhart, M. New Pd(II)- and Ni(II)-Based Catalysts for Polymerization of Ethylene and .alpha.-Olefins. *J. Am. Chem. Soc.* **1995**, *117*, 6414−6415.

(24) McCord, E. F.; McLain, S. J.; Nelson, L. T. J.; Ittel, S. D.; Tempel, D.; Killian, C. M.; Johnson, L. K.; Brookhart, M. 13C NMR Analysis of α-Olefin Enchainment in Poly(α-olefins) Produced with Nickel and Palladium α-Diimine Catalysts. *Macromolecules* **2007**, *40*, 410−420.

(25) Tempel, D. J.; Johnson, L. K.; Huff, L. R.; White, P. S.; Brookhart, M. Mechanistic Studies of Pd(II)-α-Diimine Catalyzed Olefin Polymerizations1. *J. Am. Chem. Soc.* **2000**, *122*, 6686−6700.

(26) Guo, L.; Dai, S.; Sui, X.; Chen, C. Palladium and Nickel Catalyzed Chain Walking Olefin Polymerization and Copolymerization. *ACS Catal.* **2016**, *6*, 428−441.

(27) Bomfim, J. A. S.; Dias, M. L.; Filgueiras, C. A. L.; Peruch, F.; Deffieux, A. The Effect of Polymerization Temperature on the Structure and Properties of Poly(1-hexene) and Poly(1-decene) Prepared with a Ni(II)–diimine Catalyst. *Catalysis Today* **2008**, *133-135*, 879−885.

(28) Hu, H.; Gao, H.; Chen, D.; Li, G.; Tan, Y.; Liang, G.; Zhu, F.; Wu, Q. Ligand-Directed Regioselectivity in Amine–Imine Nickel-Catalyzed 1-Hexene Polymerization. *ACS Catal.*, **2015**, *5*, 122–128.

(29) Dai, S.; Sui, X.; Chen, C. Synthesis of High Molecular Weight Polyethylene Using Iminopyridyl Nickel Catalysts. *Chem. Commun.* **2016**, *52*, 9113–9116.

(30) Killian, C. M.; Johnson, L. K.; Brookhart, M. Living Polymerization of α-Olefins Using Ni(II)-α-Diimine Catalysts. Synthesis of New Block Polymers Based on α-Olefins. *J. Am. Chem. Soc.* **1996**, *118*, 11664−11665.

(31) Leone, G.; Mauri, M.; Bertini, F.; Canetti, M.; Piovani, D.; Ricci, G. Ni(II) α-Diimine-Catalyzed α-Olefins Polymerization: Thermoplastic Elastomers of Block Copolymers. *Macromolecules* **2015**, *48*, 1304−1312.

(32) Vaidya, T.; Klimovica, K.; LaPointe, A. M.; Keresztes, I.; Lobkovsky, E. B.; Daugulis, O.; Coates, G. W. Secondary Alkene Insertion and Precision Chain-Walking: A New Route to Semicrystalline "Polyethylene" from α-Olefins by Combining Two Rare Catalytic Events. *J. Am. Chem. Soc.* **2014**, *136*, 7213−7216.

(33) Zhang, D.; Nadres, E. T.; Brookhart, M.; Daugulis, O. Synthesis of Highly Branched Polyethylene Using "Sandwich" (8-p-Tolyl naphthyl α-diimine)nickel(II) Catalysts. *Organometallics* **2013**, *32*, 5136−5143.

(34) Busico, V.; Cipullo, R.; Cutillo, F.; Friederichs, N.; Ronca, S.; Wang, B. Improving the Performance of Methylalumoxane: A Facile and Efficient Method to Trap "Free" Trimethylaluminum. *J. Am. Chem. Soc.* **2003**, *125*, 12402−12403.

(35) Macchioni, A. Ion Pairing in Transition-Metal Organometallic Chemistry. *Chem. Rev.* **2005**, *105*, 2039–2074.

(36) Ayoub, G.; Zaïri, F.; Fréderix, C.; Gloaguen, J. M.; Naït-Abdelaziz, M.; Seguela, R.; Lefebvre, J. M. Effects of Crystal Content on the Mechanical Behaviour of Polyethylene under Finite Strain: Experiments and Constitutive Modelling. *Int. J. Plast.* **2011**, *27*, 492−511.

(37) Toki, S.; Fujimaki, T.; Okuyama, M. Strain-induced Crystallization of Natural Rubber as Detected Real-time by Wide-angle X-ray Diffraction Technique. *Polymer J.* **2000**, *41*, 5423−5429.

(38) Hotta, A.; Cochran, E.; Ruokolainen, J.; Khanna, V.; Fredrickson, G. H.; Kramer, E. J.; Shin, Y. W.; Shimizu, F.; Cherian, A. E.; Hustad, P. D.; Rose, J. M.; Coates, G. W. Semicrystalline Thermoplastic Elastomeric Polyolefins: Advances through Catalyst Development and Macromolecular Design. *Proc. Natl. Acad. Sci. USA* **2006**, *103*, 15327−15332.

(39) Bates, F. S.; Fredrickson., Glenn H.; Hucul, D.; Hahn, S. F. PCHE-based Pentablock Copolymers: Evolution of a New Plastic. *AlChE J.* **2001**, *47*, 762−765.

(40) Poon, B. C.; Dias. P.; Ansems, P.; Chum, S. P.; Hiltner, A.; Baer, E. Structure and Deformation of an Elastomeric Propylene−Ethylene Copolymer. *J. Appl. Polym. Sci.* **2007**, *104*, 489−499.

(41) Wang, H. P.; Khariwala, D. U.; Cheung, W.; Chum, S. P.; Hiltner, A.; Baer, E. Characterization of Some New Olefinic Block Copolymers. *Macromolecules* **2007**, *40*, 2852−2863.

(42) Wang, H. P.; Chum, S. P.; Hiltner, A.; Baer, E. Comparing Elastomeric Behavior of Block and Random Ethylene−Octene Copolymers. *J. Appl. Polym. Sci.* **2009**, *113*, 3236−3244.

(43) Luo, X.; Xie, S.; Liu, J.; Hu, H.; Jiang, J.; Huang, W.; Gao, H.; Zhou, D.; Lü, Z.; Yan, D. The Relationship Between the Degree of Branching and Glass Transition Temperature of Branched Polyethylene: Experiment and Simulation. *Polym. Chem.* **2014**, *5*, 1305−1312.

(44) Meinhard D.; Wegner, M.; Kipiani, G.; Hearley, A.; Reuter,P.; Fischer, S.; Marti, O.; Rieger, B. New Nickel (II) Diimine Complexes and the Control of Polyethylene Microstructure by Catalyst Design. *J. Am. Chem. Soc.* **2007**, 129, 9182−9191.

(45) Azoulay, J.D.; Bazan, G.C.; Galland, G.B. Microstructural Characterization of Poly(1-hexene) Obtained Using a Nickel α-Keto- β-diimine Initiator. *Macromolecules* **2010**, *43*, 2794-2800.

Bibliography

Adhikari, B.; De, D.; Maiti, S. Reclamation and Recycling of Waste Rubber. *Prog. Polym. Sci.* **2000**, *25*, 909–948.

Akiba, M.; Hashim, A. S. Vulcanization and Crosslinking in Elastomers. *Prog. Polym. Sci.* **1997**, *22*, 475–521.

Akindoyo, J. O.; Beg, M. D. H.; Ghazali, S.; Islam, M. R.; Jeyaratnam, N.; Yuvaraj, A. R. Polyurethane Types, Synthesis and Applications-a Review. *RSC Adv.* **2016**, *6*, 114453–114482.

Albertsson, A.-C.; Hakkarainen, M. Designed to Degrade. *Science* **2017**, *358*, 872–873.

Albertsson, A.-C.; Varma, I. K. Recent Developments in Ring Opening Polymerization of Lactones for Biomedical Applications. *Biomacromolecules* **2003**, *4*, 1466–1486.

Anastas, P.; Eghbali, N. Green Chemistry: Principles and Practice. *Chem. Soc. Rev.* **2010**, *39*, 301–312.

Anderson, K. S.; Hillmyer, M. A. The Influence of Block Copolymer Microstructure on the Toughness of Compatibilized Polylactide/Polyethylene Blends. *Polymer* **2004**, *45*, 8809–8823.

Anderson, K. S.; Schreck, K. M.; Hillmyer, M. A. Toughening Polylactide. *Polym. Rev.* **2008**, *48*, 85–108.

Andreeßen, B.; Steinbüchel, A. Biosynthesis and Biodegradation of 3-Hydroxypropionate-Containing Polyesters. *Appl. Environ. Microbiol.* **2010**, *76*, 4919–4925.

Andronova, N.; Albertsson, A.-C. Resilient Bioresorbable Copolymers Based on Trimethylene Carbonate, L-Lactide, and 1,5-Dioxepan-2-One. *Biomacromolecules* **2006**, *7*, 1489–1495.

Appel, W. P. J.; Portale, G.; Wisse, E.; Dankers, P. Y. W.; Meijer, E. W. Aggregation of Ureido-Pyrimidinone Supramolecular Thermoplastic Elastomers into Nanofibers: A Kinetic Analysis. *Macromolecules* **2011**, *44*, 6776–6784.

Arpe, H.-J. *Industrial Organic Chemistry*; 5th ed.; Weinheim, Germany, 2010.

Arriola, D. J.; Carnahan, E. M.; Hustad, P. D.; Kuhlman, R. L.; Wenzel, T. T. Catalytic Production of Olefin Block Copolymers via Chain Shuttling Polymerization. *Science* **2006**, *312*, 714−719.

Ayoub, G.; Zaïri, F.; Fréderix, C.; Gloaguen, J. M.; Naït-Abdelaziz, M.; Seguela, R.; Lefebvre, J. M. Effects of Crystal Content on the Mechanical Behaviour of Polyethylene under Finite Strain: Experiments and Constitutive Modelling. *Int. J. Plast.* **2011**, *27*, 492−511.

Azoulay, J.D.; Bazan, G.C.; Galland, G.B. Microstructural Characterization of Poly(1-hexene) Obtained Using a Nickel α-Keto- β-diimine Initiator. *Macromolecules* **2010**, *43*, 2794-2800.

Baeurle, S. a.; Hotta, A.; Gusev, A. a. A New Semi-Phenomenological Approach to Predict the Stress Relaxation Behavior of Thermoplastic Elastomers. *Polymer* **2005**, *46*, 4344–4354.

Baimark, Y.; Molloy, R. Synthesis and Characterization of Poly (L-Lactide-Co-ε-

Caprolactone) Copolymers: Effects of Stannous Octoate Initiator and Diethylene Glycol Coinitiator Concentrations. *Sci. Asia* **2004**, *30*, 327–334.

Bao, J.; Chang, X.; Xie, Q.; Yu, C.; Shan, G.; Bao, Y.; Pan, P. Preferential Formation of β-Form Crystals and Temperature-Dependent Polymorphic Structure in Supramolecular Poly(l-Lactic Acid) Bonded by Multiple Hydrogen Bonds. *Macromolecules* **2017**, *50*, 8619–8630.

Bates, F. S.; Fredrickson, G. H. Block Copolymer Thermodynamics: Theory and Experiment. *Annu. Rev. Phys. Chem.* **1990**, *41*, 525–557.

Bates, F. S.; Fredrickson., Glenn H.; Hucul, D.; Hahn, S. F. PCHE-based Pentablock Copolymers: Evolution of a New Plastic. *AlChE J.* **2001**, *47*, 762−765.

Bates, F. S.; Rosedale, J. H.; Fredrickson, G. H. Fluctuation Effects in a Symmetric Diblock Copolymer near the Order-Disorder Transition. *J. Chem. Phys.* **1990**, *92*, 6255–6270.

Bechtold, K.; Hillmyer, M. A.; Tolman, W. B. Perfectly Alternating Copolymer of Lactic Acid and Ethylene Oxide as a Plasticizing Agent for Polylactide. *Macromolecules*, **2001**, *34*, 8641–8648.

Beckingham, B. S.; Sanoja, G. E.; Lynd, N. a. Simple and Accurate Determination of Reactivity Ratios Using a Nonterminal Model of Chain Copolymerization. *Macromolecules* **2015**, *48*, 6922–6930.

Beijer, F. H.; Sijbesma, R. P.; Kooijman, H.; Spek, A. L.; Meijer, E. W. Strong Dimerization of Ureidopyrimidones via Quadruple Hydrogen Bonding. *J. Am. Chem. Soc.* **1998**, *120*, 6761–6769.

Bergström, J. S.; Boyce, M. C. Constitutive Modeling of the Large Strain Time-Dependent Behavior of Elastomers. *J. Mech. Phys. Solids* **1998**, *46*, 931–954.

Bero, M.; Kasperczyk, J.; Jedlinski, Z. J. Coordination Polymerization of Lactides, 1. Structure Determination of Obtained Polymers. *Die Makromol. Chemie* **1990**, *191*, 2287–2296.

Bertrand, A.; Lortie, F.; Bernard, J. Routes to Hydrogen Bonding Chain-End Functionalized Polymers. *Macromol. Rapid Commun.* **2012**, *33*, 2062–2091.

Bomfim, J. A. S.; Dias, M. L.; Filgueiras, C. A. L.; Peruch, F.; Deffieux, A. The Effect of Polymerization Temperature on the Structure and Properties of Poly(1-hexene) and Poly(1-decene) Prepared with a Ni(II)–diimine Catalyst. *Catalysis Today* **2008**, *133-135*, 879−885.

Bosman, A. W.; Sijbesma, R. P.; Meijer, E. W. Supramolecular Polymers at Work. *Mater. Today* **2004**, *7*, 34–39.

Botterhuis, N. E.; van Beek, D. J. M.; van Gemert, G. M. L.; Bosman, A. W.; Sijbesma, R. P. Self-Assembly and Morphology of Polydimethylsiloxane Supramolecular Thermoplastic Elastomers. *J. Polym. Sci. Part A Polym. Chem.* **2008**, *46*, 3877–3885.

Bouyahyi, M.; Pepels, M. P. F.; Heise, A.; Duchateau, R. ω-Pentandecalactone Polymerization and ω-Pentadecalactone/ε-Caprolactone Copolymerization Reactions Using Organic Catalysts. *Macromolecules* **2012**, *45*, 3356–3366.

Breteler, M. R. T.; Zhong, Z.; Dijkstra, P. J.; Palmans, A. R. A.; Peeters, J.; Feijen, J. Ring-Opening Polymerization of Substituted Ɛ-Caprolactones with a Chiral (Salen) AlOiPr Complex. *J. Polym. Sci. Part A Polym. Chem.* **2007**, *45*, 429–436.

Breulmann, M.; Künkel, A.; Philipp, S.; Reimer, V.; Siegenthaler, K. O.; Skupin, G.; Yamamoto, M. Polymers, Biodegradable. *Ullmann's Encycl. Ind. Chem.* **2009**, 266.

Brobny, J.G. Handbook of Thermoplastic Elastomers; William Andrews: New York, 2007.

Brunsveld, L.; Folmer, B. J. B.; Meijer, E. W.; Sijbesma, R. P. Supramolecular Polymers. *Chem. Rev.* **2001**, *101*, 4071–4098.

Brutman, J. P.; De Hoe, G. X.; Schneiderman, D. K.; Le, T. N.; Hillmyer, M. A. Renewable, Degradable, and Chemically Recyclable Cross-Linked Elastomers. *Ind. Eng. Chem. Res.* **2016**, *55*, 11097–11106.

Burns, A. B.; Register, R. A. Mechanical Properties of Star Block Polymer Thermoplastic Elastomers with Glassy and Crystalline End Blocks. *Macromolecules* **2016**, *49*, 9521–9530.

Burns, A. B.; Register, R. A. Mechanical Properties of Star Block Polymer Thermoplastic Elastomers with Glassy and Crystalline End Blocks. *Macromolecules* **2016**, *49*, 9521–9530.

Busico, V.; Cipullo, R.; Cutillo, F.; Friederichs, N.; Ronca, S.; Wang, B. Improving the Performance of Methylalumoxane: A Facile and Efficient Method to Trap "Free" Trimethylaluminum. *J. Am. Chem. Soc.* **2003**, *125*, 12402−12403.

Chabot, F.; Vert, M.; Chapelle, S.; Granger, P. Configurational Structures of Lactic Acid Stereocopolymers as Determined by 13C-{1H} N.M.R. *Polymer* **1983**, *24*, 53–59.

Chang, R.; Huang, Y.; Shan, G.; Bao, Y.; Yun, X.; Dong, T.; Pan, P. Alternating Poly(Lactic Acid)/Poly(Ethylene-Co-Butylene) Supramolecular Multiblock Copolymers with Tunable Shape Memory and Self-Healing Properties. *Polym. Chem.* **2015**, *6*, 5899–5910.

Chang, R.; Shan, G.; Bao, Y.; Pan, P. Enhancement of Crystallizability and Control of Mechanical and Shape-Memory Properties for Amorphous Enantiopure Supramolecular Copolymers via Stereocomplexation. *Macromolecules* **2015**, *48*, 7872–7881.

Chen, M.; Zhang, Y.; Zhou, Y.; Zhang, Y.; Lang, M.; Ye, Z.; Tan, W. S. Pendant Small Functional Groups on Poly(ε-Caprolactone) Substrate Modulate Adhesion, Proliferation and Differentiation of Human Mesenchymal Stem Cells. *Colloids Surfaces B Biointerfaces* **2015**, *134*, 322–331.

Chen, Y.; Zhang, H.; Fang, X.; Lin, Y.; Xu, Y.; Weng, W. Mechanical Activation of Mechanophore Enhanced by Strong Hydrogen Bonding Interactions. *ACS Macro Lett.* **2014**, *3*, 141–145.

Chen, Y.-D. M.; Cohen, R. E. The Influence of Molecular Weight on the Large Deformation Behavior of SBS Triblock Copolymer Elastomers. *J. Appl. Polym. Sci.* **1977**, *21*, 629–643.

Chung, S. H.; Stevens, J. R. Time-dependent Correlation and the Evaluation of the Stretched Exponential or Kohlrausch–Williams–Watts Function. *Am. J. Phys.* **1991**, *59*, 1024–1030.

Coates, G. W.; Waymouth, R. M. Oscillating Stereocontrol: A Strategy for the Synthesis of Thermoplastic Elastomeric Polypropylene. *Science* **1995**, *267*, 217−219.

Cohn, D.; Hotovely Salomon, A. Designing Biodegradable Multiblock PCL/PLA Thermoplastic Elastomers. *Biomaterials* **2005**, *26*, 2297–2305.

Craver, C.; Carraher, C.; Applied Polymer Science: 21st Century, Elsevier Science, Oxford, 2000.

Cunningham, R. E.; Auerbach, M.; Floyd, W. J. Preparation and Stress–strain Properties of SBS and SIS Block Polymers Made with Dilithium Initiators. *J. Appl. Polym. Sci.* **1972**, *16*, 163–173.

Dai, S.; Sui, X.; Chen, C. Synthesis of High Molecular Weight Polyethylene Using Iminopyridyl Nickel Catalysts. *Chem. Commun.* **2016**, *52*, 9113–9116.

Dainton, F. S.; Ivin, K. J. Reversibility of the Propagation Reaction in Polymerization Processes and Its Manifestation in the Phenomenon of a 'Ceiling Temperature.' *Nature* **1948**, *162*, 705–707.

Dale, J. Conformational Aspects of Many-Membered Rings. *Angew. Chemie Int. Ed. English* **1966**, *5*, 1000–1021.

Dávila, J. A.; Rosenberg, M.; Cardona, C. A. Techno-Economic and Environmental Assessment of p-Cymene and Pectin Production from Orange Peel. *Waste and Biomass Valorization* **2015**, *6*, 253–261.

de Geus, M.; van der Meulen, I.; Goderis, B.; van Hecke, K.; Dorschu, M.; van der Werff, H.; Koning, C. E.; Heise, A. Performance Polymers from Renewable Monomers: High Molecular Weight Poly(Pentadecalactone) for Fiber Applications. *Polym. Chem.* **2010**, *1*, 525–533.

De Hoe, G. X.; Zumstein, M. T.; Tiegs, B. J.; Brutman, J. P.; McNeill, K.; Sander, M.; Coates, G. W.; Hillmyer, M. A. Sustainable Polyester Elastomers from Lactones: Synthesis, Properties, and Enzymatic Hydrolyzability. *J. Am. Chem. Soc.* **2018**, *140*, 963–973.

Dechy-Cabaret, O.; Martin-Vaca, B.; Bourissou, D. Controlled Ring-Opening Polymerization of Lactide and Glycolide. *Chem. Rev.* **2004**, *104*, 6147–6175.

Delgado, P. A.; Hillmyer, M. A. Combining Block Copolymers and Hydrogen Bonding for Poly(Lactide) Toughening. *RSC Adv.* **2014**, *4*, 13266–13273.

Dimopoulos, A.; Wietor, J. L.; Wübbenhorst, M.; Napolitano, S.; Van Benthem, R. A. T. M.; De With, G.; Sijbesma, R. P. Enhanced Mechanical Relaxation below the Glass Transition Temperature in Partially Supramolecular Networks. *Macromolecules* **2010**, *43*, 8664–8669.

Dong, C.; Qiu, K.; Gu, Z.; Feng, X. Synthesis of Poly(D,L-Lactic Acid-Alt-Glycolic Acid) from D,L-3-Methylglycolide. *J. Polym. Sci. Part A Polym. Chem.* **2000**, *38*, 4179–4184.

Dorgan, J. R.; Williams, J. S.; Lewis, D. N. Melt Rheology of Poly(Lactic Acid): Entanglement and Chain Architecture Effects. *J. Rheol.* **1999**, *43*, 1141.

Dove, A. P. Organic Catalysis for Ring-Opening Polymerization. *ACS Macro Lett.* **2012**, *1*, 1409–1412.

Dubé, M. A.; Salehpour, S. Applying the Principles of Green Chemistry to Polymer Production Technology. *Macromol. React. Eng.* **2014**, *8*, 7–28.

Duda, A.; Kowalski, A.; Libiszowski, J.; Penczek, S. Thermodynamic and Kinetic Polymerizability of Cyclic Esters. *Macromol. Symp.* **2005**, *224*, 71–84.

Duda, A.; Kowalski, A.; Penczek, S.; Uyama, H.; Kobayashi, S. Kinetics of the Ring-Opening Polymerization of 6-, 7-, 9-, 12-, 13-, 16-, and 17-Membered Lactones. Comparison of Chemical and Enzymatic Polymerizations. *Macromolecules* **2002**, *35*, 4266–4270.

Duda, A.; Penczek, S. Thermodynamics, Kinetics, and Mechanisms of Cyclic Esters Polymerization. In *Polymers from Renewable Resources*; Scholz, C.; Gross, R. A., Eds.; ACS Symposium Series; American Chemical Society: Washington, DC, 2001; Vol. 764, pp. 160–198.

Eckhard, H. BASF AG. *Tert*-butylesters of substituted 3-hydroxyproponoic acid. DE Application No. 3925256A1, January 31, 1991.

Feldman, K. E.; Kade, M. J.; Meijer, E. W.; Hawker, C. J.; Kramer, E. J. Model Transient Networks from Strongly Hydrogen-Bonded Polymers. *Macromolecules* **2009**, *42*, 9072–9081.

Fetters, L. J.; Lohse, D. J.; Milner, S. T.; Graessley, W. W. Packing Length Influence in Linear Polymer Melts on the Entanglement, Critical, and Reptation Molecular Weights. *Macromolecules* **1999**, *32*, 6847–6851.

Fiege, H. Cresols and Xylenols. In *Ullmann's Encyclopedia of Industrial Chemistry*; Wiley-VCH Verlag GmbH & Co. KGaA: Weinheim, Germany, 2000; pp. 419–461.

Fisher, E. W.; Sterzel, H. J.; Wegner, G. *Kolloid Z. Z. Polym.* **1973**, *251*, 980–990.

Folmer, B. J. B.; Sijbesma, R. P.; Versteegen, R. M.; Van Der Rijt, J. A. J.; Meijer, E. W. Supramolecular Polymer Materials: Chain Extension of Telechelic Polymers Using a Reactive Hydrogen-Bonding Synthon. *Adv. Mater.* **2000**, *12*, 874–878.

Fox, T. G. Influence of Diluent and of Copolymer Composition on the Glass Temperature of a Polymer System. *Bull. Am. Phys. Soc.*, **1956**, *1*, 123.

Frick, E. M.; Zalusky, A. S.; Hillmyer, M. A. Characterization of Polylactide-b-Polyisoprene-b-Polylactide Thermoplastic Elastomers. *Biomacromolecules* **2003**, *4*, 216–223.

Fukumori, K.; Kurauchi, T.; Kamigaito, O. Pulsed NMR Study of Elastomeric Block Copolymer under Deformation. *J. Appl. Polym. Sci.* **1989**, *38*, 1313–1334.

Gallezot, P. Catalytic Routes from Renewables to Fine Chemicals. *Catal. Today* **2007**, *121*, 76–91.

Gallezot, P. Conversion of Biomass to Selected Chemical Products. *Chem. Soc. Rev.* **2012**, *41*, 1538–1558.

Garcia, J. M.; Robertson, M. L. The Future of Plastics Recycling. *Science* **2017**, *358*, 870–872.

Gardella, L.; Cavallo, D.; Colonna, S.; Fina, A.; Monticelli, O. Novel Poly(l-Lactide)/Poly(d-Lactide)/Poly(Tetrahydrofuran) Multiblock Copolymers with a Controlled Architecture: Synthesis and Characterization. *J. Polym. Sci. Part A Polym. Chem.* **2014**, *52*, 3269–3282.

Gent, A. N. Relaxation Processes in Vulcanized Rubber. *J. Appl. Polym. Sci.* **1962**, *VI*, 442–448.

Gilding, D. K.; Reed, A. M. Biodegradable Polymers for Use in Surgery-Polyglycolic/Poly(Lactic Acid) Homo- and Copolymers: 1. *Polymer* **1979**, *20*, 1459–1464.

Glasebrook, A. L. Dehydrogenation of Sulfur-Contaminated Monocyclic Terpenes. US Patent 2857439A, 1958.

Graglia, M.; Kanna, N.; Esposito, D. Lignin Refinery: Towards the Preparation of Renewable Aromatic Building Blocks. *ChemBioEng Rev.* **2015**, *2*, 377–392.

Guan, Z.; Roland, J. T.; Bai, J. Z.; Ma, S. X.; McIntire, T. M.; Nguyen, M. Modular Domain Structure: A Biomimetic Strategy for Advanced Polymeric Materials. *J. Am. Chem. Soc.* **2004**, *126*, 2058–2065.

Guo, L.; Dai, S.; Sui, X.; Chen, C. Palladium and Nickel Catalyzed Chain Walking Olefin Polymerization and Copolymerization. *ACS Catal.* **2016**, *6*, 428−441.

Guth, E. Theory of Filler Reinforcement. *J. Appl. Phys.* **1945**, *16*, 20–25.

Gwo-Wen, W.; Ging-Ho, H.; Jin-Sheng, Y. Stress Relaxation Behavior of Low Epoxidized Poly(Styrene-b-Butadiene-b-Styrene) Triblock Copolymers. *Mater. Chem. Phys.* **1994**, *39*, 29–33.

Han, C. D.; Baek, D. M.; Kim, J. K.; Ogawa, T.; Sakamoto, N.; Hashimoto, T. Effect of Volume Fraction on the Order-Disorder Transition in Low Molecular Weight Polystyrene-Block-Polyisoprene Copolymers. 1. Order-Disorder Transition Temperature Determined by Rheological Measurements. *Macromolecules* **1995**, *28*, 5043–5062.

Handbook of Elastomers; Bhowmick, A. K.; Stephens, H. L., Eds.; 2nd ed.; Mercel Dekker, Inc.: New York, 2001.

Handbook of Ring-Opening Polymerization; Dubois, P.; Coulembier, O.; Raquez, J.-M., Eds.; Wiley-VCH Verlag GmbH & Co. KGaA: Weinheim, Germany, 2009.

Harney, M. B.; Zhang, Y.; Sita, L. R. Discrete, Multiblock Isotactic–Atactic Stereoblock Polypropene Microstructures of Differing Block Architectures through Programmable Stereomodulated Living Ziegler–Natta Polymerization. *Angew. Chem. Int. Ed.* **2006**, *45*, 2400−2404.

Hayashi, M.; Noro, A.; Matsushita, Y. Highly Extensible Supramolecular Elastomers with Large Stress Generation Capability Originating from Multiple Hydrogen Bonds on the Long Soft Network Strands. *Macromol. Rapid Commun.* **2016**, *37*, 678–684.

Hentschel, J.; Kushner, A. M.; Ziller, J.; Guan, Z. Self-Healing Supramolecular Block Copolymers. *Angew. Chemie* **2012**, *124*, 10713–10717.

Hillmyer, M. A.; Tolman, W. B. Aliphatic Polyester Block Polymers: Renewable, Degradable, and Sustainable. *Acc. Chem. Res.* **2014**, *47*, 2390–2396.

Hirao, A.; Goseki, R.; Ishizone, T. Advances in Living Anionic Polymerization: From Functional Monomers, Polymerization Systems, to Macromolecular Architectures. *Macromolecules* **2014**, *47*, 1883–1905.

Ho, C. H.; Jang, G. W.; Lee, Y. Der. Crystallization of Poly(l-Lactide-Dimethyl Siloxane-l-Lactide) Triblock Copolymers and Its Effect on Morphology of Microphase Separation. *Polymer* **2010**, *51*, 1639–1647.

Holden, G.; Bishop, E. T.; Legge, N. R. Thermoplastic Elastomers. *J. Polym. Sci. Part C Polym. Symp.* **1969**, *26*, 37–57.

Honeker, C. C.; Thomas, E. L. Impact of Morphological Orientation in Determining Mechanical Properties in Triblock Copolymer Systems. *Chem. Mater.* **1996**, *8*, 1702–1714.

Hong, M.; Chen, E. Y.-X. Chemically Recyclable Polymers: A Circular Economy Approach to Sustainability. *Green Chem.* **2017**, *19*, 3692–3706.

Hori, Y.; Hongo, H.; Hagiwara, T. Ring-Opening Copolymerization of (R)-β-Butyrolactone with Macrolide: A New Series of Poly(Hydroxyalkanoate)S. *Macromolecules* **1999**, *32*, 3537–3539.

Hotta, A.; Clarke, S. M.; Terentjev, E. M. Stress Relaxation in Transient Networks of Symmetric Triblock Styrene−Isoprene−Styrene Copolymer. *Macromolecules* **2002**, *35*, 271–277.

Hotta, A.; Cochran, E.; Ruokolainen, J.; Khanna, V.; Fredrickson, G. H.; Kramer, E. J.; Shin, Y. W.; Shimizu, F.; Cherian, A. E.; Hustad, P. D.; Rose, J. M.; Coates, G. W. Semicrystalline Thermoplastic Elastomeric Polyolefins: Advances through Catalyst Development and Macromolecular Design. *Proc. Natl. Acad. Sci. USA* **2006**, *103*, 15327−15332.

Hsiue, G. -H; Wu, G. -W. The Stress Relaxation of the Thermoplastic Elastomer (SBS Type). *J. Appl. Polym. Sci.* **1980**, *25*, 2119–2121.

Hsiue, G.; Chen, D.; Liew, Y.-K. Stress Relaxation and the Domain Structure of Thermoplastic Elastomer. *J. Appl. Polym. Sci.* **1988**, *35*, 995–1002.

Hu, H.; Gao, H.; Chen, D.; Li, G.; Tan, Y.; Liang, G.; Zhu, F.; Wu, Q. Ligand-Directed Regioselectivity in Amine–Imine Nickel-Catalyzed 1-Hexene Polymerization. *ACS Catal.*, **2015**, *5*, 122–128.

Huang, Y.; Chang, R.; Han, L.; Shan, G.; Bao, Y.; Pan, P. ABA-Type Thermoplastic Elastomers Composed of Poly(ε-Caprolactone-co-δ-Valerolactone) Soft Midblock and Polymorphic Poly(Lactic Acid) Hard End Blocks. *ACS Sustain. Chem. Eng.* **2016**, *4*, 121–128.

Hutin, M.; Burakowska-Meise, E.; Appel, W. P. J.; Dankers, P. Y. W.; Meijer, E. W. From Molecular Structure to Macromolecular Organization: Keys to Design Supramolecular Biomaterials. *Macromolecules* **2013**, *46*, 8528–8537.

In't Veld, P. J. A.; Velner, E. M.; Van De Witte, P.; Hamhuis, J.; Dijkstra, P. J.; Feijen, J. Melt Block Copolymerization of ε-Caprolactone and L-Lactide. *J. Polym. Sci. Part A Polym. Chem.* **1997**, *35*, 219–226.

Jamshidi, K.; Hyon, S.-H.; Ikada, Y. Thermal Characterization of Polylactides. *Polymer* **1988**, *29*, 2229–2234.

Jing, Z.; Shi, X.; Zhang, G. Synthesis and Properties of Biodegradable Supramolecular Polymers Based on Polylactide- Block -Poly(δ -Valerolactone)- Block -Polylactide Triblock Copolymers. *Polym. Int.* **2017**, *66*, 1487–1497.

Jing, Z.; Shi, X.; Zhang, G.; Gu, J. Synthesis and Properties of Poly(Lactide)/Poly(ε-Caprolactone) Multiblock Supramolecular Polymers Bonded by the Self-Complementary Quadruple Hydrogen Bonding. *Polymer* **2017**, *121*, 124–136.

Johnson, L. K.; Killian, C. M.; Brookhart, M. New Pd(II)- and Ni(II)-Based Catalysts for Polymerization of Ethylene and .alpha.-Olefins. *J. Am. Chem. Soc.* **1995**, *117*, 6414−6415.

Kajita, T.; Noro, A.; Matsushita, Y. Design and Properties of Supramolecular Elastomers. *Polymer* **2017**, *128*, 297–310.

Kale, G.; Kijchavengkul, T.; Auras, R.; Rubino, M.; Selke, S. E.; Singh, S. P. Compostability of Bioplastic Packaging Materials: An Overview. *Macromol. Biosci.* **2007**, *7*, 255–277.

Kambour, R. P. A Review of Crazing and Fracture in Thermoplastics. *J. Polym. Sci. Macromol. Rev.* **1973**, *7*, 1–154.

Kan, H.-C.; Ferry, J. D.; Fetters, L. J. Rubber Networks Containing Unattached Macromolecules. 5. Stress Relaxation in Styrene-Butadiene-Styrene Block Copolymer with Unattached Linear and Star Polybutadienes. *Macromolecules* **1980**, *13*, 1571–1577.

Kautz, H.; van Beek, D. J. M.; Sijbesma, R. P.; Meijer, E. W. Cooperative End-to-End and Lateral Hydrogen-Bonding Motifs in Supramolecular Thermoplastic Elastomers. *Macromolecules* **2006**, *39*, 4265–4267.

Keller, T. H.; Neeland, E. G.; Rettig, S.; Trotter, J.; Weiler, L. Conformational Analysis of 14-Membered Macrolides Using x-Ray Crystallography and Molecular Mechanics Calculations. *J. Am. Chem. Soc.* **1988**, *110*, 7858–7868.

Kiesewetter, M. K.; Shin, E. J.; Hedrick, J. L.; Waymouth, R. M. Organocatalysis: Opportunities and Challenges for Polymer Synthesis. *Macromolecules* **2010**, *43*, 2093–2107.

Killian, C. M.; Johnson, L. K.; Brookhart, M. Living Polymerization of α-Olefins Using Ni(II)-α-Diimine Catalysts. Synthesis of New Block Polymers Based on α-Olefins. *J. Am. Chem. Soc.* **1996**, *118*, 11664−11665.

Kobayashi, S.; Uyama, H.; Namekawa, S.; Hayakawa, H. Enzymatic Ring-Opening Polymerization and Copolymerization of 8-Octanolide by Lipase Catalyst. *Macromolecules* **1998**, *31*, 5655–5659.

Kong, J. F.; Lipik, V.; Abadie, M. J. M.; Roshan Deen, G.; Venkatraman, S. S. Characterization and Degradation of Elastomeric Four-Armed Star Copolymers Based on Caprolactone and L-Lactide. *J. Biomed. Mater. Res. Part A* **2012**, *100A*, 3436–3445.

Kong, J. F.; Lipik, V.; Abadie, M. J.; Deen, G. R.; Venkatraman, S. S. Biodegradable Elastomers Based on ABA Triblocks: Influence of End-Block Crystallinity on Elastomeric Character. *Polym. Int.* **2012**, *61*, 43–50.

Koo, C. M.; Hillmyer, M. A.; Bates, F. S. Structure and Properties of Semicrystalline–Rubbery Multiblock Copolymers. *Macromolecules* **2006**, *39*, 667–677.

Kowalski, A.; Duda, A.; Penczek, S. Kinetics and Mechanism of Cyclic Esters Polymerization Initiated with Tin(II) Octoate. 3. † Polymerization of L ,L -Dilactide. *Macromolecules* **2000**, *33*, 7359–7370.

Kowalski, A.; Duda, A.; Penczek, S. Mechanism of Cyclic Ester Polymerization Initiated with Tin(II) Octoate. 2. Macromolecules Fitted with Tin(II) Alkoxide Species Observed Directly in MALDI−TOF Spectra. *Macromolecules* **2000**, *33*, 689–695.

Kricheldorf, H. R.; Boettcher, C.; Tönnes, K.-U. Polylactones: 23. Polymerization of Racemic and Mesod,l-Lactide with Various Organotin Catalysts—stereochemical Aspects. *Polymer* **1992**, *33*, 2817–2824.

Kricheldorf, H. R.; Kreiser-Saunders, I.; Stricker, A. Polylactones 48. SnOct2-Initiated Polymerizations of Lactide: A Mechanistic Study. *Macromolecules* **2000**, *33*, 702–709.

Kricheldorf, H. R.; Rost, S. Biodegradable Multiblock Copolyesters Prepared from ε-Caprolactone, L-Lactide, and Trimethylene Carbonate by Means of Bismuth Hexanoate. *Macromolecules* **2005**, *38*, 8220–8226.

Kulinski, Z.; Piorkowska, E. Crystallization, Structure and Properties of Plasticized Poly(L-Lactide). *Polymer* **2005**, *46*, 10290–10300.

Kumar, A.; Kalra, B.; Dekhterman, A.; Gross, R. A. Efficient Ring-Opening Polymerization and Copolymerization of ε-Caprolactone and ω-Pentadecalactone Catalyzed by Candida Antartica Lipase B. *Macromolecules* **2000**, *33*, 6303–6309.

Kumar, V.; Ashok, S.; Park, S. Recent Advances in Biological Production of 3-Hydroxypropionic Acid. *Biotechnol. Adv.* **2013**, *31*, 945–961.

Le Roux, E. Recent Advances on Tailor-Made Titanium Catalysts for Biopolymer Synthesis. *Coord. Chem. Rev.* **2016**, *306*, 65–85.

Lee, I.; Panthani, T. R.; Bates, F. S. Sustainable Poly(Lactide-b-Butadiene) Multiblock Copolymers with Enhanced Mechanical Properties. *Macromolecules* **2013**, *46*, 7387–7398.

Lee, R.; Huang, Y.; Chen, W. Synthesis and Characterization of Temperature-Sensitive Block Copolymers from Poly(N-isopropylacrylamide) and 4-Methyl-ε-Caprolactone or 4-Phenyl-ε-Caprolactone. *J. Appl. Polym. Sci.* **2010**, *118*, 1634–1642.

Lee, R.-S.; Hung, C.-B.; Huang, Y.; Chen, W. Synthesis and Characterization of Amphiphilic Block Copolymers from Poly(Ethylene Glycol)Methyl Ether and 4-Methyl-ε-Caprolactone or 4-Phenyl-ε-Caprolactone. *Polymer* **2007**, *48*, 2605–2612.

Leone, G.; Mauri, M.; Bertini, F.; Canetti, M.; Piovani, D.; Ricci, G. Ni(II) α-Diimine-Catalyzed α-Olefins Polymerization: Thermoplastic Elastomers of Block Copolymers. *Macromolecules* **2015**, *48*, 1304−1312.

Li, S.; Vert, M. Biodegradation of Aliphatic Polyesters. In *Degradable Polymers*; Scott, G., Ed.; Kluwer Academic Publishers, 2002; 71–131.

Li, Y.; Hoskins, J. N.; Sreerama, S. G.; Grayson, M. A.; Grayson, S. M. *Journal of Mass Spectrometry,* **2010**, *45*, 587–611

Linnekoski, J. A.; Asikainen, M.; Heikkinen, H.; Kaila, R. K.; Räsänen, J.; Laitinen, A.; Harlin, A. Production of p-Cymene from Crude Sulphate Turpentine with Commercial Zeolite Catalyst Using a Continuous Fixed Bed Reactor. *Org. Process Res. Dev.* **2014**, *18*, 1468–1475.

Liu, H.; Zhang, J. Research Progress in Toughening Modification of Poly(Lactic Acid). *J. Polym. Sci. Part B Polym. Phys.* **2011**, *49*, 1051–1083.

Loefgren, A.; Albertsson, A.-C.; Dubois, P.; Jerome, R.; Teyssie, P. Synthesis and Characterization of Biodegradable Homopolymers and Block Copolymers Based on 1,5-Dioxepan-2-One. *Macromolecules* **1994**, *27*, 5556–5562.

Luckachan, G. E.; Pillai, C. K. S. Biodegradable Polymers- A Review on Recent Trends and Emerging Perspectives. *J. Polym. Environ.* **2011**, *19*, 637–676.

Lundberg, D. J.; Lundberg, D. J.; Hillmyer, M. A.; Dauenhauer, P. J. Techno-economic analysis of a chemical process to manufacture methyl-ε-caprolactone from cresols. *ACS Sustain. Chem. Eng.* **2018**, Article ASAP.

Luo, X.; Xie, S.; Liu, J.; Hu, H.; Jiang, J.; Huang, W.; Gao, H.; Zhou, D.; Lü, Z.; Yan, D. The Relationship Between the Degree of Branching and Glass Transition Temperature of Branched Polyethylene: Experiment and Simulation. *Polym. Chem.* **2014**, *5*, 1305−1312.

Lynd, N. A.; Oyerokun, F. T.; O'Donoghue, D. L.; Handlin, D. L.; Fredrickson, G. H. Design of Soft and Strong Thermoplastic Elastomers Based on Nonlinear Block Copolymer Architectures Using Self-Consistent-Field Theory. *Macromolecules* **2010**, *43*, 3479–3486.

Macchioni, A. Ion Pairing in Transition-Metal Organometallic Chemistry. *Chem. Rev.* **2005**, *105*, 2039–2074.

Mahoney, J. E. Acrylic Acid Production Methods. U.S. Application No. 15,247,833, August 25, 2016.

Makarouni, D.; Lycourghiotis, S.; Kordouli, E.; Bourikas, K.; Kordulis, C.; Dourtoglou, V. Transformation of Limonene into p-Cymene over Acid Activated Natural Mordenite Utilizing Atmospheric Oxygen as a Green Oxidant: A Novel Mechanism. *Appl. Catal. B Environ.* **2018**, *224*, 740–750.

Marín, F. R.; Soler-Rivas, C.; Benavente-García, O.; Castillo, J.; Pérez-Alvarez, J. A. By-Products from Different Citrus Processes as a Source of Customized Functional Fibres. *Food Chem.* **2007**, *100*, 736–741.

Martello, M. T.; Burns, A.; Hillmyer, M. Bulk Ring-Opening Transesterification Polymerization of the Renewable δ-Decalactone Using an Organocatalyst. *ACS Macro Lett.* **2012**, *1*, 131–135.

Martello, M. T.; Hillmyer, M. A. Polylactide-Poly(6-Methyl-ε-Caprolactone)-Polylactide Thermoplastic Elastomers. *Macromolecules* **2011**, *44*, 8537–8545.

Martello, M. T.; Schneiderman, D. K.; Hillmyer, M. A. Synthesis and Melt Processing of Sustainable Poly(ε-Decalactone)-block-Poly(Lactide) Multiblock Thermoplastic Elastomers. *ACS Sustain. Chem. Eng.* **2014**, *2*, 2519–2526.

Mathisen, T.; Albertsson, A.-C. Polymerization of 1,5-Dioxepan-2-One. 1. Synthesis and Characterization of the Monomer 1,5-Dioxepan-2-One and Its Cyclic Dimer 1,5,8,12-Tetraoxacyclotetradecane-2,9-Dio. *Macromolecules* **1989**, *22*, 3838–3842.

Matsumiya, Y.; Watanabe, H.; Takano, A.; Takahashi, Y. Uniaxial Extensional Behavior of (SIS)P-Type Multiblock Copolymer Systems: Structural Origin of High Extensibility. *Macromolecules* **2013**, *46*, 2681–2695.

McCord, E. F.; McLain, S. J.; Nelson, L. T. J.; Ittel, S. D.; Tempel, D.; Killian, C. M.; Johnson, L. K.; Brookhart, M. 13C NMR Analysis of α-Olefin Enchainment in Poly(α-olefins) Produced with Nickel and Palladium α-Diimine Catalysts. *Macromolecules* **2007**, *40*, 410−420.

Meinhard D.; Wegner, M.; Kipiani, G.; Hearley, A.; Reuter,P.; Fischer, S.; Marti, O.; Rieger, B. New Nickel (II) Diimine Complexes and the Control of Polyethylene Microstructure by Catalyst Design. *J. Am. Chem. Soc.* **2007**, 129, 9182−9191.

Meng, F.; Pritchard, R. H.; Terentjev, E. M. Stress Relaxation, Dynamics, and Plasticity of Transient Polymer Networks. *Macromolecules* **2016**, *49*, 2843–2852.

Miyata, T.; Masuko, T. Crystallization Behaviour of Poly(l-Lactide). *Polymer* **1998**, *39*, 5515–5521.

Molero, C.; de Lucas, A.; Romero, F.; Rodríguez, J. F. Glycolysis of Flexible Polyurethane Wastes Using Stannous Octoate as the Catalyst. *J. Mater. Cycles Waste Manag.* **2009**, *11*, 130–132.

Moore, J. S., & Stupp, S. I. Room Temperature Polyesterification. *Macromolecules*, **1990**, *23*, 65–70.

Morton, M.; McGrath, J. E.; Juliano, P. C. Structure–Property Relationships for Styrene–Diene Thermoplastic Elastomers. *J. Polym. Sci., Part C: Polym. Symp.* **1969**, *26*, 99–115.

Müller, A. J.; Balsamo, V.; Arnal, M. L. Nucleation and Crystallization in Diblock and Triblock Copolymers. *Adv. Polym. Sci.* **2005**, *190*, 1–63.

Myers, D.; Witt, T.; Cyriac, A.; Bown, M.; Mecking, S.; Williams, C. K. Ring Opening Polymerization of Macrolactones: High Conversions and Activities Using an Yttrium Catalyst. *Polym. Chem.* **2017**, *8*, 5780–5785.

Nagarajan, S.; Gowd, E. B. Cold Crystallization of PDMS and PLLA in Poly(L-Lactide-b-Dimethylsiloxane-b- L-Lactide) Triblock Copolymer and Their Effect on Nanostructure Morphology. *Macromolecules* **2015**, *48*, 5367–5377.

Nagarajan, V.; Mohanty, A. K.; Misra, M. Perspective on Polylactic Acid (PLA) Based Sustainable Materials for Durable Applications: Focus on Toughness and Heat Resistance. *ACS Sustain. Chem. Eng.* **2016**, *4*, 2899–2916.

Nakayama, Y.; Aihara, K.; Yamanishi, H.; Fukuoka, H.; Tanaka, R.; Cai, Z.; Shiono, T. Synthesis of Biodegradable Thermoplastic Elastomers from ε-Caprolactone and Lactide. *J. Polym. Sci. Part A Polym. Chem.* **2015**, *53*, 489–495.

Nandan, B.; Hsu, J.; Chen, H. Crystallization Behavior of Crystalline-Amorphous Diblock Copolymers Consisting of a Rubbery Amorphous Block. *J. Macromol. Sci. Part C Polym. Rev.* **2006**, *46*, 143–172.

Nelißen, M.; Keul, H.; Höcker, H. Ring-Closing Depolymerization of Poly(ε-Caprolactone). *Macromol. Chem. Phys.* **1995**, *196*, 1645–1661.

Nørskov-Lauritsen, L.; Bürgi, H.-B.; Hofmann, P.; Schmidt, H. R. Bond Angles in Lactones and Lactams. *Helv. Chim. Acta* **1985**, *68*, 76–82.

O'Connell, P. A.; McKenna, G. B. Arrhenius-Type Temperature Dependence of the Segmental Relaxation below Tg. *J. Chem. Phys.* **1999**, *110*, 11054–11060.

O'Keefe, B. J.; Hillmyer, M. A.; Tolman, W. B. Polymerization of Lactide and Related Cyclic Esters by Discrete Metal Complexes. *J. Chem. Soc. Dalt. Trans.* **2001**, 2215–2224.

Ocando, C.; Fernández, R.; Tercjak, A.; Mondragon, I.; Eceiza, A. Nanostructured Thermoplastic Elastomers Based on SBS Triblock Copolymer Stiffening with Low

Contents of Epoxy System. Morphological Behavior and Mechanical Properties. *Macromolecules* **2013**, *46*, 3444–3451.
Ohtaki, H.; Deplace, F.; Vo, G. D.; LaPointe, A. M.; Shimizu, F.; Sugano, T.; Kramer, E. J.; Fredrickson, G. H.; Coates, G. W. Allyl-Terminated Polypropylene Macromonomers: A Route to Polyolefin Elastomers with Excellent Elastic Behavior. *Macromolecules* **2015**, *48*, 7489–7494.
Ohtaki, H; Shimizu, F; Coates, G. W.; Fredrickson, G. H. Thermoplastic Elastomer Compositions with High Mechanical Strength and their Manufacture. *PCT Int. Appl.* WO 2013061974 A1 20130502, 2013.
Olsén, P.; Borke, T.; Odelius, K.; Albertsson, A.-C. ε-Decalactone: A Thermoresilient and Toughening Comonomer to Poly(L-Lactide). *Biomacromolecules* **2013**, *14*, 2883–2890.
Olsén, P.; Odelius, K.; Albertsson, A. C. Thermodynamic Presynthetic Considerations for Ring-Opening Polymerization. *Biomacromolecules* **2016**, *17*, 699–709.
Ono, N.; Miyake, H.; Fujii, M.; Kaji, A. *Tet. Lett.* **1983**, *24*, 3477–3480.
Otake, Y.; Kobayashi, T.; Asabe, H.; Murakami, N.; Ono, K. Biodegradation of Low-Density Polyethylene, Polystyrene, Polyvinyl Chloride, and Urea Formaldehyde Resin Buried under Soil for over 32 Years. *J. Appl. Polym. Sci.* **1995**, *56*, 1789–1796.
Overberger, C. G.; Kaye, H. The Syntheses of Some Optically Active ε-Caprolactones. *J. Am. Chem. Soc.* **1967**, *89*, 5640–5645.
Panthani, T. R.; Bates, F. S. Crystallization and Mechanical Properties of Poly(L-Lactide)-Based Rubbery/Semicrystalline Multiblock Copolymers. *Macromolecules* **2015**, *48*, 4529–4540.
Parker, A. J.; Rottler, J. Molecular Mechanisms of Plastic Deformation in Sphere-Forming Thermoplastic Elastomers. *Macromolecules* **2015**, *48*, 8253–8261.
Payne, A. R. Hysteresis in Rubber Vulcanizates. *J. Polym. Sci. Polym. Symp.* **2007**, *48*, 169–196.
Peeters, J. W.; van Leeuwen, O.; Palmans, A. R. A.; Meijer, E. W. Lipase-Catalyzed Ring-Opening Polymerizations of 4-Substituted ε-Caprolactones: Mechanistic Considerations. *Macromolecules* **2005**, *38*, 5587–5592.
Penczek, S.; Cypryk, M.; Duda, A.; Kubisa, P.; Słomkowski, S. Living Ring-Opening Polymerizations of Heterocyclic Monomers. *Prog. Polym. Sci.* **2007**, *32*, 247–282.
Perego, G.; Cella, G.; Bastioli, C. Effect of Molecular Weight and Crystallinity on Poly (Lactic Acid) Mechanical Properties. *J. Appl. Polym.* **1996**, *59*, 37–43.
Phenolic Resins: A Century of Progress; Pilato, L., Ed.; Springer: Berlin, Heidelberg, 2010.
Pitt, C. G.; Gratzl, M. M.; Kimmel, G. L.; Surles, J.; Schindler, A. Aliphatic Polyesters II. The Degradation of Poly (D,L-lactide), Poly (ε-caprolactone), and Their Copolymers in Vivo. *Biomaterials* **1981**, *2*, 215−220.
Poly(Lactic Acid): Synthesis, Structures, Properties, Processing, and Applications; Auras, R. A.; Lim, L.-T.; Selke, S. E. M.; Tsuji, H., Eds.; John Wiley & Sons, Inc.: Hoboken, NJ, USA, 2010.

Poon, B. C.; Dias. P.; Ansems, P.; Chum, S. P.; Hiltner, A.; Baer, E. Structure and Deformation of an Elastomeric Propylene−Ethylene Copolymer. *J. Appl. Polym. Sci.* **2007**, *104*, 489−499.

Ragauskas, A. J.; Nagy, M.; Kim, D. H.; Eckert, C. A.; Hallett, J. P.; Liotta, C. L. From Wood to Fuels: Integrating Biofuels and Pulp Production. *Ind. Biotechnol.* **2006**, *2*, 55–65.

Rainbolt, E. A.; Washington, K. E.; Biewer, M. C.; Stefan, M. C. Recent Developments in Micellar Drug Carriers Featuring Substituted Poly(ε-Caprolactone)s. *Polym. Chem.* **2015**, *6*, 2369–2381.

Riande, E.; De la Campa, J. G.; Guzman, J.; De Abajo, J. Ring-Opening Polymerization of 3-Methyloxetane: NMR Spectroscopy and Configurational Properties of the Polymer. *Macromolecules* **1984**, *17*, 1431–1436.

Roberge, D. M.; Buhl, D.; Niederer, J. P. M.; Hölderich, W. F. Catalytic Aspects in the Transformation of Pinenes to p-Cymene. *Appl. Catal. A Gen.* **2001**, *215*, 111–124.

Robertson, M. L; Hillmyer, M. A.; Mortamet, A. -C.; Ryan, A. J. Biorenewable Multiphase Polymers. *MRS Bull.* **2010**, *35*, 194–200.

Rose, J. M.; Deplace, F.; Lynd, N. A.; Wang, Z.; Hotta, A.; Lobkovsky, E. B.; Kramer, E. J.; Coates, G. W. C2-Symmetric Ni(II) α-Diimines Featuring Cumyl-Derived Ligands: Synthesis of Improved Elastomeric Regioblock Polypropylene. *Macromolecules* **2008**, *41*, 9548−9555.

Roy, P. K.; Hakkarainen, M.; Varma, I. K.; Albertsson, A. C. Degradable Polyethylene: Fantasy or Reality. *Environ. Sci. Technol.* **2011**, *45*, 4217–4227.

Rubinstein, M.; Semenov, A. N. Dynamics of Entangled Solutions of Associating Polymers. *Macromolecules* **2001**, *34*, 1058–1068.

Ryner, M.; Albertsson, A.-C. Resorbable and Highly Elastic Block Copolymers from 1,5-Dioxepan-2-One and L-Lactide with Controlled Tensile Properties and Hydrophilicity. *Biomacromolecules* **2002**, *3*, 601–608.

Sardon, H.; Pascual, A.; Mecerreyes, D.; Taton, D.; Cramail, H.; Hedrick, J. L. Synthesis of Polyurethanes Using Organocatalysis: A Perspective. *Macromolecules* **2015**, *48*, 3153–3165.

Sato, T.; Watanabe, H.; Osaki, K. Rheological and Dielectric Behavior of a Styrene−Isoprene−Styrene Triblock Copolymer in n -Tetradecane. 1. Rubbery−Plastic−Viscous Transition. *Macromolecules* **1996**, *29*, 6231–6239.

Save, M.; Schappacher, M.; Soum, A. Controlled Ring-Opening Polymerization of Lactones and Lactides Initiated by Lanthanum Isopropoxide, 1. General Aspects and Kinetics. *Macromol. Chem. Phys.* **2002**, *203*, 889–899.

Schmidt, T.; Kirschnig, A. Total Synthesis of Carolacton, a Highly Potent Biofilm Inhibitor. *Angew. Chem. Int. Ed.* **2012**, *51*, 1063–1066.

Schneiderman, D. K.; Hill, E. M.; Martello, M. T.; Hillmyer, M. A. Poly(Lactide)-Block-Poly(ε-Caprolactone-co-ε-Decalactone)-Block-Poly(Lactide) Copolymer Elastomers. *Polym. Chem.* **2015**, *6*, 3641–3651.

Schneiderman, D. K.; Hillmyer, M. A. Aliphatic Polyester Block Polymer Design. *Macromolecules* **2016**, *49*, 2419–2428.

Schneiderman, D. K.; Vanderlaan, M. E.; Mannion, A. M.; Panthani, T. R.; Batiste, D. C.; Wang, J. Z.; Bates, F. S.; Macosko, C. W.; Hillmyer, M. A. Chemically Recyclable Biobased Polyurethanes. *ACS Macro Lett.* **2016**, *5*, 515–518.

Schutyser, W.; Van Den Bosch, S.; Dijkmans, J.; Turner, S.; Meledina, M.; Van Tendeloo, G.; Debecker, D. P.; Sels, B. F. Selective Nickel-Catalyzed Conversion of Model and Lignin-Derived Phenolic Compounds to Cyclohexanone-Based Polymer Building Blocks. *Chem. Sus. Chem.* **2015**, *8*, 1805–1818.

Seefried, C. G.; Koleske, J. V. Lactone Polymers. VI. Glass-Transition Temperatures of Methyl-Substituted ε-Caprolactones and Polymer Blends. *J. Polym. Sci. Polym. Phys. Ed.* **1975**, *13*, 851–856.

Self-Healing Materials; Hager, M. D.; van der Zwaag, S.; Schubert, U. S., Eds.; Springer International Publishing: Cham, 2016; Vol. 273.

Shi, X.; Jing, Z.; Zhang, G.; Xu, Y.; Yao, Y. Fully Bio-Based Poly(ε-Capolactone)/Poly(Lactide) Alternating Multiblock Supramolecular Polymers: Synthesis, Crystallization Behavior, and Properties. *J. Appl. Polym. Sci.* **2017**, *134*, 1–12.

Shin, J.; Kim, Y.-W.; Kim, G.-J. Sustainable Block Copolymer-Based Thermoplastic Elastomers. *Appl. Chem. Eng.* **2014**, *25*, 121–133.

Shin, J.; Martello, M. T.; Shrestha, M.; Wissinger, J. E.; Tolman, W. B.; Hillmyer, M. A. Pressure-Sensitive Adhesives from Renewable Triblock Copolymers. *Macromolecules* **2011**, *44*, 87–94.

Simón, D.; de Lucas, A.; Rodríguez, J. F.; Borreguero, A. M. Flexible Polyurethane Foams Synthesized Employing Recovered Polyols from Glycolysis: Physical and Structural Properties. *J. Appl. Polym. Sci.* **2017**, *134*, 1–9.

Singh, N. K.; Lesser, A. J. A Physical and Mechanical Study of Prestressed Competitive Double Network Thermoplastic Elastomers. *Macromolecules* **2011**, *44*, 1480–1490.

Slivniak, R.; Domb, A. J. Macrolactones and Polyesters from Ricinoleic Acid. *Biomacromolecules* **2005**, *6*, 1679–1688.

Small, B. L.; Brookhart, M. Iron-Based Catalysts with Exceptionally High Activities and Selectivities for Oligomerization of Ethylene to Linear α-Olefins. *J. Am. Chem. Soc.* **1998**, *120*, 7143–7144.

Södergård, A.; Stolt, M. Properties of Lactic Acid Based Polymers and Their Correlation with Composition. *Prog. Polym. Sci.* **2002**, *27*, 1123–1163.

Söntjens, S. H. M.; Sijbesma, R. P.; Van Genderen, M. H. P.; Meijer, E. W. Stability and Lifetime of Quadruply Hydrogen Bonded 2-Ureido-4[1H]-Pyrimidinone Dimers. *J. Am. Chem. Soc.* **2000**, *122*, 7487–7493.

Spaans, R. D.; Williams, M. C. Nonlinear Viscoelasticity of ABA Block Copolymer Melts: Stress Relaxation and Recovery. *Ind. Eng. Chem. Res.* **1995**, *34*, 3496–3507.

Spurr, O. K.; Niegisch, W. D. Stress Crazing of Some Amorphous Thermoplastics. *J. Appl. Polym. Sci.* **1962**, *6*, 585–599.

Stayshich, R. M.; Meyer, T. Y. New Insights into Poly(Lactic-co-Glycolic Acid) Microstructure: Using Repeating Sequence Copolymers to Decipher Complex NMR and Thermal Behavior. *J. Am. Chem. Soc.* **2010**, *132*, 10920–10934.

Stjerndahl, A.; Finne-Wistrand, A.; Albertsson, A.-C.; Bäckesjö, C. M.; Lindgren, U. Minimization of Residual Tin in the Controlled Sn(II)Octoate-Catalyzed Polymerization of ε-Caprolactone. *J. Biomed. Mater. Res. A* **2008**, *87*, 1086–1091.

Storey, R. F.; Sherman, J. W. Kinetics and Mechanism of the Stannous Octoate-Catalyzed Bulk Polymerization of ε-Caprolactone. *Macromolecules* **2002**, *35*, 1504–1512.

Subramanyam, U.; Sivaram, S. Synthesis and Characterization of Poly(higher-α-olefins) with a Nickel(α-diimine)/Methylaluminoxane Catalyst System: Effect of Chain Running on the Polymer Properties. *J. Polym. Sci., Part A: Polym. Chem*. **2007**, *45*, 191−210.

Supramolecular Polymer Networks and Gels; Seiffert, S., Ed.; Advances in Polymer Science; Springer International Publishing: Cham, 2015; Vol. 268.

Tabone, M. D.; Cregg, J. J.; Beckman, E. J.; Landis, A. E. Sustainability Metrics: Life Cycle Assessment and Green Design in Polymers. *Environ. Sci. Technol.* **2010**, *44*, 8264–8269.

Takahara, I.; Saito, M.; Inaba, M.; Murata, K. Dehydration of Ethanol into Ethylene over Solid Acid Catalysts. *Catal. Lett.* **2005**, *105*, 249−252.

Taskila, S.; Ojamo, H. The Current Status and Future Expectations in Industrial Production of Lactic Acid by Lactic Acid Bacteria. In *Lactic Acid Bacteria - R & D for Food, Health and Livestock Purposes*; Kongo, M., Ed.; InTech, 2013; pp. 615–632.

Tempel, D. J.; Johnson, L. K.; Huff, L. R.; White, P. S.; Brookhart, M. Mechanistic Studies of Pd(II)-α-Diimine Catalyzed Olefin Polymerizations1. *J. Am. Chem. Soc.* **2000**, *122*, 6686−6700.

The Physics of Glassy Polymers, 2nd ed.; Haward, R. N.; Young, R. J., Eds.; Chapman & Hall: London, 1997.

Thermoplastic Elastomers; Holden, G.; Kricheldorf, H. R.; Quirk, R. P., Eds.; 3rd ed.; Hanser Gardner Publications, Inc.: Cincinnati, 2004.

Thomas, R. M.; Keitz, B. K.; Champagne, T. M.; Grubbs, R. H. Highly Selective Ruthenium Catalysts for Ethenolysis. *J. Am. Chem. Soc.* **2011**, *133*, 7490−7496.

Toki, S.; Fujimaki, T.; Okuyama, M. Strain-induced Crystallization of Natural Rubber as Detected Real-time by Wide-angle X-ray Diffraction Technique. *Polymer J.* **2000**, *41*, 5423−5429.

Tomita, S.; Lei, L.; Urushihara, Y.; Kuwamoto, S.; Matsushita, T.; Sakamoto, N.; Sasaki, S.; Sakurai, S. Strain-Induced Deformation of Glassy Spherical Microdomains in Elastomeric Triblock Copolymer Films: Simultaneous Measurements of a Stress–Strain Curve with 2D-SAXS Patterns. *Macromolecules* **2017**, *50*, 677–686.

Tong, J.; Jerôme, R. Dependence of the Ultimate Tensile Strength of Thermoplastic Elastomers of the Triblock Type on the Molecular Weight between Chain Entanglements of the Central Block. *Macromolecules* **2000**, *33*, 1479–1481.

Trollsås, M.; Kelly, M. a.; Claesson, H.; Siemens, R.; Hedrick, J. L. Highly Branched Block Copolymers: Design, Synthesis, and Morphology. *Macromolecules* **1999**, *32*, 4917–4924.

Tsuji, H. Poly(Lactide) Stereocomplexes: Formation, Structure, Properties, Degradation, and Applications. *Macromol. Biosci.* **2005**, *5*, 569–597.

Tsuji, H.; Ikada, Y. Stereocomplex Formation between Enantiomeric Poly(Lactic Acid)s. XI. Mechanical Properties and Morphology of Solution-Cast Films. *Polymer* **1999**, *40*, 6699–6708.

Ugarte, L.; Saralegi, A.; Fernández, R.; Martín, L.; Corcuera, M. A.; Eceiza, A. Flexible Polyurethane Foams Based on 100% Renewably Sourced Polyols. *Ind. Crops Prod.* **2015**, *62*, 545–551.

United States Department of Agriculture. USDA Biopreferred® program guidelines, June 2016; https://www.biopreferred.gov/BioPreferred/faces/pages/DocumentBrowser.xhtml (Accessed 24 October 2018).

US Food and Drug Administration. Title 21. PART 175 - Indirect Food Additives: Adhesives and Components of Coatings, 2014.

Vaidya, T.; Klimovica, K.; LaPointe, A. M.; Keresztes, I.; Lobkovsky, E. B.; Daugulis, O.; Coates, G. W. Secondary Alkene Insertion and Precision Chain-Walking: A New Route to Semicrystalline "Polyethylene" from α-Olefins by Combining Two Rare Catalytic Events. *J. Am. Chem. Soc.* **2014**, *136*, 7213−7216.

van Beek, D. J. M.; Gillissen, M. A. J.; van As, B. A. C.; Palmans, A. R. A.; Sijbesma, R. P. Supramolecular Copolyesters with Tunable Properties. *Macromolecules* **2007**, *40*, 6340–6348.

van Beek, D. J. M.; Peters, G. M. W.; Sijbesma, R. P. Rheological Behavior of a Quadruple Hydrogen-Bonded Suprarmolecular Polyester. *Mater. Technol.* **2005**, 433–434.

van Beek, D. J. M.; Spiering, A. J. H.; Peters, G. W. M.; te Nijenhuis, K.; Sijbesma, R. P. Unidirectional Dimerization and Stacking of Ureidopyrimidinone End Groups in Polycaprolactone Supramolecular Polymers. *Macromolecules* **2007**, *40*, 8464–8475.

van der Mee, L.; Helmich, F.; de Bruijn, R.; Vekemans, J. A. J. M.; Palmans, A. R. A.; Meijer, E. W. Investigation of Lipase-Catalyzed Ring-Opening Polymerizations of Lactones with Various Ring Sizes: Kinetic Evaluation. *Macromolecules* **2006**, *39*, 5021–5027.

Vangeyte, P.; Jérôme, R. Amphiphilic Block Copolymers of High-Molecular-Weight Poly(Ethylene Oxide) and Either ε-Caprolactone or γ-Methyl-ε-Caprolactone: Synthesis and Characterization. *J. Polym. Sci. Part A Polym. Chem.* **2004**, *42*, 1132–1142.

Wanamaker, C. L.; Bluemle, M. J.; Pitet, L. M.; O'Leary, L. E.; Tolman, W. B.; Hillmyer, M. A. Consequences of Polylactide Stereochemistry on the Properties of Polylactide-Polymenthide-Polylactide Thermoplastic Elastomers. *Biomacromolecules* **2009**, *10*, 2904–2911.

Wanamaker, C. L.; Bluemle, M. J.; Pitet, L. M.; O'Leary, L. E.; Tolman, W. B.; Hillmyer, M. A. Consequences of Polylactide Stereochemistry on the Properties of Polylactide-Polymenthide-Polylactide Thermoplastic Elastomers. *Biomacromolecules* **2009**, *10*, 2904–2911.

Wanamaker, C. L.; O'Leary, L. E.; Lynd, N. A.; Hillmyer, M. A.; Tolman, W. B. Renewable-Resource Thermoplastic Elastomers Based on Polylactide and Polymenthide. *Biomacromolecules* **2007**, *8*, 3634–3640.

Wang, H. P.; Chum, S. P.; Hiltner, A.; Baer, E. Comparing Elastomeric Behavior of Block and Random Ethylene−Octene Copolymers. *J. Appl. Polym. Sci.* **2009**, *113*, 3236−3244.

Wang, H. P.; Khariwala, D. U.; Cheung, W.; Chum, S. P.; Hiltner, A.; Baer, E. Characterization of Some New Olefinic Block Copolymers. *Macromolecules* **2007**, *40*, 2852−2863.

Watts, A.; Kurokawa, N.; Hillmyer, M. A. Strong, Resilient, and Sustainable Aliphatic Polyester Thermoplastic Elastomers. *Biomacromolecules* **2017**, *18*, 1845–1854.

Weisz, P. B. Basic Choices and Constraints on Long-Term Energy Supplies. *Physics Today* **2004**, *57*, 47–52.

Wietor, J. L.; Van Beek, D. J. M.; Peters, G. W.; Mendes, E.; Sijbesma, R. P. Effects of Branching and Crystallization on Rheology of Polycaprolactone Supramolecular Polymers with Ureidopyrimidinone End Groups. *Macromolecules* **2011**, *44*, 1211–1219.

Williams, C. K.; Breyfogle, L. E.; Choi, S. K.; Nam, W.; Young, V. G.; Hillmyer, M. A.; Tolman, W. B. A Highly Active Zinc Catalyst for the Controlled Polymerization of Lactide. *J. Am. Chem. Soc.* **2003**, *125*, 11350–11359.

Witzke, D. R.; Narayan, R.; Kolstad, J. J. Reversible Kinetics and Thermodynamics of the Homopolymerization of L-Lactide with 2-Ethylhexanoic Acid Tin(II) Salt. *Macromolecules* **1997**, *30*, 7075–7085.

World Economic Forum, Ellen MacArthur Foundation, and McKinsey and Company. The New Plastics Economy: Rethinking the future of plastics. 2016, report. http://www.ellenmacarthurfoundation.org/publications

Wu, G.-W.; Hsiue, G.-H.; Yang, J.-S. Stress Relaxation in Poly(Styrene-Butadiene-Styrene) and Poly(Styrene-Isoprene-Styrene) Triblock Copolymers and Their Derivatives. *Mater. Chem. Phys.* **1994**, *37*, 191–196.

Wu, J.; Yu, T.; Chen, C.; Lin, C. Recent Developments in Main Group Metal Complexes Catalyzed/Initiated Polymerization of Lactides and Related Cyclic Esters. *Coord. Chem. Rev.* **2006**, *250*, 602–626.

Wu, L.; Cochran, E. W.; Lodge, T. P.; Bates, F. S. Consequences of Block Number on the Order-Disorder Transition and Viscoelastic Properties of Linear (AB)N Multiblock Copolymers. *Macromolecules* **2004**, *37*, 3360–3368.

Wu, S. Phase Structure and Adhesion in Polymer Blends: A Criterion for Rubber Toughening. *Polymer* **1985**, *26*, 1855–1863.

Xiao, Y.; Cummins, D.; Palmans, A. R. A.; Koning, C. E.; Heise, A. Synthesis of Biodegradable Chiral Polyesters by Asymmetric Enzymatic Polymerization and Their Formulation into Microspheres. *Soft Matter* **2008**, *4*, 593–599.

Xiong, M.; Schneiderman, D. K.; Bates, F. S.; Hillmyer, M. A.; Zhang, K. Scalable Production of Mechanically Tunable Block Polymers from Sugar. *Proc. Natl. Acad. Sci.* **2014**, *111*, 8357–8362.

Yamauchi, K.; Kanomata, A.; Inoue, T.; Long, T. E. Thermoreversible Polyesters Consisting of Multiple Hydrogen Bonding (MHB). *Macromolecules* **2004**, *37*, 3519–3522.

Yamauchi, T.; Hattori, K.; Nakao, K.; Tamaki, K. Preparation of 2-Arylpropanoates by the Reaction of 2-Hydroxypropiophenone Dimethyl Acetals with Sulfuryl Chloride in the Presence of an Amide or a Weak Base. *Bull. Chem. Soc. Jpn.* **1987**, *60*, 4015–4018.

Yevstropov, A. A.; Lebedev, B. V.; Kiparisova, Y. G. *Vysokomol. Soyed.*, **1983**, *A25*, 1679─1685

Yu, T.; Ren, J.; Gu, S.; Yang, M. Preparation and Characterization of Biodegradable Poly(Lactic Acid)-block-Poly(ε-Caprolactone) Multiblock Copolymer. *Polym. Adv. Technol.* **2010**, *21*, 183–188.

Zhang, D.; Hillmyer, M. A.; Tolman, W. B. A New Synthetic Route to Poly[3-Hydroxypropionic Acid] (P[3-HP]): Ring-Opening Polymerization of 3-HP Macrocyclic Esters. *Macromolecules* **2004**, *37*, 8198–8200.

Zhang, D.; Nadres, E. T.; Brookhart, M.; Daugulis, O. Synthesis of Highly Branched Polyethylene Using "Sandwich" (8-p-Tolyl naphthyl α-diimine)nickel(II) Catalysts. *Organometallics* **2013**, *32*, 5136−5143.

Zhang, D.; Xu, J.; Alcazar-Roman, L.; Greenman, L.; Cramer, C. J.; Hillmyer, M. A.; Tolman, W. B. Isotactic Polymers with Alternating Lactic Acid and Oxetane Subunits from the Endoentropic Polymerization of a 14-Membered Ring. *Macromolecules* **2004**, *37*, 5274–5281.

Zhang, X. D.; Macosko, C. W.; Davis, H. T.; Nikolov, A. D.; Wasan, D. T. Role of Silicone Surfactant in Flexible Polyurethane Foam. *J. Colloid Interface Sci.* **1999**, *215*, 270–279.

Zhang, Z.; Grijpma, D. W.; Feijen, J. Triblock Copolymers Based on 1,3-Trimethylene Carbonate and Lactide as Biodegradable Thermoplastic Elastomers. *Macromol. Chem. Phys.* **2004**, *205*, 867–875.

Zhao, Y.; Ning, N.; Hu, X.; Li, Y.; Chen, F.; Fu, Q. Processing Temperature Dependent Mechanical Response of a Thermoplastic Elastomer with Low Hard Segment. *Polymer* **2012**, *53*, 4310–4317.

Zhu, Y.; Radlauer, M. R.; Schneiderman, D. K.; Shaffer, M. S. P.; Hillmyer, M. A.; Williams, C. K. Multiblock Polyesters Demonstrating High Elasticity and Shape Memory Effects. *Macromolecules* **2018**, *51*, 2466–2475.

Zhu, Y.; Romain, C.; Williams, C. K. Sustainable Polymers from Renewable Resources. *Nature* **2016**, *540*, 354–362.

Zing, J-B.; Srinivansan, M.; Li, Y-D.; Narayan, R.; Wang, Y-Z. *Journal of Polymer Science: Part A: Polymer Chemistry*, **2010**, *48*, 5885–5890

Zupancich, J. A.; Bates, F. S.; Hillmyer, M. A. Aqueous Dispersions of Poly(Ethylene Oxide)- b -Poly(γ-Methyl-ε-Caprolactone) Block Copolymers. *Macromolecules* **2006**, *39*, 4286–4288.

Appendix A.

Impact of thermal history on the properties of poly(L-lactide) block polymers [†]

[†] The work in this chapter was carried out in part in collaboration with Emma M. Rettner and Naruki Kurokawa. The TEM images were obtained by Jun Xu.

A.1. Introduction

Due to the growing end-of-life concerns for single use plastics, biorenewable and biodegradable plastics such as polylactide (PLA) have found many applications in substituting petroleum-based and non-compostable plastics.[1] The Young's modulus (E = 3.8 GPa) and the ultimate tensile strength (σ_B = 59 MPa) for high molar mass semicrystalline poly(L-lactide) (PLLA) is comparable to the tensile properties of polystyrene (PS) and poly(ethylene terephthalate) (PET).[2] One limitation to PLLA is the brittle nature of the thermoplastic due to the low strain at break (3 – 4%). A broader range of properties of increased toughness without compromised ultimate tensile strength and modulus can be achieved by incorporating PLLA in blends or block polymers.[3]

Similar to rubber fillers in immiscible polymer blends, microphase separated rubbery domains in block polymers provide a method improve toughness.[4] Reports of block polymers with a large fraction of PLLA to yield tough plastics have mostly focused on a triblock and multiblock architectures.[5,6] ABA block polymers with an amorphous, low T_g midblock and PLLA end blocks have been shown to exhibit increased toughness over homopolymer PLLA.[7] The toughness is improved after chain-extending low molar mass ABA triblock polymers to yield high molar mass $(AB)_n$ multiblock polymers. However, the urethane linkages that bridge the ABA segments in multiblock polymers are thermally sensitive and are not amendable to melt-processing above the melting temperature of PLLA (T_m = 180 °C). Additionally, the high toughness values of multiblock polymers comes at the cost of lower modulus, lower yield stress, and lower ultimate tensile strength compared to homopolymer PLLA. One method to increase PLLA

toughness that has limited reports is the use of high molar mass (>100 kg mol^{-1}) triblock polymers with semicrystalline PLLA.[8]

Enhancing the crystallinity in homopolymer PLLA increases the ultimate tensile strength and impact strength.[9] When crystalline polymers such as PLLA are incorporated into block polymers, the competing thermodynamic factors of microphase separation and crystallization need to be considered. Crystallization can result in (i) crystalline breakout, where the formation of crystalline lamellae disrupts the block polymer morphology, or (ii) crystalline confinement, where the crystalline lamellae remain confined within the microphase separated domains.[10] A low segregation strength and/or low molar mass can result in crystalline breakout, which reduces the toughness of PLLA block polymers. The microphase separated rubbery domains, acting like rubber fillers in the PLLA matrix, allow stress to be dissipated through cavitation and debonding for a toughening effect.[11] When crystalline breakout disrupts the microphase separated rubber domains, the stress can no longer be dissipated in this way, causing the reduction in toughness. High segregation strength and/or high molar mass that results in crystallization confinement can mitigate these concerns.

In addition to the balance between microphase separation and crystallinity, thermal history of the polymers also has an impact on the final microstructure. Rapid cooling of the block polymer from the melt can prevent crystallization and reduce crystalline breakout while annealing the polymers can promote crystalline breakout.[12] Although increasing the degree of crystallinity in homopolymer PLLA improves the tensile properties, there are more parameters to consider in PLLA block polymers. Most reports of PLLA block

polymers do not address the crystallinity of the sample after processing, limiting the understanding of the parameters that contribute to the mechanical properties observed.

Chapter 3 demonstrates the high performance of PLLA-*block*-poly(γ-methyl-ε-caprolactone)-*block*-PLLA (LLMLL) thermoplastic elastomers. Block polymers with a high fraction of PLLA (f_{LLA} = 0.80, M_n = 159 kg mol^{-1}) exhibit high elongations at break (ε_b = 314%) while maintaining high ultimate tensile strength (42 MPa) and Young's modulus (1.3 GPa). To further understand the compositions that will yield tough PLLA through the block polymer system LLMLL, we synthesized high molar mass polymers with a range of PLLA (f_{LLA} = 0.72 – 0.91). High molar-mass PLLA homopolymer was also synthesized as a control to compare the toughening effect γMCL has in these block polymers. Furthermore, the crystallinity of PLLA in all polymer samples were enhanced through thermal annealing and further tested in uniaxial extension. The impact of block polymer composition and crystallinity of PLLA on the tensile properties are reported.

A.2. Results and discussion

Tough PLLA can be obtained by incorporating a rubbery component dispersed within the PLLA matrix.[2,3] PLLA blends with an immiscible rubbery polymer have demonstrated high levels of toughening, yet most additives are petroleum-based and are not biodegradable.[2] In the sustainable LLMLL block polymer system, we can achieve microphase separated poly(γ-methyl-ε-caprolactone) (PMCL) domains as rubber fillers within a PLLA matrix. To study the impact of PMCL on the toughness

of PLLA, high molar mass polymers with high volume fraction of PLLA (f_{LLA} = 0.72 – 0.91) were synthesized (Table A.1). Homopolymer PLLA (122 kg mol^{-1}, f_{LLA} = 1.00) was synthesized through similar conditions. SEC traces of block polymers are unimodal with low dispersities ($Đ$ = 1.2 – 1.4) and exhibit a clear shift from PMCL homopolymer (Figure A.1). All block polymers exhibit a T_g around −60 °C for the PMCL block and a T_g of 54 – 59 °C for the PLA block. Crystallization and melting peaks are also observed during the second heat by DSC, with the peak T_m reported for the PLLA block (Table A.1).

Table A.1.
Properties of triblock polymers LLMLL with high PLLA composition.

Sample ID ($M_{n,total}$, f_{LLA})	$M_{n,PMCL}$[a] (kg mol^{-1})	$M_{n,total}$[a] (kg mol^{-1})	$Đ$[b]	f_{LLA}[c]	$T_{g,PLLA}$[d] (°C)	$T_{m,PLLA}$[d] (°C)
LLMLL (122, 1.00)	-	122	1.4	1.00	59	176
LLMLL (169, 0.91)	13	169	1.3	0.91	54	177
LLMLL (111, 0.85)	15	111	1.5	0.85	57	175
LLMLL (173, 0.78)	33	173	1.3	0.78	54	176
LLMLL (148, 0.72)	36	148	1.3	0.72	59	175
LLMLL (43, 0.66)	13	43	1.2	0.66	55	167

[a]Determined by ^{1}H NMR analysis; [b]measured by $CHCl_3$ SEC equipped with an RI detector, referenced to polystyrene standards;.[c]Calculated using ρ_{LLA} =1.25 and $\rho_{\gamma MCL}$ = 1.037; [d]DSC results during the second heat.

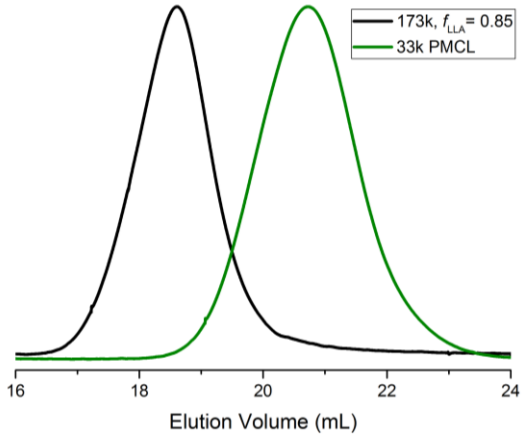

Figure A.1.
Representative SEC trace of triblock polymer LLMLL and PγMCL prepolymer.

Polymer samples were subjected to the following processing conditions to achieve films with different degrees of crystallinity, keeping all other factors the same (Figure A.2). The samples are denoted as quenched (Q) when cooled rapidly (~ 35 °C min^{-1}) from the melt state, which would afford samples with low to moderate degrees of crystallinity.[5] Half of the quenched samples were resubjected to the melt press at 100 °C to promote crystallization and is denoted as annealed (A). The Q and A processed samples were characterized through the first heat by DSC (Figure A.3) to determine the percent crystallinity (X_{PLLA}) using equation A.1:

$$X_{PLLA} = \frac{H_m}{H_m^{\infty} w_{PLLA}} \times 100 \qquad \text{(A.1)}$$

H_m^{∞} is the heat of fusion for an infinite PLLA crystal (93 J/g), w_{PLLA} is the weight fraction of PLLA in the sample, and H_m is the enthalpy of melting taken from the first heat in DSC.[12] The crystallinity of all samples are reported in Table A.2. The quenched samples exhibit crystallinities ranging from 9 – 20%. After annealing, the

percent crystallinity is increased to 38 – 49%. This is a similar degree of crystallinity observed after annealing homopolymer PLLA (M_n = 71 kg mol^{-1}, X_{PLLA} = 45%) after much longer annealing times, 90 min.[9] In the polymers studied, we did not observe an increase in crystallinity with increased annealing times.

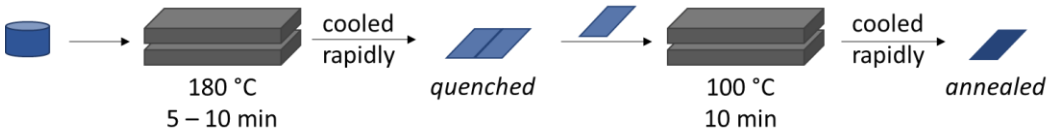

Figure A.2.
Image illustrates the thermal history of quenched and annealed samples.

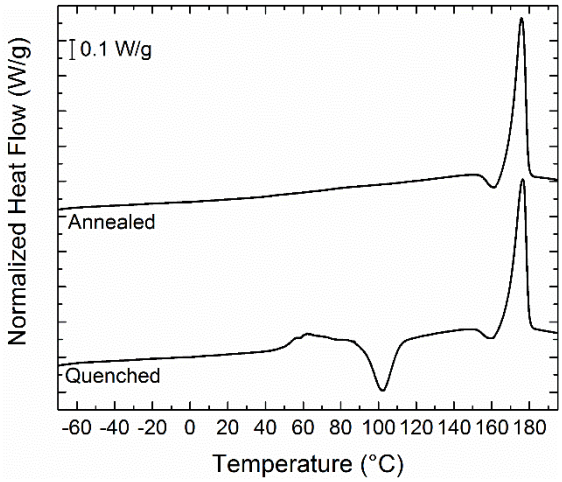

Figure A.3.
DSC trace of LLMLL (169, 0.91) quenched and annealed during the first heat, heating at 10 °C min^{-1}.

Table A.2.
Summary of the ultimate tensile properties of samples with low (Q) and high (A) degrees of crystallinity.

Sample ID[a] (M_n, f_{LLA})-Q/A	X_{LLA}[b] (%)	σ_B[c] (MPa)	ε_B[c] (%)	σ_y[c,d] (MPa)	E (GPa)	Tensile toughness (MJ m^{-3})
(122, 1.00)-Q	9	58.2 ± 9.2	4.8 ± 1.7		1.8	1.6
(122, 1.00)-A	38	73.1 ± 7.9	4.0 ± 0.7		2.2	1.9
(169, 0.91)-Q	17	38.8 ± 5.8	27 ± 14	53.0 ± 1.2	1.1	10
(169, 0.91)-A	41	39.1 ± 0.8	27 ± 25	53.0 ± 1.6	1.5	11
(111, 0.85)-Q	14	31.1 ± 0.8	130 ± 71	53.3 ± 2.5	1.2	40
(111, 0.85)-A	41	40.6 ± 1.8	77 ± 54	52.3 ± 1.1	1.3	31
(173, 0.78)-Q	20	26.0 ± 2.1	142 ± 92	43.2 ± 1.6	1.3	35
(173, 0.78)-A	38	32.8 ± 1.7	105 ± 64	41.6 ± 0.1	1.2	33
(148, 0.72)-Q	16	30.4 ± 3.2	294 ± 75	41.2 ± 1.2	1.4	91
(148, 0.72)-A	44	36.1 ± 6.7	308 ± 103	32.3 ± 0.7	1.2	77
(43, 0.66)-Q	20	20.4 ± 2.0	218 ± 116	34.4 ± 2.4	0.94	42
(43, 0.66)-A	49	23.9 ± 0.2	316 ± 67	20.4 ± 0.3	0.86	58

[a]sample ID with Q for quenched samples and A for annealed samples; [b]calculated by integrating the melting endotherm and subtracting out any crystallization peaks during the first heat in DSC; [c]average and standard deviation reported for six samples; [d]yield stress, the maximum stress at low strain.

When crystallization in block polymers results in crystalline breakout, the original melt morphology is disrupted to form predominantly crystalline lamellae.[13,14] Quenched and annealed LLMLL were characterized by transmission electron microscopy (TEM) (Figure A.4). In LLMLL samples (169, 0.91)-Q and (173, 0.78)-Q, the melt block polymer microstructure is observed. Rapid cooling from the melt limits crystallization, preventing crystalline breakout. After annealing, TEM images of LLMLL (169, 0.91)-A demonstrate lower contrast between blocks, yet the microstructure is still visible (Figure A.4). LLMLL (173, 0.78)-A maintains good contrast while exhibiting a smearing effect. This could be a result of PLLA crystalline regions breaking into the domain boundary to a small extent. Another

contribution that cannot be ruled out is the crystallization of PLLA mixed in the PMCL domain as these block polymers exhibit a depressed T_g of 54 °C, indicating possible mixing between blocks.

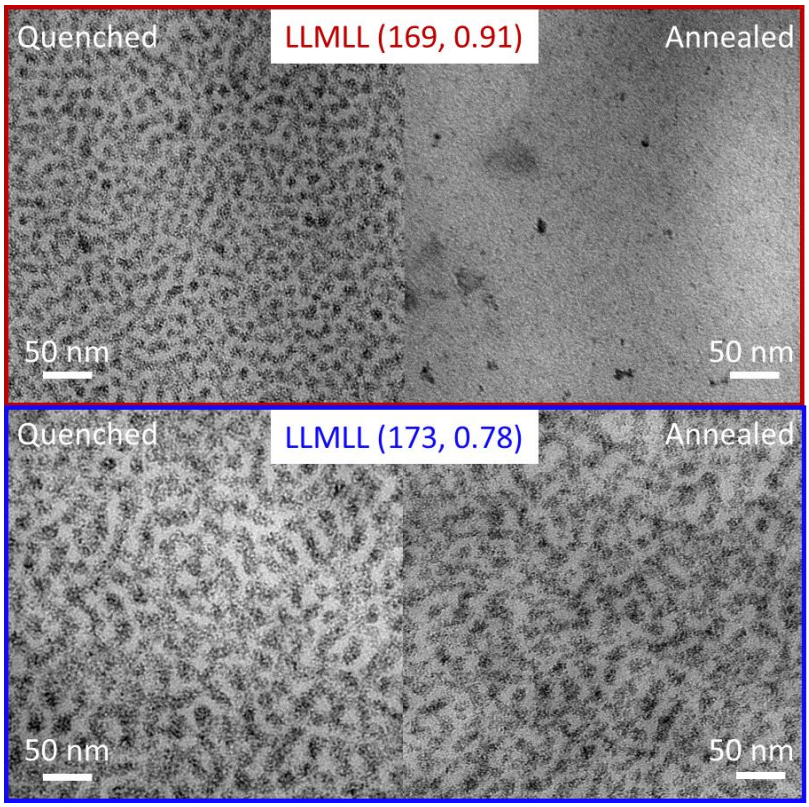

Figure A.4.
Transmission electron microscopy images of select LLMLL samples quenched and annealed, stained with RuO_4

To corroborate the observations made by TEM, we report the small-angle X-ray scattering (SAXS) of these samples (Figure A.5). Quenched samples exhibit a broad primary peak with a higher q shoulder suggesting liquid-like spherical domains. Samples (169, 0.91)-A and (173, 0.78)-A exhibit loss of long-range order by SAXS, corroborating the smearing observed in TEM. SAXS patterns maintain the

same q^* after annealing in both polymer samples, indicating the domain size does not change. The lower intensity observed after annealing corroborates the domain boundaries being less well-defined. The disappearance of the higher q shoulder after crystallization indicates a loss of long-range order. These TEM and SAXS results demonstrate the domain microstructure becomes less well-defined after crystallization through annealing. Likely due to the high molar mass of the samples, we do not observe complete crystalline breakout to yield a lamellar morphology.

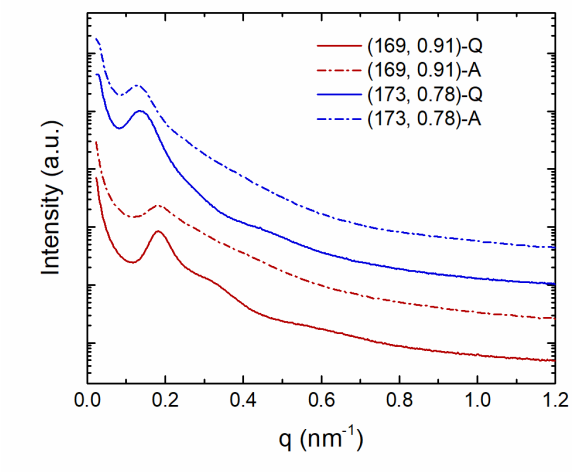

Figure A.5.
Small-angle X-ray scattering patterns of select LLMLL samples quenched and annealed.

When block polymers crystallize above the order-disorder transition temperature (T_{ODT}), the crystalline lamellae microstructure dominates. If the block polymer is microphase separated at the crystallization temperature ($T_g < T_{ODT} > T_m$), crystallization is likely to be confined within the microphase separated domain of the semicrystalline block. SAXS patterns were collected at elevated temperatures for LLMLL (173, 0.78) (Figure A.6) to better understand the morphology at processing

temperatures. The SAXS patterns below 180 °C are similar to the annealed sample at room temperature (173, 0.78)-A, exhibiting a low intensity, low q principle scattering peak. Between the crystallization temperature (100 °C) and melting temperature (180 °C), the microstructure is disturbed due to PLLA crystallization. Above the melting temperature at 210 °C and 240 °C, samples exhibit similar scattering patterns to (173, 0.78)-Q, demonstrating that these LLMLL materials are microphase separated above the melting temperature. The high molar mass of these polymers contributes to high order-disorder transition temperatures (T_{ODT}), resulting in melt microstructure being maintained in LLMLL samples.[10]

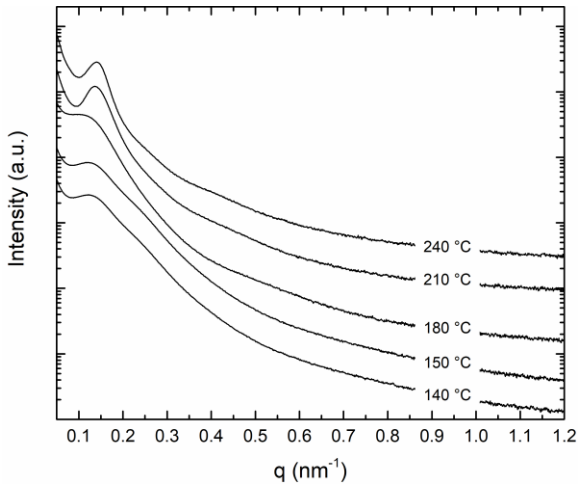

Figure A.6.
Small-angle X-ray scattering patterns at the indicated temperatures of LLMLL (173, 0.78).

Block polymers LLMLL and homopolymer PLLA processed with different thermal histories were tested in uniaxial extension until failure. Representative stress-strain curves are shown in Figure A.7. The ultimate tensile strength (σ_B), strain

at break (ε_B), Young's modulus (E), and tensile toughness (area under the stress-strain curve) are reported as average values with the standard deviation (Table A.2). Some of the reported strain at break values are likely underestimates as imperfections at the edges of the tensile bars resulted in early failure, which also increased the standard deviation of these values. Samples were aged over 48 h after processing; the impact of aging time on the tensile properties were not considered and could be an area of future investigation.

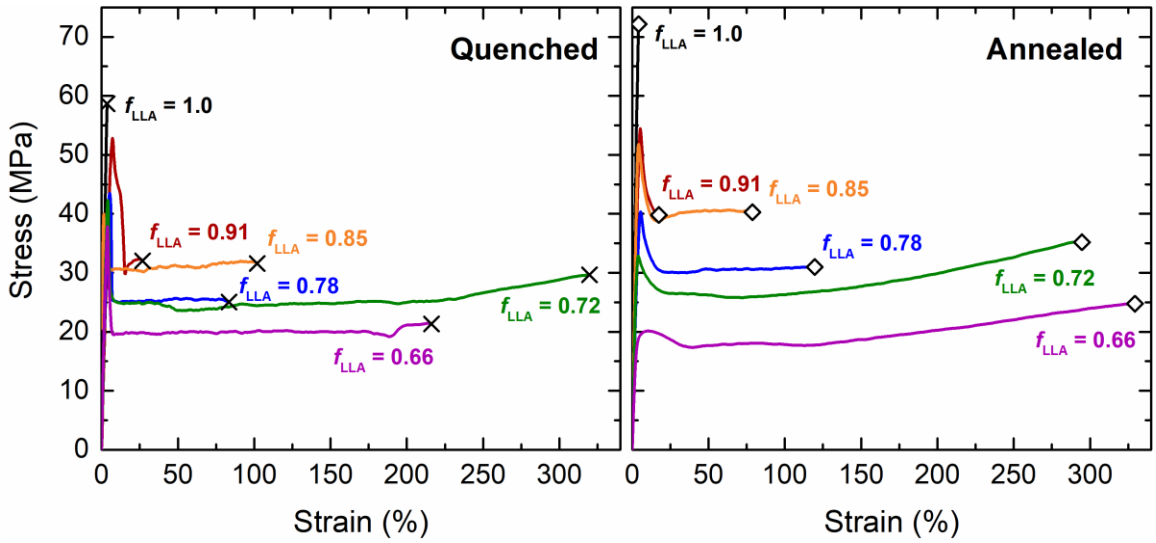

Figure A.7.
Representative stress strain curves of quenched and annealed samples, extending at 5 mm min^{-1}.

Homopolymer PLLA is strong and brittle, exhibiting high stress at break (58.2 ± 9.2 MPa) and low strain at break <5%. Annealing the polymer to higher degree of crystallinity increases the stress at break (73.1 ± 7.9 MPa) at similar strain at break, consistent with literature.[1] The opposite trend is observed in LLMLL triblock

polymer samples with the exception of LLMLL (169, 0.91), which has identical properties before and after annealing. Quenched LLMLL generally exhibits higher ultimate tensile strength and higher strains at break when compared to the annealed samples. The largest difference between quenched and annealed samples is the trend in the yield stress where enhanced crystallinity results in a decrease in yield stress. This difference becomes more pronounced with decreasing f_{LLA}; samples with higher PLLA content have similar yield stress values while low PLLA content exhibits a large difference between yield stress values. Overall, a decrease in f_{LLA} results in a decrease in the ultimate tensile strength and increase in strain at break, consistent with reports in literature.[9,15]

Incorporating 9 vol% PMCL in PLLA, LLMLL (169, 0.91), results in a significant change in mechanical properties when compared to PLLA. Upon extension, LLMLL (169, 0.91) extends to 27% strain before breaking. This results in an increased toughness (10 – 11 MJ m^{-3}) compared to homopolymer PLLA (1.6 – 1.9 MJ m^{-3}). Furthermore, LLMLL exhibits a high yield stress and high modulus, demonstrating the desirable properties of PLLA are not compromised when toughness is increased. The stress-strain behavior of LLMLL (169, 0.91) is comparable to multiblock polymers (poly(D,L-lactide)-*b*-polybutadiene)$_n$ (86, 0.90) (σ_B = 29 MPa, ε_B = 32%, E = 1.3 GPa) and PLLA blends (e.g. ~10% poly(ethylene oxide) (PEO) in PLLA).[3,16] Regardless of the architecture, incorporating 10 vol% of a rubbery block can drastically improve the tensile toughness of PLLA. The

increased PLLA toughness previously observed in multiblock polymers and blends can be achieved through simple ABA triblock polymers.

LLMLL (148, 0.72) exhibits a strain at break ~300% leading to the highest tensile toughness values (77 – 91 MJ m^{-3}) observed in the LLMLL system. A similar polymer composition is reported by Panthani and coworkers in PLLA-*b*-poly(ethyl-*co*-ethylene)-*b*-PLLA (LLELL) with the corresponding chain-extended multiblock polymers $(LLE)_n$.[5] The multiblock polymer $(LLE)_n$ (37.8, 0.7) exhibits similar tensile properties as processed (σ_B = 24 MPa, ε_B = 632%, E = 0.55 GPa, σ_y = 28 MPa) compared to the annealed derivative (σ_B = 22 MPa, ε_B = 422%, E = 0.67 GPa, σ_y = 31 MPa). LLMLL does not exhibit as high of an elongation at break as $(LLE)_n$ at this composition. Yet, LLMLL exhibits higher Young's modulus, higher yield stress, and higher ultimate tensile strength demonstrating stiffer properties overall (σ_B = 30–36 MPa, ε_B = 294–308%, E = 1.2–1.4 GPa, σ_y = 32–41 MPa).

While the multiblock approach taken by Panthani et al and Lee et al are an effective method to improve the toughness of PLLA, the results of LLMLL demonstrate that tough PLLA can be achieved through a simple triblock polymer architecture with high molar mass.[5,16] Additionally, the low stiffness and low ultimate tensile strength that is observed in multiblock polymers and blends are able to be mitigated in high molar mass LLMLL.

A.3. Conclusion

We report the synthesis and tensile properties of high molar mass LLMLL with various composition. Increasing the crystallinity by annealing has a minor impact on the tensile properties, becoming more significant with lower f_{LLA}. The thermal history has an impact on the microstructure. Though due to the high molar masses used in this study, the polymers do not exhibit crystalline breakout supported by TEM and SAXS results. The toughness of PLLA was increased by decreasing the f_{LLA} to 0.72. The use of semicrystalline PLLA and high molar mass (>100 kg mol^{-1}) resulted in the block polymers maintaining Young's modulus > 1 GPa. We demonstrate this use of high molar mass block polymers with semicrystalline PLLA blocks as an effective method to achieve tough PLLA.

A.4. Experimental methods

Most of the synthesis and characterization methods for Appendix A followed the same experimental methods as reported in Chapter 3. Deviations from those methods are outlined below. TA Instruments Discovery DSC was used to determine thermal properties. Samples loaded into hermetically sealed aluminum DSC pans were cooled to −75 °C then heated to 200 °C at 10 °C min^{-1} to determine percent crystallization in the processed samples. The glass transitions and peak melting temperatures reported are from the second heat.

Tensile Testing: Uniaxial tensile tests were performed on a Shimadzu AGS-X 50 kN tabletop tensile tester at room temperature (20–22 °C). Polymer films with a thickness ~0.6 mm were prepared using a Wabash hot press at a temperature of 180 °C, heating without pressure for 3 min then compressing at 4000 lbs for 4 min then quenched at 35 °C min^{-1}. Half of each sample was placed back into the hot press at 100 °C for ten minutes to promote PLLA crystallite growth, before being cooled at 35 °C min^{-1}. All samples were stored at room temperature for at least 48 h before testing. Specimens were drawn until failure at a constant rate of 5 mm min^{-1}. Stress ($\sigma = F/A_0$) was calculated from the applied force (F) and the initial cross-sectional area of the gauge (A_0); strain ($\varepsilon = (l - l_0)/l_0 \times 100$) was determined from the change in grip-to-grip distance ($l - l_0$) and the initial gauge length (l_0). Young's modulus (E) was obtained from the slope of the linear regime of the stress−strain curve. Tensile toughness was determined by taking the area beneath the stress-strain curve over the full range of elongation. At least six specimens were tested for each sample and all statistics reported are the average values obtained.

A.5. References

(1) *Poly(Lactic Acid): Synthesis, Structures, Properties, Processing, and Applications*; Auras, R. A.; Lim, L.-T.; Selke, S. E. M.; Tsuji, H., Eds.; John Wiley & Sons, Inc.: Hoboken, NJ, USA, 2010.

(2) Anderson, K. S.; Schreck, K. M.; Hillmyer, M. A. Toughening Polylactide. *Polym. Rev.* **2008**, *48*, 85–108.

(3) Liu, H.; Zhang, J. Research Progress in Toughening Modification of Poly(Lactic Acid). *J. Polym. Sci. Part B Polym. Phys.* **2011**, *49*, 1051–1083.

(4) Wu, S. Phase Structure and Adhesion in Polymer Blends: A Criterion for Rubber Toughening. *Polymer* **1985**, *26*, 1855–1863.

(5) Panthani, T. R.; Bates, F. S. Crystallization and Mechanical Properties of Poly(L-Lactide)-Based Rubbery/Semicrystalline Multiblock Copolymers. *Macromolecules* **2015**, *48*, 4529–4540.

(6) Yu, T.; Ren, J.; Gu, S.; Yang, M. Preparation and Characterization of Biodegradable Poly(Lactic Acid)-block-Poly(ε-Caprolactone) Multiblock Copolymer. *Polym. Adv. Technol.* **2010**, *21*, 183–188.

(7) Anderson, K. S.; Hillmyer, M. A. The Influence of Block Copolymer Microstructure on the Toughness of Compatibilized Polylactide/Polyethylene Blends. *Polymer* **2004**, *45*, 8809–8823.

(8) Nagarajan, V.; Mohanty, A. K.; Misra, M. Perspective on Polylactic Acid (PLA) Based Sustainable Materials for Durable Applications: Focus on Toughness and Heat Resistance. *ACS Sustain. Chem. Eng.* **2016**, *4*, 2899–2916.

(9) Perego, G.; Cella, G.; Bastioli, C. Effect of Molecular Weight and Crystallinity on Poly (Lactic Acid) Mechanical Properties. *J. Appl. Polym.* **1996**, *59*, 37–43.

(10) Nandan, B.; Hsu, J.; Chen, H. Crystallization Behavior of Crystalline-Amorphous Diblock Copolymers Consisting of a Rubbery Amorphous Block. *J. Macromol. Sci. Part C Polym. Rev.* **2006**, *46*, 143–172.

(11) *The Physics of Glassy Polymers*, 2nd ed.; Haward, R. N.; Young, R. J., Eds.; Chapman & Hall: London, 1997.

(12) Miyata, T.; Masuko, T. Crystallization Behaviour of Poly(l-Lactide). *Polymer* **1998**, *39*, 5515–5521.

(13) Ho, C. H.; Jang, G. W.; Lee, Y. Der. Crystallization of Poly(l-Lactide-Dimethyl Siloxane-l-Lactide) Triblock Copolymers and Its Effect on Morphology of Microphase Separation. *Polymer* **2010**, *51*, 1639–1647.

(14) Müller, A. J.; Balsamo, V.; Arnal, M. L. Nucleation and Crystallization in Diblock and Triblock Copolymers. *Adv. Polym. Sci.* **2005**, *190*, 1–63.

(15) Kulinski, Z.; Piorkowska, E. Crystallization, Structure and Properties of Plasticized Poly(L-Lactide). *Polymer* **2005**, *46*, 10290–10300.

(16) Lee, I.; Panthani, T. R.; Bates, F. S. Sustainable Poly(Lactide-b-Butadiene) Multiblock Copolymers with Enhanced Mechanical Properties. *Macromolecules* **2013**, *46*, 7387–7398.

Appendix B.

Chemically recyclable polyurethane foams from poly(γ-methyl-ε-caprolactone) †

† The work in this chapter was carried out in collaboration with Emily Abdo and Derek C. Batiste. SEM images were obtained with help from Sebla Onbulak.

B.1. Introduction

Flexible polyurethane (PU) foams are used in a variety of applications such as furniture, packaging, and other cushioning applications.[1] PU foams are thermosets predominantly composed of polyols crosslinked with isocyanates, derived from petrochemical feedstocks. Sustainable PU foam development has focused on the use of renewable feedstocks.[2,3] However, the recycling of PUs is a considerable challenge in the current waste management infrastructure due to their covalently crosslinked nature. Chemical recycling methods have gained attention as the original polyol can be recovered through glycolysis or hydrolysis. Due to the equilibrium nature of the urethane exchange reaction in chemical recycling, obtaining the original polyol with no oligomers is a challenge.[4] The recycled material cannot act as a drop-in replacement for pristine polyol due to this oligomer impurity.[5,6]

The use of polyesters is of interest for PU applications due to the potential to derive starting materials from renewable feedstocks and the ability for the polymers to degrade through hydrolysis. Even more desirable in tuning the properties of PU foams, control over architecture and molar mass can be achieved in the ring-opening transesterification polymerization (ROTEP) of cyclic esters. Biobased PUs from β-methyl-δ-valerolactone (MVL) were demonstrated to be chemically recyclable to recover high purity monomer.[7] The low ceiling temperature T_c of MVL (226 °C in bulk and 27 °C in 1 M solution) provides an excellent system for chemical recycling, as the unzipping of the polymer to form monomer becomes more favorable at elevated temperature.[8] Due to these same properties, however, the polymerization of

MVL requires low temperatures to achieve high conversions. In contrast to the glycolysis/hydrolysis of PU foams to yield the original polyol and their oligomers, the reverse ROTEP reaction recovers high value monomer for reuse towards any future application.

As demonstrated in Chapter 3, we are interested in the use of γ-methyl-ε-caprolactone (MCL) as a sustainable monomer due to its thermodynamic (T_c > 500 °C in bulk and > 250 °C in 1 M solution) properties that yield high conversions at elevated temperatures.[9] Poly(MCL) (PMCL) is an amorphous, low-T_g polymer that can be derived from renewable feedstocks and is degradable under enzymatic hydrolysis conditions.[10,11] Herein, we report the change in the properties of PMCL flexible foams as the formulations are modified. Preliminary results demonstrate the impact of changing the formulation on the cell structure. Taking advantage of the reversible nature of ROTEP, we explore the chemical recyclability of PMCL foams to recover MCL monomer.

B.2. Results and discussion

To obtain flexible foams, low molar mass PMCL-triol (3.4 kg mol^{-1}) was synthesized using previously reported methods (Chapter 3). In the foam formulation, toluene diisocyanate (TDI) reacts to form the hard segment, water is the blowing agent, amine catalysts promote the reaction of isocyanate with polyol and water, and surfactant stabilizes bubble formation (Scheme B.1). PMCL foams exhibit properties in compression that are consistent with commercial flexible polyurethane foams (Table

B.1, Figure B.1). Due to the uneven foam dimensions, a positive force was applied to ensure the full surface of the foam was in contact with the testing plates (Figure B.1). The compressive strength was determined as the stress at 50 % compression (σ_{50}). The compressive modulus (K) was taken as the slope of the linear portion of the stress-strain curve. PMCL foams exhibited similar modulus, ranging from 7 to 15 kPa, regardless of the formulations. The compressive strength and compressive modulus for PMCL foams synthesized are on the same order of magnitude as the commercial foam tested.

Scheme B.1.
Synthesis of foams from MCL

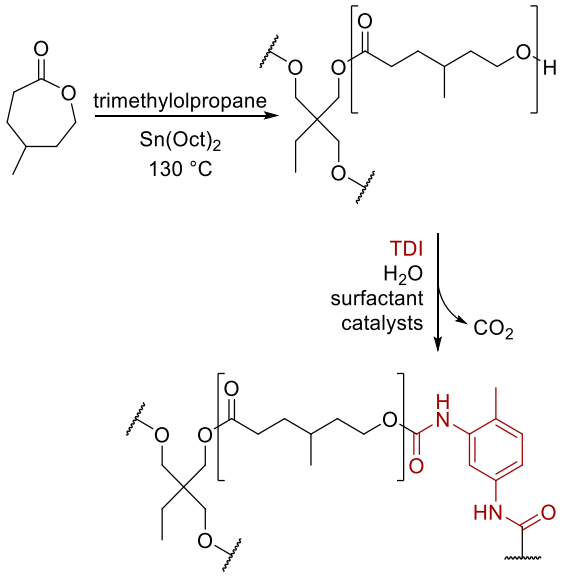

Table B.1.
Summary of properties of PMCL PU foams

Sample ID	Isocyanate index	Surfactant	σ_{50}[a] (kPa)	K[b] (kPa)	Hysteresis[c] Cycle 1 (J)	Hysteresis[c] Cycle 20 (J)
II70-D	70	Dabco 5164	3.7 ± 0.6	12 ± 8	47 ± 7	31 ± 8
II70-DC	70	Dow corning 5987	9.0 ± 0.8	13 ± 5	35 ± 1	21 ± 1
II100-D	100	Dabco 5164	8.1 ± 1.3	15 ± 3	43 ± 3	32 ± 3
II100-D-2[d]	100	Dabco 5164	2.8	7.0	28	15
Commercial	NA	NA	4.9 ± 0.3	17 ± 2	26 ± 1	NT

Three samples were tested in compression and the average values are reported with the standard deviation. [a]the stress at 50% compression; [b]compression modulus taken as the slope of the low strain region; [c]the energy loss between the compression and relaxation cycle; [d]only one sample was tested thus no standard deviation is reported. NA = not available. NT = not tested.

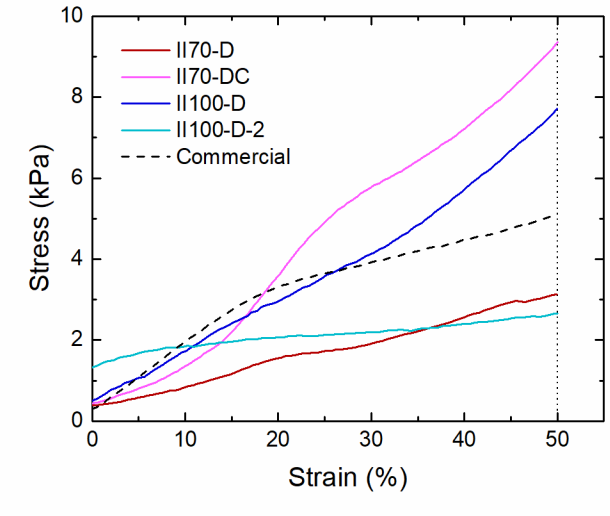

Figure B.1.
Compression of PMCL foams compared to a commercial foam, compressing at 12 mm min^{-1}. The initial positive stress is applied to ensure full contact of the foam on the testing plates.

Changing the isocyanate index in flexible PU foams impacts the cell size, cell morphology, and density. These factors ultimately impact the mechanical properties of the foam. Keeping the water content and surfactant identity the same, PMCL foams with

isocyanate index of 70 (II70-D) and 100 (II100-D) were compared. II100-D exhibits a higher compressive strength of 8.1 ± 1.3 kPa than II70-D, 3.7 ± 0.6 kPa. These foams were tested under cyclic compression to 50% strain for 20 cycles (Figure B.2). II100-D and II70-D exhibit similar hysteresis at each cycle (Table B.1). However, after allowing the foam to rest for 10 min, II100-D exhibits very similar stress-strain behavior as the first compression cycle, recovering the original compression strength after resting. II70-D does not recover the original properties, exhibiting lower compression strength after rest (Figure B.2). For these PMCL foams, a higher amount of isocyanate maintains foam properties after multiple compressions. The increased isocyanate index also results in larger cell sizes (Figure B.3). In summary, the higher ratio of TDI in II100-D results in higher compression strength with better recovery and larger pore sizes when compared to II70-D.

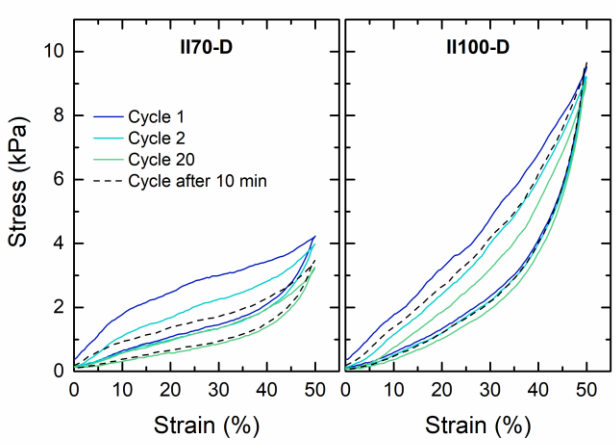

Figure B.2.
Hysteresis of II70-D and II100-D in compression at 12 mm min^{-1}. Dashed line indicates the cycle after resting the sample for 10 min after the 20th cycle.

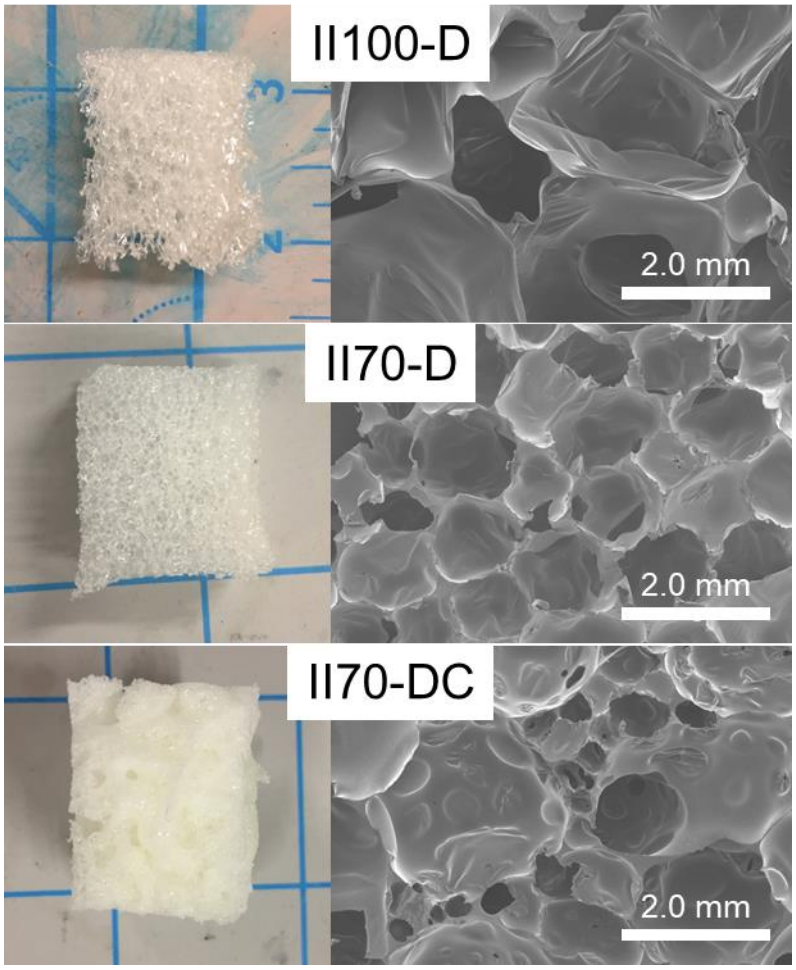

Figure B.3.
Pictures (left) and SEM images (right) of PMCL foam samples.

Surfactants in the formulation stabilize the CO_2 bubbles and ultimately impacts the cell size and structure.[12] The microphase separation of the hard segment and the covalent crosslinks trap the foam morphology. Two different surfactants were used to modify the properties of the foams with an isocyanate index of 70. Dabco 5164 (II70-D) is a silicone surfactant that typically forms a course cell structure. Dow Corning 5987 (II70-DC) is a silicone surfactant that is advertised to provide a fine cell structure. SEM images of PMCL foams show both samples have a mostly closed cell structure with no obvious

directionality. The cells in II70-DC exhibit a wide range of cell sizes in the sample area with a small number of open cells. In contrast, II70-D exhibits uniform cell structure and cell size. II70-DC exhibits the highest compression modulus 9.0 ± 0.8 kPa of the samples tested. More work is necessary to determine if other surfactants and additives can be used to yield open-cells with uniform cell size in PMCL foams.

Water in the formulation acts as the blowing agent, forming CO_2 gas upon reaction with isocyanate groups. Preliminary experiments were conducted to observe the impact of changing the water content in foams. Less water was added to the formulation of II100-D-2 (0.06 mL, 5 g scale) than II100-D (0.10 mL, 5 g scale) to produce less CO_2 gas. This resulted in a 2.5 cm rise compared to the 3.5 cm rise in II100-D. This formulation change resulted in foams with very low compression strength of 2.8 kPa. Due to the small 5 g scale of these foams, more samples were not able to be obtained from the core for testing. Future work on scaling up the foams and further characterization is important to understand how this formulation change impacts the cell morphology.

There are a variety of mechanisms that occur during thermal degradation of polyesters, affected by the amount of residual catalyst and water. Possible degradation mechanisms include hydrolysis, depolymerization, transesterification, and random chain scission.[13] This degradation results in low molecular weight compounds ranging from chain scission products, monomers, cyclic oligomers, and other small molecules. Taking advantage of the zipper-like depolymerization, cyclic monomers can be recovered from polyesters. This depolymerization of polyesters has long been utilized in the process to manufacture lactide.[14] Additionally, our group has previously demonstrated the chemical

recyclability of PMVL PU foams to recover the relatively stable 6-membered lactone.[7] Even though 7-membered lactones are more stable and have a higher ceiling temperature than MVL and lactide, ε-caprolactone has been recovered through depolymerization.[15] The chemical recycling of thermosets to recover monomer is one method towards achieving a circular economy for plastics by closing the loop in the plastic life cycle.[16]

Based on previous reports of the depolymerization of polycaprolactone and its derivatives, we wanted to demonstrate the ability to recover of MCL from PU foams. The crosslinking urethane linkages are thermally stable up to 180 °C. The thermal decomposition temperature at 5% weight loss for PMCL polyol $T_{d,5\%}$ = 251 °C and for PU foam II100-D $T_{d,5\%}$ = 247 °C were measured using thermogravimetric analysis (Figure B.4). These thermal decomposition temperatures are essentially the same. Even though the isocyanate bond can revert to form an alcohol end group at elevated temperatures (> 180 °C), the thermal decomposition of PMCL does not release to release volatile molecules until ~250 °C. The chemical recycling of PU foam (II70-D) was carried out in the presence of $Sn(Oct)_2$ catalyst, heating to 270 °C under reduced pressure. The depolymerized monomer was distilled away and collected as a clear liquid (74% recovery by mass). Analysis by ^{1}H NMR spectroscopy and GC-MS demonstrate pure MCL monomer is collected with no higher order oligomers (Figure B.5). Achieving 100% recovery would require optimization to limit other thermal decomposition reactions that do not yield cyclic monomer at these temperatures.

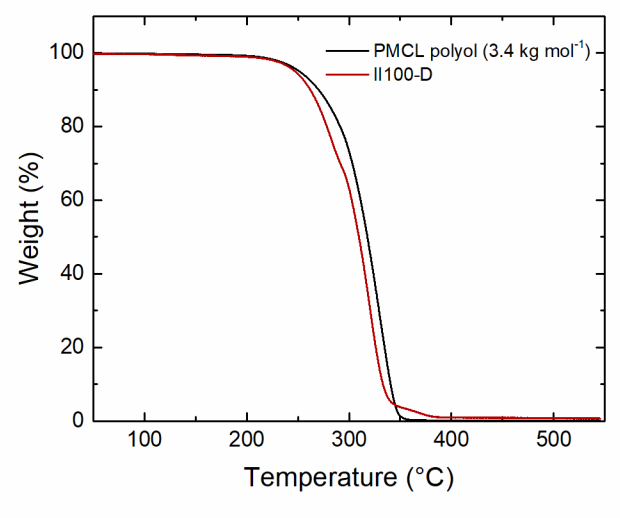

Figure B.4.
Thermogravimetric analysis of PMCL polyol and II100-D foam, heating 10 °C min^{-1} under nitrogen.

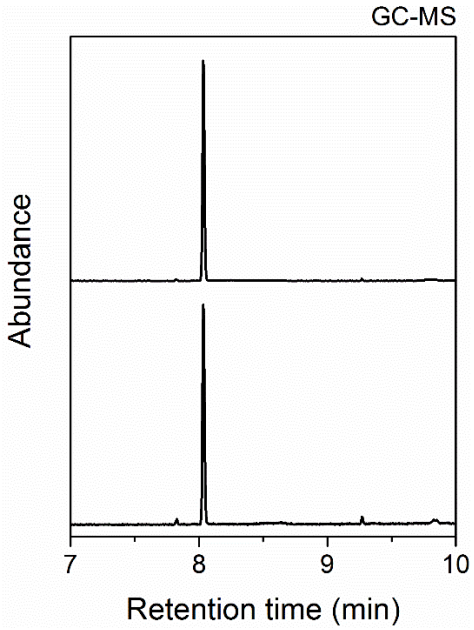

Figure B.5.
Gas chromatograph of MCL monomer as synthesized (top) and recovered from PU foam (bottom).

B.3. Conclusion

The mechanical performance and cell structure of PMCL-based PU foams can be modulated through changing the surfactant identity, amount of blowing agent, and isocyanate index in formulations. These preliminary results demonstrate that higher isocyanate indices result in foams that can withstand higher stress at similar compressions. We observe mostly closed-cell structure of the foams synthesized in this study. Overall, these PMCL foams have similar compression behavior as flexible foams available commercially. Additionally, we have demonstrated the ability to chemically recycle these foams to yield pure monomer through distillation.

Further work in using higher molar mass polyol (6 – 12 kg mol^{-1}) would be of interest as this can provide foams with different properties such as higher resiliency and tear strength. Additionally, low-density open-cell PU foams could be achieved through changing the surfactant, adding additives, optimizing processing, and/or modifying the relative ratios of isocyanate and water in the formulation. Work on the general chemical recyclability of PMCL-based materials are ongoing.

B.4. Experimental methods

General methods

Dabco 5164, Dabco 5179, Dow Corning 5987, N,N-dimethylcyclohexylamine (DMCHA), N,N,N',N'',N'''-pentamethyldiethylenetriamine (PMDETA), and

toluene diisocyanate (TDI) were used as received. γ-methyl-ε-caprolactone was synthesized as previously described in Chapter 3.

Bruker Avance III 500 was used for ^{1}H NMR spectroscopy and molar masses were calculated from end-group analysis. Thermogravimetric analysis was conducted in nitrogen atmosphere using a TA instruments TGA Q500 heating at 10 °C min^{-1}. Samples from the core of the foam was cut out using a razor with dimensions 10 (w) x 8 (d) x 8 (h) mm for compression testing. Samples were tested using Shimadzu Autograph AGS-X Tensile Tester with modified compression plates and a compression rate of 12 mm min^{-1}. GC-MS was collected using an Agilent 6890 GC equipped with a HP-5ms column (30 m x 0.25 mm) and Agilent 5973 MS detector. The method used in GC-MS held the sample at 50 °C for 1.5 min, heated to 250 °C at 20 °C min^{-1}, and then finally held at 250 °C for 3.5 min. For SEM imaging, foam samples were sputtered with iridium (5 nm thickness) and imaged with 5 kV field.

PMCL synthesis

A pressure vessel was equipped with γ-methyl-ε-caprolactone (50 g, 0.39 mol), trimethylolpropane (2.4 g, 17 mmol), and $Sn(Oct)_2$ (0.16 g, 0.39 mmol) in a glovebox and sealed. The reaction vessel was heated to 130 °C and left to react for 1.5 h, then cooled in an ice bath. The polymer was diluted in chloroform and precipitated into cold methanol. The polymer phase separated to a layer at the bottom of the beaker, methanol was decanted. The clear, colorless liquid polymer was dried *in vacuo*. The polymer was stored in a desiccator and dried before use.

General foam synthesis

One of two methods were to homogenize the formulations: (i) hand mixing with a metal spatula and (ii) prop-mixing using a propeller pixer equipped with a 0.5" pitched 3-blade impeller and operated at 5000 RPMs for ~ 10 s. Poly(γ-methyl-ε-caprolactone) (4.0 g) was homogenized with DMCHA (11.8 μL), PMDETA (12.1 μL), DI water (0.12 mL), surfactant Dabco 5164 or Dow Corning 5987 (0.12 mL), and TDI (0.6 mL). The foam was left undisturbed to rise and cure over 24 h. Table B.2 lists the formulations of PU foams. The formulation variables studied were TDI volume, DI water volume, and surfactant identity. The formulation was modified as necessary to maintain a consistent batch size of 5 g. The core of the foam was cut out for further testing.

Table B.2.
Formulation table for foams tested in this work.

Sample ID	Surfactant	PMCL polyol (g)	DMCHA (μL)	PMDETA (μL)	Surfactant (mL)	DI water (mL)	TDI (mL)	Rise (cm)
II70-D	Dabco 5164	3.78	11.10	11.40	0.11	0.11	0.79	+2.0
II70-DC	Dow corning 5987	3.78	11.10	11.40	0.11	0.11	0.80	−6.0
II100-D	Dabco 5164	3.49	10.30	10.50	0.10	0.10	1.10	+3.5
II100-D-2	Dabco 5164	3.93	11.60	11.85	0.11	0.06	0.72	+2.5

Depolymerization

A sample of foam (3 g, 80 wt% PMCL) was cut into small pieces and placed in a round-bottom flask with $Sn(Oct)_2$ (10.6 mg) and a stir bar. The vessel was heated to 270 °C under vacuum (100 – 500 mtorr) and the distillate was collected as a clear colorless liquid (1.77 g, 74% recovery).

B.5. References

(1) Akindoyo, J. O.; Beg, M. D. H.; Ghazali, S.; Islam, M. R.; Jeyaratnam, N.; Yuvaraj, A. R. Polyurethane Types, Synthesis and Applications-a Review. *RSC Adv.* **2016**, *6*, 114453–114482.

(2) Ugarte, L.; Saralegi, A.; Fernández, R.; Martín, L.; Corcuera, M. A.; Eceiza, A. Flexible Polyurethane Foams Based on 100% Renewably Sourced Polyols. *Ind. Crops Prod.* **2015**, *62*, 545–551.

(3) Sardon, H.; Pascual, A.; Mecerreyes, D.; Taton, D.; Cramail, H.; Hedrick, J. L. Synthesis of Polyurethanes Using Organocatalysis: A Perspective. *Macromolecules* **2015**, *48*, 3153–3165.

(4) Molero, C.; de Lucas, A.; Romero, F.; Rodríguez, J. F. Glycolysis of Flexible Polyurethane Wastes Using Stannous Octoate as the Catalyst. *J. Mater. Cycles Waste Manag.* **2009**, *11*, 130–132.

(5) Simón, D.; de Lucas, A.; Rodríguez, J. F.; Borreguero, A. M. Flexible Polyurethane Foams Synthesized Employing Recovered Polyols from Glycolysis: Physical and Structural Properties. *J. Appl. Polym. Sci.* **2017**, *134*, 1–9.

(6) Akindoyo, J. O.; Beg, M. D. H.; Ghazali, S.; Islam, M. R.; Jeyaratnam, N.; Yuvaraj, A. R. Polyurethane Types, Synthesis and Applications-a Review. *RSC Adv.* **2016**, *6*, 114453–114482.

(7) Schneiderman, D. K.; Vanderlaan, M. E.; Mannion, A. M.; Panthani, T. R.; Batiste, D. C.; Wang, J. Z.; Bates, F. S.; Macosko, C. W.; Hillmyer, M. A. Chemically Recyclable Biobased Polyurethanes. *ACS Macro Lett.* **2016**, *5*, 515–518.

(8) Schneiderman, D. K.; Hillmyer, M. A. Aliphatic Polyester Block Polymer Design. *Macromolecules* **2016**, *49*, 2419–2428.

(9) Olsén, P.; Odelius, K.; Albertsson, A.-C. Thermodynamic Presynthetic Considerations for Ring-Opening Polymerization. *Biomacromolecules* **2016**, *17*, 699–709.

(10) Watts, A.; Kurokawa, N.; Hillmyer, M. A. Strong, Resilient, and Sustainable Aliphatic Polyester Thermoplastic Elastomers. *Biomacromolecules* **2017**, *18*, 1845–1854.

(11) De Hoe, G. X.; Zumstein, M. T.; Tiegs, B. J.; Brutman, J. P.; McNeill, K.; Sander, M.; Coates, G. W.; Hillmyer, M. A. Sustainable Polyester Elastomers from Lactones: Synthesis, Properties, and Enzymatic Hydrolyzability. *J. Am. Chem. Soc.* **2018**, *140*, 963–973.

(12) Zhang, X. D.; Macosko, C. W.; Davis, H. T.; Nikolov, A. D.; Wasan, D. T. Role of Silicone Surfactant in Flexible Polyurethane Foam. *J. Colloid Interface Sci.* **1999**, *215*, 270–279.

(13) Södergård, A.; Stolt, M. Properties of Lactic Acid Based Polymers and Their Correlation with Composition. *Prog. Polym. Sci.* **2002**, *27*, 1123–1163.

(14) *Poly(Lactic Acid): Synthesis, Structures, Properties, Processing, and Applications*; Auras, R. A.; Lim, L.-T.; Selke, S. E. M.; Tsuji, H., Eds.; John Wiley & Sons, Inc.: Hoboken, NJ, USA, 2010.

(15) Nelißen, M.; Keul, H.; Höcker, H. Ring-Closing Depolymerization of Poly(ε-Caprolactone). *Macromol. Chem. Phys.* **1995**, *196*, 1645–1661.

(16) Hong, M.; Chen, E. Y.-X. Chemically Recyclable Polymers: A Circular Economy Approach to Sustainability. *Green Chem.* **2017**, *19*, 3692–3706.

Appendix C.

Life cycle assessment of γ-methyl-ε-caprolactone[†]

[†] The work in this chapter was carried out in part in collaboration with Rylie E.O. Pelton and Timothy M. Smith in the Department of Bioproducts and Biosystems Engineering, University of Minnesota. Funding support provided by the Center for Sustainable Polymers and NorthStar Initiative for Sustainable Enterprise, Institute on the Environment.

C.1. Introduction

In Chapter 1, the sustainability considerations in feedstock, production, lifetime, recycling, and end-of-life in plastics were briefly described. Addressing some of these topics, the work of this dissertation has utilized a compound, γ-methyl-ε-caprolactone (MCL). MCL was used to produce a wide range of plastics that compete with commercially available materials: thermoplastic elastomers (Chapter 3 and 4), tough polylactide (Appendix A), and soft polyurethane foams (Appendix B). In this section, the environmental impact of feedstock choice on the production of MCL is quantified through a preliminary life cycle assessment (LCA).

The chemical industry relies on raw materials derived from fossil-fuels, e.g. coal, natural gas, and oil. This industry alone accounts for 6% of total energy consumption, making it one of the most energy-intensive industrial sectors.[1] The energy source structure continues to change as economically feasible processes are developed. Oil used to meet 25% of world energy consumption in 1950, increasing to 36% in 1999. Within this same time span, coal's shares decreased from ~60% of world energy consumption to 23%.[1] The increase in energy demand, decrease in supply, and concerns regarding global warming have led to the exploration of alternate sources to meet future energy requirements. However, the chemical industry continues to rely heavily on non-renewable fossil feedstocks for raw materials.

A large factor in the future of chemical feedstocks is economic viability and availability of resources. While synthetic ethanol production from ethylene in the US

is dictated by external economic factors, Japan and Germany have relied mostly on agricultural ethanol where price is less impacted by the market.[1] As petroleum resources are depleted, there will be increasing competition between use for energy production vs. chemical feedstock. Current estimates predict that the reserves of oil, natural gas, and coal will meet energy demands for a long time.[1] However, there are concerns regarding the environmental impacts (e.g. CO_2 release) of extracting this energy through coal mining, oil sands extraction, etc. History has shown that an industry once heavily reliant on coal can adapt to different feedstocks, e.g. oil and natural gas. With supply changes and improved processes, the chemical industry will also change to utilize abundant and cost-effective resources.

There are many parameters that chemists can address to improve the sustainability of a product.[2] Due to broad and imprecise definitions of sustainability, we set out to quantify the environmental impacts of MCL production through LCA. First, the data and information on the raw materials, production, and use of a product during its lifetime are collected. The entire picture of the process is considered, including transportation, energy consumption, water usage, waste handling, etc. The social, environmental, and economic impacts are evaluated in the following categories: ozone depletion, global warming, acidification, eutrophication, and human health (cancer and non-cancer). One of the complications in conducting an LCA is the availability of inventory information of a process, as it is likely proprietary and inaccessible. When processes are not available in inventory databases, the assessment is reliant on published literature. The impact assessment

in LCAs should not be interpreted as the absolute conclusion for the use of one product over another. Instead, it can be utilized to highlight the areas in which improvements can be made.

The work in Chapter 3 outlines the scalable synthesis of MCL via the Baeyer-Villiger oxidation of 4-methylcyclohexanone, a commercially available reagent sourced from cresols derived from coal and oil (Figure C.1). The transformation of a renewable feedstock, pulegone, can yield MCL directly; however, the process requires many synthetic transformations resulting in low overall yield.[3] One way to approach the use of renewable feedstocks is to consider the formation of the precursors to MCL. The production of aromatic compounds from renewable resources is a growing area of research. This section investigates the LCA of the process to form MCL from various feedstocks through a *p*-cresol intermediate (Figure C.).

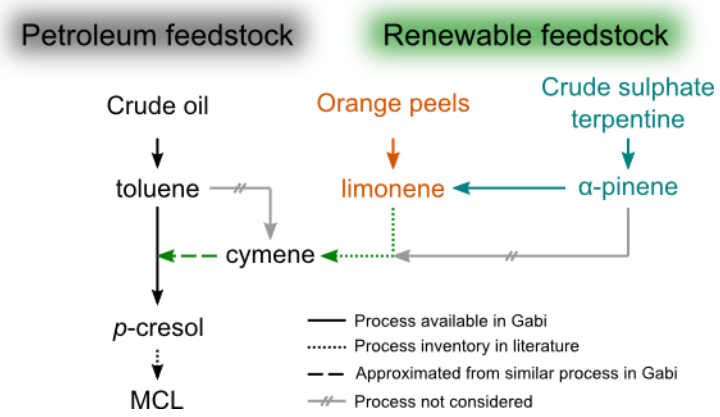

Figure C.1.
Process to form MCL from crude oil, orange peels, and crude sulphate turpentine.

C.2. Results and discussion

Although cresols exist in nature, they are produced commercially from toluene found in fossil fuels.[4] Toluene is first isolated from a mixture of benzene, toluene, and xylene (BTX).[1] BTX is obtained from hard coal, reformate gasoline, and pyrolysis gasoline. Sulfonation of toluene and subsequent treatment with a strong base yields cresols (Scheme C.1). In this process, *o*-cresol is a minor byproduct, able to be separated from *p*-cresol by distillation. Another method for industrial production of cresols rely on alkylation of toluene, discussed later in this section. The inventory data available for this process is the sulfonation of toluene that is isolated from reformate gasoline (Figure C.1).

Scheme C.1.
Sulfonation of toluene to produce *p*-cresol.

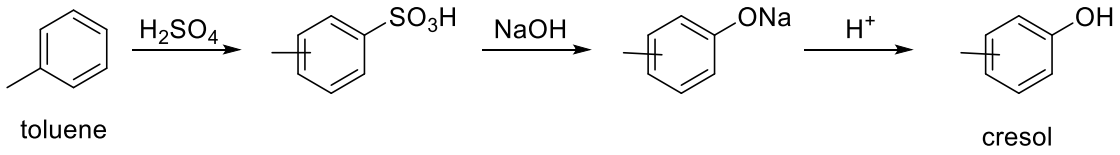

Cresols have the potential to be produced from renewable feedstocks through a *p*-cymene intermediate (Figure C.1). In fact, Hercules Powder Co. produced *p*-cresol industrially from monocyclic terpenes extracted from crude sulphate terpentine (CST) until 1972.[5] CST is a renewable feedstock that is a byproduct of the Kraft pulping process.[6,7] We consider two terpenes, limonene and α-pinene, that can be converted to *p*-cymene (Figure C.1). CST has a large fraction of α-pinene (40 – 90%) that can be isomerized to yield limonene; additionally, limonene can be extracted directly from orange peels obtained during the production of orange juice.[8] Due to the large amount of waste in citrus

processing (ca. 15 million tons per year), there has been interest in valorizing the waste products through the production of limonene and pectin.[9,10] Inventory information is available to produce limonene from orange peels and crude sulphate turpentine (Figure C.1). Dehydrogenation of limonene produces *p*-cymene (Scheme C.2). Although the industrial process inventory is not available, the process information for this transformation reported in a technoeconomic analysis is used in this work.[11]

Scheme C.2.
Limonene to cymene process

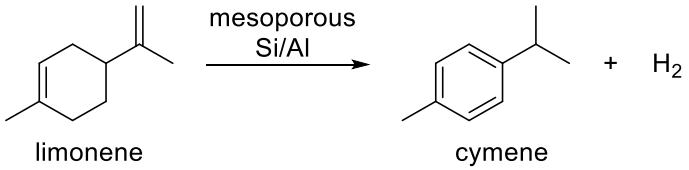

The cymene to cresol process is analogous to the cumene process, developed by Hock and Lang in 1944 and used industrially since 1953.[1] The oxidation of *p*-cymene and subsequent hydroperoxide cleavage results in the formation of *p*-cresols (Scheme C.3).[4] This cymene/cumene process is currently used commercially by Sumitomo Chemical and Mitsui, operating plants with a capacity of 10 thousand tons per year.[12] The cymene process has been used industrially to convert toluene to cresol, though the main source of cresols today is from the sulfonation process (Scheme C.1).[12] Since the propylation of toluene results in formation of all three cymene isomers, the process requires costly distillation procedures to reduce *o*-cymene concentrations. This complication is avoided by obtaining cymene from limonene, as *p*-cymene is formed exclusively. Due to the lack of inventory data for the cymene process, the inventory information from the cumene process is used in

this work. This is likely to be a close approximation due to the extent of similarities in the two processes when starting with *p*-cymene.

Scheme C.3.
Cymene to cresol process

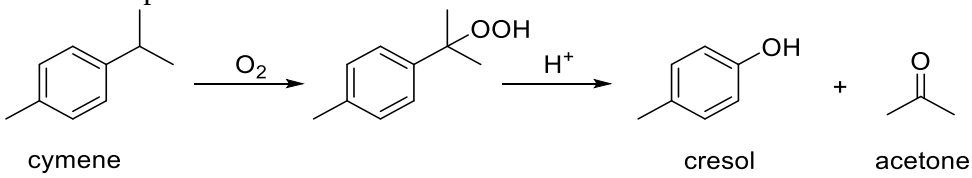

Regardless of its ultimate source, the cresol to MCL process (Scheme C.4) is very similar to the process used commercially to form ε-caprolactone from phenol. Previously developed as an intermediate to ε-caprolactam, the Union Carbide Corporation (UCC) oxidation process is currently used to manufacture ε-caprolactone for polyester manufacturing and the ammonolysis step to yield caprolactam has been discontinued.[1] The inventory data of this process is not available, therefore the industrially relevant hydrogenation and oxidation process is considered through information reported in literature.[13]

Scheme C.4.
Cresol to MCL process

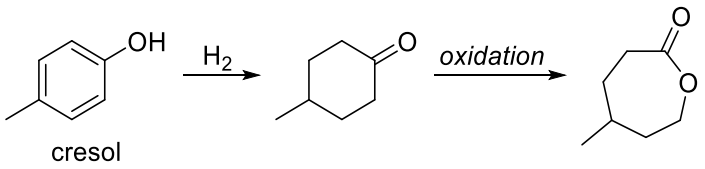

Lundberg and coworkers modeled the cresol-to-MCL process in a technoeconomic analysis of MCL production.[13] The following reaction information from this model was considered to evaluate the environmental impacts of the process. First, hydrogenation of

cresol is carried out in *n*-dodecane under atmospheric pressure of hydrogen gas over a heterogeneous palladium catalyst to yield 4-methylcyclohexanone. The oxidation process of 4-methylcyclohexanone uses hydrogen peroxide at 50 °C, similar to the UCC process. MCL can be purified to high purity, 99.9 mol%, through vacuum distillation. Unreacted reagents from each step are recycled through a vapor recycling system. A fraction of the recycled vapor is removed for hazardous waste disposal to prevent accumulation of impurities. Byproducts, 4-methylcyclohexanol and 4-methyl-6-hydroxyhexanoic acid, are removed through distillation for hazardous waste disposal.

For the process of MCL production described above, the environmental impacts in the categories of greenhouse gas (GHG) emissions, acidification, ozone depletion, terrestrial eutrophication, and human toxicity (cancer and non-cancer) were evaluated. Figure C.2 plots the relative contributions from the cresol-to-MCL process in these environmental impact categories. The top contributors to GHG emissions, acidification, terrestrial eutrophication, and human toxicity (non-cancer) are from use of natural gas and hydrogen peroxide. As for ozone depletion and human toxicity (cancer), hazardous waste disposal and cooling water are the biggest contributors.

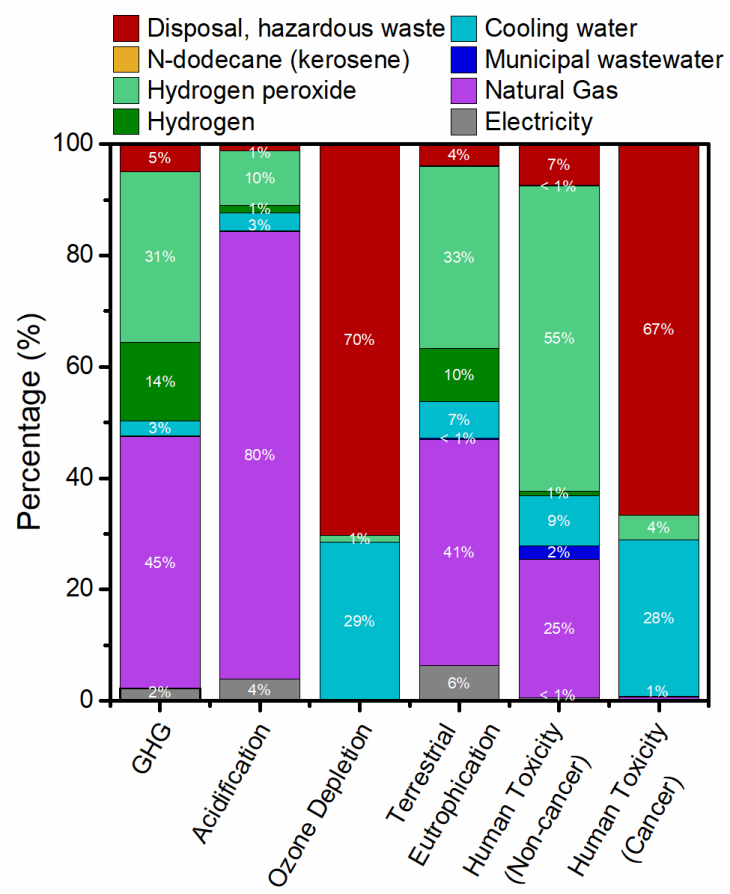

Figure C.2.
Environmental assessment of the cresol-to-MCL process described by Lundberg et al.[13]

C.3. Future Direction

The process detailed in Figure C.1 considers the various starting materials to produce MCL through a common *p*-cresol intermediate. The assumptions made in this work rely on literature reports that are comparable to the processes used on a commercial scale today. This provides a better estimate of what the environmental impact is if MCL were to be commercially produced from a variety of starting points, using either fossil fuels or renewable resources.

The environmental impacts of the entire MCL production process comparing between the various starting materials will be evaluated through contributions to GHG emissions, acidification, terrestrial eutrophication, ozone depletion, and human toxicity. The preliminary data obtained for two processes, orange peels-to-limonene and *p*-cresol-to-MCL, are plotted in Figure C.3. However, there are processes for limonene-to-cymene and cymene-to-cresol that still need to be quantified.

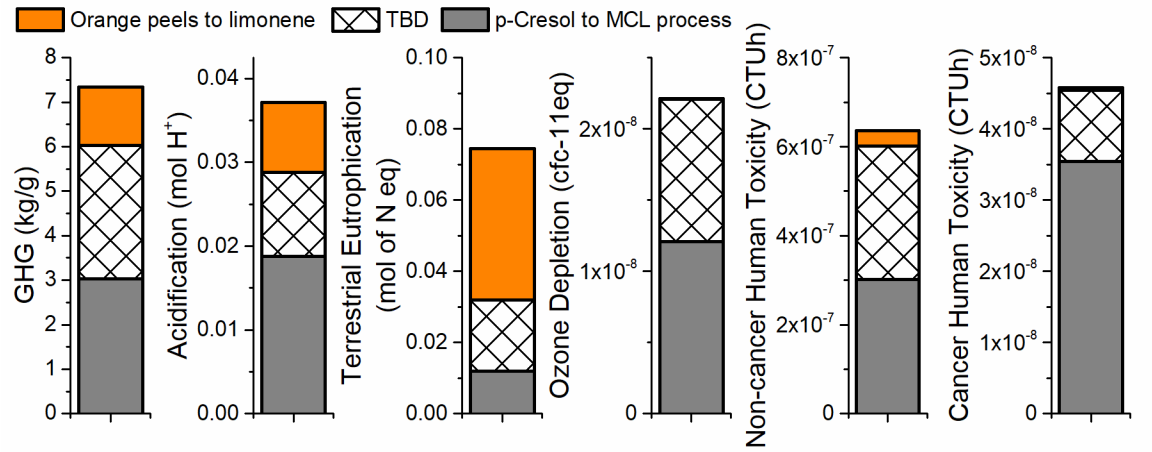

Figure C.3.
Preliminary LCA data for MCL process from orange peels. The quantity of the crosshatched bar will be determined in future work.

The inventory data of commercial processes for crude oil-to-cresol, turpentine-to-limonene, and cumene-to-phenol still need to be obtained and the literature values reported for the orange peel-to-cymene process will be evaluated to quantify the environmental impacts. Once the inventory information has been collected for these processes, the production of MCL from petroleum feedstocks will

be compared to production from renewable feedstocks for the environmental impacts listed above.

C.4. References

(1) Arpe, H.-J. *Industrial Organic Chemistry*; 5th ed.; Weinheim, Germany, 2010.

(2) Tabone, M. D.; Cregg, J. J.; Beckman, E. J.; Landis, A. E. Sustainability Metrics: Life Cycle Assessment and Green Design in Polymers. *Environ. Sci. Technol.* **2010**, *44*, 8264–8269.

(3) Overberger, C. G.; Kaye, H. The Syntheses of Some Optically Active ε-Caprolactones. *J. Am. Chem. Soc.* **1967**, *89*, 5640–5645.

(4) Fiege, H. Cresols and Xylenols. In *Ullmann's Encyclopedia of Industrial Chemistry*; Wiley-VCH Verlag GmbH & Co. KGaA: Weinheim, Germany, 2000; pp. 419–461.

(5) Glasebrook, A. L. Dehydrogenation of Sulfur-Contaminated Monocyclic Terpenes. US Patent 2857439A, 1958.

(6) Ragauskas, A. J.; Nagy, M.; Kim, D. H.; Eckert, C. A.; Hallett, J. P.; Liotta, C. L. From Wood to Fuels: Integrating Biofuels and Pulp Production. *Ind. Biotechnol.* **2006**, *2*, 55–65.

(7) Graglia, M.; Kanna, N.; Esposito, D. Lignin Refinery: Towards the Preparation of Renewable Aromatic Building Blocks. *ChemBioEng Rev.* **2015**, *2*, 377–392.

(8) Linnekoski, J. A.; Asikainen, M.; Heikkinen, H.; Kaila, R. K.; Räsänen, J.; Laitinen, A.; Harlin, A. Production of p -Cymene from Crude Sulphate Turpentine with Commercial Zeolite Catalyst Using a Continuous Fixed Bed Reactor. *Org. Process Res. Dev.* **2014**, *18*, 1468–1475.

(9) Marín, F. R.; Soler-Rivas, C.; Benavente-García, O.; Castillo, J.; Pérez-Alvarez, J. A. By-Products from Different Citrus Processes as a Source of Customized Functional Fibres. *Food Chem.* **2007**, *100*, 736–741.

(10) Dávila, J. A.; Rosenberg, M.; Cardona, C. A. Techno-Economic and Environmental Assessment of p-Cymene and Pectin Production from Orange Peel. *Waste and Biomass Valorization* **2015**, *6*, 253–261.

(11) Makarouni, D.; Lycourghiotis, S.; Kordouli, E.; Bourikas, K.; Kordulis, C.; Dourtoglou, V. Transformation of Limonene into p-Cymene over Acid Activated Natural Mordenite Utilizing Atmospheric Oxygen as a Green Oxidant: A Novel Mechanism. *Appl. Catal. B Environ.* **2018**, *224*, 740–750.

(12) *Phenolic Resins: A Century of Progress*; Pilato, L., Ed.; Springer: Berlin, Heidelberg, 2010.

(13) Lundberg, D. J.; Lundberg, D. J.; Hillmyer, M. A.; Dauenhauer, P. J. Techno-economic analysis of a chemical process to manufacture methyl-ε-caprolactone from cresols. *ACS Sustain. Chem. Eng.* **2018**, Article ASAP.